



**Studies to validate the Comet assay in measuring differential radiation-  
induced DNA damage in cancer cells.**

Thesis submitted for the degree of  
Doctor of Philosophy at the University of Leicester  
by  
Saraa Hanna Barsoom

Leicester Cancer Research Centre  
University of Leicester

2018

## Abstract

DNA damage, induced by both exogenous and exogenous sources, is a key cause of cancer. However, further induced DNA damage, in the form of radiotherapy and genotoxic-chemotherapy, are key means of treating cancer. Consequently, methods to assess DNA damage are important in studies of both cancer causation and treatment. The alkaline comet assay (ACA) has become a standard method for detection of differential DNA damage formation and repair, both *in vitro* and *in vivo*. In this study two different theories were investigated to determine the reason for the differential measures of comet formation noted between bladder cancer cell lines. First, that differential comet formation reflects actual differences in DNA damage formation between the radioresistant and radiosensitive cell lines. Second, that differential comet formation is simply due to the additional release of DNA sequences/loops from the comet head to the tail, for the same level of DNA damage. To determine which scenario occurs, cell lines, which exhibited differential ACA responses, were examined using alternate DNA damage assays (including LC-MS/MS,  $\gamma$ -H2AX & PFGE). An equivalent differential response noted between the assays would indicate that the comet assay does indeed measure differences in IR- induced DNA damage between cell lines; whilst the absence of a differential effect for the alternate methods could indicate that the differential effect noted by the comet assay is possibly due to the additional release of the adjacent/contiguous loops of DNA from the comet head. The key finding of this project is that an equivalent differential response noted between ACA and both LC-MS/MS and PFGE reveals that the comet assay does indeed measure differences in induced DNA damage between cells lines. This project also suggests further new insight regarding  $\gamma$ -H2AX foci formation, with foci formation being marker of DSBs that are 'marked' for repair, and therefore possibly considered as markers indicative of resistance.

*To the soul of my mother who died 27/07/2016.*

# Acknowledgments

*Thanks and praise are going to God for His blessing and protecting during this project work and in fact, throughout all my life.*

**I am particularly indebted to my supervisor, Prof. George DD Jones, for his excellent guidance, enduring and constant encouragement. I acknowledge his insightful discussions and invaluable comments and suggestions.**

**I owe a great deal of gratitude to Dr. Kees Straatman Genetics Department for helping me with the  $\gamma$ -H2AX samples and for his assistance in analysing the results, and to Dr. Nicolas Sylvius of Nucleus of Nucleus Genomics, Genetics Department for helping me with DNA extraction by the Maxwell® 16 MDx Instrument.**

**Thank you very much to Raj Singh for being a great help around all mass spec related issues.**

**I would like to thank Prof. Don Jones, and Dr Chris Talbot for making part of this project possible by his helpful comments, encouragement which I really appreciated**

**I would like to record my thanks to my mother who passed away before she saw my achievement for her continual praying, blessing and for her love, kindness, and supporting during my entire life.**

**Very special thanks to my husband Bahaa, who has given me constant support and patience throughout the PhD study. I could not have done it without you! I also thank my family for their continued support and encouragement over the years.**

**My sincere thanks go to Dr. Ferwerdin Al-Barazanji, Ms. Aisha Al-misnad and all my friends at home for keeping in touch and for their support in every step of my work.**

**My gratitude also goes to everyone in the Radiobiology & DNA Damage group, who have made my PhD experience truly memorable. Specifically, I would like to thank Dr.Karen Bowman, Dr. Kamla Al-Salmani, Aleksandra Bzura and Taniqua Adderley for all their support and the good times we had together.**

**Finally, I would like to acknowledge my thanks to the Ministry of Higher Education of Kurdistan Region government for giving me this opportunity to study in one of the most famous university's in the UK.**

## List of Contents

<b>Abstract</b> .....	<b>II</b>
Acknowledgments.....	IV
List of Tables and Figures.....	XVIII
List of Equations.....	XXVI
List of Abbreviations.....	XXVII
<b>Chapter 1</b> .....	<b>1</b>
<b>Introduction</b> .....	<b>1</b>
1.1 DNA basic structure and functions.....	2
1.1.1 DNA damage in cancer.....	3
1.1.2 ROS induced DNA damage in cancer.....	4
1.2 Cancer incidence.....	6
1.3 Bladder cancer.....	6
1.3.1 The causes of bladder cancer.....	6
1.3.2 The stages and grades of bladder cancer.....	7
1.3.3 The epidemiology of bladder cancer.....	10
1.3.4 Treatment of Bladder Cancer.....	11
1.4 Radiotherapy (RT) in cancer treatment.....	12
1.4.1 RT, Surgery and Chemotherapy in treating cancer.....	14
1.5 Ionising Radiation (IR).....	15
1.5.1 Units used in radiobiology.....	16
1.5.2 Types of ionising radiation.....	16

1.5.3 The physics of IR interaction with matter.....	17
1.5.4 DNA and ionising radiation: DNA is the key target to IR.....	19
1.5.5 The interaction of ionising radiation with cells.....	21
1.5.5.1 The direct and indirect effects of ionising radiation on cells.....	21
1.5.6 Radiation-induced DNA damage.....	23
1.5.6.1 Strand breaks.....	23
1.5.6.2 Base lesions.....	24
1.5.7 The isolated DNA lesions and/or clustered DNA lesions.....	25
1.5.7.1 Single lesions.....	25
1.5.7.2 Clustered lesions.....	26
1.6 Cellular response.....	27
1.6.1 The DNA damage response and DNA repair pathways.....	28
1.6.1.1 DNA damage signaling induction.....	28
1.6.1.2 DNA damage checkpoint induction.....	28
1.6.1.3 DNA damage repair pathways.....	30
1.7 DNA damage measure as markers of RT treatment efficacy.....	33
1.8 Overview of methods to assess DNA damage in this study.....	35
1.8.1 Alkaline Comet assay for the assessment of radiation-induced DNA damage..	35
1.8.2 Liquid chromatography mass spectrometry LC-MS/MS.....	38
1.8.3 Pulsed field gel electrophoresis (PFGE) assay for evaluation of radiation-induced DNA damage.....	39
1.8.4 $\gamma$ -H2AX immunoassay for assessment of radiation-induced DNA damage.....	40

1.9 Comet formation – the two models.....	40
1.10 Aims and Objectives.....	43
1.11 Hypothesis to be tested.....	45
<b>Chapter 2.....</b>	<b>46</b>
<b>Materials and Methods.....</b>	<b>46</b>
2.1 Cell-lines for in vitro studies.....	47
2.1.1 Cell culture medium and supplements.....	47
2.2 Chemicals and Reagents.....	48
2.3 Kits, Enzymes and antibodies.....	48
2.4 Summary of the techniques included in this project.....	49
2.5 Preparation of buffers and working reagents.....	49
Tissue culture and general use	
2.5.1 PBS.....	49
2.5.2 1x Trypsin-EDTA.....	50
Comet Assay	
2.5.3 Low melting point agarose (LMP).....	50
2.5.4 Normal melting point agarose (NMP).....	50
2.5.5 Lysis buffer.....	50
2.5.6 Alkaline electrophoresis buffer.....	50
2.5.7 Neutralisation buffer.....	51
2.5.8 Propidium iodide (PI).....	51
$\gamma$ -H2AX assay	
2.5.9 10x KCM buffer.....	51



2.5.10 1x KCM washing buffer.....	51
2.5.11 KCM blocking buffer.....	51
LC-MS/MS	
2.5.12 Digestion buffer.....	52
2.5.13 Shrimp Alkaline Phosphatase (SAP).....	52
2.5.14 Deoxyribonuclease I (DNase I).....	52
2.5.15 Snake Venom Phosphodiesterase I (SVP).....	52
PFGE assay	
2.5.16 Lysis buffer solution.....	52
2.5.17 Washing buffer.....	53
2.5.18 Low Melting Temperature agarose stock (LMT).....	53
2.5.19 Pulse Field Certified Agarose stock (PFCA).....	53
2.5.20 Running Buffer 1X TBE.....	53
2.6 Medium preparation	
2.6.1 Eagle's Minimum Essential Media (MEM).....	53
2.6.2 Dulbecco's Modified Eagle's Medium (DMEM).....	53
2.6.3 McCoy's A (a modified medium).....	54
2.6.4 Dulbecco's Modified Eagle's Medium (DMEM) with high glucose and L-glutamine.....	54
2.7 Cells lines and culture conditions.....	
2.7.1 Reviving of cell lines from storage.....	54
2.7.2 Maintenance of cell lines.....	54
2.7.3 Freezing of the cells for storage.....	55

2.7.4 Cell counting using trypan blue assay.....	54
2.8 Exposure of cells to ionising radiation.....	56
2.9 Cell viability and proliferation assay.....	57
2.9.1 Determination of cell viability by cell count after IR exposure.....	57
2.10 Estimating DNA damage using alkaline comet assay (ACA).....	58
2.10.1 Pre-coating frosted slides.....	59
2.10.2 Cell-slide preparation.....	59
2.10.3 X-ray radiation.....	59
2.10.4 Cells lysis.....	60
2.10.5 DNA unwinding and electrophoresis.....	60
2.10.6 Neutralisation step.....	60
2.10.7 Slide staining.....	61
2.10.8 Image capture and analysis.....	61
2.11 Liquid Chromatography-mass spectrometry/mass spectrometry (LC-MS/MS) method for the determination of 8-oxodG in DNA bladder cancer cell samples.....	62
2.11.1 DNA extraction by Maxwell 16 Cell DNA Purification.....	63
2.11.1.1 Samples preparation.....	63
2.11.1.2 X-ray irradiation of the samples.....	63
2.11.1.3 Maxwell 16 cell DNA purification.....	63
2.11.1.4 Cell preparation.....	64
2.11.1.5 Automated DNA Purification on the Maxwell® 16 MDx Instrument.....	64

2.11.2 Enzymatic digestion of DNA.....	64
2.11.3 Online column-switching LC-MS/MS analysis.....	67
2.11.4 Sample loading.....	68
2.11.5 Sample elution.....	68
2.11.6 Mass spectrometer.....	68
2.11.7 Determination of the moles of DNA adduct detected on column.....	69
2.11.8 Calculation of the levels of the DNA adducts detected.....	69
2.12 Estimation of DNA DSBs using the PFGE assay.....	70
2.12.1 Plug preparation.....	70
2.12.2 X-ray irradiation of the cell-plugs.....	71
2.12.3 Plugs washing.....	71
2.12.4 Preparation of pulse field certified agarose (PFCA).....	71
2.12.5 Plug preparation to electrophoresis.....	71
2.12.6 Electrophoresis.....	72
2.12.7 Gel staining and visualising.....	72
2.13 Estimation of DNA damage level (DSBs) using $\gamma$ -H2AX assay.....	73
2.13.1 Cells seeding.....	73
2.13.2 X-ray radiation dose.....	73
2.13.3 Fixation and permeabilisation.....	73
2.13.4 Cells imaging and $\gamma$ -H2AX foci visualisation and analysis.....	74
2.14 Statistical analysis.....	75

<b>Chapter 3.....</b>	<b>76</b>
<b>Examination of IR-induced DNA damage (SSB and ALS) by single cell gel electrophoresis (Comet assay).....</b>	<b>76</b>
3.1 Introduction	
3.1.1 Examination of IR-induced DNA damage (SSB and ALS) by single cell gel electrophoresis (Comet assay).....	77
3.1.2 Determination of cell viability in the four bladder cancer cell by trypan blue exclusion assay.....	79
3.1.3 Specific aims of study.....	80
3.1.4 Summary of the techniques/approach.....	80
3.2 Results	
3.2.1 Estimation of radiation-induced comet formation in four bladder cancer cell lines using the alkaline comet assay (ACA).....	82
3.2.1.1 Estimation of IR-induced comet formation in the RT4 bladder cancer cell line as determined by ACA.....	82
3.2.1.2 Estimation of IR-induced comet formation in the J82 bladder cancer cell line as determined by ACA.....	84
3.2.1.3 Estimation of IR-induced comet formation in the RT112 bladder cancer cell line as determined by ACA.....	86
3.2.1.4 Estimation of IR-induced comet formation in UMUC3 bladder cancer cells line as determined by the ACA.....	88
3.2.1.5 The combined results for J82, RT4, RT112 and UMUC3 cancer cells to estimate comet formation as measured by the ACA.....	90
3.2.2 Comparison of IR-induced comet formation response for the four bladder cancer cell lines as determined by ACA, with inclusion of background/basal levels of DNA damage.....	92

3.2.3 Further evaluation of the relative comet formation response for the four bladder cancer cell lines after radiation exposure, as determined by ACA, with inclusion of background/basal levels of DNA damage.....	97
3.2.4 Comparison of IR-induced comet formation response for the four bladder cancer cell lines as determined by ACA, following the subtraction of background/basal levels of DNA damage.....	100
3.2.5 Further evaluation the relative comet formation response for the four bladder cancer cell lines after radiation exposure, as determined by the ACA, with subtraction of background/basal levels of DNA damage.....	106
3.2.6 Assessment of RT4, J82, RT112 and UMUC3 bladder cancer cells viability following IR exposure by trypan blue exclusion assay.....	109
3.2.7 Radiosensitivity in bladder cancer as assessed by Comet Assay and Trypan blue exclusion assay.....	110
<b>3.3 Discussion</b>	
3.3.1 ACA for evaluation the comet formation responses in the four bladder cancer cell lines.....	111
3.3.2 The effect of IR doses in the four bladder cancer cell lines.....	112
3.3.3 Evaluation of IR-induced DNA damage formation through counting cells viability.....	116
<b>Chapter 4.....</b>	<b>117</b>
<b>Liquid chromatography-tandem mass spectrometry (LC-MS/MS) for determination of radiation-induced 8-oxodG in bladder cancer cell DNA.....</b>	<b>117</b>
4.1 Introduction	
4.1.1 Formation of DNA base adducts.....	118
4.1.2 Oxidative DNA damage.....	119

4.1.3 Liquid chromatography/mass spectrometry in the analysis of DNA adducts..	121
4.1.3.1 Instrumentation of mass spectrometric detection.....	121
4.1.3.2 Tandem mass spectrometry (MS/MS).....	122
4.1.4 The detection methods for determination of DNA adducts.....	124
4.1.4.1 Online column-switching system.....	124
4.1.5 General information about the chromatograms.....	125
4.2 Aim.....	126
4.3 Summary of the techniques/approach.....	126
4.4 Results	
4.4.1 The analysis of the prepared DNA bladder cancer cell samples that exposed to (0, 20 and 100 Gy of ionising radiation doses).....	128
4.4.1.1 Optimised method for the genomic DNA extraction.....	128
4.4.1.2 Standards.....	128
4.4.1.3 Online column-switching LC-MS/MS SRM analysis.....	129
4.5 Discussion.....	140
<b>Chapter 5.....</b>	<b>144</b>
<b>IR-induced DNA DSBs damage by the Pulsed Field Gel Electrophoresis (PFGE).....</b>	<b>144</b>
5.1 Introduction	
5.1.1 Analysis of IR-induced DNA DSBs damage by the Pulsed Field Gel Electrophoresis (PFGE).....	145
5.1.2 Pulsed field gel electrophoresis (PFGE) technique.....	145
5.1.2.1 The basic equipment and features of the PFGE System.....	147

5.1.2.2 Running conditions for the PFGE assay.....	148
5.1.2.3 PFGE by Contour-Clamped Homogeneous Electric Fields (CHEF).....	150
5.2 Study Aims.....	152
5.3 Summary of the technique/approach.....	152
5.4 Results	
5.4.1 Assessment of radiation-induced DNA damage formation in the four bladder cancer cell lines as assessed by PFGE/CHEF.....	153
5.4.2 Evaluation of IR-induced DNA DSBs formation in the RT4 bladder cancer cell line.....	153
5.4.3 Evaluation of IR-induced DNA DSBs formation in the J82 bladder cancer cell line.....	154
5.4.4 Evaluation of IR-induced DNA DSBs formation in the RT112 bladder cancer cell line.....	156
5.4.5 Evaluation of IR-induced DNA DSBs formation in the UMUC3 bladder cancer cell.....	157
5.4.6 The combined results for RT4, J82, RT112 and UMUC3 for estimation of the rank-order of IR-induced DNA DSB levels in these cell lines.....	158
5.4.7 Measurement of the relative DNA DSB formation increase induced by IR in the four bladder cancer cell lines, as determined by the PFGE assay.....	160
5.4.8 Investigation of the effect of IR-induced DNA DSBs formation response on the four bladder cancer cell lines following the subtraction of background/basal levels of DNA damage, as determined by PFGE.....	162

5.4.9 Measurement of relative DNA DSBs formation level induced by IR in the four bladder cancer cell lines following the subtraction of background/basal levels....	164
5.4.10 Correlation of total summation of IR-induced DNA SSBs damages as assessed by ACA with total summation of IR-induced DNA DSBs damages as assessed by PFGE assay in UMUC3, RT112, J82 and RT4 bladder cancer cell lines.....	166
5.5 Discussion.....	168
<b>Chapter 6.....</b>	<b>171</b>
<b>Estimation of IR-induced DNA DSBs damage in the four bladder cancer cells using the <math>\gamma</math>-H2AX assay.....</b>	<b>171</b>
6.1 Introduction	
6.1.1 Estimation of IR-induced DNA DSBs damage in the four bladder cancer cells using the $\gamma$ -H2AX assay.....	172
6.2 Summary of the techniques/approach.....	175
6.3 Aim.....	175
6.4 Results	
6.4.1 Optimisation the $\gamma$ -H2AX assay.....	175
6.4.2 IR-induced DNA DSBs damage (foci formation) as assessed via $\gamma$ -H2AX assay in RT4, J82, RT112 and UMUC3 cells.....	177
6.4.2.1 Estimation of DNA DSBs damage levels induced by ionising radiation in RT4 bladder cancer cells as assessed by $\gamma$ -H2AX foci counting.....	177
6.4.2.2 Estimation of DNA DSBs damage levels induced by ionising radiation in the J82 bladder cancer cell line as assessed by $\gamma$ -H2AX foci counting.....	181



6.4.2.3 Estimation of DNA DSBs damage levels induced by ionising radiation in the RT112 bladder cancer cell line as assessed by $\gamma$ -H2AX foci counting.....	185
6.4.2.4 Estimation of DNA DSBs damage levels induced by ionising radiation in UMUC3 bladder cancer cell line as assessed by $\gamma$ -H2AX foci counting.....	189
6.4.3 Assessment of IR-induced DNA DSBs (foci formation) for the four bladder cancer cell lines over the five different time points post-irradiation, including background/basal levels of DNA foci, via $\gamma$ -H2AX assay.....	193
6.5 Discussion.....	197
<b>Chapter 7.....</b>	<b>202</b>
<b>General Discussion and Thesis Summary.....</b>	<b>202</b>
7.1 Final Discussion.....	203
7.1.1 Assessment of IR-induced comet formation response for the four bladder cancer cells via ACA.....	204
7.1.2 Measurement of 8-oxodG DNA adducts in bladder cancer cell lines after ionising radiation treatment using LC-MS/MS.....	205
7.1.3 Investigation of the effect of IR-induced DNA DSBs formation response on the four bladder cancer cell lines as determined by the PFGE assay.....	206
7.1.4 Assessment of IR-induced DNA DSBs damage via the $\gamma$ -H2AX assay in UMUC3, RT112, J82 and RT4 bladder cancer cells.....	206
7.2 Conclusion.....	209
7.3 Future work.....	211
<b>References.....</b>	<b>212</b>
<b>Appendix.....</b>	<b>253</b>

## List of Tables and Figures

Figure 1.1 (A) Anti-parallel double strand DNA showing the base pairing of AT and CG. (B) Pairs of complementary nucleosides present in double-stranded DNA along with their hydrogen bonds .....	3
Figure 1.2 The Stages and grades of TCC of Bladder Cancer (Knowles and Hurst, 2015)....	8
Table 1.1 The T stages of the bladder cancer which shows the progress of cancer cells in the bladder layers .....	9
Table 1.2 The Lymph nodes stages (N stages) of bladder cancer.....	10
Table 1.3 The metastasis stages (M stages) of bladder cancer.....	10
Figure 1.3 Bladder cancer treatment.....	12
Figure 1.4 Schematic diagram of simple and complex lesions that could be formed by the effect of a single radiation track. Low LET radiation track induces lower concentrations of ionisation events, which produce fewer DNA damage sites than high LET tracks. The coloured stars represent base or sugar lesions .....	18
Figure 1.5 Energy deposition ‘spur’ and ‘blob’ events produced by X-ray radiation.....	20
Figure 1.6 Direct and indirect cellular effects of ionising radiation on macromolecules....	22
Figure 1.7 DSB and non-DSB clustered DNA damage. DSB can be simple or more complex with associated base lesions and AP sites. Non-DSB clustered damaged is defined as two or more lesions within one or two helical turns of DNA.....	27
Figure 1.8 DNA damage and DNA repair pathways. The DNA backbone can be affected by endogenous or exogenous factors (for instance, ionising radiation, alkylating agents, or oxygen radicals), leading to the activation and undertaking of specific of DNA repair pathways .....	31
Figure 1.9 Simplified models of DSB-repair by NHEJ and HRR.....	32
Figure 1.10 Example of ‘comets’ as seen using comet 5.5 software.....	38

Figure 1.11 Comet formation and cell's survival rate in six bladder cancer cell lines as determined by the ACA and clonogenic assay .....	42
Table 2.1 The Origin of RT4, J82, RT112 and UMUC3 human TCC cell lines.....	47
Figure 2.1 The key steps of the Comet Assay procedure.....	62
Figure 2.2 The basic components (A, B and C) and steps (D) of the Max well DNA purification instrument.....	66
Figure 2.3 Scheme for the online column-switching.....	67
Figure 2.4 The key steps of the pulse-field gel electrophoresis procedure.....	72
Figure 2.5 Olympus Cyto-system microscope Analysis of $\gamma$ -H2AX foci per field of treated sample using image J software, which was done in duplicate. ....	75
Figure 3.1 IR-induced comet formation response, measured by alkaline comet assay, in the RT4 bladder cancer cell line. IR-induced comet formation in RT4 cells as measured by (A) % tail DNA, (B) Olive tail moment, (C) Tail extent moment, and (D) Tail length, as determined by the ACA.....	83
Figure 3.2 IR-induced comet formation response, measured by alkaline comet assay, in the J82 bladder cancer cell line. IR-induced comet formation as measured by (A) %Tail DNA, (B) Olive tail moment, (C) Tail extent moment, and (D) Tail length, as determined by the ACA. ....	85
Figure 3.3. IR-induced comet formation, measured by alkaline comet assay, in the RT112 bladder cancer cell line. IR-induced comet formation as measured by (A) % Tail DNA, (B) Olive tail moment, (C) Tail extent moment, and (D) Tail length, as determined by the ACA. ....	87
Figure 3.4 IR-induced comet formation response, measured by alkaline comet assay, in UMUC3 bladder cancer cell line. Quantification of IR-induced comet formation as measured by (A) % Tail DNA, (B) Olive tail moment, (C) Tail extent moment, and (D) Tail length, as determined by the ACA.....	89

Figure 3.5a Combined results of IR-induced comet formation, measured by alkaline comet assay, for the four bladder cancer cell lines. Quantification of IR-induced comet formation in RT4, J82, and RT112, and UMUC3 bladder cancer cell lines as measured by % Tail DNA, and Olive tail moment. ....	90
Figure 3.5b Combined results of IR-induced comet formation, measured by alkaline comet assay, for the four bladder cancer cell lines. Quantification of IR-induced comet formation in RT4, J82, and RT112, and UMUC3 bladder cancer cell lines as measured by Tail extent moment, and Tail length. ....	91
Figure 3.6a IR-induced comet formation response, measured by alkaline comet assay, for RT4, J82, RT112 and UMUC3 bladder cancer cell lines.....	93
Figure 3.6b IR-induced comet formation response, measured by alkaline comet assay, for RT4, J82, RT112 and UMUC3 bladder cancer cell lines. ....	94
Figure 3.7 The relative increase in comet formation as assessed by the relative dose response gradient of the four comet parameters, relative to the lowest responding cell line RT4, as assessed by %TD, OTM, TEM, and TL using the ACA (The Figure update from figure 3.6a &b).....	96
Figure 3.8 Comparison of the relative comet formation response, in bladder cancer cell lines exposed to IR as determined by %TD, OTM, TEM, and TL by using the ACA. ....	99
Figure 3.9a IR-induced comet formation response, measured by alkaline comet assay, for UMUC3, RT112, J82, and RT4 bladder cancer cells. ....	102
Figure 3.9b IR-induced comet formation response, measured by alkaline comet assay, for UMUC3, RT112, J82, and RT4 bladder cancer cells.....	103
Figure 3.10 shows the relative increase in comet formation as assessed by the relative dose response gradient of the four comet parameters, relative to the lowest responding cell line RT4, as assessed by %TD, OTM, TEM, and TL using the ACA.....	105
Figure 3.11 Relative comet formation responses in bladder cancer cells after eliminating background/basal levels of DNA damage from each cell lines separately using ACA as assessed by (A) % TD, (B) OTM, (C) TEM, and (D) TL.....	108

Figure 3.12 The viable cell curve responses for the four bladder cancer cell lines investigated, over a dose range of 0–15 Gy, 7 days post irradiation as determined by trypan blue assay.....	109
Figure 3.13 (A) The extent of initial comet formation, as measured by mean %TD, for the four bladder cancer cell lines, over a dose range of 0–10 Gy, as determined by ACA. (B) The radiation cell viable curve responses for the four bladder cancer cell lines investigated, over a dose range of 0–15 Gy, as determined by Trypan blue exclusion assay.....	110
Figure 4.1 An illustration of the various DNA sites frequently modified by carcinogens and their metabolites.....	118
Figure 4.2 Simplified diagram and function of instrumentation of typical mass spectrometry.....	122
Figure 4.3 Principal components of a tandem mass spectrometer. (A) The sample is ionised in the source, and passes into the 1st mass filter (Q1), then into the collision cell (Q2), followed by the 2nd mass filter (Q3), and finally the detector (Grebe and Singh, 2011b) (B) The ionisation method(electrospray ionisation (ESI)) which is used in current clinical LC-MS/MS instruments.....	123
Figure 4.4 Schematic representation of the main detection modes of a triple quadrupole mass spectrometer that have been used to study DNA adducts .....	124
Figure 4.5 typical chromatogram obtained for the analysis of the 8-oxodG and 8-oxodA and its labelled standard using LC-MS/MS SRM.....	125
Figure 4.6a Typical chromatogram obtained for the analysis of the 8-oxo-dG and 8-oxo-dA adducts and its labelled standards using LC-MS/MS SRM.....	131
Figure 4.6b typical chromatogram obtained for the analysis of the 8-oxo-dG and 8-oxo-dA adducts and its labelled standards using LC-MS/MS SRM.....	133
Figure 4.6c typical chromatogram obtained for the analysis of the 8-oxo-dG and 8-oxo-dA adducts and its labelled standards using LC-MS/MS SRM.....	135

Figure 4.6d typical chromatogram obtained for the analysis of the 8-oxo-dG and 8-oxo-dA adducts and its labelled standards using LC-MS/MS SRM.....	137
Table 4.1a. Formation of 8-oxodG following the treatment of the four bladder cancer cell lines DNA with different IR doses as determined by online column-switching LC-MS/MS SRM with background/basal damage.....	139
Table 4.1b. Formation of 8-oxodG following the treatment of the four bladder cancer cell lines DNA with different IR doses as determined by online column-switching LC-MS/MS SRM .....	139
Figure 4.7 Formation of 8-oxodG following the treatment of the four bladder cancer cell lines DNA with different IR doses as determined by online column-switching LC-MS/MS SRM.....	140
Figure 5.1a. Schematic drawings showing CHEF instrument.....	151
Figure 5.1b. Homogeneous pulsed electric field in a CHEF instrument.....	151
Figure 5.2 (A) Image of a de-stained gel produced by PFGE for RT4 bladder cancer cells. (B) DNA damage response for RT4 bladder cancer cell line after exposure to 5, 10, 20, 40 and 50 Gy of IR doses compared to control sample (non-irradiated cells) using PFGE assay.....	154
Figure 5.3 (A) Image of a de-stained gel produced by PFGE for J82 bladder cancer cells. (B) DNA damage response for J82 bladder cancer cell line after exposure to 5, 10, 20, 40 and 50 Gy of IR doses compared to control sample (non-irradiated cells) using PFGE assay.....	155
Figure 5.4 (A) Image of a de-stained gel produced by PFGE for RT112 bladder cancer cells. (B) DNA damage response for RT112 bladder cancer cell line after exposure to 5, 10, 20, 40 and 50 Gy of IR doses compared to control sample (non-irradiated cells) using PFGE assay.....	156
Figure 5.5 (A) Image of a de-stained gel produced by PFGE for UMUC3 bladder cancer cells. (B) DNA damage response for UMUC3 bladder cancer cell line after exposure	

to 5, 10, 20, 40 and 50 Gy of IR doses compared to control sample (non-irradiated cells) using PFGE assay.....	157
Figure 5.6 IR-induced DNA damage in RT4, J82, RT112, and UMUC3 bladder cancer cell lines. The percentage of DNA DSBs damage response was measured by the PFGE assay.....	158
Figure 5.7 The DNA DSBs damage response for four bladder cancer cell line after exposing to 0, 5, 10, 20, 40, and 50 Gy of IR doses as assessed by PFGE assay.....	160
Figure 5.8 The relative of DNA damage increase for the four-bladder cancer cell line, inclusive of the background/basal levels of damage, after exposure to 0, 5, 10, 20, 40 and 50 Gy of IR doses as measured by PFGE.....	161
Figure 5.9 IR-induced DNA damage in RT4, J82, RT112, and UMUC3 bladder cancer cell lines after subtraction the background/basal levels of DNA damage following 5, 10,20, 40 and 50 Gy of IR, as assessed by PFGE assay.....	162
Figure 5.10 The DNA damage (DSBs) for the four bladder cancer cell lines, after subtraction the endogenous damage, following 5, 10, 20, 40 and 50 Gy of IR as assessed by PFGE assay.....	164
Figure 5.11 The relative of DNA damage increase for the four bladder cancer cell lines, after subtraction the endogenous damage from 5, 10, 20, 40 and 50 Gy of IR doses results, as assessed by PFGE assay. Each bar represents Mean $\pm$ SD of four independent experiments. Two-way ANOVA test was used to compare the mean of the four bladder cancer cell lines .....	165
Figure 5.12a Relationship between total summation of IR-induced DNA damage as assessed by Comet assay %TD and the total summation of IR-induced DNA damage as assessed by PFGE assay; with inclusion of background/basal levels of DNA damage in UMUC3, RT112, J82 and RT4 cells.....	167
Figure 5.12b Relationship between total summation of IR-induced DNA damage as assessed by Comet assay %TD and the total summation of IR-induced DNA damage as	

assessed by PFGE assay; with subtraction of the background/basal levels of DNA damage.....	167
Figure 6.1a Examples of DNA damage foci in Bladder cancer cells. Immunofluorescence staining for $\gamma$ -H2AX (green) and DNA counterstaining with Dapi (blue) in RT4 bladder cancer cell line .....	179
Figure 6.1b Examples of DNA damage foci in Bladder cancer cells. Immunofluorescence staining for $\gamma$ -H2AX (green) and DNA counterstaining with Dapi (blue) in RT4 bladder cancer cell line after .....	180
Figure 6.1c IR-induced DNA formation and repair as presented by the number of foci per cell in RT4 bladder cancer cell line.....	181
Figure 6.2a Examples of DNA damage foci in bladder cancer cells. Immunofluorescence staining for $\gamma$ -H2AX (green) and DNA counterstaining with Dapi (blue) in J82 bladder cancer cell line .....	183
Figure 6.2b Examples of DNA damage foci in bladder cancer cells. Immunofluorescence staining for $\gamma$ -H2AX (green) and DNA counterstaining with Dapi (blue) in J82 bladder cancer cell line .....	184
Figure 6.2c IR-induced DNA formation and repair as presented by the number of foci per cell in J82 bladder cancer cell line.....	185
Figure 6.3a Examples of DNA damage foci in bladder cancer cells. Immunofluorescence staining for $\gamma$ -H2AX (green) and DNA counterstaining with Dapi (blue) in RT112 bladder cancer cell line .....	187
Figure 6.3b Examples of DNA damage foci in bladder cancer cells. Immunofluorescence staining for $\gamma$ -H2AX (green) and DNA counterstaining with Dapi (blue) in RT112 bladder cancer cell line after exposing to 0, 0.5, 1 and 2 Gy of IR .....	188
Figure 6.3c IR-induced DNA formation and repair as presented by the number of foci per cell in RT112 bladder cancer cell line. DNA DSB formation and repair were analysed using the $\gamma$ -H2AX assay after exposure to 0.5, 1, and 2 Gy of IR .....	189



Figure 6.4a Examples of DNA damage foci in bladder cancer cells. Immunofluorescence staining for $\gamma$ -H2AX (green) and DNA counterstaining with Dapi (blue) in UMUC3 bladder cancer cell line after exposing to 0, 0.5,1 and 2 Gy of IR .....	191
Figure 6.4b Examples of DNA damage foci in bladder cancer cells. Immunofluorescence staining for $\gamma$ -H2AX (green) and DNA counterstaining with Dapi (blue) in UMUC3 bladder cancer cell line after exposing to 0, 0.5,1 and 2 Gy of IR .....	192
Figure 6.4c IR-induced DNA formation and repair as presented by the number of foci per cell in UMUC3 bladder cancer cell line. DNA DSB formation and repair were analysed using the $\gamma$ -H2AX assay after exposure to 0.5, 1, and 2 Gy of IR .....	193
Figure 6.5 The level of DNA DSBs (foci formation) for the five time points post-irradiation (30 mins, 2 hrs, 6 hrs, 16 hrs, and 24 hrs) of the four bladder cancer cell lines after exposure to 0.5 Gy, 1 Gy, and 2 Gy of IR doses as measured by $\gamma$ -H2AX assay. ....	196

## List of Equations

Equation 2.1 Digestion buffer volume formula.....	52
Equation 2.2 Total cell number in 1ml complete medium formula.....	56
Equation 2.3a and b Number of cell and viable percentage formula.....	58
Equation 2.4 % Tail DNA formula.....	61
Equation 2.5 Formula for calculating DNA adduct on column.....	69
Equation 2.6 Formula for levels of DNA adducts detected.....	69
Equation 2.7 Formula for calculating $\gamma$ -H2AX foci per Nuclei.....	74

## List of Abbreviations

<b>A</b>	Adenine
<b>ACN</b>	Acetonitrile
<b>AEB</b>	Alkaline electrophoresis buffer
<b>ACA</b>	Alkaline comet assay
<b>AJCC</b>	American Joint Committee on Cancer
<b>ALS</b>	Alkali labile sites
<b>ATCC</b>	American Type Culture Collection
<b>ATM</b>	Ataxia telangiectasia mutated
<b>APCI</b>	Atmospheric pressure chemical ionisation
<b>ATP</b>	Adenosine triphosphate
<b>ATR</b>	Ataxia telangiectasia and Rad3-related protein
<b>BC</b>	Bladder cancer
<b>BER</b>	Base excision repair
<b>bp</b>	Base pair
<b>BSA</b>	Bovine serum albumin
<b>C</b>	Cytosine
<b>CCD</b>	Charge-coupled device
<b>CG</b>	Centre of gravity
<b>CID</b>	Collision induced dissociation
<b>CT-DNA</b>	Calf thymus DNA
<b>DDR</b>	DNA damage response
<b>DMEM</b>	Dulbecco's Modified Eagle Medium
<b>DMSO</b>	Dimethyl sulfoxide

<b>DNA</b>	Deoxyribonucleic acid
<b>DNA-PKcs</b>	DNA-dependent protein kinase complex DNA-PK
<b>DNA-PKcs</b>	Protein kinase catalytic subunit
<b>DNase I</b>	Deoxyribonuclease I
<b>EDTA</b>	Ethylenediaminetetraacetic acid
<b>EMEM</b>	Eagle's Minimum Essential Medium
<b>DSBs</b>	Double-strand breaks
<b>ESI</b>	Electrospray ionisation
<b>EtBr</b>	Ethidium bromide
<b>FBS</b>	Fetal bovine serum
<b>FCS</b>	Fetal calf serum
<b>fmol</b>	Femtomole
<b>g</b>	Gram
<b>G</b>	Guanine
<b>G1</b>	Phase Gap 1 phase
<b>G2</b>	Phase Gap 2 phase
<b>Gy</b>	Gray
<b>hr</b>	Hour
<b>H<sub>2</sub>O<sub>2</sub></b>	Hydrogen peroxide
<b>HCl</b>	Hydrochloric acid
<b>HPLC</b>	High performance liquid chromatography
<b>HR</b>	Homologous recombination repair
<b>ICL</b>	Inter-strand crosslinks
<b>IDLs</b>	Insertion/deletion loops

<b>IR</b>	Ionising Radiation
<b>Kb</b>	Kilo base
<b>KCl</b>	Potassium Chloride
<b>L</b>	Litter
<b>LC-MS</b>	Liquid Chromatography-mass spectrometry
<b>LET</b>	The linear energy transfer
<b>Lig I</b>	DNA ligase I
<b>LMA</b>	Low-melting-point agarose
<b>LMP</b>	Low melting point
<b>M</b>	Molar
<b><i>m/z</i></b>	Mass-to-charge ratio
<b>Mb</b>	Mega base
<b>MEM</b>	Minimal essential medium
<b>MeOH</b>	Methanol
<b>mg</b>	Milligram
<b>MgCl<sub>2</sub></b>	Magnesium chloride
<b>min</b>	Minute
<b>mL</b>	Millilitre
<b>mm</b>	Millimetre
<b>MMR</b>	Mismatch repair
<b>MOTM</b>	Mean Olive tail moment
<b>MS</b>	Mass spectrometry
<b>MS/MS</b>	<b>Tandem mass spectrometry</b>
<b>Na<sub>2</sub>EDTA</b>	Ethylenediaminetetraacetic acid disodium salt dehydrate

<b>Na<sub>2</sub>CO<sub>3</sub></b>	Sodium carbonate
<b>NaCl</b>	Sodium chloride
<b>NaI</b>	Sodium Iodide
<b>NaOH</b>	Sodium hydroxide
<b>NEAA</b>	Non-essential amino acids
<b>NER</b>	Nucleotide excision repair
<b>ng</b>	nano gram
<b>NHEJ</b>	Non-homologous end joining
<b>Nm</b>	Nanometer
<b>NM</b>	Nuclear matrix
<b>NMP</b>	Normal melting point
<b>NO</b>	Nitric oxide
<b>OTM</b>	Olive tail moment
<b>PARP1</b>	Poly(ADP-ribose) polymerase 1
<b>PBS</b>	Phosphate buffered saline
<b>PFCA</b>	Pulse Field Certified agarose stock
<b>PFGE</b>	Pulsed field gel electrophoresis
<b>PI</b>	Propidium iodide
<b>PIKK</b>	Phosphoinositide three-kinase-related protein kinases
<b>pmol</b>	Picomole
<b>RNase</b>	Ribonuclease
<b>ROS</b>	Reactive oxygen species
<b>rpm</b>	Revolutions per minute
<b>RT</b>	Room temperature

<b>S</b>	Synthesis phase
<b>S. pombe</b>	Schizosaccharomyces pombe
<b>S/MARs</b>	Scaffold/Matrix attachment regions
<b>SAP</b>	Shrimp Alkaline Phosphatase
<b>SCGE</b>	Single-cell gel electrophoresis
<b>SD</b>	Standard deviation
<b>SDS</b>	Sodium dodecyl sulphate
<b>SEM</b>	Standard error of the mean
<b>SIM</b>	Single ion monitoring
<b>SRM</b>	Selected reaction monitoring
<b>MRM</b>	Multiple reaction monitoring
<b>SSB</b>	Single strand break
<b>SSPE</b>	Sodium Chloride/Sodium Phosphate/EDTA
<b>SVP</b>	Snake venom phosphodiesterase I
<b>T</b>	Thymine
<b>TCC</b>	Transitional cells carcinoma
<b>TE buffer</b>	Tris-EDTA buffer
<b>TE/EDTA</b>	Trypsin/Ethylene Diamine Tetraacetic Acid
<b>TEM</b>	Tail Extent Moment
<b>TL</b>	Tail length
<b>TLS</b>	Translesion synthesis
<b>Tris -HCl</b>	Tris hydrochloride
<b>Trypsin-EDTA</b>	Trypsin-ethylenediaminetetraacetic acid
<b>U</b>	Unit

<b>U</b>	Uracil
<b>% TD</b>	The percentage of tail DNA
<b>(d)dH2O</b>	(Double-)distilled water
<b>°C</b>	Degrees Celsius
<b>•OH</b>	Hydroxyl radical
<b>8-oxodG</b>	8-oxo-7,8-dihydro-2'-deoxyguanosine
<b>IF</b>	Immunofluorescence
<b>IHC</b>	Immunohistochemistry
<b>LMDS</b>	locally multiply damaged sites
<b>OCDL</b>	Oxidative clustered DNA lesions
<b>V</b>	Volt
<b>v/v</b>	Volume/volume
<b>w/v</b>	Weight/volume
<b>xg</b>	Times gravity
<b>γ-H2AX</b>	Gamma H2A Histone family member X
<b>μg</b>	Microgram
<b>μL</b>	Microliter



# **Chapter 1**

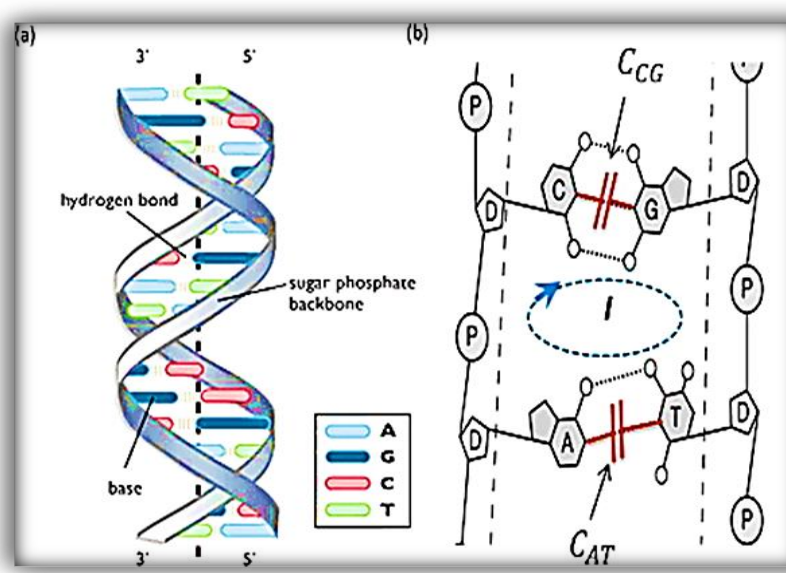
## **Introduction**

## **Introduction**

### **1.1 DNA basic structure and functions**

DNA is the main hereditary material in humans. Most DNA is in the cell nucleus which occupies ~10% of the total cell volume, but a small amount of DNA is also located within the mitochondria (mtDNA). The DNA molecule is a double helix that consists of two long polynucleotide chains composed of four types of nucleotide subunits that are held together by hydrogen bonds. The nucleotide subunit consists of a sugar and phosphate moiety, and one of four DNA bases. The DNA bases are classified into two classes: purines and pyrimidines. The purines are adenine and guanine, and the pyrimidines are cytosine and thymine. The base pairing occurs normally between adenine (A) and thymine (T), and between guanine (G) and cytosine (C) to present AT and GC pairs (Watson and Crick, 1953; Saenger, 1984; Jeffrey and Saenger, 2012).

The nucleotide consists of a phosphate linked to a sugar known as 2'-deoxyribose to which a base is also attached. The sugar is a 2'-deoxyribose as there is no hydroxyl moiety at position 2' (just two hydrogens). The sugar and base together are called a nucleoside. The addition of a phosphate to a nucleoside creates a nucleotide. Nucleotides are then joined together in polynucleotide chains through the 3'-hydroxyl of 2'-deoxyribose of one nucleotide, and the phosphate attached to the 5'-hydroxyl of another nucleotide (Watson and Crick, 1953; Saenger, 1984; Jeffrey and Saenger, 2012) (as shown in Figure 1.1). DNA encodes information through specific arrangements of the nucleotides along each strand. Thus, the complete set of information in the DNA structure is called the genome which is contains the vital information of protein synthesis. Genes contain the instructions that can produce specific proteins. Therefore, DNA is the most important part of the cell, because of its ability to carry all the genetic information for all proteins that organisms will continually synthesise and use (Alberts et al., 2002). Every single DNA strand contains a specific sequence of nucleotides exactly complementary to the second strand (known as the complementary strand). Subsequently, DNA duplication can take place with one strand being employed as a template for the synthesis of a new second strand.



**Figure 1.1** (A) Anti-parallel double strand DNA showing the base pairing of AT and CG. (B) Pairs of complementary nucleosides present in double-stranded DNA along with their hydrogen bonds (Al Ahmad et al., 2016).

### 1.1.1 DNA damage in cancer

DNA is constantly being damaged by either exogenous sources such as ionising radiation and drugs, or endogenous sources such as cellular metabolism, immune responses, and inflammation (Kryston et al., 2011a).

DNA mutation is the modification in the primary structure of the DNA molecule, induced by a chemical addition or base DNA disruption, which result in the formation of an abnormal nucleotide or a break in one or both DNA strand chains. Although damage to the DNA has occurred, the damaged DNA might still be able to undergo DNA replication, therefore, an incorrect base would be inserted on the opposite side of the damaged base in the complementary strand. This can subsequently cause a mutation in the next round of DNA replication. Additionally, mutations can be generated during the double-strand repair process because of inaccuracies in the repair process (Bernstein et al., 2013). Mutations can trigger a variety of genes that are oncogenes or suppress tumour suppressor genes or induce genomic instability in cells and these traits can be initiated via epigenetics. However, mutations can be inhibited or evaded by accurate DNA repair mechanisms, which can recognise the damage site before DNA replication. Furthermore, during cell proliferation, if DNA damages in the

replicating cells are not repaired because of inadequate DNA repair, this can increase the risk of cancer formation. In the non-proliferating cells, the DNA damages, if not repaired properly, can cause premature aging (Akbari and Krokan, 2008; Negrini et al., 2010).

DNA repair mechanisms are a crucial strategy to preserve the genomic integrity of cells. Accordingly, cells have developed mechanisms and DNA damage response networks for dealing with these damages through repairing the damage to restore the integrity of the DNA molecule or by initiating programmed cell death to eliminate severely damaged or highly uncontrolled cells (Hoeijmakers, 2009; Shimizu et al., 2014; Fontes et al., 2015; Uryga et al., 2016).

### **1.1.2 ROS induced DNA damage in cancer**

Reactive oxygen species (ROS) is a group of chemically reactive molecules containing either molecular oxygen ( $O_2$ ) or atomic oxygen (O). These are constantly produced in cells as products of normal oxygen metabolism. They may be highly reactive molecules due to the presence of one or more unpaired electrons in the outer orbital, such as for superoxide anion ( $O_2^{\bullet-}$ ), peroxide ( $O_2^{\bullet-2}$ ), hydroxyl radical ( $OH^\bullet$ ), nitric oxide ( $NO^\bullet$ ), peroxy ( $ROO^\bullet$ ), and lipid peroxy ( $LOO^\bullet$ ) (Aiken et al., 2011). However, there are also non-free-radical ROS species, which do not possess unpaired electrons in the outer orbital. For instance, hydrogen peroxide ( $H_2O_2$ ), nitrous acid ( $HNO_2$ ), and lipid peroxide ( $LOOH$ ). Nevertheless, whilst not free radical they can readily generate free radicals (Genestra, 2007; Trachootham et al., 2009). ROS can be generated via means of enzymatic and non-enzymatic reactions. The enzymatic reactions take place during common intracellular metabolism, mainly due to activities such as mitochondrial respiration, prostaglandin synthesis, cell differentiation and proliferation, inflammation, immune cell activation following attack from pathogens or foreign bodies, mental stress, infection, cancer, and aging (Halliwell and Cross, 1994; Finkel and Holbrook, 2000; Valko et al., 2005; Valko et al., 2006; Halliwell, 2007; Trachootham et al., 2009). However, the non-enzymatic reactions can occur via oxygen reacting with organic compounds like those initiated by ionising radiations (Droge, 2002). Cell injury can occur as a result of ROS formation through a series of different alterations in the DNA structure. ROS can occur in various organelles; however, mitochondria is the essential source of ROS production (Beckman and Ames, 1998; Balaam et al., 2005). Therefore, the excess

production of ROS within mitochondria can lead to oxidative damage to mitochondrial proteins, membranes, and its DNA (Higgins et al., 2010). Endogenous ROS can produce mutations in the DNA if the damages are not repaired accurately (Kohn and Bohr, 2002).

Exogenous sources of ROS-mediated damage can result from UV irradiation (from exposure to sunlight), gamma and X-ray sources, air and water pollution, cigarette smoke, alcohol, drugs, industrial solvents, and cooking (smoked meat, used oil, fat) (Young and Woodside, 2001; Mashima et al., 2001; Valko et al., 2005; Valko et al., 2006). These exogenous sources of damage can penetrate the body through different paths and can generate free radicals. ROS interaction with genetic materials may possibly cause a variety of lesions (Loft and Poulson, 1996). Therefore, the sensitivity of cells to ROS-induced DNA damage is dependent upon the ROS members and their effects. Hydroxyl radicals ( $\text{OH}\bullet$ ) are the most effective oxidising agent amongst ROS species, because of their ability to attack DNA by removing a hydrogen atom from the sugar backbone of DNA strand causing strand breakage (mainly SSBs) (Wang et al., 1998; Evans et al., 2004) and by adding to the double bonds of any one of the four DNA bases to cause oxidatively damaged base lesions (de Miguel and Cordero, 2012). Therefore, ROS can be an effective agent of cancer causation, cell death, ageing, and neurological disorders (Floyd, 1999).

Normal cells have low endogenous ROS levels; however, cancer cells have an elevated amount of ROS which stimulates cell proliferation, differentiation as well as increase their ability to survive (Boonstra and Post, 2004; Gibellini et al., 2010). However, increasing ROS levels in cancer cells can lead to the induction of a temporary cellular damage which can lead to the accumulation of ROS-induced damage within cancer cells that subsequently can promote cellular death, and provoke cells to initiate toxic chain reactions (Ahmad et al., 2004). Hence, this action is capable of causing a permanent oxidative damage to the biological components (specifically DNA) of cancer cells (Lopez-Lázaro, 2007). From this point, further exogenous treatment-sources of damage such as drugs and ionising radiation can elevate ROS levels in cancer cells by increasing the oxidative stress above the toxic threshold which can escalate cancer cell lethality (Lopez-Lázaro, 2007; Trachootham et al., 2009). Whilst DNA damage is a cause of cancer, inducing further DNA damage is the basis of the current successful strategies for treating cancer, notably by radiotherapy.

## **1.2 Cancer incidence**

Cancer represents the second most prominent cause of death worldwide. Cancer is a class of diseases characterised by uncontrolled cell growth, resulting from unregulated division of the cells which grows locally but possesses the capacity to metastasise to different organs within the body (Jemal et al., 2010; Baskar et al., 2012). This unregulated cell division can be caused by DNA mutations, which greatly impact cellular functions. DNA mutations can activate oncogenes, inactivate tumour suppressor genes, and can initiate genomic instability within the replication process. Thus, the accumulation of such mutations within a cell can lead to cancer (Vogelstein et al., 2013). The accumulation of cancerous cells is known as a tumour (Almeida and Barry, 2011).

## **1.3 Bladder cancer**

Bladder cancer (BC) is an irregular growth, which concerns the bladder urothelium (Pang & Catto, 2013). It is a common type of disease in the UK. Patients with transitional cell carcinomas (TCCs) represent 90% of all cases. The transitional cell carcinoma that grows in the mucosa or submucosa, is identified as “non-muscle invasive” (NMIBC) or superficial bladder cancer, while the remaining common rare subtypes include squamous cell carcinoma (SCC), adenocarcinoma carcinoma, micropapillary carcinoma (MPC), plasmacytoid urothelial carcinoma (PUC) and small cell carcinoma of the bladder (SCCB) (Burger et al, 2013).

### **1.3.1 The causes of bladder cancer**

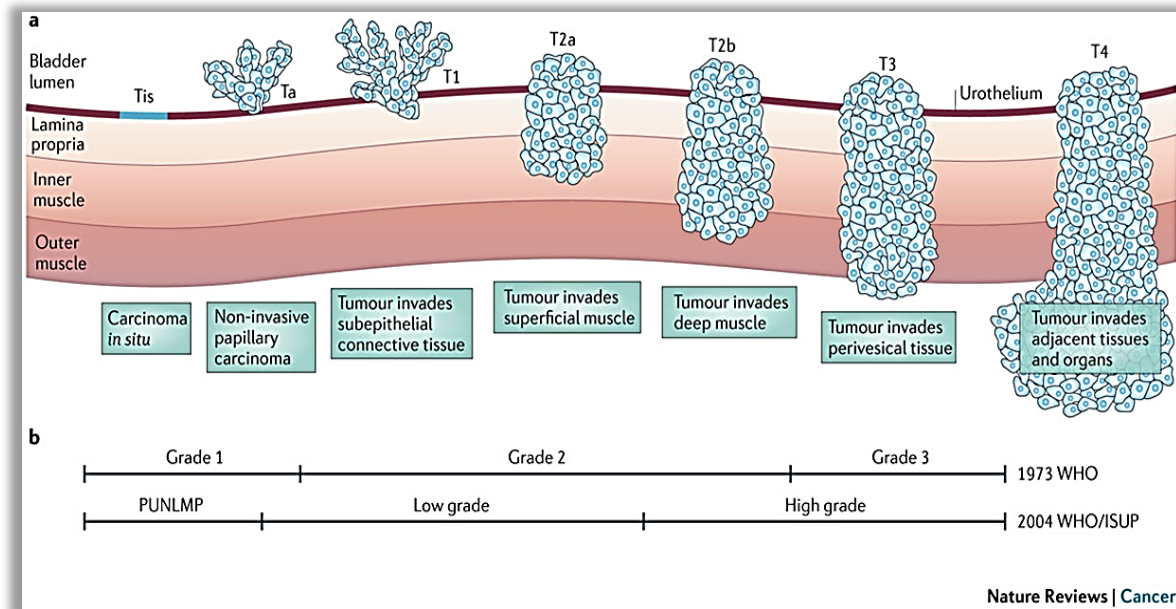
**A.** External environmental and non-genetic factors play a role in the development of bladder cancer. The most well known risk factors of bladder cancer are smoking and occupational exposure. Tobacco consumption is the most significant factor that increases the risk of developing bladder cancer in both males and females. The duration of smoking and the number of cigarettes increases the level of bladder cancer incidence (Freedman et al., 2011; Yang, 2011). Moreover, people who began smoking at an earlier age or non-smokers whose are exposed to second hand smoke (SHS), which is also known as environmental tobacco

smoke (ETS), could increase their risk of BC incidence (Freedman, et al., 2011; Yang, 2011). Occupational carcinogens are also considered to be among the prominent reasons for bladder incidence, causes approximately 20-25% of bladder cancers incidence. Furthermore, acute urinary tract infections, which consist of fungal and viral infections (Fioriti D, et al., 2012), or bacterial, and parasitic infections (Mostafa et al., 1999), seem to have a great influence on bladder cancer causation. For example, schistosomiasis (bilharzia) is a type of parasite that can infect the urinary tract. It is now a widespread, common disease currently found in 75 countries, and it can have a crucial impact on bladder cancer causation, specifically invasive SCC. It is expected that more than 200 million people residing in rural and agricultural areas are infected and also between 500 million and 600 million people might be at a risk of infection with this parasite (Mostafa et al., 1999).

**B.** Physiological or internal factors (genetic inheritance factors) can also result in the formation of bladder tumours. If genetic mutation occurs, the DNA is permanently altered as genetic changes are irreversible. For instance, there may be a transformation in the sequence of nucleotides or rearrangements of whole chromosomes, both of which can be associated with increases in gene expression. For instance, if part or all of chromosome 9 were missing, this could have a great impact on BC recurrence (Lindgren et al., 2006). Age and gender factors also impact urothelial carcinoma of the bladder (Fajkovic et al., 2011). However, the variance between the sexes with regard urothelial carcinoma could be associated with environmental exposure, physiological, or other internal factors such as inherited genetic defects, the immune system defects, and hormone defects (Shariat et al., 2010).

### **1.3.2 The stages and grades of bladder cancer**

Bladder cancer can be classified according to the TNM (Tumour-Node-Metastasis) staging system, in which the tumour (T) stage of the primary tumour depends on the depth of tumour penetration of the bladder layers and whether it has reached the lymph nodes or has spread (metastases) (American Joint Committee on Cancer (AJCC), 2002). The diagnosis, medication and tumour progression are dependent upon tumour stage and grade (Rene et al., 2009) (Figure 1.2).



**Figure 1.2** The Stages and grades of TCC of Bladder Cancer (Knowles and Hurst, 2015).

BC patients may be approximately partitioned into two groups: those having a non-muscle-invasive bladder cancer (NMIBC), staged Ta and T1, which represent 75% of the patients, and those with a muscle-invasive bladder cancer (MIBC), staged T2 to T4, which account for 25% of the patients (Stenzl et al., 2011; Babjuk et al., 2012) (Table 1.1, 1.2, 1.3).

On the other hand, according to WHO and the International Society of Urological Pathology agreement (2004), bladder malignancy is categorised into four grades which depends on their cellular characteristics:

- Urothelial papilloma – benign tumour
- Papillary Urothelial Neoplasm of Low Malignant Potential (PUNLMP) – grows very slowly and unlikely distribution to bladder muscles layers.
- Low grade papillary urothelial carcinoma – grows slowly and unlikely to diffuse. This type is well differentiated and it remains in the bladder lining layer.
- High grade papillary urothelial carcinoma – poorly differentiated, quick growing and with the ability to spread into bladder muscles layers.



80% of bladder cancer is represented by Low grade papillary urothelial carcinoma which grows slowly and remains in the bladder lining layer (Cheng, et al., 2012).

**Table 1.1 The T stages of the bladder cancer which shows the progress of cancer cells in the bladder layers (Di Pierro et al., 2012).**

TX	Primary tumour cannot be evaluated.
T0	No evidence of primary tumour.
Ta	Tumour is starting to grow in the innermost (papillary) layer of the bladder lining.
Tis (Cis)	Carcinoma in the innermost layer of bladder lining (the epithelial tissues). Cells are hard to differentiate.
T1	Tumour has begun to grow into sub-epithelial connective tissue.
T2	Tumour has grown and reached bladder muscle layer.
T2a	Tumour has invaded superficial muscle.
T2b	Tumour has reached the deepest muscle.
T3	Tumour has grown in to the muscle layers to reach the fat tissue.
T3a	In this stage the cancer in fat tissue could only be seen under a microscope (Microscope invasion).
T3b	Macroscopic invasion.
T4	Tumour has reached other organs: Prostate, Uterus, Vagina, Pelvic Wall, and Abdominal Wall.
T4a	Tumour has invaded prostate, uterus, or vagina.
T4b	Tumour finally has invaded pelvic or abdominal wall.

**Table 1.2 The Lymph nodes stages (N stages) of bladder cancer (Di Pierro et al., 2012).**

NX	Regional Lymph nodes cannot be assessed.
N0	The lymph nodes are not affected.
N1	Metastasis in one lymph node, 2 cm or less in measurement.
N2	Metastasis in multiple lymph nodes in the pelvis.
N3	Metastasis in one or more lymph nodes which reach the groin.

**Table 1.3 The metastasis stages (M stages) of bladder cancer (Di Pierro et al., 2012).**

X	Metastasis cannot be evaluated.
M0	Cancer has not spread to other organs.
M1	Cancer has spread to others organs which are most likely to be the lungs, bones, or liver.

### **1.3.3 The epidemiology of bladder cancer**

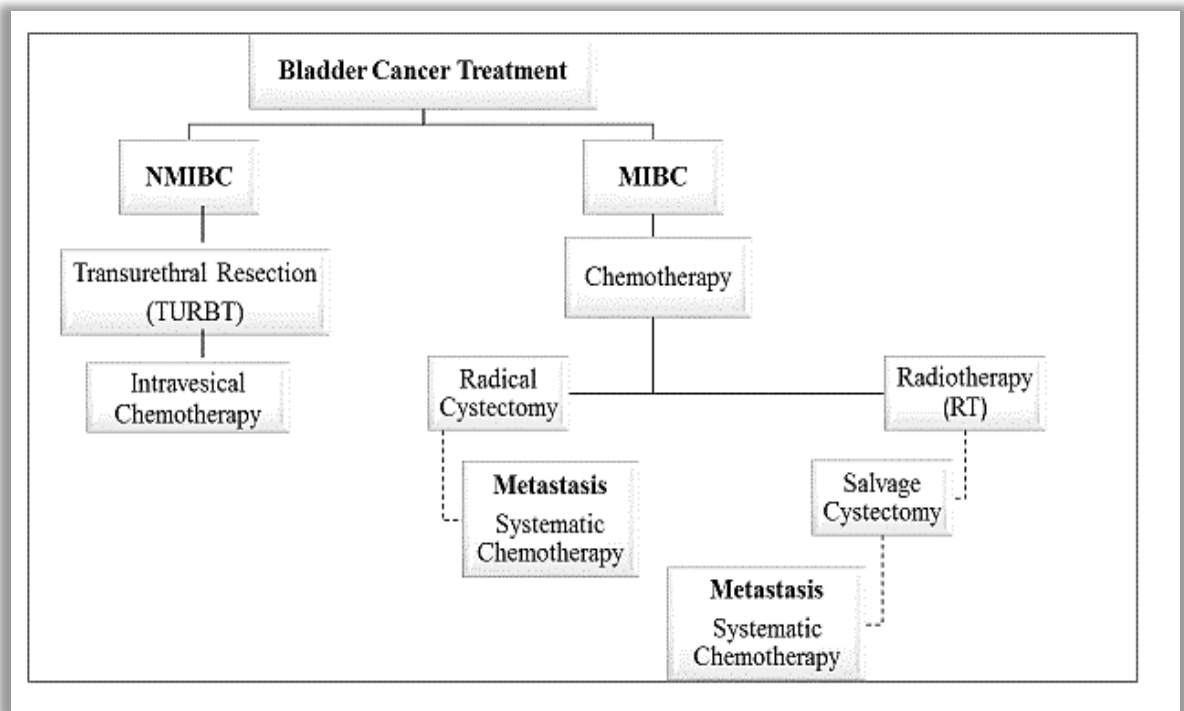
Bladder cancer is the most common cancer of the urinary tract with ~380,000 new cases and ~150,000 deaths per year worldwide (Ferlay et al., 2010). Bladder cancer is recognised as the ninth most prevalent malignancy worldwide (Stenzl et al., 2011). It has also become the fifth malignant disease in the developed countries and represents 5% of cancer types (Cheng, et al., 2012, Jemal et al., 2011). The rate of bladder cancer increases with age and is most common between 50 and 70 years of age. Additionally, bladder cancer is five times more common among men than women (Goodison et al., 2013).

In Europe and North America, > 90% of bladder cancers are TCC. The majority of bladder cancers (~60%) are non-muscle invasive (stage Ta) papillary tumours of low grade (figure1.1). Stage T1 tumours, which have penetrated the epithelial basement membrane but

have not invaded the muscle, are mostly of high grade. The NMIBCs frequently recurrence (50–70%) but infrequently progress to invasion (10–15%) (Prout, et al, 1992). MIBCs (of stage T2 and above) have a poor diagnosis with five-year survival < 50% and common progression to metastasis (Soloway, 2013).

### **1.3.4 Treatment of Bladder Cancer**

Based on clinical and pathological assessments, patients with NMIBC (Ta, Tis, T1) would be treated by transurethral resection of the bladder tumour (TURBT) followed by chemotherapy. The recurrence rates of non-muscle-invasive bladder cancer can be as high as 50-80% with 10-25% progressing to a muscle-invasive bladder tumour (T2a-T4) (Herr, 1992). On the other hand, for patients with MIBC, there are two choices: cystectomy or organ-preserving treatment. A comprehensive and accurate transurethral resection (TUR) is the correct way to make an appropriate diagnosis and eliminate all visible lesions (Babjuk et al., 2012). However, the convenient treatment of organ preserving for MIBC patients is radiotherapy (RT) (James et al., 2012) primarily radical external beam RT. RT can assist in preventing unnecessary surgery, and it is also the main treatment for patients who are considered inappropriate for surgery. Furthermore, RT achieves the same cure levels as cystectomy (Kotwal et al., 2008; James et al., 2012). However, 50% of MIBC patients who receive radical RT suffer local cancer recurrence that requires further treatment in the form of salvage cystectomy (Cooke et al., 2000) (Figure, 1.3).



**Figure 1.3** Bladder cancer treatment

#### 1.4 Radiotherapy (RT) in cancer treatment

Radiation therapy or radiotherapy is a highly effective tool for the treatment of cancer, and a vital component of cancer management including palliative treatment (Guadagnolo et al., 2013; Liauw et al., 2013). RT is the option for patients with inoperable tumours, also for patients who have had surgery but suffer from tumour recurrence after surgery (Durante and Loeffler, 2010). RT is the mainstay of organ preserving therapy, and it is also the main treatment for patients who are considered unfit for surgery. Ionising radiation (IR) kills cancerous cells by extensively damaging the cells' DNA. The main goal of radiotherapy is to eradicate cancer cells growth ability and to kill cancer cells. Radiotherapy

does not kill cancer cells directly, as cancer cells require hours, days, or weeks of treatment before they die/are totally eradicated (Hanahan and Weinberg, 2011; Burrell et al., 2013).

Radiotherapy is a localised therapy treatment, and it is utilised as an essential treatment for ~50% of all cancer patients at some stage of their illness. Radiotherapy can also be used as a form of palliative treatment, to relieve the patients from symptoms caused by the cancer but is commonly delivered with curative intent (Delaney et al., 2005; Bhide and Nutting, 2010; Begg et al., 2011). Indeed, the majority of patients (~60%) are treated by radiotherapy with the intention of cure (Barnett et al., 2009), and presently RT accounts for ~40% of all cancer that are cured (Bentzen, 2006; Ahmad et al., 2012). Radiotherapy, along with surgery and cytotoxic chemotherapy, can increase survival rates of cancer patients (Delaney et al., 2005). A considerable genetic and epigenetic abnormality distinguishes cancer from other diseases, and cancer possesses the capacity to metastasise to different organs within the body (Hanahan and Weinberg, 2011; Burrell et al., 2013). The cytotoxic effects of IR can be employed on cancer cells (Lawrence et al., 2008), because the high-energy radiation damages genetic material (DNA) of cells. Consequently, it promotes blockage of their ability to divide and proliferate further (Jackson and Bartek, 2009a).

Even though radiation damages both normal cells as well as cancer cells, the main goal of radiation therapy is to increase the radiation dose on the cancer cells whilst reducing exposure to normal cells, although normal cells will always be in the range of the radiation margins (Begg et al., 2011). Yet, despite the vast benefits derived from medical applications, radiation can be harmful, and it may lead to genetic modifications in normal cells. Consequently, radiation is carcinogenic to living organisms (Little, 2003).

Several radioprotection strategies including physical targeting of the radiation to the tumour cells and excluding as much as possible the normal tissues from the path of radiation target, were developed including conformal radiotherapy, intensity modulated therapy, and image guided radiotherapy (Brizel, 2005; Verellen et al., 2007). Likewise, fractionating the radiation dose considerably increases in the effectiveness of radiotherapy on cancer cells as well as decreasing the harmful effects on non-cancerous normal tissues which surround the tumour and the tumour bed (Emami et al., 1991; Bentzen et al., 2010). Furthermore, the capacity of radiation to intensely damage tumour cells is dependent upon the radiation's

LET, fractionation schedules, total dose, and the relative radiosensitivity of the targeted cells or tissues (Hall, 2007; Baskar, 2010).

### **1.4.1 RT, Surgery and Chemotherapy in treating cancer**

In recent years, many treatment and management options for cancer are available including surgery, radiotherapy, and systemic therapy (e.g., chemotherapy, hormonal therapy, immune therapy, and molecularly targeted therapy). Radiotherapy is an often used and successful cancer treatment, with approximately 50% of all cancer patients receiving radiotherapy during the course of their illness (Delaney et al., 2005; Begg et al., 2011). Radiotherapy provides a local therapy treatment (Moding et al., 2013) as well as a very efficient palliative treatment for cancer patients for alleviation of pain as a result of the cancer (Delaney et al., 2005; Prise, 2006; Guadagnolo et al., 2013; Liauw et al., 2013). Radiotherapy is the main option for patients with inoperable cancer or partially resected disease (Durante and Loeffler, 2010), as well as for those who are suffering from recurrent tumours post-surgery. Therefore, many patients are treated with the intent to cure (Barnett et al., 2009).

Radiotherapy treatment may be delivered alone or in combination with other treatment modalities such as surgery, chemotherapy, or immunotherapy to utilize the ability of ionising radiation to limit cancer cell division and to potentially to induce cell death. If implemented pre-surgery (neoadjuvant therapy), radiation is used to shrink the tumour pre-resection, so allowing for a greater chance of fully removing the tumour and killing/removing any locally metastatic cells. If used after surgery (adjuvant therapy), radiation is used to destroy any residual microscopic tumour cells left behind post-surgery. It is well known that tumours differ in their sensitivity to radiation treatment with some tumour/cancer types (sarcomas) being sensitive to the killing effects of radiation and some resistant (lung cancer). Radiotherapy exploits low and high linear energy transfer (LET) radiations to effectively eradicate cancer cells, while to prevent toxic effects on normal tissues (Lawrence et al., 2008, Baskar et al., 2012). Fractionation of the total radiation dose over a time frame of several weeks reduces the risk of normal cell toxicity, with the lower dose per fraction allowing normal tissue, with their full repair capacity, to better recover (Bentzen, 2006).

There are two ways to deliver radiation to the location of the cancer. External beam radiation is one way in which radiation is delivered from outside the body by aiming high-energy rays (photons, protons or particle radiation) to the location of the tumour. Still, the surrounding normal tissues are unavoidably exposed to radiation during the delivery of external-beam radiation, which escalates the normal tissues complication probability. However, Radiation can also be delivered internally (e.g., brachytherapy) which involves the delivery of radiation from inside the body by radioactive sources sealed in catheters or seeds directly implanted into the tumour site. This form of radiation delivery is used particularly in the routine treatment of gynaecological and prostate malignancies (Baskar et al., 2012).

Over the years, technological improvements in radiotherapy delivery have aimed to widen the therapeutic window while reducing the normal tissue impact and increase tumour control (Durante and Loeffler, 2010; Loeffler and Durante, 2013) and the benefits will be three-fold: patient cure, organ preservation, and cost-efficiency.

To fully appreciate radiation-induced DNA damage, it is important to consider the underpinning radiation physical effects and associated terminology to enable a better understanding of the importance of basic concepts of ionising radiation interactions with living cells.

## **1.5 Ionising Radiation (IR)**

Radiation is the result of energy emitted by a specific body, and subsequently transmitted and absorbed by another body. Radiation can be classified into two major forms: ionising radiation and non-ionising radiation. Environmental radiation (exogenous sources) is a main form of non-ionising radiation, such as ultraviolet (UV) rays from the sun. Radiation is believed to be ionising if composed of particles or photons that carry sufficient kinetic energy to interact with and eject electrons from atoms or molecules of the absorbing material. Ionising radiation can be the result of the natural decay of unstable atomic nuclei (radioactivity), but can also be artificially generated, for example by particle accelerators (Valente, 2011). The interaction of IR with biomolecules is, however, much more aggressive than non-IR due to its greater ability of IR to induce atom ionisation. When IR traverses through matter, it progressively deposits energy by ionising atoms through many interaction processes along the length of its target track. Ionising radiation, therefore, is a high-energy

type of radiation that is measured in electron volts (eV). For instance, the water molecule ( $\text{H}_2\text{O}$ ), is ionised by the absorption of  $\sim 14\text{eV}$  of energy from IR (Maier et al., 2014).

### **1.5.1 Units used in radiobiology**

The Gray (Gy), named after British physicist Louis Harold Gray, is the international unit of measurement for ionising radiation (radiation dose). It is defined as the absorption of one joule of radiation energy per kilogram of matter. This measurement takes into consideration the Linear Energy Transfer (LET) of ionising radiation, but changes with the IR type and the atomic number of the traversed material. In addition, dose rate is the dose absorbed per unit of time, and a variety of dose rates illicit distinct biological responses (R. Boreham et al., 2000).

### **1.5.2 Types of ionising radiation**

An understanding of the biologic effects of radiation requires a basic understanding of the types of radiation, and the ways in which radiation interacts with cells and tissues. Radiation can interact with matter in diverse ways, largely driven by the type of radiation and the type of material with which it interacts. Radiation is a form of energy, and its absorption by biological matter can lead to two different effects: excitation and ionisation. When excitation of an electron occurs, the electron is elevated to a higher energy level in an atom, but it is not ejected. Ionising radiation, however, results when an electron obtains enough energy to leave the orbit around an atom or molecular (Rebois and Ray, 2012; Ray et al., 2014).

Ionising radiation can be distinguished into two types: electromagnetic radiation and particle radiation.  $\gamma$ -rays and X-rays are two examples of electromagnetic radiations that are frequently used in medical and biological applications. These types can be considered as photons (packets of energy) and are distinguished by their high energies and short wavelengths.  $\gamma$ -rays are produced without a machine and can be emitted from radioactive isotopes. The radioactive substances experience nuclear decay until the nucleus becomes stable by releasing energy in the form of  $\gamma$ -rays. In contrast, X-rays are produced mechanically. Nevertheless, both X-rays and  $\gamma$ -rays have similar physical characters and the biological responses of  $\gamma$ -rays and X-rays are due to the interaction of their photons with the absorbing biological materials (Hall and Giaccia, 2006; Pernot et al., 2012a). However,



electrons, protons, neutrons,  $\alpha$ -particles, and heavy charged ions are examples of particle radiation, and these also can be utilised clinically or experimentally (Sørensen et al., 2011; Pernot et al., 2012a).

Ionising radiation can be further classified into either direct or indirect ionising in mediating their biological effects (for further details of direct vs indirect effects, see 1.3.5). Most of the particulate types of radiation are directly ionising. For instance, individual particles with sufficient kinetic energy can interrupt the atomic structure directly of the absorbing substance through which their path passes. Therefore, chemical and biological damage can occur in the absorbing molecules. In contrast, electromagnetic radiations are mostly indirect ionising radiations, because they produce secondary electrons (charged particles) following energy absorption in the material (Hall and Giaccia, 2006).

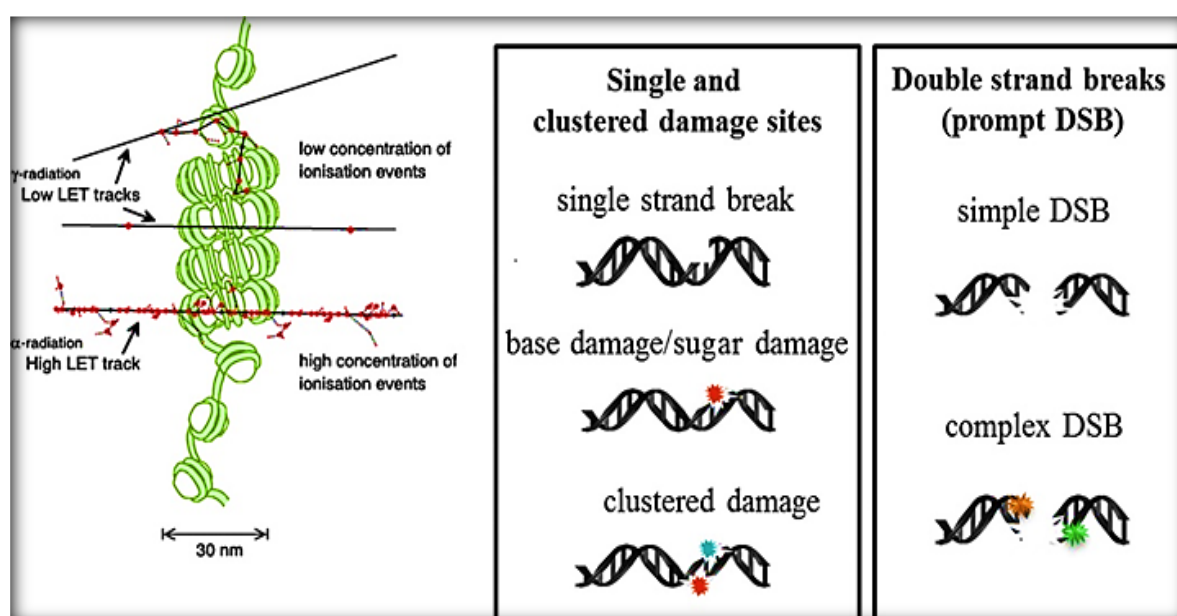
Although alpha and beta particles can lose its action when hindered by physical barriers such as a sheet of paper or an aluminum plate, X-rays and  $\gamma$ -rays are more powerful and have penetration ability. In addition, X-rays and  $\gamma$ -rays have been successfully developed for therapeutic purposes, as they can cause significant cellular damage (Devita Jr et al., 2012).

### **1.5.3 The physics of IR interaction with matter**

Linear Energy Transfer (LET) is the amount of energy transferred to matter (such as tissues) per unit length of the track of ionising radiation passing through it. When LET is utilised to indicate the dosimetry of ionising radiation in a biomedical context, LET is usually expressed in keV/ $\mu$ M (Emami et al., 1991; Maier et al., 2014). The rate at which energy is lost depends on the type and the energy of the radiation itself, as well as the density of material and these characteristics are described by the radiation's LET. According to the emitted particle and density energy power, ionising radiation can be broadly categorized to two groups: high LET and low LET radiation (as illustrated in Figure 1.4). The clustered damage sites, that include DSBs, are abundantly produced by high LET, such as alpha particles and neutrons (Eccles et al., 2011; Schipler and Iliakis, 2013). Meanwhile, X-rays or beta and  $\gamma$ -rays are ionising radiation with lower ionisation densities, thus of lower LET, cause less complex DNA damage (Nikjoo, et al, 1998).

Low LET radiations deposit tiny amounts of energy. In contrast, radiation particles (either electrons which are negatively charged, or protons, alpha rays, and other heavy ions which

are positively charged) deposit further energy on the targeted areas and causes more biological effects than the low LET radiations (Seiwert et al., 2007). Just as for lower-energy radiation, high-energy radiation damage genetic material of cells which, subsequently, can lead to blockage of their ability to divide and proliferate (Thariat et al., 2013). The ability of normal cells to repair damage, and so maintain their normal function, is at a faster rate in comparison to tumour cells. This is because cancer cells are not as efficient as normal cells in repairing damage caused, for instance by radiotherapy, due to loss of some repair function or efficacy (Begg et al., 2011).



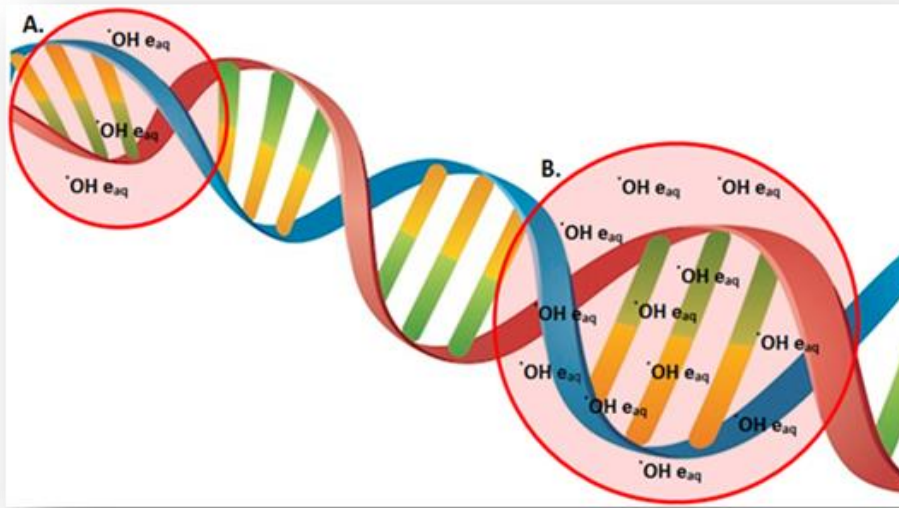
**Figure 1.4 Schematic diagram of simple and complex lesions that could be formed by the effect of a single radiation track.** Low LET radiation track induces lower concentrations of ionisation events, which produce fewer DNA damage sites than high LET tracks. The coloured stars represent base or sugar lesions (Lomax et al., 2013).

Features of sparsely ionising radiations (X-rays and  $\gamma$ -rays) and densely ionising radiations (charged particle radiation) can be estimated by LET. Sparsely ionising radiations (X-rays and  $\gamma$ -rays) are low-LET radiations, with an energy deposition range of 0.2 to 5keV/ $\mu$ m. Whereas, the densely ionising radiations (charged particle radiations) are high-LET radiation with an energy deposition range of 10-100keV/ $\mu$ m for neutrons, 100-200keV/ $\mu$ m for  $\alpha$ -particles and >1000keV/ $\mu$ m for heavy ions (Herskind and Wenz, 2014). When the effects of equal doses of diverse types of radiation are compared, they produce unequal biological effects. Hence, it is necessary to consider the biological effect of a radiation. The efficiency of different quality of IR can be expressed as relative biological effectiveness (RBE). RBE is defined as the ratio of a dose of photons to a dose of any other particle to produce the same biological effect. High LET radiation is characterised by a higher biological effectiveness compared to photons of low LET. Since high LET radiation is densely ionising, the DNA damage becomes more difficult to be repaired which can significantly increase efficiency of cell killing (Goodhead, 1999). High LET beams may have RBEs ranging from 1.5 to 3 (Jäkel, 2008), while the RBE values for low-LET radiations are close to 1. RBE values for one type of radiation may differ for various endpoints, and different cell types (Sørensen et al., 2011).

#### **1.5.4 DNA and ionising radiation: DNA is the key target to IR**

The biological response of IR exposure may become noticeable when molecules that regulate vital cell processes are changed or altered to eradicate or alter their function. DNA, cell membranes and proteins are all targets for ionising radiation. Yet, as already discussed, amongst all these alterations, DNA is the most important target for the biological effects of ionising radiation, because it contains the genetic materials that hold information for cell functioning and reproduction that are essential to cell survival (Domenech, 2017). The effects on these structures can be produced by direct damage causing ionisation of the biological molecule. On the other hand, the effects may act indirectly through free radicals resulting from the ionisation of molecules, notably water molecules, that surround the cell, leading to the formation of reactive oxygen and reactive nitrogen species (ROS and RNS, respectively) (Daly et al., 2007).

Radiation deposits energy in high energy, multiple ionisation events known as ‘spurs’ or ‘blobs’. Radiation spurs are the most frequent and main energy deposition event. These involve the generation of approximately three ion pairs, with a diameter of ~4nm that can be nearly twice the size of the double helix. Radiation blobs occur less frequently but are larger in energy and size. Radiation blobs include the production of up to twelve ion pairs and are ~7nm in diameter. Therefore, spurs and blobs events can deposit large amounts of energy within the DNA helical strands (as shown in Figure 1.5). Via both direct and indirect effects, damage will occur on the DNA strands notably as double strand breaks (DSB) which are key cytotoxic lesions and are considered responsible for cell death following ionising radiation exposure (Hall and Giaccia, 2006).



**Figure 1.5** Energy deposition ‘spur’ and ‘blob’ events produced by X-ray radiation (Hall and Giaccia, 2006).

## **1.5.5 The interaction of ionising radiation with cells**

### **1.5.5.1 The direct and indirect effects of ionising radiation on cells**

Ionising radiation generates free radicals in substantial numbers, due to the process of energy absorption and breakage of chemical bonds in molecules. The free radicals are molecules or parts of molecules which are characterised by having unpaired electrons and can promote high reactivity with other nearby molecules. Free radicals play a key role in radiation effects on biological tissues and organisms through a combination of direct and indirect actions of IR. Many biological changes take place due to interactions of free radicals with processes such as metabolism, oxidation, reduction, potentially leading to pathological diseases and cancer induction (Khaled and Held, 2012).

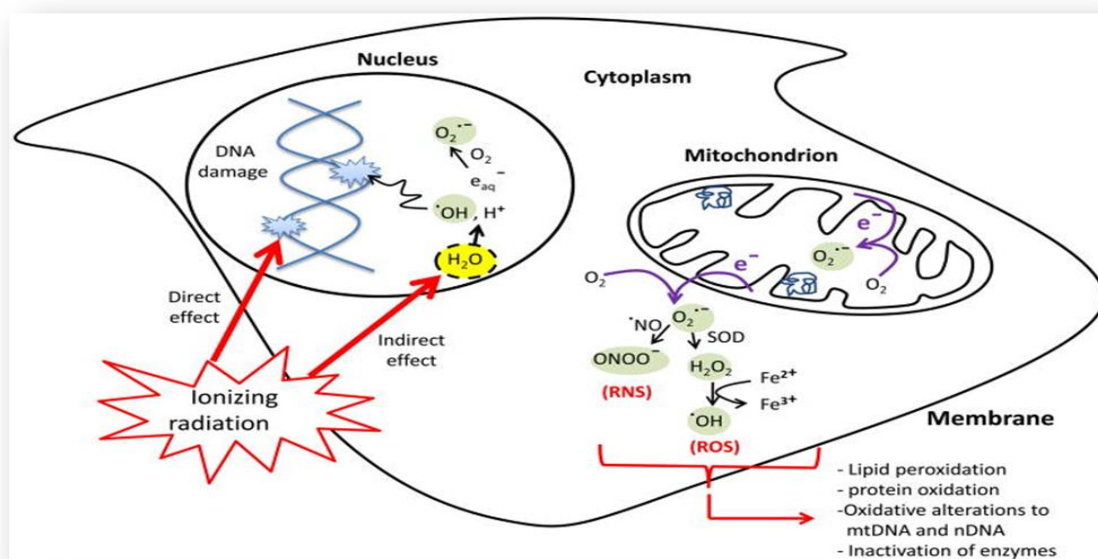
#### **● The direct interaction of IR on cells**

Radiation can act directly on biological molecules. IR may deposit energy in a DNA macromolecule and interact with atomic structures of the target molecule, thus, initiating a chain of events and disrupt the DNA molecular structure. Chemical bonds can be broken which can lead to unpaired electrons in atoms or molecules. This is called a direct action of radiation. This process predominates with high-LET radiations such as  $\alpha$ -particles and neutrons, and at high radiation doses. Accordingly, this process may interfere with the ability of the cell to replicate and, thus, hinder its life-sustaining system (Valentin, 2006; Lehnert, 2007).

#### **● The indirect interactions of IR on cells – (water radiolysis)**

Both electromagnetic radiation and particulate radiation can cause indirect effects to the atoms or molecules of target cells (Hall and Giaccia, 2006). The indirect effects of radiation occur when the radiation interacts with ‘off-target’ molecules, such as water molecules (the most abundant molecule in the cell) and produces free radicals such as reactive oxygen species (ROS). The radicals can then migrate to and be transferred to other nearby molecules. Indirectly induced free radicals, such as hydrogen atoms ( $H^\bullet$ ), hydrated electrons ( $e^-_{aq}$ ), superoxide radicals ( $O_2^{\bullet-}$ ), have unpaired electrons, and may have high chemical reactivity such as hydroxyl radical ( $OH^\bullet$ ) the most highly reactive of ROS free radical species (Cadet

et al., 2003a; Ward, 1988). The  $\text{OH}^\bullet$  may diffuse over distances to interact with DNA, proteins and enzymes to cause damage to these molecules and disrupt physiological processes. The total dose of ionising radiation specifies the number of free radicals (Valentin, 2006; Lehnert, 2007). The majority of radiation-induced damage in cells results from the indirect action mechanism, because water constitutes ~70% of the composition of cells (Saha, 2012). Ionising radiation may also interrupt mitochondrial functions through alterations to lipids, proteins, and mitochondrial DNA (mtDNA) (Azzam et al., 2012). Yet, internal cellular damage can occur also due to continuous generation of ROS that arise as a side effect of mitochondrial energy metabolism disruption and both ROS and reactive nitrogen species (RNS) formation by the stimulation of oxidases and nitric oxide synthases (Wardman, 2009). Remarkably, these oxidative alterations might remain functional for many days to several months after the first initial IR exposure (Kryston et al., 2011a). In conclusion, many of the biological and physiological alterations can result from direct and indirect actions, which also induce genetic and epigenetic changes in the macromolecules structure (Koturbash et al., 2008) (as illustrated in Figure 1.6).



**Figure 1.6** Direct and indirect cellular effects of ionising radiation on macromolecules (Azzam et al., 2012).

## **1.5.6 Radiation-induced DNA damage**

Accumulated evidence from radiological studies has shown that DNA is the critical target for the biologic impacts of ionising radiation.

### **1.5.6.1 Strand breaks**

Strand breaks are a most dangerous forms of damage, since they involve the loss of the integrity of the DNA structure itself. High energy ionising radiation can cause detrimental effects through the sugar phosphate backbone causing either DNA single strand breaks (SSBs) or DSBs (Price and D'Andrea, 2013).

- **DNA single strand breaks (SSBs)**

SSBs are one of the most common DNA lesions which occur following IR exposure. This forms as a discontinuity in one strand of the DNA double helix and is usually accompanied by loss of a single nucleotide, with damaged 5'- and/or 3'-termini at the site of the break due to an oxidative attack on the deoxyribose sugar. The radical attack initiates the rupture of the sugar unit, leading to the release of the attached nucleotide from the DNA molecule. This type of damage is very common and can easily be repaired. This type of damage can be produced *in vivo* at a rate estimated to be ~600 per hour, which is equivalent to that induced by radiation delivered at a dose rate of ~0.5cGy/min. Even though most of the SSBs are repaired by error-free mechanisms, still at least 1% of SSBs may avoid the repair process. SSBs are considered a major source of endogenous double strand breaks, because of their ability to collapse or stall replication forks (Polo and Jackson, 2011). Therefore, genetic instability may emerge if SSBs are not repaired. For instance, SSBs may be converted into DNA DSBs during DNA replication (Kuzminov, 2001) leading to chromosome aberrations (Carrano et al., 1986; Domínguez et al., 1998), and subsequently tumorigenesis may arise (Hanahan and Weinberg, 2000; Caldecott, 2008). However, the majority of SSBs induced by ionising radiation can be repaired by the four basic steps of base excision repair (BER) which include damage detection and base excision, endonuclease action and end processing, gap filling, and DNA ligation (Caldecott, 2001; Caldecott, 2007).

- **DNA Double strand breaks (DSBs)**

DNA DSBs are breaks in the phosphodiester backbone of both strands of the DNA separated by about  $\leq 10$  base pairs. Therefore, both strands of the double helix are completely broken, leaving no intact template strand to enable easy accurate repair. A DSB can be produced as a direct break of the two strands or can be formed from the interaction between two close single damages in opposite strands during repair. DSBs caused by ionising radiation are considered the most important lesions with respect to the induction of gene mutations and chromosomal aberrations. This is the result of DSBs potentially leading to the breakdown of chromosomes into fragments which may rejoin incorrectly. Subsequently, these processes can influence the integrity of DNA molecules and thus, modify cell functions or can be particularly lethal to cells (Rich et al., 2000; Ghardi et al., 2012; Kavanagh et al., 2013). DSBs can also be produced in cells because of natural biological processes including oxidative metabolisms, replication, meiosis, and production or formation of antibodies (Dahm-Daphi, 2000). In normal human cells, ~1% of endogenous SSBs lead to ~50 endogenous DSBs/cell per cell cycle, which is estimated to be approximately equal to that generated by 1.5 Gy of ionising radiation (Vilenchik and Knudson, 2003). However, DSBs can be repaired by two major DSB-repair pathways: non-homologous end joining (NHEJ) and homologous recombination repair (HRR) (Collis et al., 2005; Lieber, 2010).

### **1.5.6.2 Base lesions**

The vast majority of DNA damage from radiation involves chemical modification of the bases themselves. DNA molecules are subject to base loss, because of spontaneous reactions due to internal and external factors (Sancar et al., 2004; Alberts et al., 2008). Apurinic/apyrimidinic site (AP site), also known as an abasic site, is a location in the DNA molecule that presents neither a purine nor a pyrimidine base, although the sugar phosphate backbone remains intact with a hydroxyl group in the place of the nucleobase. Loss of DNA bases can be particularly mutagenic and, if left unrepaired, can inhibit transcription. Loss of pyrimidine bases (cytosine and thymine) occurs similarly to depurination, which is an alteration of DNA where the purine base (adenine or guanine) is removed from the deoxyribose sugar by hydrolysis of glycosidic bond between the base and the sugar but this



noticeably occurs at low rates. A damaged nucleotide can mistakenly interact with another neighbouring nucleotide, and different situations can cause base lesion (Sancar et al., 2004).

### **1.5.7 The isolated DNA lesions and/or clustered DNA lesions**

Many cytotoxic and mutagenic effects (gene mutation and chromosome aberration) can occur following the induction of radiation-induced DNA lesions; these lesions can initiate cellular transformation, carcinogenesis, and can end with cell death. IR generates a wide variety of DNA damage which can either be isolated DNA lesions and/or clustered DNA lesions. The latter types of lesions are also known as locally multiply damaged sites (LMDS) (Ward, 1994), or, non-DSB oxidative clustered DNA lesions (OCDL) (Sutherland et al., 2000; Georgakilas, 2008). The isolated DNA damages include single strand breaks (SSBs), DNA bases lesions and abasic sites. These isolated lesions can normally be repaired without adverse biological consequences (Ward, 1994); (Sutherland et al., 2000). However, clustered DNA damages appear when two or more lesions occur in both DNA strands. For instance, two base damages (BD) or one BD and the presence of a SSB in opposite strands, or the formation of strand breaks in opposite DNA strands resulting in a double strand break (DSB) (Goodhead, 1994; Purkayastha et al., 2007).

Also, DSBs can be formed when OCDL interferes with DNA function, such as replication and transcription (illustrated in Figure 1.5) (Dickey et al., 2009; Sedelnikova et al., 2010). Amongst the various types of DNA damage induced by ionising radiation, DSBs are crucial lesions as they are responsible of the radiogenic cell death (Ward, 1988). Complex lesions are more difficult to be repaired than isolated DNA lesions (Ward, 1981; Harrison et al., 1999; Georgakilas et al., 2002; Georgakilas, 2008). The persistence of unrepaired or mis-repaired DNA damages, which result from both accumulated DSBs and OCDL, are lethal to cells and can lead to cytotoxicity, genome instability, chromosomal abnormalities, carcinogenesis, and apoptosis (Jeggo and Löbrich, 2007; McKinnon and Caldecott, 2007; Jackson and Bartek, 2009a).

#### **1.5.7.1 Single lesions**

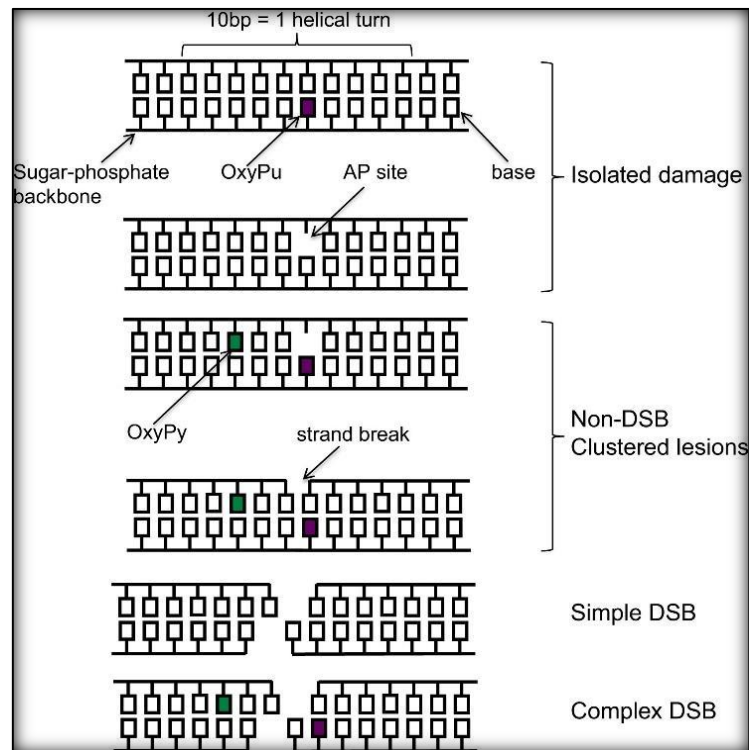
The single lesions can be induced by exogenous and endogenous factors. The predominant single lesions are base lesions such as oxidised purines or pyrimidines and AP sites (apurinic

or apyrimidinic), and sugar modifications. When phosphodiester bond between the sugars is broken, a single-strand break is formed.

### **1.5.7.2 Clustered lesions**

Clustered damage sites contain two or more lesions within the DNA helices by passage of a single radiation track (Ward, 1981; Goodhead, 1994). This could be bi-stranded (lesions on both strands of the DNA helix), or tandem (two or more lesions adjacent on the same strand of DNA) (Nikjoo et al., 2001). Clustered damage is made up of double strand breaks (DSB) with associated base lesions or abasic (AP) sites, and non-DSB clusters are comprised of base lesions, AP sites, and single strand breaks (Georgakilas, 2008).

Clustered lesions are estimated to be 50–80% of the total complex DNA damage that are produced by ionising radiation (Ward, 1994; Sutherland et al., 2002). An increase in radiation LET can increase the number of clustered/complex DNA lesions which reflects the increased of clustering of energy deposition lesions. For instance, in high-LET radiation (densely ionising radiation), ~90% of the energy deposited can produce clustered damage with greater complexity. Whereas, for low LET radiation, ~30% of the energy deposited induces clustered damage sites of varying structural and chemical complexity (Semenenko and Stewart, 2004). Consequently, clustered DNA lesions are more difficult to repair, and these lesions can produce cytotoxic and mutagenic effects (Georgakilas et al., 2004; Malyarchuk et al., 2004) as well as chromosomal instability that can be lethal to cells (Suzuki et al., 2003). Subsequently, clustered DNA lesions are considered as highly non-repairable damages, or incorrectly repaired DNA lesions (Lindahl and Wood, 1999) that lead to significant biological lesions (Goodhead, 1994; Dianov et al., 2001) that contributes more effectively in tumour cells killing by ionising radiation (as show in Figure 1.7).



**Figure 1.7 DSB and non-DSB clustered DNA damage.** DSB can be simple or more complex with associated base lesions and AP sites. Non-DSB clustered damaged is defined as two or more lesions within one or two helical turns of DNA (Sage and Shikazono, 2017).

## 1.6 Cellular response

To limit genomic instability, cells are equipped with DNA damage response (DDR) pathways and DNA repair mechanisms to remove and/or tolerate DNA lesions (Hoeijmakers, 2001; Roos et al., 2016). A complicated network of signalling pathways and repair mechanisms have evolved to enable the mammalian cells to cope with a variety of DNA lesions to protect genomic stability. In humans, at least 130 genes are implicated in DNA repair process (Wood et al., 2001).

The response to DNA damage is carefully regulated, often specific to the type of damage incurred. Thus, DNA repair pathways can be categorized into six crucial categories which are

dependent upon the form and location of damage: (1) direct repair, (2) base excision repair (BER), (3) nucleotide excision repair (NER), (4) mismatch repair (MMR), (5) the double-strand break (DSB) repair: non-homologous end-joining (NHEJ) and homology recombination repair (HRR), and (6) inter-strand crosslink repair (Kohn and Bohr, 2002; Sancar et al., 2004; Hoeijmakers, 2009; Tornaletti, 2009; Shimizu et al., 2014; Fontes et al., 2015; Uryga et al., 2016).

## **1.6.1 The DNA damage response and DNA repair pathways**

### **1.6.1.1 DNA damage signaling induction**

A variety of powerful and complex repair and signaling mechanisms have evolved within cells to preserve the genetic integrity of DNA following damage induction (Gauthier and Bechhoefer, 2009). When damage occurs within the DNA molecule, eukaryotic cells cope with the damage by initially detecting the DNA damage via sensor proteins, which bind to DNA randomly and then translocate to the damage site (Halford and Marko, 2004). However, due to the DNA helical structure, it becomes easier to distinguish between the damage and undamaged DNA by the use of several steps of DNA damage recognition (Sancar et al., 2004; David, 2005). Consequently, the cells attempt to focus their own activity towards the lesions in such a way to repair the damage or reduce its effects. The progression in the cell-cycle is usually delayed until the DNA repair process is complete. The cell signaling pathway is a key response to DNA damage detection. This step includes the activation of a specific cell-cycle control systems which can slow down, delay, arrest and/or stop the cell-cycle.

### **1.6.1.2 DNA damage checkpoint induction**

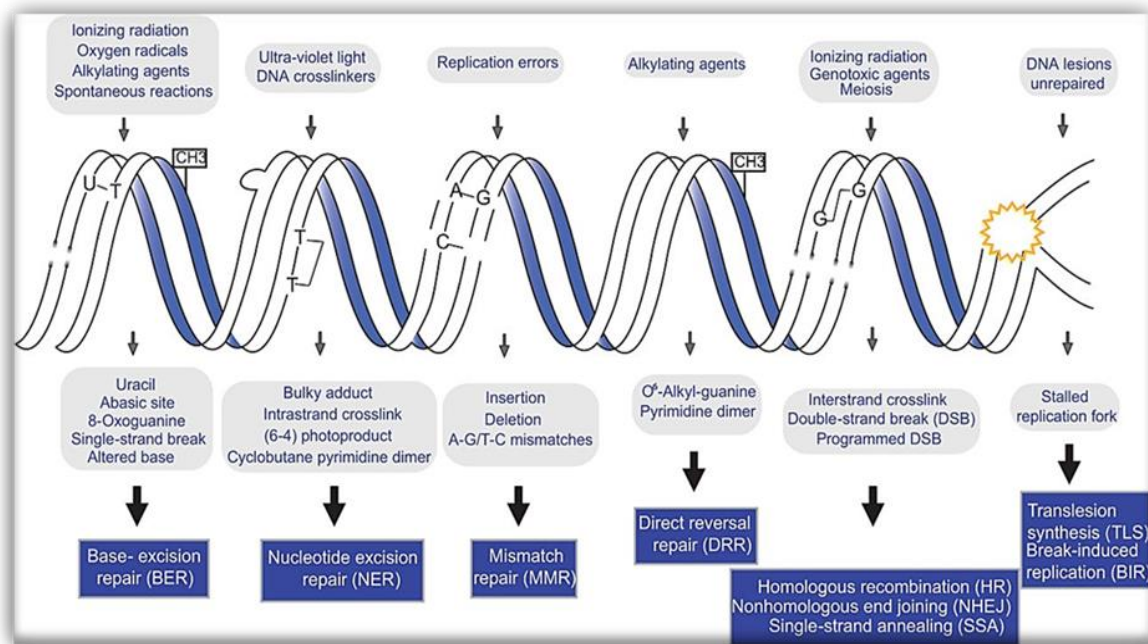
The cell works to eliminate or cope with the acquired DNA damage through activation of DNA damage checkpoints, which arrest or halt cell-cycle progression while repair mechanisms, transcriptional modulation, and/or apoptotic pathways are activated (Sancar et al., 2004). These checkpoints are biochemical pathways that help maintain the genetic information by monitoring cell-cycle events by mediating cascades of phosphorylation

events that alter the activity, stability, or localisation of many proteins, until DNA damage is repaired. The proteins involved in the DNA damage checkpoint responses are the same as those responsible for the normal progression of the cell-cycle. The DNA damage checkpoints employ damage sensor proteins that detect DNA damage and/or chromatin alterations that occur after damage induction. These then initiate the signal that's transmitted by transducer proteins, which are usually kinases that increase the damage signal. Additionally, the signal transducers activate or inactivate other proteins, the effectors which directly participate in inhibiting the cell-cycle progression (Ciccia and Elledge, 2010). Additional types of DNA damage response (DDR) proteins are the mediators, which promote interaction between the other proteins. The DDR is regulated by the phosphoinositide three-kinase-related protein kinases (PIKK) which are central to the entire DNA damage response, specifically for the radiation-induced damage, especially DSBs. The PIKK is responsible for initiating the presence of DNA damage proteins which include: ATM (Ataxia Telangiectasia Mutated), ATR (Ataxia Telangiectasia and Rad3-related protein) and DNA-PKcs (the DNA-dependent protein kinase complex DNA-PK). The signal that activates ATM and DNA-PKcs is a double strand break, whilst ATR responds to single-stranded DNA gaps. All three kinases are recruited to the DNA lesion site, which promotes kinase activation. These PIKK phosphorylate hundreds of proteins that maintain genome integrity through regulation of cell-cycle progression, DNA repair, apoptosis, and cellular senescence (Lovejoy and Cortez, 2009).

Additionally, the p53 tumour suppressor protein is a multi-functional transcription factor that regulates cellular processes affecting proliferation of the cell-cycle checkpoints and triggers apoptotic pathways. The damage of DNA caused by mutagens, like radiation, induces the synthesis of the p53 protein which initiates the repair process or brings the cell to death if the damage cannot be repaired. Most DNA damage is removed by DNA repair enzymes, but these repair processes are not completely efficient. The reason for this is that if the level of DNA damage is high the lesions may not all be repaired. In such a circumstance, a cell may take the path of programmed cell death, thereby preventing propagation of the DNA lesion and potential mutagenesis (Galluzzi et al., 2015)

### **1.6.1.3 DNA damage repair pathways**

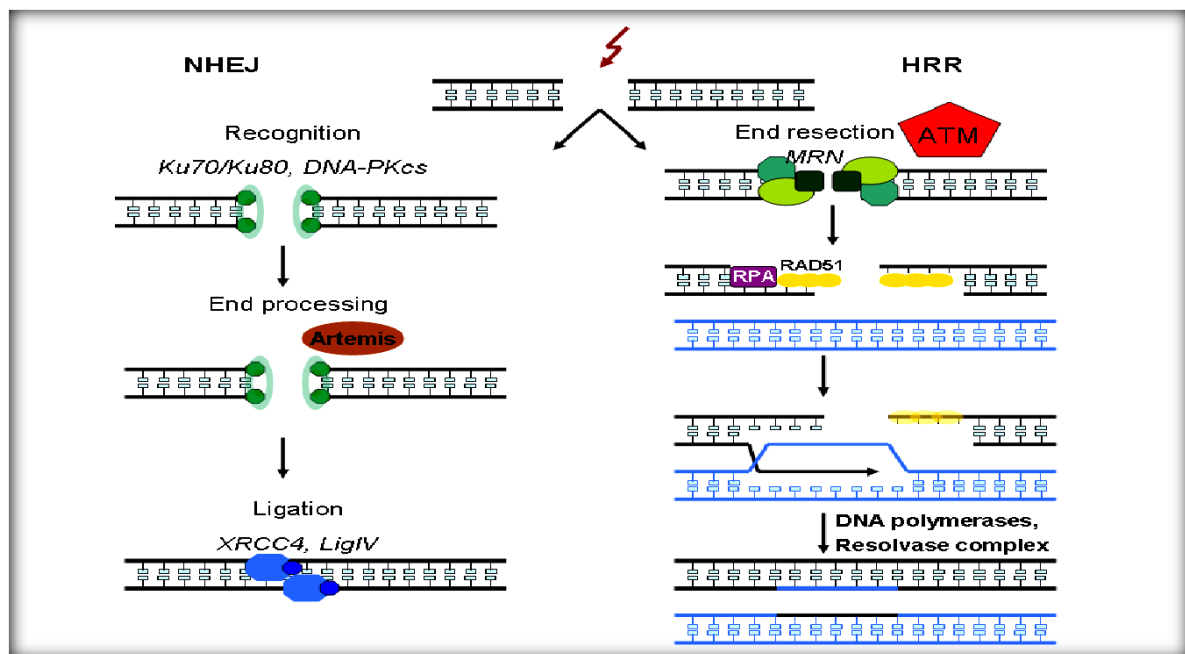
Ionising radiation may be considered as a ‘two-edged sword’, because it can lead to genetic modifications in exposed, surviving normal cells or tissue. Still, radiation is able to damage the clonogenic survival of tumour cells or tissues, which can primarily deliver an essential benefit after radiotherapy. Ionising radiation exposure leads to damaging the DNA of exposed tumour tissue, which gives rise to cell death (Lomax et al., 2013). However, when DNA damages occur, DNA repair mechanism is a vital protective process that can block the entry of cells into carcinogenesis, and maintain genomic integrity (Bernstein et al., 2013). According to the type of DNA damage, cells may upregulate specific DNA repair pathways to preserve a cells’ genomic information. For instance, BER pathway can restore the minor changes to DNA such as oxidised or alkylated bases, small base adducts, and SSBs (Barnes and Lindahl, 2004; Caldecott, 2007). BER repairs DNA damage that is therapeutically induced by ionising radiation and DNA methylating agents (Plo et al., 2003). The main components of this repair pathway are glycosylases, endonucleases, DNA polymerases and DNA ligases, and Poly adenosine diphosphate ribose (PAR) polymerase (PARP) which facilitates the repair of SSBs process. The more complicated lesions, such as DNA helix-distorting base lesions like those produce by UV light, are repaired by the NER pathway (Hoeijmakers, 2009). The NER mechanism can recognize and repair base lesions which are associated with distortion of the DNA helical structure. NER is able to remove helix distorting adducts on DNA and promote the repair of both intrastrand and interstrand crosslinks (ICLs). Covalent links between the two strands of the double helix represent a type of DNA damage referred to as interstrand crosslinks (ICLs) (Deans and West, 2011). ICL repair is complex and involves the cooperation of several repair pathways, such as NER, translesion synthesis (TLS), and homologous recombination (HR) (Schärer, 2005). The xeroderma pigmentosum (XP) proteins and excision repair cross-complementation group 1 (ERCC1) also have essential roles in both the NER and ICL repair pathways (Naegeli and Sugawara, 2011). Another type of damage disturbing the helical structure of DNA are base mismatches. The MMR mechanism recognises, and repairs errors introduced during DNA replication. Furthermore, MMR also recognises and repairs insertion/deletion loops (IDLs), particularly within microsatellite DNA (Jiricny, 2006; Iorns et al., 2009; Sourisseau et al., 2010) (as shown in Figure 1.8).



**Figure 1.8 DNA damage and DNA repair pathways.** The DNA backbone can be affected by endogenous or exogenous factors (for instance, ionising radiation, alkylating agents, or oxygen radicals), leading to the activation and undertaking of specific of DNA repair pathways (Genois et al., 2014).

DNA DSBs are the one of the most widely investigated DNA damages, as these are a complex form of damage. DSBs are the most critical type of IR-induced DNA lesion; associated not only with cell death, but also with the induction of mutations and with carcinogenesis. Nevertheless, besides IR, several chemical and physical cytotoxic agents can generate DSBs, as well as during the normal life cycle of the cell, particularly during DNA replication or in meiosis (Baudat and de Massy, 2007; Longhese et al., 2009). Therefore, the two important mechanisms for DNA DSBs repair in mammalian cells have been described: NHEJ and HR. For both NHEJ and HR, the initial DNA damage response and DNA repair proteins may overlap; indeed, several proteins are distinguished to be involved in both DSB repair pathways: BRCA1, H2AX, PARP-1, Rad18, DNA-PKcs, Mre11, and ATM. Yet, NHEJ factors are recruited to DSB faster than HR factors. NHEJ and HR factors are independently recruited to DSB repair (Kim et al., 2005). However, there is a specific period when NHEJ and HR factors are present at DSB damage sites. Additionally, one or more proteins involved in both repair pathways can regulate and choose either of the repair

pathways (Shrivastav et al., 2008). Still, the NHEJ pathway operates throughout the entire cell cycle (Rothkamm et al., 2003). However, this DSB-repair pathway is more error prone, and may lead to mutations and even cell death (Lieber, 2010). NHEJ involves the binding of Ku heterodimers to the two ends of a DSB that in turn recruits DNA-PK (DNA-dependent protein kinase), Artemis nuclease, and X-ray repair cross-complementing protein XRCC4-DNA ligase IV complex, which then ligate the two duplex termini (Drouet et al., 2005; Gu et al., 2007). On the other hand, HR is activated during the S- and G2-phases of the cell cycle. This DSB-repair pathway is regarded as error free, since HR uses an undamaged homologous sister chromatid as a template (Chapman et al., 2012). HR involves the 5' to 3' resection of the DNA strands from the site of the DSB and strand invasion into the homologous chromosome. Homologous recombination in eukaryotes is carried out by the RAD52 group genes (Rad50, Rad51, Rad52, Rad54, Rdh54/Tid1, Rad55, Rad57, Rad59, Mre11, and Xrs2). Nevertheless, depending on the process, a Holliday junction may then be generated, followed by branch migration, resolution of the Holliday junction, and finally ligation (Compton et al., 2010), (as displayed in Figure 1.9).



**Figure 1.9** Simplified models of DSB-repair by NHEJ and HRR (Bajinskis, 2012).



## **1.7 DNA damage measure as markers of RT treatment efficacy**

The assessment of DNA damage has an essential role in understanding cancer causation and treatment. Moreover, many therapeutic treatments achieve their anticancer by creating cytotoxic DNA lesions. For instance, the impacts of radiotherapy and other cancer therapies cause single- and double-strand breaks, DNA interstrand crosslinks (ICLs – a particularly toxic form of DNA damage), replication lesions, and base damage. These forms of DNA damage can inhibit cancer cell replication and induce cell death. Thus, if cancer cells can repair the therapeutic-induced damage, this can make the cancerous cells insensitive to these therapeutic agents. Accordingly, the measurement of DNA damage and repair should be performed by characterising key molecules and mediators in the biological structure that play a pivotal role in determining cancer cell sensitivity to DNA damage inducing agents (Nikitaki et al., 2015); therefore, the measurement of DNA damage is central to the study of cancer (both formation and treatment). different strategies are employed for the purpose of detecting and quantifying DNA damage in cells. The direct methods depend on analytical chemistry and require extraction and digestion of DNA, which is then followed by measurement of specific DNA lesions at the nucleotide, nucleoside or base level (Ravanat, 2012). Chromatographic methods, such as high-performance liquid chromatography (HPLC), are used to separate the hydrolysed products, and a specific detection method is used to detect and quantify the lesions such as electrochemical detection (ECD) (Floyd et al., 1984). Other analogous protocols include gas chromatography coupled to mass spectrometry (GC-MS) (Dizdaroglu, 1984) or HPLC coupled to tandem mass spectrometry (HPLC-MS/MS) (Ravanat, 2012). Another direct method of detection of DNA strand breaks is the Comet assay which involves the detection of strand breakages and the electrophoretic approach such as the pulse field gel electrophoresis (PFGE) assay for measurement of DSBs (Hada and Georgakilas, 2008).

Indirect methods are also used, which involves the measurement of the downstream consequences of DNA strand breaks. First attempts have been made by using specific antibodies that react against specific types of proteins belonging to DNA damage response (DDR) mechanisms that allow for the detection of DNA repair foci which correlates to DNA lesions. Additionally, many biological lesions, such as chromosomal aberrations, can also be used to evaluate DNA damages. Other indirect methods are the immunostaining assay such

as  $\gamma$ -H2AX immunofluorescence assay for measuring DNA DSBs (Li et al., 2013), and “DNA staining” methods that were adapted recently for assessing DNA damage such as immunohistochemistry (IHC), immunocytochemistry (ICC), immunofluorescence (IF), flow cytometry, ELISA, and Western Blotting. These techniques utilise a required antibody to detect the presence of a specific protein for detection of DSBs or OCDLs.

## **1.8 Overview of methods to assess DNA damage in this study**

### **1.8.1 Alkaline Comet assay for the assessment of radiation-induced DNA damage**

The Comet assay is a sensitive microscopy-based method to measure DNA strand breaks in eukaryotic cells without extracting the DNA. The alkaline version of the comet assay (alkaline Comet assay; ACA) is a highly sensitive method for the assessment of single-strand breaks (SSBs) and alkali labile sites (ALSs), and can detect levels of damage induced by clinically relevant doses of radiation (Ward, 1988; Singh, 1996; Azqueta et al., 2009; Collins, 2009). The basic principle of ACA is dependent upon the preparation of a specific number of cells which embedded in a thin gel of low melting point agarose (LMP) on a microscope slide. The prepared cells are then subject to lysis to remove both the plasma and nuclear membranes and the nucleosomes, leaving nucleoid bodies composed of negatively supercoiled loops of DNA attached to lysis-resistant nuclear matrix scaffolding proteins. Following lysis, the agarose-embedded nucleoids slides are then subject to alkaline unwinding, which denatures any broken DNA, followed by electrophoresis in the same buffer for a short duration using a low voltage which causes the broken loops that have lost their supercoiling to migrate towards the anode (Collins, 2002). The broken, relaxed, denatured DNA can migrate away from undamaged supercoiled DNA leading to the formation of the structures resembling a ‘comets’ (as depicted in Figure 1.10), in which the ‘head’ consists of the nucleoid body containing intact DNA and the ‘tail’ consists of the damaged DNA. The level of DNA damage induced is assessed by the extent of comet tail formation. The intensity of the comet tail (consisting of the broken damaged DNA) reflects the amount of DNA strand breaks present in the DNA of each cell (Olive, 1999). After electrophoresis, the samples are neutralised and stained with a DNA binding fluorescent dye (typically propidium iodide (PI) or ethidium bromide (EtBr)) to allow comet visualisation, and this allows for image analysis and quantification of strand break damage levels which is observed by fluorescence microscopy. The comets are analysed to measure a variety of densitometric and geometric comet parameters using fluorescence microscopy plus image analysis software packages specifically designed to interrogate comet images, and to determine DNA damage parameters of individual cells in a sample population. Presently, different software packages are used for measurement of comet parameters on the basis of

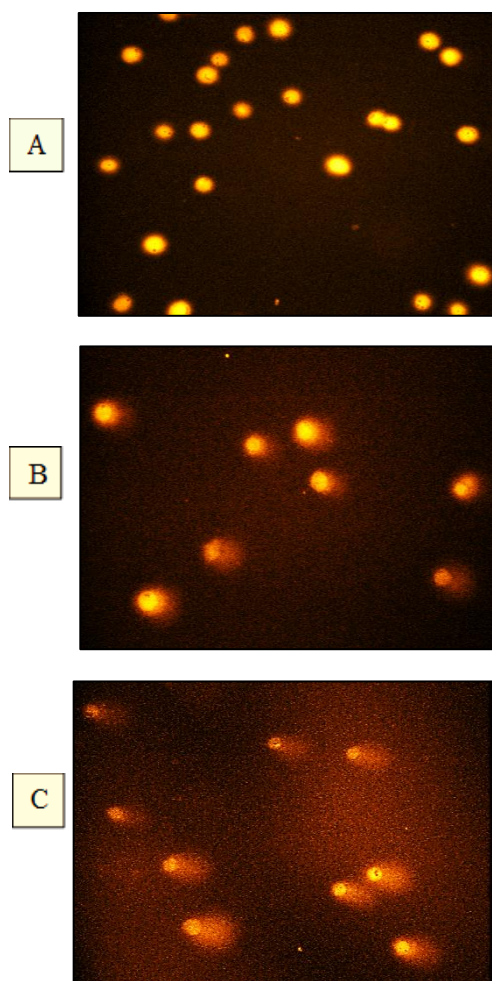
image analysis. Although these software packages may differ slightly the way they calculate DNA damage, the underlying principles of image analysis are the same (Vilhar 2004; <http://www.botanika.biologija.org/exp/comet/Comet-principles>).

Singh et al. (1988) amplified ACA making this assay dependent upon the length of DNA migration (define as Tail Length) to determine how far the DNA has migrated out of the cell to quantify the extent of damage (Kumaravel and Jha, 2006). However, TL can probably be affected by changes in the threshold settings which are utilised for image analysis. Consequently, it is not easy to compare results inter-laboratories. Tail extent moment (TEM) is a parameter that takes into account tail length and tail intensity, thus, it can undergo the same limitations Olive *et al.* (1990) defined Olive tail moment as the product of the percentage DNA in the comet tail and the distance between the centres of gravity (CG) for DNA in the head and tail of the comet. This parameter is helpful in describing heterogeneity within a cell, as OTM accounts for variations in DNA distribution within the tail (Olive et al., 1990). The percentage of DNA in tail (% TD) is linearly related to strand break frequency over a wide range of damage levels. %TD is recommended as the best descriptor for DNA break occurrences, as it is independent from threshold settings and gives a clear indication of the appearance of the comet which is referred to as the extent of damage which can easily be visualized (Langie et al., 2015) so the results are easily interpreted by researchers in different laboratories. A potential drawback of using % TD as a measure of DNA damage is the fact that it assumes that the staining efficiency of the fluorescent dye is the same for migrated (*i.e.* damaged) and non-migrated (*i.e.* intact) DNA. Still, it is important to note that the same parameters (e.g., tail moment) may be calculated differently among image analysis systems (Speit and Hartmann, 2006).

Kumaravel and Jha (2006) defined the most reliable comet measurements that would truly reflect the extent of DNA damage induced by low linear energy transfer ionising radiation. As DNA damage produced is directly proportional to the radiation dose, any change in dose should be reflected in proportional change in the comet measurements. Further retrospective analysis from in vitro and in vivo experiments using chemicals also suggested that OTM and % TD gave good correlations with the dose of genotoxic agents used and were the most reliable comet measurements. They recommended that, for scientific purposes, both OTM and % Tail DNA could be used.

Comet assay is being a very popular choice to determine DNA damage. Therefore, it is being implicated in translational research to assess whether tumour radiosensitivity (Fisher et al., 2007) and chemo-sensitivity (Smith et al., 2007) can be determined. This would allow clinicians to individualise patient management, allocating cancer therapy to those for whom it will be of most benefit and reducing the likelihood of patients receiving toxic (and as such ineffective) therapy. This assay has also been used to show protective effects of different dietary factors in chemo-preventive studies (Bichler et al., 2007; Collins et al., 2001a, b). In combination with the fluorescence in situ hybridisation (FISH) technique (Comet-FISH), the application of this assay has also been extended to determine sequence or gene-specific damage and repair (McKenna et al., 2003) as well as of possible diagnostic use (Kumaravel and Bristow, 2005; Kumaravel et al., 2009).

For this study, four parameters have used (%TD, TEM, OTM, and TL) to identify the best parameter to assess bladder cancer cells radiosensitivity and to distinguish between the radiosensitive and radioresistant bladder cancer cells during IR exposure.



**Figure 1.10 Example of ‘comets’ as seen using comet 5.5 software.**

A. When there is little or no DNA damage.

B. The intermediate DNA damage: the tail of the comet becomes brighter as more damaged DNA is released from the head.

C. High DNA damage the tail becomes brighter as more DNA is released from the head.

### **1.8.2 Liquid chromatography mass spectrometry LC-MS/MS, an overview of mass spectrometry (LC-MS) instrumentation employed in the analysis of DNA modifications**

The liquid chromatography mass spectrometry systems can be used to separate DNA adducts (modified nucleosides, nucleotides, nucleobases, and oligonucleotides) directly from unmodified nucleosides or nucleobases, and other components of biological samples. This type of separation is vital for detection by mass spectrometry. Because of the high complexity of the biological samples, the analyte ions need to be detached and separated from the bulk of sample matrix for detection of DNA adducts levels. Hence, this process is completed by combining chromatography to mass spectrometry. LC-MS has become the preferred

approach for DNA adduct analysis. In mass spectrometers methodology, the analyte ions and any fragment ions which can be produced during the ionisation step are separated according to their mass to charge ( $m/z$ ) ratios, providing a selective process of detection of specific molecular species. Furthermore, specificity can be provided by monitoring the intact ions and mass fragment through using tandem mass spectrometry (Grebe and Singh, 2011a).

The LC-MS makes use of electrospray ionisation (ESI). Electrospray ionisation enables the direct ionisation of the analyte ions from aqueous solutions at atmospheric pressure. Consequently, the coupling of LC with MS techniques can increase the capability of MS, and develop innovative technologies for DNA modifications analysis (Tretyakova et al., 2013). Modern approaches of LC/MS have been utilised such as the column switching and nanospray operation which are able to increase the specificity of MS analyses during the detection of DNA adducts. Additionally, the utilisation of tandem MS and stable isotope internal standards can lead to an accurate usage of the LC-MS/MS which can be utilised with many biological molecules (Pitt, 2009b).

### **1.8.3 Pulsed field gel electrophoresis (PFGE) assay for evaluation of radiation-induced DNA damage**

Pulsed field gel electrophoresis (PFGE) is one of the methods that is utilised to measure DNA DSBs. PFGE is a technique for the fractionation of high-molecular-weight DNA ranging from 10kb to 10Mb by electrophoresis in agarose gel with an electric field that alternates (pulsates) in at least two directions. This technology plays a key role in modern genomics, as it allows manipulations with DNA of whole chromosomes or their large fragments (Nassonova, 2008).

The basic principal of this assay is based on cancer cells exposed to different radiation doses treated which can generate large DNA fragments that cannot be separated by usual electrophoresis. Regarding DNA preparation, intact cell populations are embedded in agarose plugs where cells are enzymatically lysed and cellular proteins digested. The agarose plugs containing the digested DNA are then submitted to PFGE, and analysed for migratory DNA using pulsed-field gel electrophoresis with ethidium bromide staining. The basis for

PFGE separation is the size-dependent time-associated reorientation of DNA migration achieved by periodic switching of the electric field in different directions. The DNA fragments will form a distinctive pattern of bands in the gel, which can be analysed visually and electronically (Goering, 2010).

#### **1.8.4 $\gamma$ -H2AX immunoassay for assessment of radiation-induced DNA damage**

The  $\gamma$ -H2AX assay is a sensitive method used to distinguish the DNA damage levels in comparison to the Comet assay (Ismail et al., 2007). The  $\gamma$ -H2AX formation takes place during the repair of DSBs (Scully and Xie, 2013), and the  $\gamma$ -H2AX assay is readily able to detect DSBs induced by ionising radiation (Kuo and Yang, 2008). Indeed, chromosomal DSBs produces a significant response of adjusting chromatin, which is characterised by phosphorylation of histone H2AX on serine 139 of its C-terminal tail by DNA kinases such as ATM, ATR, and DNA-PK to create “ $\gamma$ -H2AX” (Mah et al., 2010). The phosphorylation occurs at the site of DNA damage as it surrounds the unrepaired DNA DSBs and involves a remarkable number of histone modifications that can be visualised microscopically as spots following immunostaining (Stiff et al., 2004). In the present study,  $\gamma$ -H2AX assay was used to focus on the damage and repair that took place post-ionising radiation exposure.

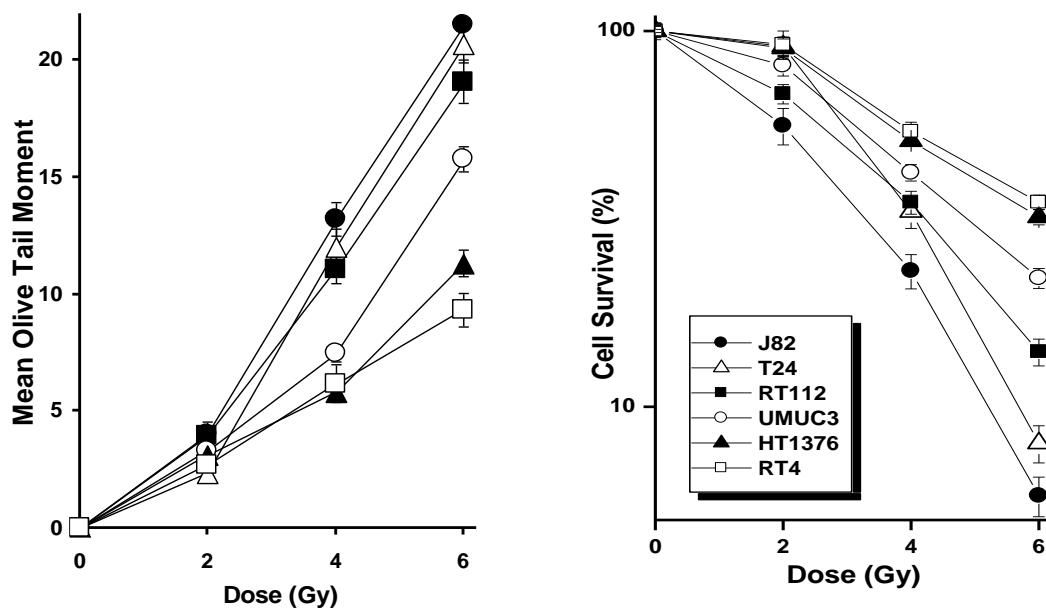
### **1.9 Comet formation – the two models**

Four cells lines of TCC were used in this study (UMUC3, RT112, J82 and RT4), and were exposed to ionising radiation over a dose range of 0-10 Gy. Although many studies have used the Comet assay to measure radiation induced DNA damage and repair, there are only very few that have used ACA to compare several tumour cell lines of the same tissue origin. There are differences in the DNA conformation and sensitivity to radiation in cells of different origins (McKeown et al., 2003). Therefore, to avoid this problem, the four cancer cell lines that have used in this project were taken from bladder cancer cells.

Methods for improving and predicting radiosensitivity in muscle-invasive bladder cancer have been reviewed (Colquhoun et al., 2003). A key factor known to influence tumour response to radiation is inherent tumour cell radiosensitivity (West, 1995; West et al., 1997; Bjork-Eriksson et al., 2000). A mechanism proposed to account for differences in inherent



radiosensitivity between cells centres on variation in the extent of DNA damage formation and repair following irradiation. Previously, using 6 bladder TCC cell lines (RT112, UMUC3, HT1376, J82, T24, and RT4), results have shown a strong, direct correlation between clonogenic cell death and radiation-induced DNA damage as assessed by the ACA, with a greater ACA response being noted in radiosensitive cells. The studied cell lines exhibit a range of radiogenic sensitivities, with J82 being the most sensitive to radiation-induced cell killing, and RT4 and HT1376 being the most resistant. Therefore, the rank order for initial comet formation matches the rank order of cell killing for all six cell lines (J82 > T24 > RT112 > UMUC3 > HT1376 > RT4). For that reason, the ACA is a good measure of bladder cancer radiosensitivity *in vitro* (Moneef et al., 2003) with the more radiosensitive bladder cancer cells showing a greater ACA response (as shown in Figure 1.11). The induction and repair of radiation-induced DNA damage, as measured by ACA, correlates bladder cancer cell radiosensitivity *in vitro* with the extent of comet formation strongly correlating with cell killing (Moneef et al., 2003; McKeown et al., 2003). Furthermore, cells from human bladder tumour biopsies reveal a wide range of ACA responses (Moneef et al., 2003; Bowman et al., 2010). Further studies showed similar trends for chemosensitivity, with greater ACA measures of cisplatin and MMC-induced crosslinks correlating with higher bladder cancer cell chemosensitivity as assessed by both clonogenic and MTT assays (Bowman et al., 2010). These studies indicate that ACA to be a good predictive measure of bladder cancer cell radiosensitivity at clinically relevant doses, with potential clinical application. It is a sensitive method that is used for measurement of radiation-induced DNA damage at the level of single cells (Singh et al., 1988; Tice et al., 2000; Collins, 2004). Therefore, the effect of ionising radiation that induces DNA damage could be measured by the ACA (Olive, 1999). Taken together these studies indicate that the nuclear DNA's sensitivity towards induced damage is a key factor in determining bladder cancer cell sensitivity towards radiation and genotoxic chemotherapy.



**Figure 1.11** Comet formation and cell's survival rate in six bladder cancer cell lines as determined by the ACA and clonogenic assay (Moneef et al., 2003).

It is proposed that the features retained in the nucleoid body could be responsible for the differential extent of comet formation. This could be the result of possible variances in the composition of the nucleoids between the radioresistant and radiosensitive cell lines which, in turn, could provide targets to improve bladder cancer cell radiosensitivity (Bowman et al., 2014). Indeed, the differential measures of comet formation may reflect actual differences in damage formation or may possibly be due to the nature of the anchoring of the DNA loops onto the nuclear matrix through specific scaffold/matrix attachment regions (S/MARs) (Pienta and Coffey, 1984). MARs have important roles in chromatin loops arrangements, enhancing gene expression, and assisting in DNA replication (Gluch et al., 2008). 'Weak' MARs would allow for the further release of adjacent DNA loops due to the effect of radiation induced strand breaks, which may lead to a higher degree of comet formation, or a 'tail' following irradiation (Bowman et al., 2014). Thus, different alterations in MAR function could affect the DNA loop attachment regions (Getzenberg et al., 1996). Therefore, two different theories can be put forward in relation to the reason for the differential measures

of comet formation noted between the bladder cancer cell lines. The first theory is that the comet formation reflects actual differences in DNA damage formation between the radioresistant and radiosensitive cell lines with the radiosensitive cells being more damage sensitive and the radiation resistant cells more damage resistant. The second theory is that extent of the comet formation is simply due to the additional release of DNA sequences/loops from the comet head to the tail, for the same level of DNA damage, with weaker MARs causing the further release of adjacent due to the effect of radiation induced strand breaks.

ACA results were then compared with other techniques to assess bladder cancer cells' damage sensitivity in this study such as LC-MS/MS, PFGE and  $\gamma$ -H2AX. The same differential response being noted between Comet and the alternate damage assays would strongly suggest that any differential response being noted with the comet is truly reflective of differential damage between the cell lines. In contrast, a similar response noted for the cell lines with the alternate assays (LC-MS/MS, PFGE &  $\gamma$ -H2AX) would be indicative of similar levels of DNA damage, with a differential release of DNA from the head to the tail region accounting for the differential measures seen with the Comet assay.

## **1.10 Aims and Objectives**

IR generates a wide variety of DNA damage such as DNA single- and double-strand breaks, as well as base deoxyribose damages, protein-DNA crosslinks and protein-protein crosslinks involving nuclear proteins such as histones and non-histone proteins. However, DNA double strand breaks (DSBs) are crucial lesions among other types of DNA damage which are responsible for the radiogenic cell death (Jackson and Bartek, 2009a).

DNA damage is both a cause of cancer and a means of clinically successfully treating cancer. Therefore, fully validated methods for measuring DNA damage are essential in studying cancer in the pre-clinical and clinical setting. The Comet assay is now widely accepted as a standard method for assessing DNA damage in individual cells indeed it has been used in a broad variety of applications including human bio-monitoring, genotoxicology, ecological monitoring and as a tool to investigate DNA damage and repair in different cell types in response to a range of DNA-damaging agents (Collins, 2004). Furthermore, many studies have demonstrated that the Comet assay can successfully measure DNA damage and

subsequent repair in a variety of human tumour cells following exposure to both radiation and mutagenic compounds. It is a sensitive, rapid and versatile technique, lending itself well to the study of a range of DNA-damaging agents, such as those used in cancer therapy (Dhawan et al., 2009). It is a sensitive method which is used to estimate the SSBs and ALSs, and other types of damage (Azqueta et al., 2009; Collins, 2009). It is therefore attainable that the Comet assay could play a central role in future cancer patient monitoring; identifying those patients with tumours who are damage sensitive and therefore appropriate for genotoxic treatments (radiotherapy & chemotherapy) or damage resistant and therefore appropriate for alternate treatments such as surgery or immunotherapy. Furthermore the assay could be used to identify patients with repair proficient tumours who may be eligible for repair/response inhibition drugs, such as PARP-inhibitors or DDR-inhibitors.

For that reason, starting with the ACA was one of the priorities for this project to detect the ability of the ACA in distinguishing cells' damage sensitivity. Therefore, to examine the effect of ionising radiation on cancerous cells, a panel of four bladder cancer cell lines (UMUC3, RT112, J82 and RT4) have been used in this study to measure cellular response (DNA damage sensitivity) to ionising radiation exposure. These cell lines were purchased from the American Tissue Culture Collection and the European Collection of Cell Culture. Previously, a preliminary study was conducted on three cell lines derived from transitional cell carcinoma (TCC) of the bladder. Cells were exposed to 0–10 Gy X-rays and an inverse correlation between cell survival (clonogenic assay) and mean tail moment (ACA) was observed (McKelvey-Martin et al, 1998). This supported the hypothesis that the ACA might be useful in predicting the radioresponsiveness of individual cell lines.

Two different theories were investigated to determine the reason for the differential measures of comet formation noted between the bladder cancer cell lines. First, it would be determined whether the comet formation reflects the differences in damage formation between the radioresistant and radiosensitive bladder cancer cell lines, or alternatively, whether the extent of the comet formation is the consequence of additional release of DNA sequences/loops from the comet head, resulting in larger comet tails for the same level of DNA damage. Studies were conducted to demonstrate that the ACA as a means of measuring DNA damage is a good measurement of bladder cancer cells' radiosensitivity *in vitro*, with both studies showing a strong inverse correlation between initial measures of comet formation and

clonogenic survival (Moneef et al., 2003; McKeown et al., 2003). However, no research has been published relating to the reasons of differential measures of comet formation associated with the effects of IR on cancer cells such as bladder cancer.

### **1.11 Hypothesis to be tested**

The four bladder cancer cell lines were analysed by both the Comet assay and by an analytical method (LC-MS/MS) or pseudo-analytical methods ( $\gamma$ -H2AX, pulsed field gel electrophoresis (PFGE)). An equivalent differential response noted for the assays can indicate that the Comet assay does indeed measure differences in induced DNA damage between cell lines; whilst the absence of a differential effect for the alternate analytical methods would indicate that the differential effect noted by the Comet assay is possibly due to the additional release of the adjacent/contiguous loops of DNA.

# **Chapter 2**

## **Materials and Methods**

## 2. Materials and Methods

### 2.1 Cell-lines for in vitro studies

J82, RT112 and UMUC3 bladder cancer cell lines were used in this project. These cells were originally derived from high grade transitional cells carcinoma (TCC) and were obtained from Prof. G D Jones (Leicester Cancer Research Center, University of Leicester, UK). RT4 cells are purchased from American Type Culture Collection from American Type Tissue Culture Collection (ATCC, LGC Standards, Teddington, and Middlesex, UK). All cell lines were maintained at a low passage as laboratory stocks. All cell lines were tested for mycoplasma contamination using the AmpFlSTR Identifiler PCR Amplification Kit (Applied Biosystems) and were assessed to be free of contamination. All cell lines were cultured at 37°C with 5 % CO<sub>2</sub>.

**Table 2.1 the Origin of RT4, J82, RT112and UMUC3 human TCC cell lines.**

Name	Tissue	Disease	Organism	Morphology	Gender	Ethnicity	Description
RT4	Urinary bladder	Bladder, urinary. Transitional cell papilloma	Homo sapiens (human)	Epithelial	Male	Caucasian	(Rigby et al., 1970)
J82	Urinary bladder	Transitional cell carcinoma	Homo sapiens (human)	Epithelial	Male	Caucasian , Swedish	(O'Toole et al., 1978)
RT112	Urinary bladder	Transitional cell carcinoma	Homo sapiens (human)	Epithelial	Female	Caucasian	( Marshall et al., 1977)
UM-UC-3	Urinary bladder	Transitional cell carcinoma	Homo sapiens (human)	Epithelial	Male	Other ethnic	(Grossman et al., 1986)

#### 2.1.1 Cell culture medium and supplements

Eagle's minimum essential media (MEM) with Earle's salts and non-essential amino acids, Dulbecco's Modified Eagle's Medium (DMEM) with high glucose and L-glutamine, McCoy's A (a modified medium), and Dulbecco's Modified Eagle's Medium (DMEM) were purchased from Fisher Scientific, (Loughborough, UK), along with sodium pyruvate, L-glutamine (GlutaMAX-I), fetal bovine serum (FBS) and non-essential amino acids (NEAA).

## 2.2 Chemicals and Reagents

All chemicals were purchased from Sigma Aldrich (Poole, UK) or Thermo Fisher Scientific (Loughborough, UK) unless indicated otherwise, for example: Ethanol, methanol, bromophenol blue, dimethyl sulfoxide (DMSO), phosphate buffer saline (PBS) tablets, normal melting point (NMP) agarose(NMP), low melting point (LMP) agarose, goat milk powder, foetal calf serum (FCS), trypan blue stain, crystal violet stain, propidium iodide (PI), hydrochloric acid (HCl), ethylenediaminetetraacetic acid disodium salt dehydrate ( $\text{Na}_2\text{EDTA}$ ), sodium chloride (NaCl), sodium hydroxide (NaOH), sodium dodecyl sulphate (SDS), sodium deoxycholate (SDC), trizma-base, propidium iodide solution stock (1mg/mL), ethidium bromide, TBE 10X, trypsin EDTA, 0.4% trypan blue stain, low melting point agarose, ethylenediaminetetraacetic acid (EDTA), tris hydrochloride (Tris HCl), potassium chloride (KCl), bovine serum albumin (BSA), tris-base, triton X-100, normal goat serum, magnesium chloride Hexahydrate ( $\text{MgCl}_2 \cdot 6\text{H}_2\text{O}$ ), 8-oxodG, desferrioximine mesylate salt, calf thymus DNA, HPLC (fluorescence) grade methanol, and HPLC grade isopropanol. Proteinase K and Triton X-100 were supplied from (Calbiochem, UK). Gold antifade/DAPI-SlowFade®, HPLC grade water, and ultra-pure  $\text{dH}_2\text{O}$  were purchased from Life Technologies (Paisley, UK). 8-oxodA was purchased from BIOLOG Life Science Institute (Bremen, Germany). HPLC grade water (18.2MV output quality) was obtained from a Maxima purification system (Elga, High Wycombe, UK). PFCA was purchased from (BioRed, Watford, UK). LMT agarose powder and PFCA agarose for PFGE assay were purchased from Bio-Rad Laboratories Ltd (Watford, UK).

## 2.3 Kits, Enzymes, and antibodies

Deoxyribonuclease I (DNase I), trypsin-ethylenediaminetetraacetic acid (Trypsin-EDTA 10x) were purchased from Sigma Aldrich (Poole, UK). Anti-phospho-histone H2A.X (ser139) antibody and A21121 Alexa Fluor 488 (goat anti-mouse IgG) were purchased from Life Technologies (Paisley, UK). Genomic DNA (Blood & Tissue) extraction kits were purchased from QIAGEN (Manchester, UK). Wako DNA extractor WB kit from (Wako Chemicals GmbH, Neuss, Germany), Maxwell® 16 DNA Purification Kits were supplied from Promega (Madison, USA). Shrimp alkaline phosphatase (SAP) was purchased from



Amersham Pharmacia Biotech (Uppsala, Sweden). Snake venom phosphodiesterase I (SVP) from *Crotalus adamanteus* were purchased from Sigma (Poole, UK). Schizosaccharomyces pombe DNA size marker was purchased from Bio-Rad laboratories (Watford, UK), and protein ladder (molecular marker) was purchased from Thermo Fisher Scientific (Horsham, UK).

## **2.4 Summary of the techniques included in this project**

RT4, J82, RT112, and UMUC3 cell lines were exposed to different radiation doses, the specific doses delivered depending on the specific DNA damage measuring technique being used/investigated. The DNA damage levels were either assessed directly, or after a period of cell incubation to allow the measure to become manifest and/or to allow damage repair. DNA response or damage was assessed using either ACA,  $\gamma$ -H2AX, PFGE and LC-MS/MS. Effects on cell viability/proliferation and cell death were investigated in all the cell lines by a cell proliferation assay whereby the cells were simply counted by PI assay.

## **2.5 Preparation of buffers and working reagents**

Buffers and working reagents were used directly from the kits supplied by the company or were newly prepared according to lab standard operating procedures. The optimisation of protocols and procedural steps used in this project were undertaken prior to the reported use. The preparations of the buffers and working reagents required for this project are detailed in the following list and were stored at the designated temperature.

### **2.5.1 PBS (For tissue culture and general use)**

PBS buffer saline (pH 7.4) was prepared by adding one tablet of PBS to 200ml of deionised water (ddH<sub>2</sub>O). This yielded 0.01M phosphate buffer, 0.0027M KCl and 0.137M NaCl, pH 7.4, which was then autoclaved and stored at 25°C prior to use.

### **2.5.2 1x Trypsin-EDTA (For tissue culture work)**

1x trypsin-EDTA was made by adding 1ml of 10x trypsin-EDTA to 9ml of sterile PBS (diluted factor is 1:10) and stored at 4°C.

### **2.5.3 Low melting point agarose (LMP) (For Comet work)**

60mg of LMP agarose powder was added to 100ml PBS solution to reach a final concentration of 0.6% (w/v) LMP agarose. This was then boiled to dissolve the agarose using a microwave oven and then stored at room temperature.

### **2.5.4 Normal melting point agarose (NMP) (For Comet work)**

1g of NMP agarose powder was dissolved in 100ml of ddH<sub>2</sub>O to achieve a final concentration of 1% (w/v) NMP agarose. This was then boiled to dissolve the agarose using a microwave oven and then stored at room temperature.

### **2.5.5 Lysis buffer (For Comet assay)**

The stock solution of lysis buffer was prepared by mixing 100mM Na<sub>2</sub>EDTA (36.40g), 2.5M NaCl (146.1g), and 10mM Tris-HCl (1.2g). The mixture was dissolved in 750ml of ddH<sub>2</sub>O, the pH was adjusted to 10 with 10M sodium hydroxide (NaOH), and this mixture was then made up to 1000ml with ddH<sub>2</sub>O. The working solution (made and used on the same day) was made by adding 1% Triton-X-100 (v/v) to the required volume of lysis buffer stock solution. The buffer was kept at 4°C and was suitable to use up to one month.

### **2.5.6 Alkaline electrophoresis buffer (For Comet assay work)**

10M NaOH was made by dissolving 200g of NaOH in 500ml ddH<sub>2</sub>O, and 200mM Na<sub>2</sub>EDTA was prepared by dissolving 7.4g of Na<sub>2</sub>EDTA in 100ml ddH<sub>2</sub>O. Alkaline electrophoresis working buffer (pH ≥13) was prepared by adding 30ml of 10M NaOH to 5ml of 200mM Na<sub>2</sub>EDTA. The final volume of the mixture was made up to 1000ml with ice-cold ddH<sub>2</sub>O.

### **2.5.7 Neutralisation buffer (For Comet assay work)**

A desired volume of neutralization buffer was prepared on the day required by adding 0.4M Tris-base (4.85g) to 80ml ddH<sub>2</sub>O and the pH was adjusted to 7.5 with concentrated HCL and was then made up to 100ml with ddH<sub>2</sub>O . The solution was kept at room temperature and was used the same working day.

### **2.5.8 Propidium iodide (PI) (For Comet assay work)**

A working solution of propidium iodide was prepared by adding 2.5µl of propidium iodide stock solution [1mg/ml (1µg/µl)] to 1ml ddH<sub>2</sub>O for every slide used during the Comet assay experiment.

### **2.5.9 10x KCM buffer (For $\gamma$ -H2AX assay work)**

The stock solution of 10x KCM was prepared by dissolving 1.2M KCl (8.95g), 200mM NaCl (1.17g), 100mM Tris-HCl (1.21g), and 10mM EDTA (0.372g) in 100ml of ddH<sub>2</sub>O then stored at 4°C until used.

### **2.5.10 1x KCM washing buffer (For $\gamma$ -H2AX assay work)**

A desired volume of 100ml of 1x KCM washing buffer was prepared on the required day by thoroughly mixing 10ml of 10x KCM buffer, 100µl Triton X-100, and 89.9ml ddH<sub>2</sub>O.

### **2.5.11 KCM blocking buffer (For $\gamma$ -H2AX assay work)**

The KCM blocking buffer was prepared immediately before use by adding 10% (w/v) normal goat serum, 10% (w/v) goat milk powder, and 2% of BSA (w/v) to KCM washing buffer. For instance, 10ml of blocking buffer was made up by mixing 1ml of 10x KCM buffer, 10µl Triton x-100, 0.2g BSA, 1g goat milk powder and 1ml of goat serum and being made up to the final volume of 10ml with ddH<sub>2</sub>O.

### **2.5.12 Digestion buffer (For LC-MS/MS work)**

The stock solution of digestion buffer was prepared by dissolving 4.844g of Trizma base and 2.033g of MgCl<sub>2</sub>·6H<sub>2</sub>O in 700ml of HPLC grade water and the pH adjusted to 8.5 with 5M HCl; then made up to 1000ml with HPLC grade water and stored at 4°C.

### **2.5.13 Shrimp Alkaline Phosphatase (SAP) (For LC-MS/MS work)**

20µl of the SAP 1U/µl was aliquot into 1ml Eppendorf tubes and stored at -20°C.

### **2.5.14 Deoxyribonuclease I (DNase I) (For LC-MS/MS work)**

The DNase I (2000U), was dissolved in a total volume of 500µl of digestion buffer, (4U/µl). 20µl was then aliquot into 1ml Eppendorf tubes and were stored at -20°C.

### **2.5.15 Snake Venom Phosphodiesterase I (SVP) (For LC-MS/MS work)**

The SVP was obtained from *Crotalus adamanteus*. Although the total enzyme activity varies from one vial to another, the preparation of SVP was made up by dissolving the entire contents of a SVP vial with digestion buffer and this could be stored for an extended period of time at -20°C. The volume of digestion buffer required to give a final concentration of SVP (0.004U/µl) was calculated using the following equation:

$$\text{Volume of digestion buffer required (}\mu\text{l)} = \frac{x \text{ units per vial (written on label)}}{0.004}$$

**Equation 2.1** Digestion buffer volume formula

### **2.5.16 Lysis buffer solution (For PFGE assay work)**

The stock solution of lysis buffer was prepared by dissolving 100mM EDTA (18.61g), 0.2% SDC (1g) and 1% SDS (5g) in 500ml ddH<sub>2</sub>O. The lysis buffer was stored at room temperature. The working solution was made up by adding 0.5ml proteinase K (20mg/ml) to 9.5ml of lysis buffer prior to use.

### **2.5.17 Washing buffer (For PFGE assay work)**

The washing buffer solution was prepared by mixing 20mM Tris-HCl (1.57g) and 50mM EDTA (9.305g) which was dissolved in 400ml of ddH<sub>2</sub>O (pH 8) and then was made up to a total volume of 500ml with ddH<sub>2</sub>O and stored at RT.

### **2.5.18 Low Melting Temperature agarose stock (LMT) (For PFGE assay work)**

2g of LMT agarose powder was dissolved using a microwave in 100ml PBS to achieve a final concentration of 2% (w/v) LMT agarose and could be stored at RT for months.

### **2.5.19 Pulse Field Certified Agarose stock (PFCA) (For PFGE assay work)**

1g of PFCA agarose was dissolved using a microwave in 100ml 1xTBE to achieve a final concentration of 1% (w/v) LMP agarose and was stored at RT prior to use.

### **2.5.20 Running Buffer 1X TBE (For PFGE assay work)**

The running buffer was prepared by adding 9L of ddH<sub>2</sub>O to 1L of 10X TBE to achieve the final concentration of 1X TBE.

## **2.6 Medium preparation**

### **2.6.1 Eagle's Minimum Essential Media (MEM)**

MEM was supplemented with 10% v/v foetal calf serum (FCS), 1% v/v sodium pyruvate, and 1% v/v GlutaMAX™, mixed and then stored at 4°C until use. This media was used for the culturing and handling of the J82 bladder cancer cell line.

### **2.6.2 Dulbecco's Modified Eagle's Medium (DMEM)**

DMEM was supplemented with 10% v/v (FCS) and 1% v/v non-essential amino acids, mixed and then stored at 4°C until use. This media was used for the culturing and handling of the RT112 bladder cancer cell line.

### **2.6.3 McCoy's A (a modified medium)**

McCoy's A (a modified medium) was supplemented with 10% v/v (FCS) and 1% sodium pyruvate, mixed and then stored at 4°C until use. This media was used for RT4 bladder cancer cell line.

### **2.6.4 Dulbecco's Modified Eagle's Medium (DMEM) with high glucose and L-glutamine**

DMEM was supplemented with 10% v/v FCS, and 1% sodium pyruvate, mixed and then stored at 4°C until use. This media was used for the culturing and handling of the UMUC3 bladder cancer cell line.

## **2.7 Cells lines and culture conditions**

### **2.7.1 Reviving of cell lines from storage**

All cells lines were collected from Dewar flask which contained liquid nitrogen, and the cell tubes were transferred to an ice box. The tubes were warmed to 37°C in the waterbath and shaken for 1-2 minutes until thawed. Cells were then re-suspended in the vial by gently pipetting the contents up and down and were then transferred to a sterile universal tube containing 10ml of complete growth medium. Cells were centrifuged at 0.4 x g for 4 minutes and the resultant pellets were re-suspended in 2ml growth medium then distributed into a T-25 flask containing 9ml of complete medium or T-75 flask containing 15ml media. The cells were then incubated at 37°C in a humidified atmosphere containing 5% CO<sub>2</sub>. The next day, the medium was changed, and incubation continued at 37°C for 3-4 days, depending on the cell type.

### **2.7.2 Maintenance of cell lines**

Cell culture protocols were undertaken in a laminar flow cabinet. Cell lines were cultured using different media, and the cells were grown at 37°C in 5% CO<sub>2</sub> incubator for 3-4 days; depending on the cell line type. For harvesting, the cell lines were sub-cultured when

monolayers reached ~80-90% confluence. The growth medium was decanted off and the cell sheets were washed twice with pre-warmed sterile phosphate buffered saline (PBS). Two to three ml of 1x trypsin/EDTA (depending on the cell lines) was then added to the monolayer cells, and the cells were re-incubated at 37°C until they detached from the flasks (verified using an optical light microscope). Once cells were detached, trypsin was inactivated with growth medium at 4X the volume of added trypsin/EDTA. The cell suspension was then centrifuged at 0.4 x g for 4 minutes after which the supernatant was poured off. The cell pellets were then re-suspended in 1-2mL of fresh growth medium and were then dispensed at the required cell numbers into new culture flasks by adding to either 9mL of medium in 25mL flask, or 15mL to of medium in 75mL flask or to 25ml in 125ml flask. The cells were then incubated at 37°C. For experiments that required seeding cells at known densities, cells were counted using trypan blue. Cells were used when ~80-90% confluent for all experiments.

### **2.7.3 Freezing of the cells for storage**

Cell lines were frozen according to the relevant ATCC protocol. Cells were trypsinised and the cell pellets were re-suspended in an appropriate volume of complete medium (typically 1ml per 10<sup>6</sup> cells) which was supplemented with 10% (v/v) FCS and 10% (v/v) dimethyl sulfoxide (DMSO). 1ml from the cell suspension was placed in cryogenic vials and transferred to a polystyrene container which was kept in a -80°C freezer at least overnight or for a few days. Following this, the vials were then placed into Dewar flask which contained liquid nitrogen for long term storage.

### **2.7.4 Cell counting using trypan blue assay**

The confluent monolayer bladder cancer cells were subcultured. The growth medium was poured off and the cell sheet was washed twice with pre-warmed sterile PBS. Two to three ml of 1x trypsin/EDTA was added to the cell sheet and the flask was rocked gently. After 3-10 minutes incubation at 37°C (depending on the cell lines types), the cells detached from the flask. Then, cells were further dispensed by pipetting them in the universal tube which contained complete growth medium. Cells were pelleted for 4 minutes at 0.4 x g then the

resultant pellets were re-suspended in 1ml of growth medium. Trypan blue assay was used to estimate the total cell number; 10µl of the cell suspension was pipetted into an Eppendorf tube and mixed with 90µl of trypan blue stain to make a dilution of 1:10. About 10µl of this mixture was placed into a haemocytometer chamber, and a phase contrast microscope was used to count and analyse the cells. The viable cells were counted within the 4 outer squares of 9 corner squares (Phillips, 1973).

**Equation 2.2** Formula for calculating total cell number in 1ml complete medium was:

$$\frac{\text{Total Cell Count}}{4} \times 10^4 \times 10 \text{ dilution factor}$$

## 2.8 Exposure of cells to ionising radiation

For studies of radiation-induced DNA damage, the cells were exposed using an Xstrahl RS320 X-Ray Irradiator system (Xstrahl LTD, Surrey, UK) located at the Hodgkin building, University of Leicester. For Comet and LC-MS/MS studies, the experiments aimed to measure the initial extent of DNA damage induced by IR, therefore, the cell samples were irradiated on ice and were protected from light exposure to avoid any additional DNA damage and to minimise repair process during exposure. However, there might be an opportunity for repair in the experiment time frames which could increase DNA damage level results of treated samples which might interfere with the outcome. Therefore, the samples were placed immediately in ice box and protected from light exposure to prevent additional DNA damage or repair process. Then, samples were collected directly to the laboratory in the Robert Kilpatrick building/University of Leicester.

However, to assess radiation-induced DSBs by  $\gamma$ -H2AX immunoassay and cell viability assay, cells were seeded and grown on sterile cover slips placed in six wells plate, and in tissue culture flasks (25ml TS flask) respectively, and then were irradiated and incubated for different time points post irradiation dependent upon the type of technique used in this study. Untreated cancer cells (the control) were exposed to the same experimental conditions.



## **2.9 Cell viability and proliferation assay**

### **2.9.1 Determination of cell viability by cell count after IR exposure**

The trypan blue exclusion assay was utilised to determine the number of viable cells. The basic principle of this assay is that living cells have intact cell membranes that can exclude trypan blue dye or any other dyes, for instance Eosin or propidium iodide; whereas, the dead cells are unable to exclude the dye, and so are stained. This assay involves the use of a haemocytometer. In this assay, a specified volume of cell suspension is mixed with a specific volume of trypan blue dye and then visually examined by light microscopic to quantify cell viability. Cells that have clear cytoplasm are viable cells (with a functional cell membrane). Whereas, cells that have blue cytoplasm are nonviable cells (with compromised cell membrane), as these cells have absorbed the stain (Strober, 2001; Strober, 2015).

For cell proliferation studies, cells were harvested by trypsinisation, seeded in a tissue culture flask (25ml TS flask) at a cell concentration of  $4 \times 10^5$  in 10ml complete medium and incubated for ~24 hours at 37°C to initiate cell recovery and growth. Cells that were exposed to IR doses (5 Gy, 10 Gy and 15 Gy of IR doses) and the control (cells in medium only without exposure to IR) were incubated for 7 days. At the end of each time period, the medium was removed, and the cells were washed with 2mL of PBS. Cells were then trypsinised and 1mL of medium was added to each tissue culture flask. This was then removed and, with the original media and washings added, was centrifuged and the resulting pellet resuspended in 1ml of media, then, approximately 10µl of the mixture was pipetted slowly into a haemocytometer chamber under a cover slip. Cells were then counted as either viable cells (white) or non-viable cells (blue) in four 1mm<sup>2</sup> areas of the chamber; this was performed within the total cell number per mL was counted (1:10 dilution of cells made using trypan blue) using a haemocytometer slide within 5 minutes or less to avoid recording false negative results. The number of viable cells per 1ml of cell suspension was obtained by multiplying the average number of white cells per 1mm<sup>2</sup> area by the dilution factor and by 10<sup>4</sup>. The viable percentage was calculated by dividing the number of viable cells by the total number of cells (viable plus non-viable cells) and multiplied by 100. The average cells in one square (1mm<sup>2</sup>) of the chamber must be between 20-50 cells. If the number of cells exceeds this range, a further dilution is required to obtain an accurate cell count, but if the number of cells per square is less than 15, a less diluted sample is recommended. The number

of cells and their viable percentage in 1ml of cell suspension were calculated as follows  
(Equation 2.3a and b):

$$(A) \text{ Number of viable cells/ mL} = \frac{\text{Sum of all viable cells counted}}{\text{Number of counted areas}} \times \text{dilution factor} \times 10^4$$

$$(B) \text{ Percentage of viable cells} = \frac{\text{Viable (unstained) cell}}{\text{The total (stained + unstained) cell count}} \times 100$$

The average results were obtained from three independent experiments conducted under identical experimental conditions.

## 2.10 Estimating DNA damage using alkaline comet assay (ACA)

ACA is a sensitive method that can be used for measurement of radiation-induced DNA damage formation and repair at the level of single cells (Singh et al., 1988; Collins, 2004). The assay is a very reliable and simple method requiring only a small number of cells (Singh et al., 1988; Singh, 1996); DNA damage is assessed through measuring the migration of DNA from individual lysed nuclei (nucleoids) upon alkaline electrophoresis (Collins, 2002). According to (Moneef et al., 2003), radiosensitive bladder cancer cells showed a greater response to ACA.

### **2.10.1 Pre-coating frosted slides**

Approximately 50ml of melted NMP agarose was transferred to a falcon tube and kept at 37°C in a water bath. Frosted microscope slides were immersed/dipped in the melted agarose until it reached just below the frosted end and the removed agarose from one side of the slide by wiping it off with a paper towel. All slides were then dried in a 37°C overnight.

### **2.10.2 Cell-slide preparation**

Cells were seeded at a density of 30,000 cells per well in a six-well plate then incubated at 37°C, for typically 24 hours (depending on rate of cell growth) to allow cells to attach and recover from manipulation. Next day, the media from the six-well plate were discarded by aspiration and the cells washed twice with pre-warmed PBS. 500µl of 1x trypsin/EDTA was added to each well following PBS removal, then the six-well plate was incubated in at 37°C for ~3-5 minutes. Once the cells were detached from the well surface, 1ml of complete medium was added to each well. 500µl of the cell suspension was collected and transferred to the pre-labelled 1.5ml Eppendorf microcentrifuge tubes, and were placed immediately on ice. 0.6% LMP agarose was prepared and placed in a water bath at 37°C. The samples were centrifuged at 11,000 x g for 10 minutes at 4°C. The supernatant was discarded, and the cell pellets placed immediately on ice. Cells were re-suspended in 200µl of 0.6 % LMP agarose, and 80µl of the LMP agarose/cell suspension mixture was applied to the centre of a pre-coated microscope slide and coverslip was placed on top of the gel. The slides were kept on ice for ~15 minutes to allow agarose gel to set under a glass coverslip. The coverslips were then carefully removed from slides, and the prepared slides were kept in Coplin Jars and placed on ice for transfer to the Xstrahl X-irradiator. The following steps were conducted in darkness or under a reduced level of light to prevent additional DNA damage.

### **2.10.3 X-ray radiation**

The prepared slides were arranged on an aluminium sheet in thermal contact with ice. Up to 12 slides are placed flat, in a prescribed manner, on an aluminium sheet in thermal contact with ice to avoid additional DNA damage. All prepared slides were then exposed to 6

different radiation doses (0, 2, 4, 6, 8 and 10 Gy) at a dose rate of 1.58 Gy/min by using an Xstrahl RS320 X-ray irradiator (195kV, 10mA) at a 30cm FSD to generate immediate DNA damage.

#### **2.10.4 Cells lysis**

After irradiation, for measures of immediate damage, slides were immediately placed in pairs back-to-back in Coplin jars which contained 30ml of ice-cold working solution of lysis buffer to avoid any further DNA damage (100mM Na<sub>2</sub>EDTA, 2.5M NaCl, 10mM Tris-base, 1% Triton X-100, pH 10.0). The Coplin jars were placed in an ice box for transport back to the lab, and kept at 4°C overnight to generate the DNA ‘nucleoids’, comprised of nuclear negatively supercoiled genomic DNA attached to remaining lysis-resistant scaffolding proteins (the nuclear matrix).

#### **2.10.5 DNA unwinding and electrophoresis**

Throughout this part of the procedure, experimental slides were covered with a dark lid to prevent any further DNA damage from light. After the lysis step, the experimental slides were completely submerged and washed twice with ice-cold ddH<sub>2</sub>O for 30 minutes (15 minutes for each wash). Slides were carefully placed in a level ice-cold electrophoresis tank filled with ice-cold electrophoresis buffer pH >13 for 20 minutes to allow DNA unwinding. The electrophoresis then was carried out in the dark at 27V and 300mA for 20 minutes. The damaged DNA migrates toward the anode as the DNA is negatively charged. The migrated damaged DNA is characterised as a “comet tail” while the undamaged DNA remains in place within the nucleoid forming the “comet head”.

#### **2.10.6 Neutralisation step**

Following electrophoresis, slides were removed from the electrophoresis tank and transferred to clean plastic trays. Slides were neutralized with 1ml of neutralization buffer pH 7.5 for 20 minutes and then washed twice with double-distilled water for 30 minutes. Afterwards, all

experimental slides were dried at 37°C for 2 hours or overnight. This procedure was carried out under conditions of darkness/reduced light to minimise further additional DNA damage.

### **2.10.7 Slide staining**

Following the neutralization step, all experimental slides were rehydrated with ddH<sub>2</sub>O for ~30 minutes. Experimental slides were then stained with 2.5µg/ml PI solution for 20 minutes and were washed with ice cold ddH<sub>2</sub>O for 20 minutes. All these processes were carried out in the dark, and the slides were left to dry overnight at 37°C.

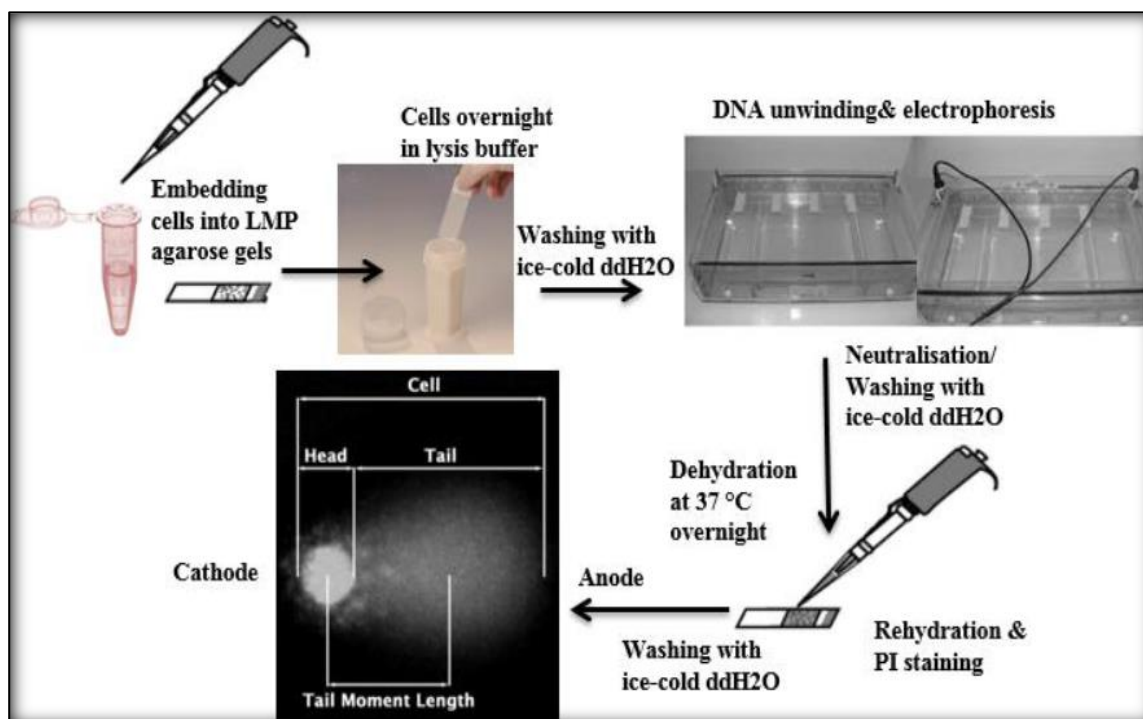
### **2.10.8 Image capture and analysis**

A total of 100 comets (50 comets from 2 gels) were scored. This was performed after adding one drop of water onto each experimental slide-gel and being covered with a coverslip for visualisation by an epi-fluorescence microscope (Olympus BH2) fitted with a green excitation filter of 515 – 535nm, a barrier filter of 590nm, and a 100W mercury lamp and operated at a magnification of 20x. Images were captured by a charge-coupled device (CCD) camera, then the comet images were analysed by the Komet software (Version 5.5, Andor Technology, Belfast, UK).

%TD, TEM, TL, and OTM were the comet parameters recorded in this study. These parameters were recorded and presented as the Mean±SEM. However, %TD is regarded as the best parameter for accurate reflection of DNA Damage formation (Collins, 2002; Kumaravel and Jha, 2006) (Figure 2.1). The percentage of tail DNA is calculated using the following equation:

$$\text{Tail DNA (\%)} = \frac{\text{Tail DNA intensity}}{\text{Total intensity of whole comet}} \times 100$$

**Equation 2.4** Formula for calculating % Tail DNA



**Figure 2.1** The key steps of the Comet Assay procedure (Al-Salmani, 2017).

## **2.11 Liquid Chromatography-mass spectrometry/mass spectrometry (LC-MS/MS) method for the determination of 8-oxodG in DNA bladder cancer cell samples.**

With the continuous development of more sensitive spectrometers, mass spectrometry is still one of the preferred analytical techniques used for the analysis of DNA adducts. Three methods were initially used to extract the genome DNA from bladder cancer cells, Maxwell 16 Cell DNA Purification, Qiagen Blood & Cell culture DNA Kit (Qiagen Genomic-tips system) and Wako DNA Extractor WB kit, however, the best results (based on recovery and the isolated DNA) were obtained using Maxwell 16 Cell DNA Purification method. (Information about Qiagen Blood & Cell culture DNA Kit (Qiagen Genomic-tips system) and Wako DNA Extractor WB kit which were used to extract the genome DNA from bladder cancer cells are given in an Appendix at the end of this thesis).

### **2.11.1 DNA extraction by Maxwell 16 cell DNA purification**

The Maxwell® 16 MDx Instrument provides automated nucleic acid purification methods for multiple analytes. The methods use sample lysis and binding to paramagnetic particles as the primary separation principle. It has two modes for different elution volumes. The Standard Elution Volume (SEV) mode allows elution in a volume of up to 400µl. The Low Elution Volume (LEV) mode allows elution in as little as 25µl. Up to 16 samples can be prepared in a single run.

#### **2.11.1.1 Samples preparation**

The cells were cultured in TC125 flasks to ~80-90 % confluence (~10 million cells). Cells were washed with PBS followed by the addition of 2-4ml of 1X trypsin/EDTA (depending on the cell line) and incubated at 37°C for 5-10 minutes. Trypsinisation was stopped by the addition of growth medium (4x trypsin/EDTA volume). Cells were pelleted via centrifugation at 400x g for 4 minutes, the supernatant discarded, and the cells re-suspended in complete medium. The cells were again washed, and after centrifugation, re-suspend with 1ml of ice-cold PBS to minimise DNA damage and transferred into pre-labelled Eppendorf tubes (each tube contained around  $10 \times 10^6$  cells). The Eppendorf tubes were kept in an ice box prior to irradiation.

#### **2.11.1.2 X-ray irradiation of the samples**

The prepared samples were irradiated with 0, 20 and 100 Gy IR doses on ice using in an Xstrahl X-ray irradiator (195kV, 10mA) at a 30cm FSD. Control cells were left on ice for the same period of time. After radiation, the labelled Eppendorf tubes were collected immediately and kept in an ice box and transferred directly to the laboratory and were stored at -20°C overnight.

#### **2.11.1.3 Maxwell 16 Cell DNA Purification**

The automated purification of genomic DNA from cell culture or bacteria cells can be undertaken by the Maxwell 16 Cell DNA Purification Kit and instrument which was used to extract DNA from bladder cancer cells line in 30–40 minutes. All enzymes and buffers were supplied in the kit.

#### **2.11.1.4 Cell preparation**

Up to  $5 \times 10^6$  tissue culture cells in a volume of 400  $\mu$ l (culture medium or PBS) was placed into well number 1 of pre-dispensed cartridge. Each cartridge was placed into the holder with the ridged side of the cartridge facing toward the labelled side of the rack. The seal of each cartridge was removed from each cartridge. The sample was loaded into well number 1 (the well closest to the cartridge label and furthest from the operator) then a plunger was placed loosely into well number 7 of each cartridge (well number 7 was closest to ridged side of the cartridge).

#### **2.11.1.5 Automated DNA Purification on the Maxwell® 16 MDx Instrument.**

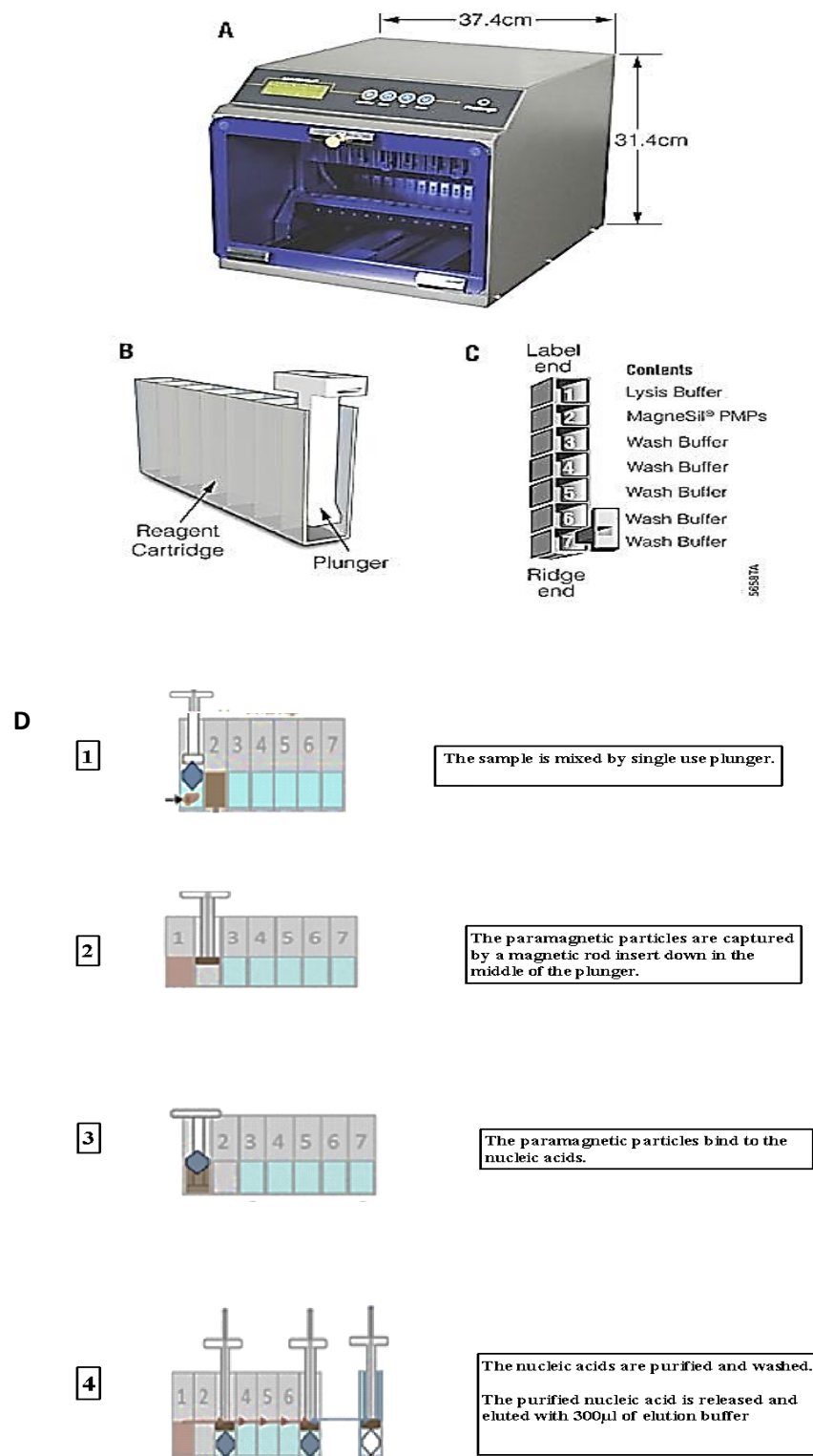
Once the certification of the SEV hardware was verified and the DNA protocol for blood and cells was selected, the labelled cartridges that contained the samples and plungers were transferred from the cartridge preparation rack into the Maxwell 16 MDx Instrument platform. A blue-labelled elution tube was placed for each cartridge into the elution tube slots that were located at the front of the platform. 300  $\mu$ l of elution buffer was added into each labelled blue elution tube. The automated purification run was completed after 30–40 minutes. The eluted samples in the elution tubes were transferred into labelled Eppendorf tubes by pipetting. Finally, the blue elution tubes, cartridges and plugs were discarded from the Maxwell 16 MDx Instrument (Figure 2.2). 10  $\mu$ l of the aliquot samples were collected and placed into pre-labelled Eppendorf tubes to measure DNA concentration. The concentration and purity of the extracted DNA was measured using a NanoDrop™ 1000 spectrophotometer (For information: example of the concentration and purity measures of the extracted DNA as measured using a NanoDrop™ 1000 spectrophotometer are given in an Appendix at the end of this thesis).

#### **2.11.2 Enzymatic digestion of DNA**

After purification of genomic DNA by the Maxwell 16 Cell DNA Purification Kit and instrument, the enzymatic digestion of DNA was done following a protocol based on that of



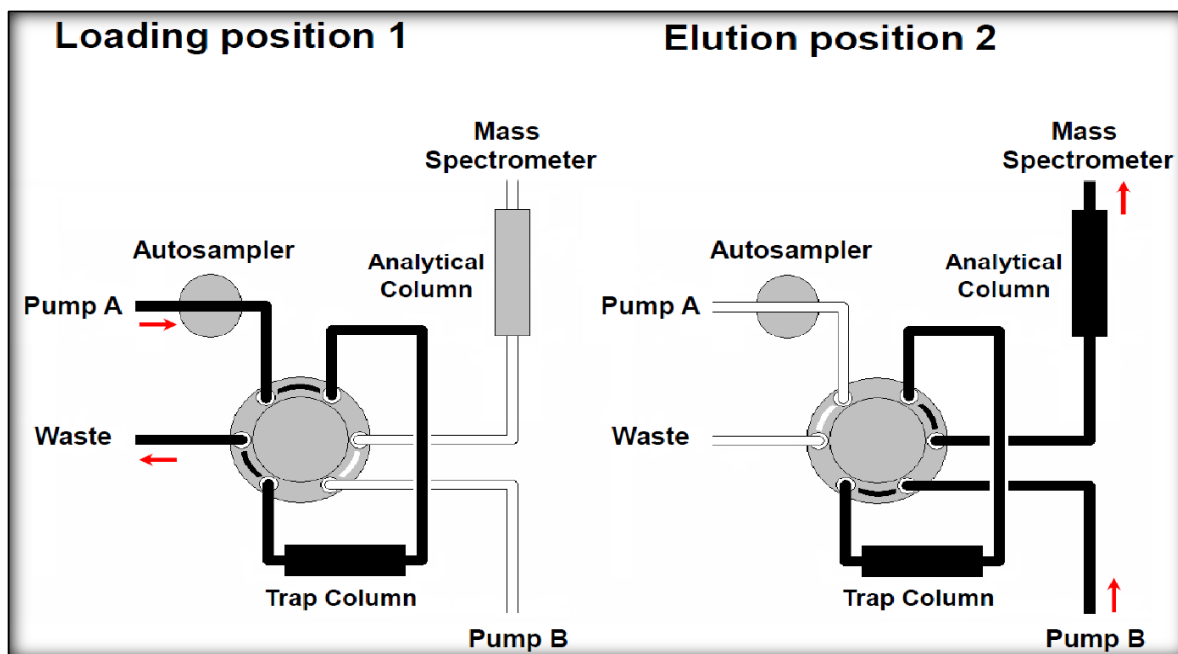
Singh *et al.* (Singh et al., 2009). A volume of 30µg of DNA from each sample was pipetted into an Eppendorf with subsequent addition of 5µL (5.0pmol) of the stable isotope internal standards [<sup>15</sup>N<sub>5</sub>]8-oxodG and [<sup>15</sup>N<sub>5</sub>]8-oxodA (each 1pmol/µL). The samples were vortexed for 30 seconds, and were centrifuged briefly at 6000 x g for 5 mins. Next, the samples were evaporated to dry in large DNA speed vac for no more than 4 hrs (no heat was required). Once the sample tubes were dried, 33µl of digestion buffer was added to each sample tube. Subsequently, 12.5µl of SVP (0.0004U/µL), 2.5µl of DNase I (4U/µL) and 2µl of SAP (1U/µL) were added and mixed. Afterward, the prepared samples were vortexed briefly (~30seconds) and incubated at 37°C for 2 hrs. The samples were then centrifuged at 14000 rpm for 5 mins. 30µl of the supernatant from each sample was transferred to a HPLC labelled vial containing low volume inserts for analysis by online column switching LC-MS/MS.



**Figure 2.2** The basic components (A, B, and C) and steps (D) of the Max well DNA purification instrument.

### 2.11.3 Online column-switching LC-MS/MS analysis

This work was carried out by Dr. Singh (Leicester Cancer Research Centre, University of Leicester). The online column-switching valve system consisted of an automated switching valve (motorised two-position six-port valve, Waters Ltd., Elstree, UK) connected to pump A incorporating the autosampler which was maintained at 10°C (Waters Alliance 2695 separations module with a 100µL injection loop) and a separate pump B (Varian prostar, California, USA). Pump A was connected via the switching valve to the trap column (Synergi Fusion-RP 80A C<sub>18</sub>, 4µm, 30x2.0mm column attached to a KrudKatcher disposable pre-column filter (0.5µm), Phenomenex, Macclesfield, UK). Pump B was connected via the switching valve to the analytical column (Synergi Fusion-RP 80A C<sub>18</sub>, 4µm, 250x2.0mm) attached to a Synergi Fusion-RP 80A C<sub>18</sub> guard column (4µm, 4.0x2.0mm) and KrudKatcher disposable pre-column filter (0.5µm). The outlet of the analytical column was directly connected to the mass spectrometer (Figure 2.3).



**Figure 2.3** Scheme for the online column-switching (Singh et al., 2009).

#### **2.11.4 Sample loading**

20µl aliquot of the DNA sample (equivalent to 30µg of hydrolysed DNA containing 3.33pmol of [<sup>15</sup>N<sub>5</sub>]8-oxodG and [<sup>15</sup>N<sub>5</sub>]8-oxodA) was injected onto the trap column using pump A with the switching valve in position 1. The impurities on the trap column were eluted to waste isocratically with solvent A, 0.1% acetic acid and solvent B, methanol (95:5, v/v), at a flow rate of 120µl/min. Isocratic flow of the DNA sample at 120µl/min via the analytical column was eluted with 0.1% acetic acid/methanol (85:15, v/v) which was maintained in the mass spectrometer by means of pump B.

#### **2.11.5 Sample elution**

At 7.5 mins, the switching valve was switched to position 2 which allowed for the purified 8-oxodG and 8-oxodA to be flushed from the trap column onto the analytical column and subsequently eluted into the mass spectrometer. Pump B maintained the isocratic flow at a flow rate of 120µl/min with 0.1% acetic acid/methanol (85:15, v/v) for 10.5 minutes. The flow from pump B bypassed the trap column and was diverted directly to waste. At 18 mins the switching valve was switched back to position 1 and the configuration of the online column-switching system was reverted to the initial conditions as previously described for the sample loading. The total run time was 50 mins.

#### **2.11.6 Mass spectrometer**

A Waters Micromass Quattro Ultima (Micromass, Waters Ltd., Manchester, UK) tandem quadrupole mass spectrometer with an electrospray ionisation (ESI) interface was used. The temperature of the ESI source was maintained at 120°C and the desolation temperature was maintained at 350°C. Nitrogen gas was used as the desolation gas (650 L/h) and the cone gas (25 L/h). The capillary voltage was set at 3.10V, and the cone voltage was 40V. The collision gas was argon (indicated cell pressure  $2.0 \times 10^{-3}$  mbar), and the collision energy was set at 12eV. The dwell time was set to 200mins and the resolution was 2 *m/z* units at peak base. Prior to use, the mass spectrometer was tuned using an 8-oxodG (10 pmol/µL) standard solution dissolved in 0.1% acetic acid/methanol (85:15, v/v) introduced by continuous

infusion at a flow rate of 10µl/min with a model 22 syringe pump (Harvard Apparatus Ltd., Edenbridge, UK). The hydrolysed DNA samples were analysed in positive ESI-MS/MS selected reaction monitoring (SRM) mode for the  $[M+H]^+$  ion to base  $[B+H_2]^+$  transitions of 8-oxodG ( $m/z$  284 to 168) and  $[^{15}N_5]$ 8-oxodG ( $m/z$  289 to 173) plus 8-oxodA ( $m/z$  268 to 152) and  $[^{15}N_5]$ 8-oxodA ( $m/z$  273 to 157). The level of 8-oxodG and 8-oxodA in each DNA sample was determined from the ratio of peak areas of the internal standards for  $[^{15}N_5]$ 8-oxodG and  $[^{15}N_5]$ 8-oxodA to the peak areas of the analyte, respectively.

### 2.11.7 Determination of the moles of DNA adduct detected on column

**Equation 2.5** Formula to estimate the DNA adduct on column:

$$Q_{anal.} = \left[ \frac{A_{anal.}}{A_{istd.}} \right] \times Q_{istd.}$$

$A_{anal.}$  = the peak area of the analyte (DNA adduct);  $A_{istd.}$  = the peak area of the DNA adduct stable isotope internal standard;  $Q_{anal.}$  = the amount of the analyte (DNA adduct) detected;  $Q_{istd.}$  = the amount of the DNA adduct stable isotope internal standard added (3.33pmol ( $3.33 \times 10^{-12}$  moles)).

### 2.11.8 Calculation of the levels of the DNA adducts detected

Assuming that 1µg of DNA is equivalent to 3240pmol ( $3240 \times 10^{-12}$  moles) of DNA nucleosides, the following equation was used to calculate the levels of DNA adducts per  $10^8$  deoxynucleosides:

$$\text{Adducts per } 10^8 \text{ deoxynucleosides} = [(Moles \text{ of DNA adduct}) / (\mu g \text{ of DNA} \times 3240 \times 10^{-12})] \div 1 \times 10^{-8}$$

**Equation 2.6** Formula for levels of DNA adducts detected.

(For information: Examples of the LC-MS/MS data reporting the levels of 8oxodG of DNA adducts in RT112 bladder cancer cell line are given in an Appendix at the end of this thesis.)

## **2.12 Estimation of DNA DSBs using the PFGE assay**

Schwartz et al. (1983) were the first to introduce the concept of fractionating large DNA molecules with the process of electrophoresis in which the DNA is separated by using two alternating electric fields. PFGE can resolve DNA molecules in excess of 2,000,000 base pairs (2.0 Mbp). PFGE is dependent upon a continuous reorientation of the DNA molecules, caused by a repeated change in electric field direction, which leads to the separation of DNA molecules primarily based on the size of the DNA molecules. DNA is a negatively charged molecule, thus it moves towards the anode in an electric field during electrophoresis. As DNA is a large molecule, it migrates as a single band. Hence, when the DNA is broken by, for instance by ionizing radiation, this leads to the formation of smaller DNA fragments. During electrophoresis, the extent of DNA fragments migration towards the anode depends on their molecular size, with the smaller sized fragments migrating quicker than larger DNA fragments. Therefore, large fragments (>20Kb) tend to combine and form a single shadowy band. By alternating the electrical field between different pairs of electrodes, the fragments are separated. Therefore, instead of continually running the voltage in one direction as in a regular electrophoresis, the voltage is switched in two or three directions: for instance, one that runs through the central axis of the gel and two that run at an angle of 120° either side.

### **2.12.1 Plug preparation**

Cells were cultured to just below confluency (70-80%). Following standard trypsinisation, and cells were counted and diluted to 250,000 cells per mL. 200µl of cell suspension was transferred to a microfuge followed by the addition of an equal volume of previously molten low melting temperature (LMT) agarose which was stabilized to 50°C by incubation in a waterbath. The agarose/cell suspension mixture was immediately mixed slowly by inversion of the microfuge several times. An aliquot of 90µL for each plug was dispensed into plug molds (which in turn were incubated at 4°C for 15 minutes. After incubation, the solidified agarose plugs were removed from the plug molds by using thin spatulas to eject the solidified agarose plugs which were placed into labelled tubes containing 1mL PBS.

### **2.12.2 X-ray irradiation of the cell-plugs**

The prepared plugs were separately irradiated with 0, 5, 10, 20, 40 and 50 Gy IR doses using an Xstrahl X-ray irradiator (195kV, 10mA) at a 30cm FSD. After radiation, the labelled tubes which contained the plugs were incubated with 1ml of lysis buffer solution (100mM EDTA, 02% Sodium Deoxycholate and 1% Sodium Lauryl Sarcosine, pH 8.0) plus 50µl Proteinase K (10mg/ml) at 37°C for 48 hrs post-IR treatment.

### **2.12.3 Plugs washing**

The lysis buffer was decanted and the agarose plugs were washed four times with 1mL washing buffer (20mM Tris-HCl and 50mM EDTA, pH 8.0) (1hr per each wash on a shaker at RT). The last wash can be done overnight at RT, and then the plugs were stored at 4°C following the final wash.

### **2.12.4 Preparation of pulse field certified agarose (PFCA)**

1% of pulse field certified agarose (PFCA) gel was dissolved in 1X TBE buffer for 1-3 minutes using a microwave, until the agarose was completely dissolved. Whilst the agarose cooled at RT, the gel casting tray with a horizontal comb was assembled to create wells. The agarose solution was poured into the cast and left at room temperature for 1-2 hrs, until it was completely solidified. The comb was carefully removed from the gel after solidification. Afterwards, both end gates and platform were unscrewed and removed, and the gel was ready for electrophoresis.

### **2.12.5 Plug preparation to electrophoresis**

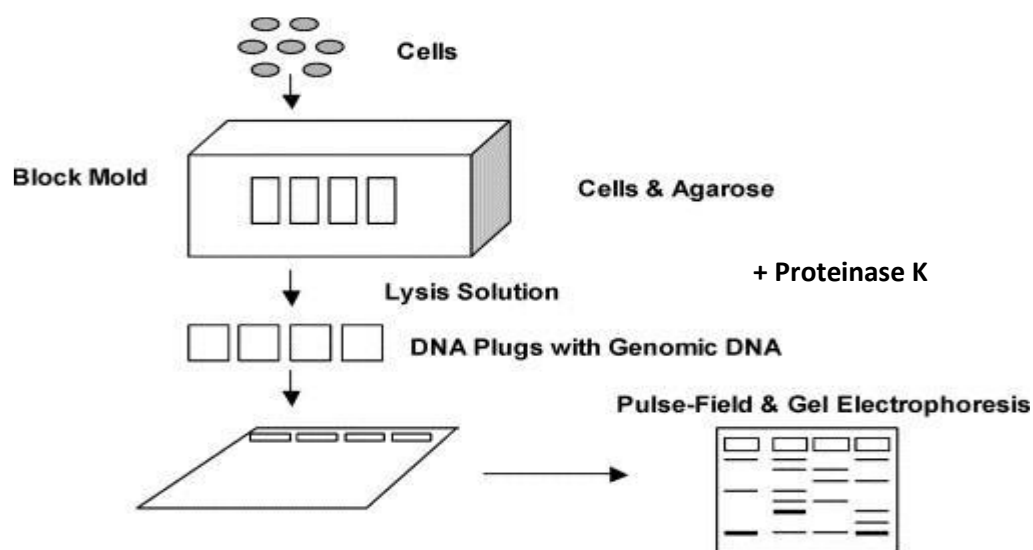
The plugs were removed from the storage buffer, and each plug was cut in half using scalpel blade and placed into the prepared well. Moreover, the well was filled with 1X TBE following vertical insertion of the half plugs to the bottom of the gel. The top of the wells were completely sealed with pulse field certified agarose, and allowing to set.

### 2.12.6 Electrophoresis

The electrophoresis step began with the preparation of 2.5 L of 1X TBE. Subsequently, the pump and the cooling system were started to pre-cool the electrophoresis buffer 30 minutes before the electrophoresis routine. Next, the gel was covered by ~2mm of 1X TBE running buffer, and the gel was soaked in this buffer for 24 hours. After entering specified electrophoresis parameters such as 14°C temperature and 90-100% variable speed pump, the electrophoresis runs were undertaken in 1X TBE buffer as follows: Run 1: 9 hours, 120° included angle, 5.5V/cm, and the initial switch time 30- final switch time 18 switch; Run 2: 6 hours, 117° included angle, 4.5V/cm, and the initial switch time 18- final switch time 19 switch and finally; Run 3: 6 hours, 112° included angle, 4.0V/cm, and the initial switch time 9- final switch time 5 switch.

### 2.12.7 Gel staining and visualising

The gel was carefully removed from the electrophoresis tank once the electrophoresis was completed. The gel was then stained with 30µl of ethidium bromide (0.25µg/ml) for 30 mins and de-stained for 1 hour with running buffer. At the end, the bands were observed and photographed for documentation. The image was analysed by SyngeneGeneSnap software (Syngene, UK) (Figure 2.4).



**Figure 2.4** The key steps of the pulse-field gel electrophoresis procedure (Farber, 1996).



## **2.13 Estimation of DNA damage level (DSBs) using $\gamma$ -H2AX assay**

In the present study,  $\gamma$ -H2AX assay was used to focus on DNA DSB damage induced after ionising radiation exposure.

### **2.13.1 Cells seeding**

RT4, J82, RT112, and UMUC3 bladder cancer cells lines were seeded on and grown on sterile cover slips attached to the bottom of wells of six-well plates at ~50,000 cells per well, supplemented with 2ml of growth medium. The cultured six-well plates were placed in an incubator at 37°C overnight. Separate six-well plates were prepared and required for each radiation dose (0, 0.5, 1 and 2 Gy).

### **2.13.2 X-ray radiation dose**

The prepared cells in the six-well plate were irradiated as required for experiment with 0, 0.5, 1 and 2 Gy IR doses using in an Xstrahl X-ray irradiator (195kV, 10mA) at a 30cm FSD. After radiation, the six-well plates were incubated for different times (30 mins, 2 hrs, 6 hrs, 16 hrs, 24 hrs) at 37°C.

### **2.13.3 Fixation and permeabilisation**

The adherent cells on coverslips in the six well plates were washed twice with 2ml of ice-cold PBS and fixed with 1ml 100% methanol and kept at -20°C overnight. After aspirating off the methanol, cells were rehydrated twice with 1ml of PBS for 20 mins (10 mins per each wash). With the PBS removed, the cells were treated with 150 $\mu$ l of fresh 1x KCM blocking buffer for 15 minutes. Then, with the blocking buffer removed, the cells were incubated at room temperature for 2 hrs on a shaker after adding 150 $\mu$ l of primary anti-phosphohistone H2AX (Ser<sup>139</sup>) antibody aliquoted in blocking buffer at a ratio 1:200. Within each well, the coverslips were next gently washed four times gently with 1ml of KCM washing buffer. The coverslips were then treated with 150 $\mu$ l of secondary antibody (A21121 Alexa Fluor 488 Goat Anti-mouse IgG) diluted in blocking buffer at a ratio of 1:200. The coverslips were placed in the dark at room temperature for 1 hr to prevent further damage to the DNA. The

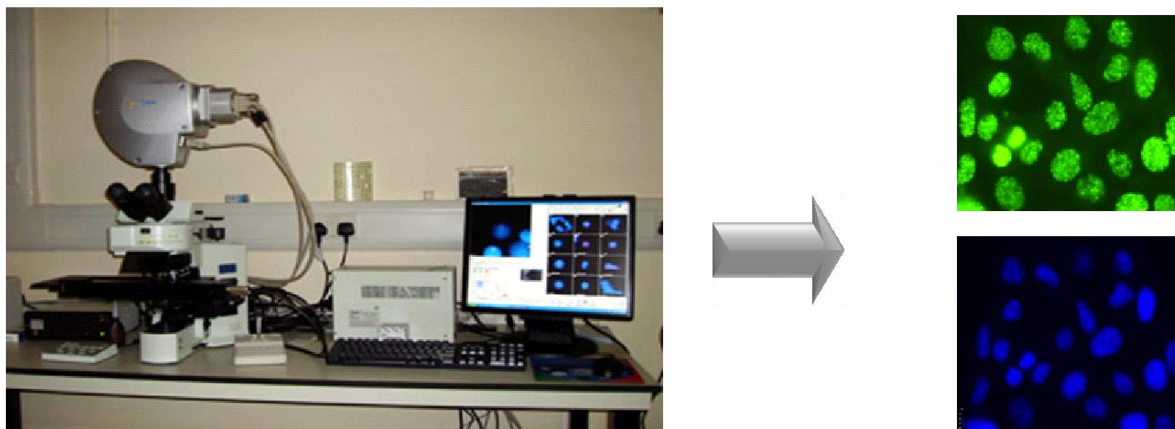
coverslips were washed 4 times with washing buffer and the washing buffer was removed after each wash (five mins per wash). Following the washing step, a drop of SlowFade® Gold antifade reagent with DAPI (10µl) was dispensed onto each new labelled slide. Carefully, each coverslip was removed from each well and placed in a specific labelled slide (sample facing down); the treated cells were pressed between the cover slip and the slide surface. Finally, the coverslip was secured by using nail polish on all sides, and the slides were then kept at 4°C prior to image viewing and analysis.

#### **2.13.4 Cells imaging and $\gamma$ -H2AX foci visualisation and analysis**

The foci were visualised at 40x magnification power and captured using Data Base Program software together with Olympus Cytological imaging system. Filters were supplied by Applied Spectral Imaging (Carlsbad CA, USA). {(Narrow-band Blue filters (GFP, Alexa 488, FITC and Cy2): exciter filter (BP 470-490), beam splitter (DM 500), barrier filter (BA 515), and the Narrow-band Green filters (Alexa 546, TRITC and Cy3): exciter filter (BP 530-550), beam splitter (DM 570), barrier filter (BA 590), Sky filter set} Filters were supplied by Applied Spectral Imaging. Automated meta-system was used to assess 6 slides each time. Scoring of up to 300 cells were randomly chosen for analysis by Fiji software (WCIF Image J version 1.42, available from research services branch NIH), two different filters were used to display  $\gamma$ -H2AX foci and the cell's nucleus. Images of clear  $\gamma$ -H2AX foci were captured using a 485µM filter, whereas the number of DAPI stained nuclei images were captured using a DAPI filter. As a part of the Fiji software's functioning,  $\gamma$ -H2AX foci and nuclei numbers were counted automatically. After exclusion of cells with more than one nucleus, the actual numbers of  $\gamma$ -H2AX foci per cell (DAPI nuclei) were obtained by dividing the total number of  $\gamma$ -H2AX foci by the total number of cells per field (Figure 2.5).

$$\text{Average } \gamma\text{-H2AX foci per Nuclei} = \frac{\text{number of total foci per field}}{\text{number of total nuclei per field}}$$

**Equation 2.7**  $\gamma$ -H2AX foci per Nuclei formula



**Figure 2.5 Olympus Cyto-system microscope Analysis of  $\gamma$ -H2AX foci per field of treated sample using image J software, which was done in duplicate.** The immune-cytochemistry images show H2AX phosphorylation (H2AX Foci) (green) which represents DSBs and the next image of nuclear dye DAPI (blue) for measuring cell numbers.

## 2.14 Statistical analysis

GraphPad Prism software version 7 (San Diego, CA, USA) was used in this study to determine statistical differences amongst sample groups. Significance of the differences in mean values among multiple groups was estimated by two-tailed one-way analysis of variance (ANOVA) with post-hoc Tukey's test. One-Way Analysis of Variance (ANOVA) followed by Tukey *post hoc* test was used to determine statistical differences between means for multiple comparisons. The probability value was considered as significant if  $<0.05$ . Data were presented as Mean  $\pm$  SEM or as Mean  $\pm$  SD.

## **Chapter 3**

**Investigation of the effects of IR-induced DNA damage  
formation by single cell gel electrophoresis (Comet assay) and  
on cell viability by trypan blue exclusion assay**

### **3.1 Introduction**

#### **3.1.1 Examination of IR-induced DNA damage (SSB and ALS) by single cell gel electrophoresis (Comet assay)**

Radiobiological studies have emphasised that DNA is the principle target for the biologic effects of ionising radiation. Ionising radiation can induce a wide range of unique DNA lesions such as modified nucleotide bases, SSBs, and DSBs (Price and D'Andrea, 2013). Any mechanisms (i.e. the enhancement or inhibition of the direct vs. indirect effects of IR) which are proposed to vary the yield of radiation-induced strand break formation (either SSB or DSB) would also be expected to similarly vary the yield of other radiation induced lesions (Ward, 1990). So a decrease in immediate SSB yield should be similarly reflected in decreased yields of SSB or 8-oxo-dG levels.

The assessment of radiation-induced DNA lesions is important for investigating and understanding the basis of radiation-induced cell killing, cell transformation and carcinogenesis, including the consequential factors of the induction of gene mutations, and chromosome aberrations (Valentin, 2006; Lehnert, 2007). Furthermore, there is a need for rapid and valid assays for the assessment of DNA damage.

The single-cell gel electrophoresis assay (SCGE) (also known as the Comet assay) was first introduced by Östling and Johanson in 1984 and was later independently modified by both Singh et al. (1988) and Olive et al. (2006). The comet assay is a sensitive microscopy-based method that has become a standard technique for the detection of DNA damage formation at the level of individual cells level. Importantly, this assay does not require the extraction of the DNA (Singh et al., 1988; Singh, 1996) that may induce adventitious damage. The comet assay, an inexpensive, simple and reliable method which has been implemented in fundamental studies on DNA damage formation and DNA damage repair (Rojas et al., 1999; Kassie et al., 2000; Collins, 2004); the assay is particularly suitable for the measurement of radiogenic damage (Olive, 1999) at the level of individual cells (Singh et al., 1988; Olive, 1999; Tice et al., 2000; Collins, 2004; Azqueta et al., 2009; Collins, 2009). The ACA, requiring only a few cells, is used to measure DNA strand breaks, which are detected by the migration of DNA from individually lysed nuclei (nucleoids) upon electrophoresis (Collins, 2002; Dhawan et al., 2009). The DNA migration, represented as the relative fluorescence of

the comet tail intensity, depicts the number of strand breaks present within the DNA of each cell (Collins, 2004), and this is an estimation of the degree of DNA damage induced post radiation exposure (Duez et al., 2003).

The alkaline version of the comet assay is a highly sensitive method for the assessment of SSBs and ALSs, and this version can detect levels of DNA damage induced by clinically relevant doses of radiation (Ward, 1988; Singh, 1996; Azqueta et al., 2009; Collins, 2004). For this project, DNA damage was assessed using the modified ACA adapted from Singh's initial protocol (Singh et al., 1988). Previously, two independent studies demonstrated that the ACA is a good measure of bladder cancer cells radiosensitivity *in vitro*, with both studies showing a strong inverse correlation between initial measures of comet formation and clonogenic survival (Moneef et al., 2003; McKeown et al., 2003) (as illustrated in Chapter 1, Figure 1.11). The studied cell lines exhibit a range of radiogenic sensitivities, with J82 being the most sensitive to radiation-induced cell killing, and RT4 and HT1376 being the most resistant. Therefore, the rank order for initial comet formation matches the rank order of cell killing for all six cell lines (J82 > T24 > RT112 > UMUC3 > HT1376 > RT4) (Moneef et al., 2003).

Studies of the irradiated nucleoids and nuclei prepared from six bladder cancer cell lines of varying radiosensitivity, exhibited similar extents of comet formation as the intact primary cells depicting an equivalent rank order for comet formation as observed in the intact parental cells (Bowman et al., 2012) (as shown in Chapter 1, Figure 1.11). It can be speculated that this observation is due to possible variances in a feature retained in the nucleoid body and presumably reflects differences in the organisation/stability of the nuclear DNA in radiation resistant and sensitive cell lines (Bowman et al., 2014).

In the above studies, for individual samples, measures of increased comet formation are due to the straightforward dose-dependency of induced damage formation. However, a further factor, which may influence the extent of comet formation, is the nature of the DNA anchoring to the nuclear matrix (NM) via matrix-associated regions (MARs), with weaker MARs allowing for the additional release and electrophoretic-migration of adjacent/contiguous loops of damaged DNA. The nuclear matrix (NM) is an essential element of the nucleus that regulates its morphology (Sjakste et al., 2004). The nuclear matrix

is the scaffolding structure of the nucleus, consisting of nuclear matrix proteins (NMPs). The matrix creates spatial order in the nucleus, providing fixed loci for sites of DNA replication, RNA transcription, and messenger RNA splicing (Berezney and Coffey, 1975; Vogelstein et al., 1980; Pienta et al., 1991; Pienta and Coffey, 1992; Misteli and Spector, 1998; Razin, 1999; Takaha et al., 2002; Elcock and Bridger, 2008; Gluch et al., 2008). Subsequently, NMPs are implemented in the control and co-ordination of gene expression. There are periodic associations of DNA chromatin with the underlying nuclear matrix through nucleoprotein interactions called matrix associated regions (MARs) (Cook and Brazell, 1976; Pienta and Coffey, 1984; Vogelstein et al., 1980; Elcock and Bridger, 2008). MARs allow the maintenance of contiguous looped regions of nuclear DNA of varying super helical densities. Changes in the DNA-matrix associations may result in weaker attachments, allowing for the additional release (and electrophoretic migration) of adjacent/contiguous loops of DNA due to the presence of radiation-induced DNA damage. A further consequence of weaker DNA-matrix associations is a decreased rewinding ability for DNA supercoils in the presence of DNA damage. Indeed, studies of radiation sensitive and resistant cells reveal that heightened radiosensitivity correlates with reduced DNA supercoil rewinding ability, in addition to the absence of various NMPs (Malyapa et al., 1994; Malyapa et al., 1996). Therefore, the differential measures of comet formation may reflect actual differences in DNA damage formation or alternatively might be due to the nature of the anchoring of the DNA loops onto the nuclear matrix through specific scaffold/matrix attachment regions (S/MARs) (Pienta and Coffey, 1984).

### **3.1.2 Determination of cell viability in the four bladder cancer cell by trypan blue exclusion assay**

Cell viability was studied by trypan blue exclusion assay to calculate viable and dead cells in irradiated RT4, J82, RT112 and UMUC3 bladder cancer cells post-irradiation. Cell viability can be defined as the number of living cells in a sample. Assessment of cell viability allows for the evaluation of the number of the living beside the dead cells. An evaluation of cell viability is essential to the assess cell growth and cell death after irradiation to understand cell's behavior after IR exposure. Trypan blue exclusion staining is based on excluding the

trypan blue dye by the intact cell membrane of the living cell so would not allow the entrance of this dye to the cell cytoplasm. Any alteration of the cell membranes can permit the dye to enter the cell. Therefore, the viable cells (with a functional cell membrane) have the ability to exclude the dye and appear unstained, and the non-viable cells (with compromised cell membrane) would obtain the Trypan blue dye as these cells have absorbed the stain and appear blue, when are visualised and counted under a light microscope at 40X magnification using a haemocytometer (Strober, 2001; Strober, 2015). Thus, the number and percentage of viable cells can be calculated in order to examine the effect of IR does effects on the bladder cancer cells (Louis and Siegel, 2011, Stoddart, 2011).

### **3.1.3 Specific aims of study**

The specific aims of this work were

- To examine the effect of IR on bladder cancer cell lines (UMUC3, RT112, J82, and RT4) as determined by the ACA to distinguish between the radiosensitive and radioresistant bladder cancer cells.
- To compare the different comet assay measurement parameters (%TD, OTM, TEM and TL) to find the fundamental parameter that distinguishes between the radiosensitive and radioresistant cells in the four bladder cancer cell lines.
- To substantiate past work results from Moneef et al., 2003 for these cells during IR exposures.
- To examine the Modulation of cell viability by IR in the four bladder cancer cell lines.

### **3.1.4 Summary of the techniques/approach**

DNA damage was assessed by the ACA. DNA denatures during the alkaline treatment and, whilst the supercoiled intact loops of DNA in the head of the comet renature upon neutralisation, the tail of the comet is thought to contain a high proportion of single-stranded broken DNA (Collins, 2004). The Materials and Methods used for this chapter have been previously described in Chapter 2. Briefly, four bladder cancer cell lines (UMUC3, RT112,



J82, and RT4) were used to investigate the ACA's capacity to distinguish the cells' damage sensitivity response after exposure to IR over a dose range of 2-10 Gy. The cells were irradiated whilst embedded in agarose gels on slides. For each dose, duplicate slides were prepared and irradiated. All experimental procedures were completed as outlined in the Materials and Methods. Slides were visualised and analysed in which a total of 200 randomly selected comets per cell line sample were scored for each dose of radiation. For visualisation of DNA damage, observations were made of ethidium bromide-stained comets at 40X magnification using a fluorescence microscope. Image analysis systems were used for quantification of the acquired DNA damage. The mean of % TD, TEM, OTM, and TL were the parameters recorded, as these parameters are commonly used. These parameters were measured and presented as the mean  $\pm$  standard error of mean (Mean $\pm$ SEM) unless otherwise stated, pooled from three independent experiments.

In addition, modulation of cell viability by IR was investigated in the four bladder cancer cells to analyse the changes in cells viability. Cell viability was examined by using trypan blue exclusion assay, to assess cell number of healthy cells in a sample. The Materials and Methods used for this Chapter have been previously described in Chapter 2.

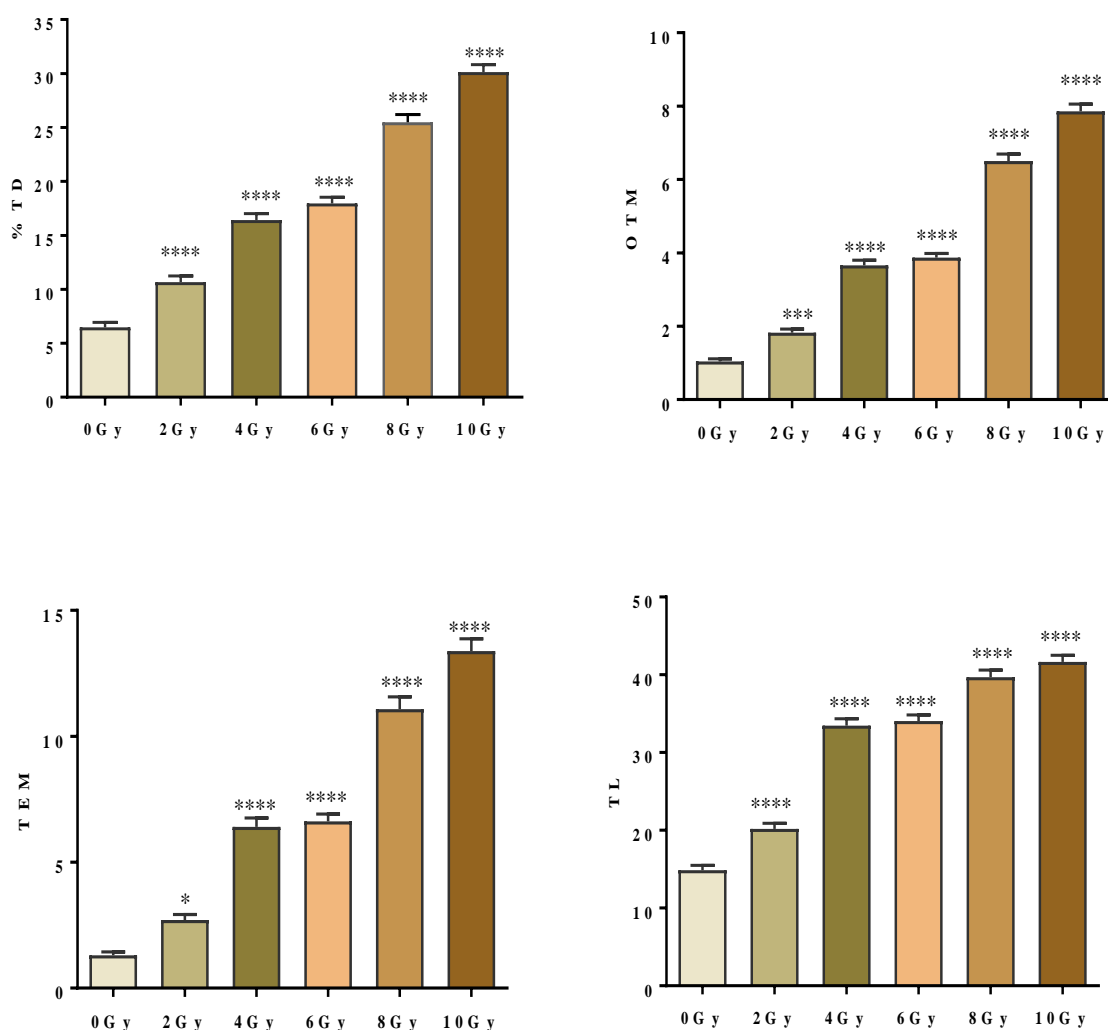
## **3.2 Results**

### **3.2.1 Estimation of radiation-induced comet formation in four bladder cancer cell lines using ACA**

The quantity of DNA damage formation, observed in UMUC3, RT112, J82 and RT4 bladder cancer cells lines, was measured after the cell were exposed to radiation over a dose range of 2-10 Gy. The induced DNA damage, in the form of SSBs and ALSs, was measured using the ACA. There was a clear positive dose response observed between the four recorded comet assay parameters (%TD, OTM, TEM, and TL) and IR dose range amongst the cell lines.

#### **3.2.1.1 Estimation of IR-induced comet formation in the RT4 bladder cancer cell line as determined by ACA**

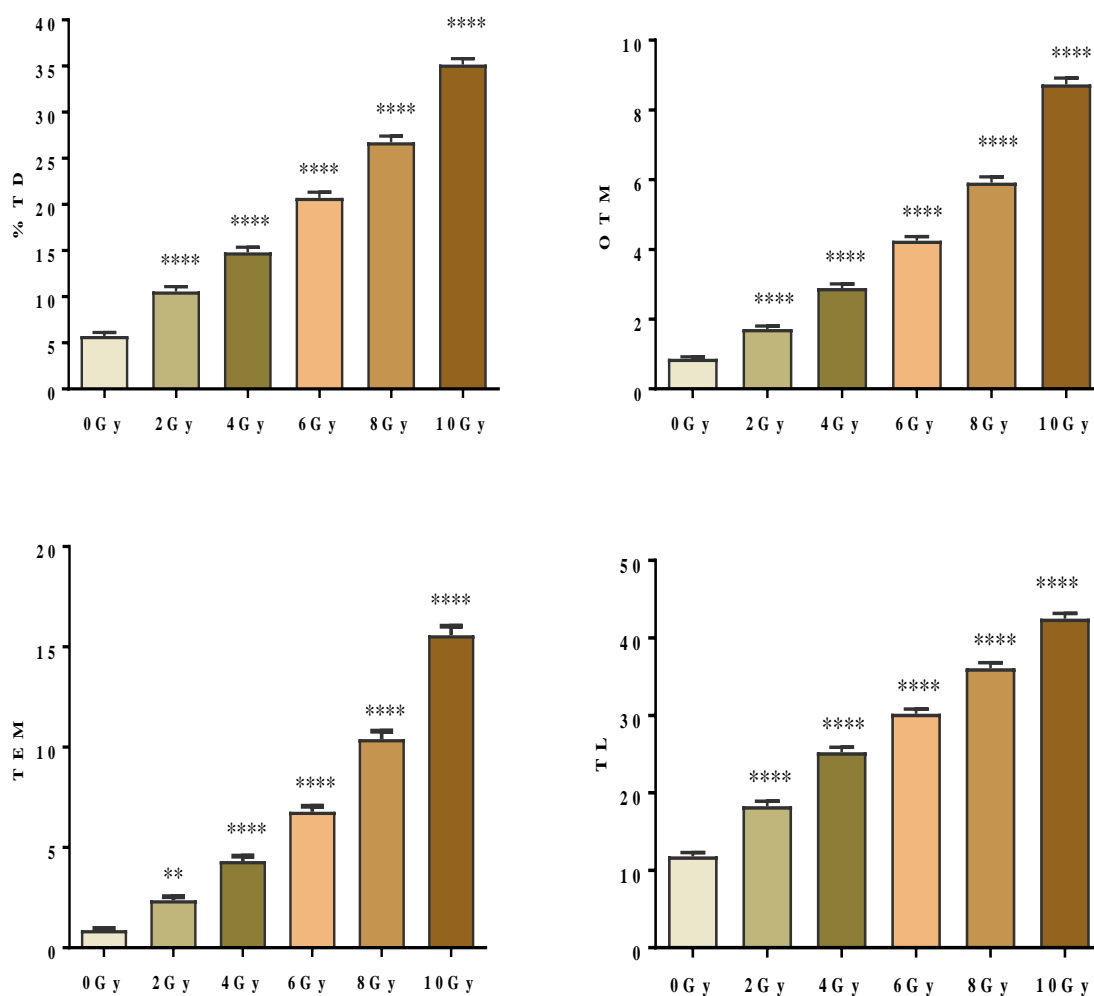
Comet formation induced by IR was examined in the RT4 bladder cancer cell line. In the replicate experiments the RT4 cells was prepared, treated, and analysed under similar experimental conditions. The ACA was utilised to investigate comet formation post exposure to IR over a dose range from 2-10 Gy. Exposing the cells to IR significantly increased the comet formation across the dose range, when compared to the untreated control sample (ANOVA:  $p < 0.0001$ ) for all the doses tested. Dunnett's multiple comparisons test showed that increasing IR doses yielded a significant increase in comet response in comparison with the untreated control sample (ANOVA:  $p < 0.0001$ ) as displayed in the plots for %TD parameter (shown in Figure 3.1A) and OTM parameter (Figure 3.1B), with exception when cells were exposed to 2 Gy measures of OTM (ANOVA:  $p < 0.001$ ) and TEM (ANOVA:  $p < 0.05$ ).



**Figure 3.1 IR-induced comet formation response, measured by alkaline comet assay, in the RT4 bladder cancer cell line.** IR-induced comet formation in RT4 cells as measured by % tail DNA, Olive tail moment, Tail extent moment, and Tail length, as determined by the ACA. Cells were exposed to IR over a dose range of 2-10 Gy and were compared to the control sample (non-irradiated cells). Results are representative of three independent experiments and expressed as Mean  $\pm$  SEM. Significance was analysed with one-way ANOVA and Dunnett's multiple comparisons (\* $p$ <0.05, \*\* $p$ <0.01, \*\*\* $p$ <0.001 and \*\*\*\* $p$ <0.0001).

### **3.2.1.2 Estimation of IR-induced comet formation in the J82 bladder cancer cell line as determined by ACA**

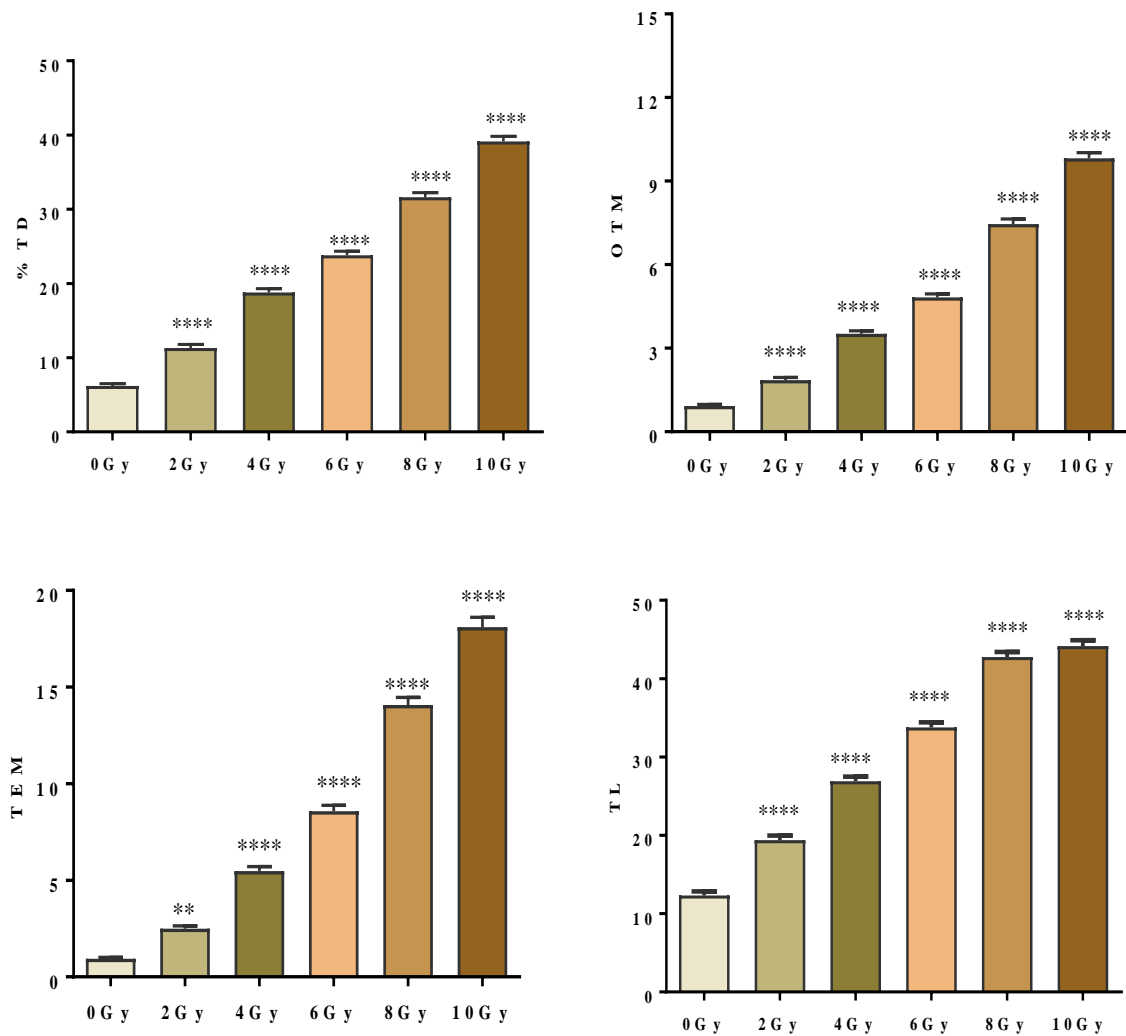
There was an evident of positive dose response between the four recorded comet parameters (%TD, OTM, TEM, and TL) and exposure to IR over a dose range of 2-10 Gy (Figure 3.2A-D). In Figure 3.2A, an illustration of immediate comet formation as measured by %TD, IR significantly increased comet formation in comparison to the untreated control sample (non-irradiated cells) (ANOVA:  $p<0.0001$ ) over the radiation dose range (2, 4, 6, 8, and 10 Gy) tested. Similarly, measurements obtained from the OTM parameter revealed that there was significant comet formation (ANOVA:  $p<0.0001$ ) over the radiation dose range of 2-10 Gy, when compared to the untreated control sample, as shown in Figure 3.2B. Likewise, Figure 3.2C shows significant increases in comet formation as measured by TEM over all radiation doses tested (ANOVA:  $p<0.0001$ ) in comparison to the control sample; with exception when cells were exposed to 2 Gy (ANOVA:  $p<0.01$ ). Finally, primary comet formation, as measured by TL (depicted in Figure 3.2D), shows that there was a significant increase in comet formation with increasing radiation doses compared to the untreated control sample (ANOVA:  $p<0.0001$ ).



**Figure 3.2 IR-induced comet formation response, measured by alkaline comet assay, in the J82 bladder cancer cell line.** IR-induced comet formation as measured by (A) %Tail DNA, (B) Olive tail moment, (C) Tail extent moment, and (D) Tail length, as determined by the ACA. Cells were exposed to IR over a dose range of 2-10 Gy and were compared to the control sample (non-irradiated cells). Results are representative of three independent experiments and expressed as Mean  $\pm$  SEM. Significance was analysed with one-way ANOVA and Dunnett's multiple comparisons (\* $p$ <0.05, \*\* $p$ <0.01, \*\*\* $p$ <0.001, and \*\*\*\* $p$ <0.0001).

### **3.2.1.3 Estimation of IR-induced comet formation in the RT112 bladder cancer cell line as determined by ACA**

Comet formation induced by IR was evaluated in the RT112 bladder cancer cell line. This cell line was treated and analysed under similar laboratory conditions previously mentioned. The ACA was used to estimate the level of comet formation resulting from DNA damage post IR exposure over a dose range of 2-10 Gy. IR-induced comet formation observed in RT112 cells was compared to the control sample (non-irradiated sample). A clear positive dose response for the four recorded comet parameters (% TD, OTM, TEM, and TL) and increasing IR dose exposure was observed. IR exposure significantly increased comet formation compared to untreated control sample as analysed by ANOVA. Dunnett's multiple comparisons test showed that increasing the IR dose yielded a significant increase in comet formation when compared to the control sample (ANOVA:  $p < 0.0001$ ) as presented in the plots depicting %TD (Figure 3.3A), OTM (Figure 3.3B), and TEM (Figure 3.3C), with the exception following exposure to 2 Gy (ANOVA:  $p < 0.01$ ) when compared with the untreated control sample. Finally, the initial comet formation, as measured by the TL (Figure 3.3D), shows that there was a significant increase in comet formation with increasing radiation dose when compared with the untreated control sample (ANOVA:  $p < 0.0001$ ).

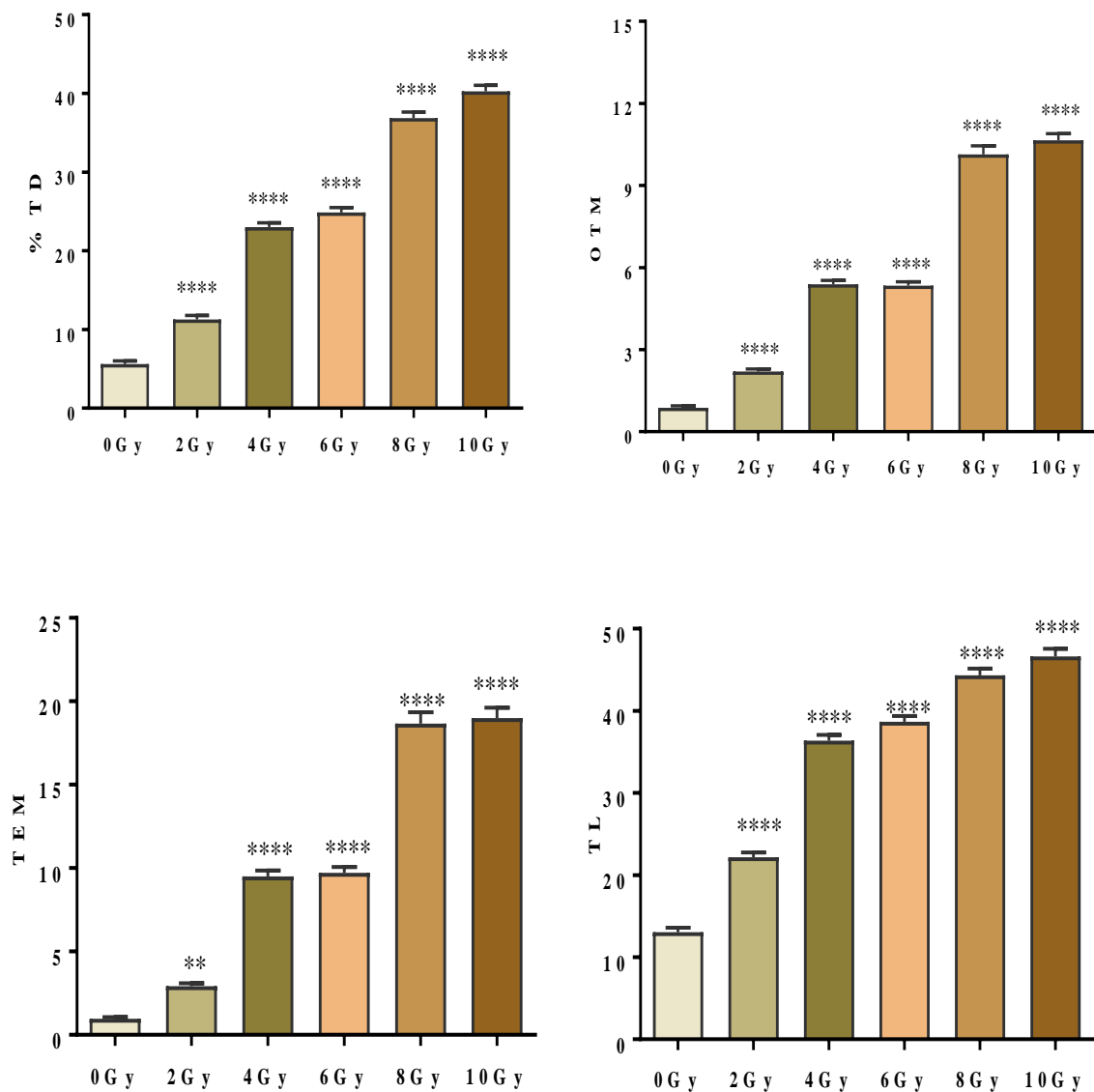


**Figure 3.3. IR-induced comet formation, measured by alkaline comet assay, in the RT112 bladder cancer cell line.** IR-induced comet formation as measured by (A) % Tail DNA, (B) Olive tail moment, (C) Tail extent moment, and (D) Tail length, as determined by the ACA. Cells were exposed to IR over a dose range of 2-10 Gy, and were compared to the control sample (non-irradiated cells). Values represent Mean  $\pm$  SEM, and were pooled from three independent experiments. Significance was analysed with one-way ANOVA and Dunnett's multiple comparisons test (\* $p$ <0.05, \*\* $p$ <0.01, \*\*\* $p$ <0.001 and \*\*\*\* $p$ <0.0001).

#### **3.2.1.4 Estimation of IR-induced comet formation in UMUC3 bladder cancer cells line as determined by the ACA**

IR-induced comet formation was assessed in UMUC3 bladder cancer cell line by utilising the ACA. The cells were exposed to IR over a dose range of 2-10 Gy. Cells were prepared, treated, and analysed under similar laboratory conditions as previously outlined. Treatment with X-ray radiation (Figure 3.4) showed a positive correlation upon examination of the % TD, OTM, TEM and TL parameters (ANOVA:  $p < 0.0001$ ) when compared to the control samples, as this observation increased significantly with increasing doses of radiation. Dunnett's multiple comparisons test showed that increasing IR dose yielded a significant increase in the TEM parameter when compared with the untreated control sample, with exception when cells were exposed to 2 Gy (ANOVA:  $p < 0.01$ ). The diagrams revealed significant response as illustrated in the graphs that depict % TD (Figure 3.4A), the OTM (Figure 3.4B), the TEM (Figure 3.4C), and the TL (Figure 3.4D) parameters.

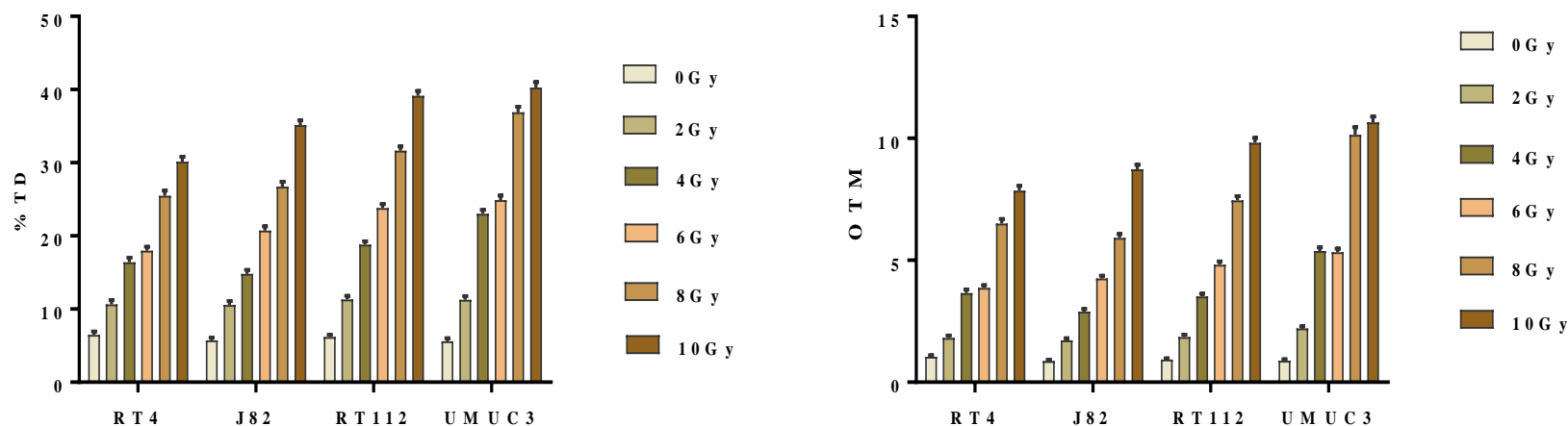




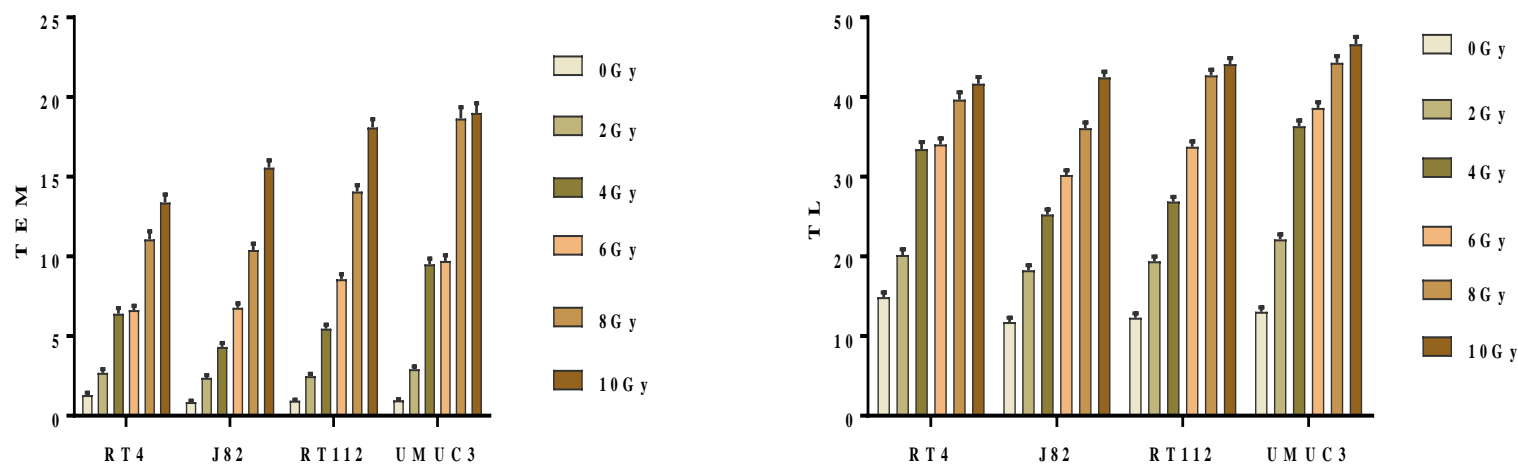
**Figure 3.4 IR-induced comet formation response, measured by alkaline comet assay, in UMUC3 bladder cancer cell line.** Quantification of IR-induced comet formation as measured by (A) % Tail DNA, (B) Olive tail moment, (C) Tail extent moment, and (D) Tail length, as determined by the ACA. Cells were exposed to IR over a dose range of 2-10 Gy, and were compared to the control sample (non-irradiated cells). Results represent Mean  $\pm$  SEM, and pooled from three independent experiments. Significance was analysed with one-way ANOVA with Dunnett's multiple comparisons test (\* $p$ <0.05, \*\* $p$ <0.01, \*\*\* $p$ <0.001 and \*\*\*\* $p$ <0.0001).

### 3.2.1.5 The combined results for UMUC3, RT112, J82, and RT4 cancer cells to estimate comet formation as measured by the ACA

Figure 3.5 directly compares the means of the individual comet measurements for the four bladder cancer cell lines post IR exposure to dose range of 0-10 Gy as measured by %TD, OTM, TEM and TL parameters.



**Figure 3.5a Combined results of IR-induced comet formation, measured by alkaline comet assay, for the four bladder cancer cell lines.** Quantification of IR-induced comet formation in RT4, J82, and RT112, and UMUC3 bladder cancer cell lines as measured by % Tail DNA, and Olive tail moment. Cells were exposed separately to 0, 2, 4, 6, 8, and 10 Gy of IR. Results represent Mean  $\pm$  SEM pooled from three independent experiments. The level of comet formation for the four bladder cancer cell lines increases considerably and significantly (see Figs. 3.1 to 3.2) with increasing IR doses, where the highest level of comet formation obtained at 10 Gy.

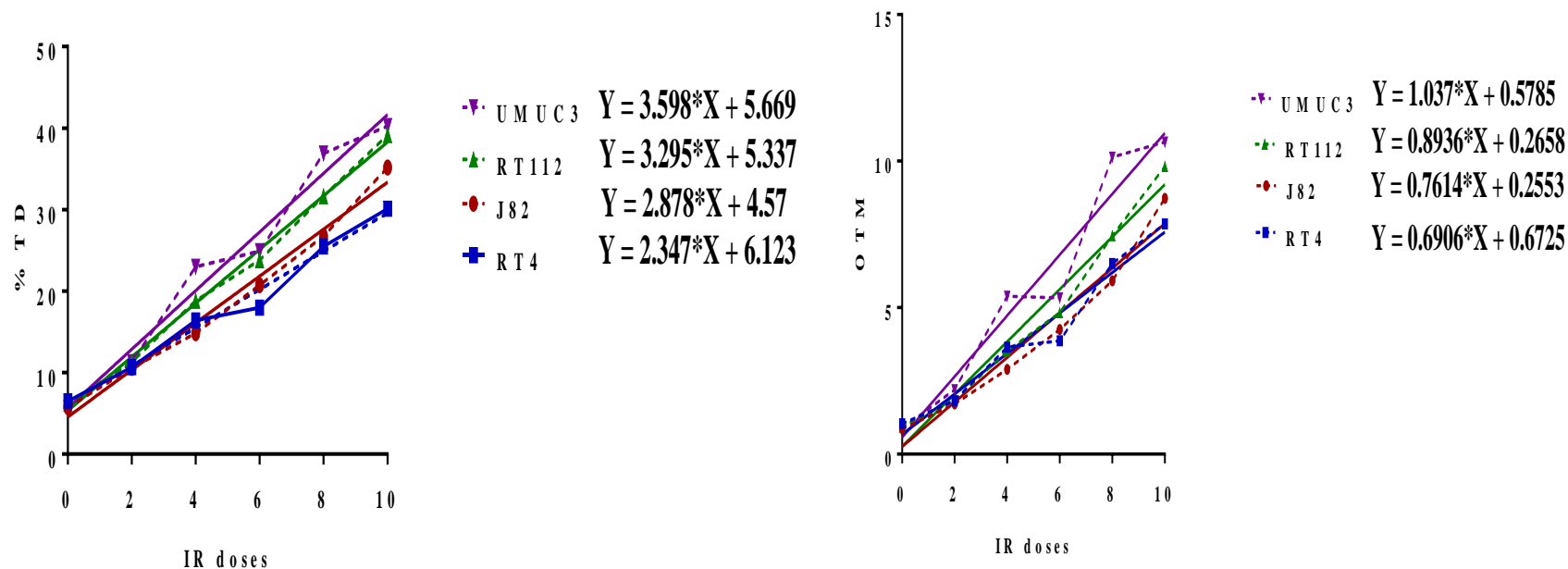


**Figure 3.5b Combined results of IR-induced comet formation, measured by alkaline comet assay, for the four bladder cancer cell lines.** Quantification of IR-induced comet formation in RT4, J82, and RT112, and UMUC3 bladder cancer cell lines as measured by Tail extent moment, and Tail length. Cells were exposed separately to 0, 2, 4, 6, 8, and 10 Gy of IR. Results represent Mean  $\pm$  SEM pooled from three independent experiments. The level of comet formation for the four bladder cancer cell lines increases considerably and significantly (see Figs. 3.3 to 3.4) with increasing IR doses, where the highest level of comet formation obtained at 10 Gy.

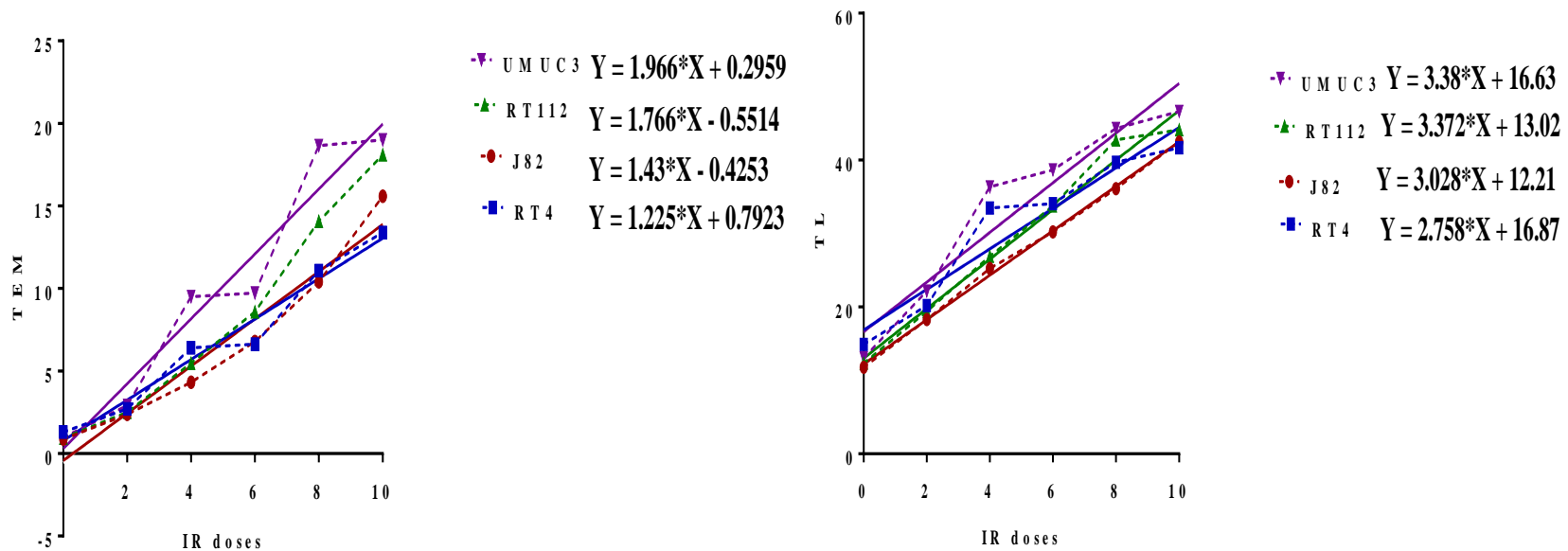
### **3.2.2 Comparison of IR-induced comet formation response for the four bladder cancer cell lines as determined by ACA, with inclusion of background/basal levels of DNA damage**

In Figure 3.6a&b, the graphs compare the means of the individual comet formation measurements observed for the four bladder cancer cell lines upon post exposure to radiation over a dose range of 0-10 Gy, as determined by %TD, OTM, TEM, and TL parameters. A linear relationship was observed independently between each parameter and the IR dose range. Two-way ANOVA tests were conducted to examine any significant differences between the responses post IR dose exposure. Tukey's multiple comparison test was used for comparative analysis of the mean for each radiation dose for each specific measure of a single dose for the four bladder cancer cell lines. %TD parameter showed no observable significant difference in the mean of comet formation post exposure to radiation dose range of 0, 2, 4, 6, and 10 Gy between UMUC3, RT112, J82 and RT4 cells. However, post radiation exposure of 8 Gy revealed a significant difference in the comet formation response between UMUC3 and RT4 cells (ANOVA:  $*p=0.0198$ ), and between UMUC3 and J82 cells (ANOVA:  $*p=0.0404$ ).

The OTM parameter revealed no significant difference in the comet formation response was observed at 0, 2, 4, 6, and 10 Gy of IR. Yet, when exposed to 8 Gy a significant difference was observed between UMUC3 and RT4 cells (ANOVA:  $*p=0.0182$ ), and between UMUC3 and J82 cells (ANOVA:  $**p=0.0062$ ). Measurements observed for the TEM parameter showed that there was no significant difference between the four bladder cancer cell lines in the mean of comet formation following exposure to 0, 2, 4, 6, and 10 Gy of IR. However, after exposure to 8 Gy of IR, there was an observable significant difference between UMUC3 and RT4 cells (ANOVA:  $*p=0.0215$ ), and between UMUC3 and J82 cells (ANOVA:  $*p=0.0121$ ). Finally, the TL parameter exhibited no observable significant responses between the four bladder cancer cell lines. However, at 4 Gy, as shown by Tukey's multiple comparison tests, there was a significant difference in responses between UMUC3 and J82 cells ( $*p=0.0119$ ), and between UMUC3 and RT112 cells (ANOVA:  $*p=0.0338$ ).

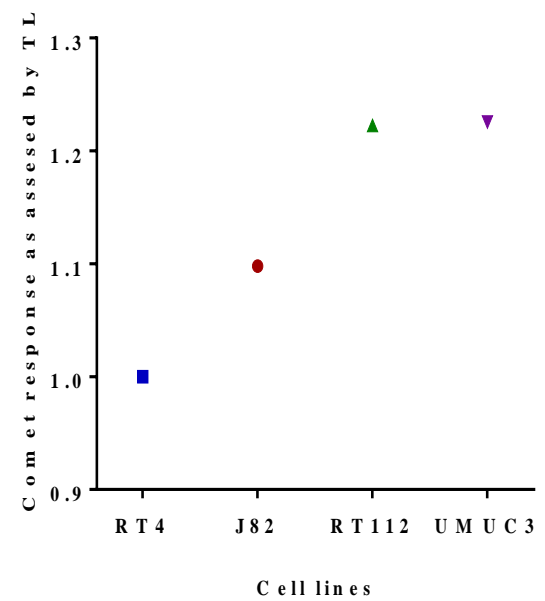
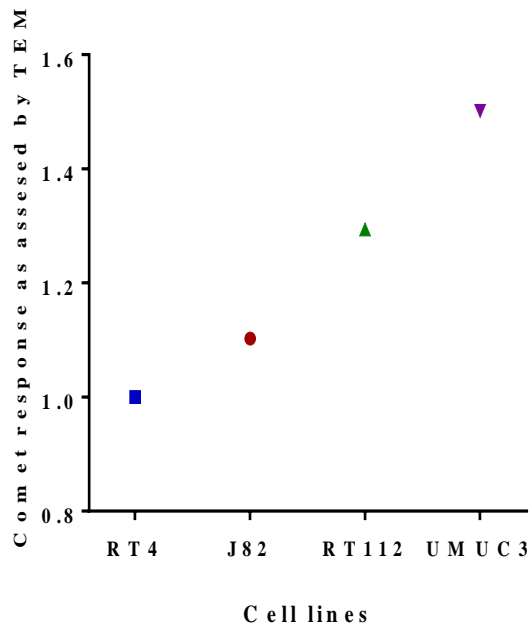
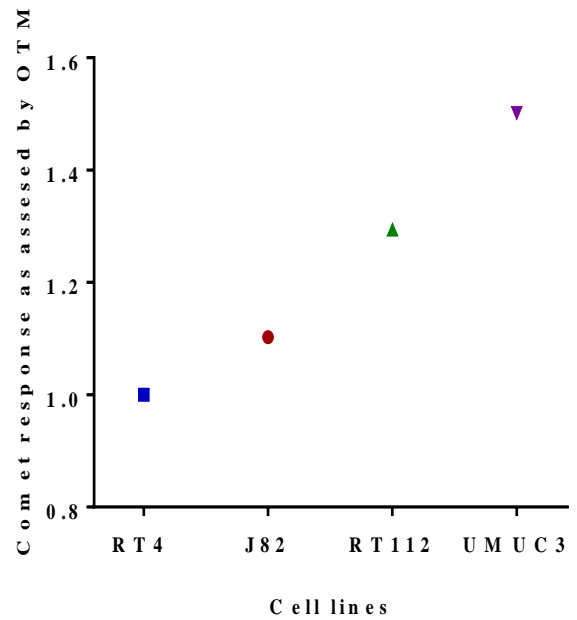
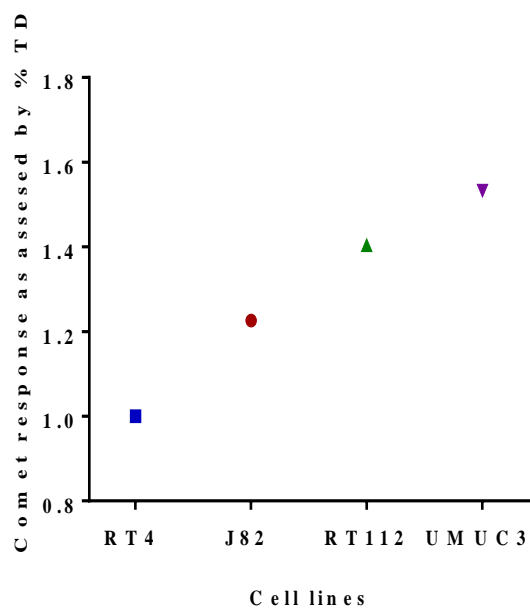


**Figure 3.6a IR-induced comet formation response, measured by alkaline comet assay, for RT4, J82, RT112 and UMUC3 bladder cancer cell lines.** Cells were seeded in 6-well plates and incubated for 24hr at 37°C/5% CO<sub>2</sub>. After 24hr incubation, the cells were exposed to 0, 2, 4, 6, 8, and 10 Gy on ice, and protected from light. Comet formation was measured by the standard ACA. Each data point represents the mean of %TD, and OTM pooled from 300 comets. Results represent Mean  $\pm$ SEM pooled from three independent experiments. A two-way ANOVA was used for statistical analysis between each of the doses (see text for details).



**Figure 3.6b IR-induced comet formation response, measured by alkaline comet assay, for RT4, J82, RT112 and UMUC3 bladder cancer cell lines.** Cells were seeded in 6-well plates and incubated for 24hr at 37°C/5% CO<sub>2</sub>. After 24hr incubation, the cells were exposed to 0, 2, 4, 6, 8, and 10 Gy on ice, and protected from light. Comet formation was measured by the standard ACA. Each data point represents the mean of TEM, and TL pooled from 300 comets. Results represent Mean  $\pm$ SEM pooled from three independent experiments. A two-way ANOVA was used for statistical analysis between each of the doses (see text for details).

In Figure 3.7, the graphs show the relative increase in comet formation as assessed by the relative dose response gradient of the four comet parameters, relative to the lowest responding cell line RT4as assessed by alkaline comet assay, for RT4, J82, RT112 and UMUC3 bladder cancer cell lines. RT4 cancer cells were consistently shown to exhibit the lowest level of comet formation in comparison to the other bladder cancer cell lines. In contrast, UMUC3 cell line consistently showed the highest level of comet formation following radiation exposure. Indeed, the rank order of comet formation for the four cell lines, from the lowest to highest comet formation response was RT4 > J82 > RT112 > UMUC3.



**Figure 3.7** The relative increase in comet formation as assessed by the relative dose response gradient of the four comet parameters, relative to the lowest responding cell line RT4, as assessed by %TD, OTM, TEM, and TL using the ACA (The Figure update from figure 3.6a &b).



### **3.2.3 Further evaluation of the relative comet formation response for the four bladder cancer cell lines after radiation exposure, as determined by ACA, with inclusion of background/basal levels of DNA damage**

To further analyse the data and to better resolve the differential effects of IR doses on the four bladder cancer cell lines, the following analysis was undertaken. For the RT4 cells (the lowest responding cell line) each individual parameter, following exposure to each individual radiation dose, was noted. Then, for each other cell line, the relative comet response increase noted at the exact same doses was determined relative to the RT4 cell line. The relative responses for each individual cell were averaged and values present as the mean  $\pm$  standard deviation (Mean $\pm$ SD) (Figure 3.8).

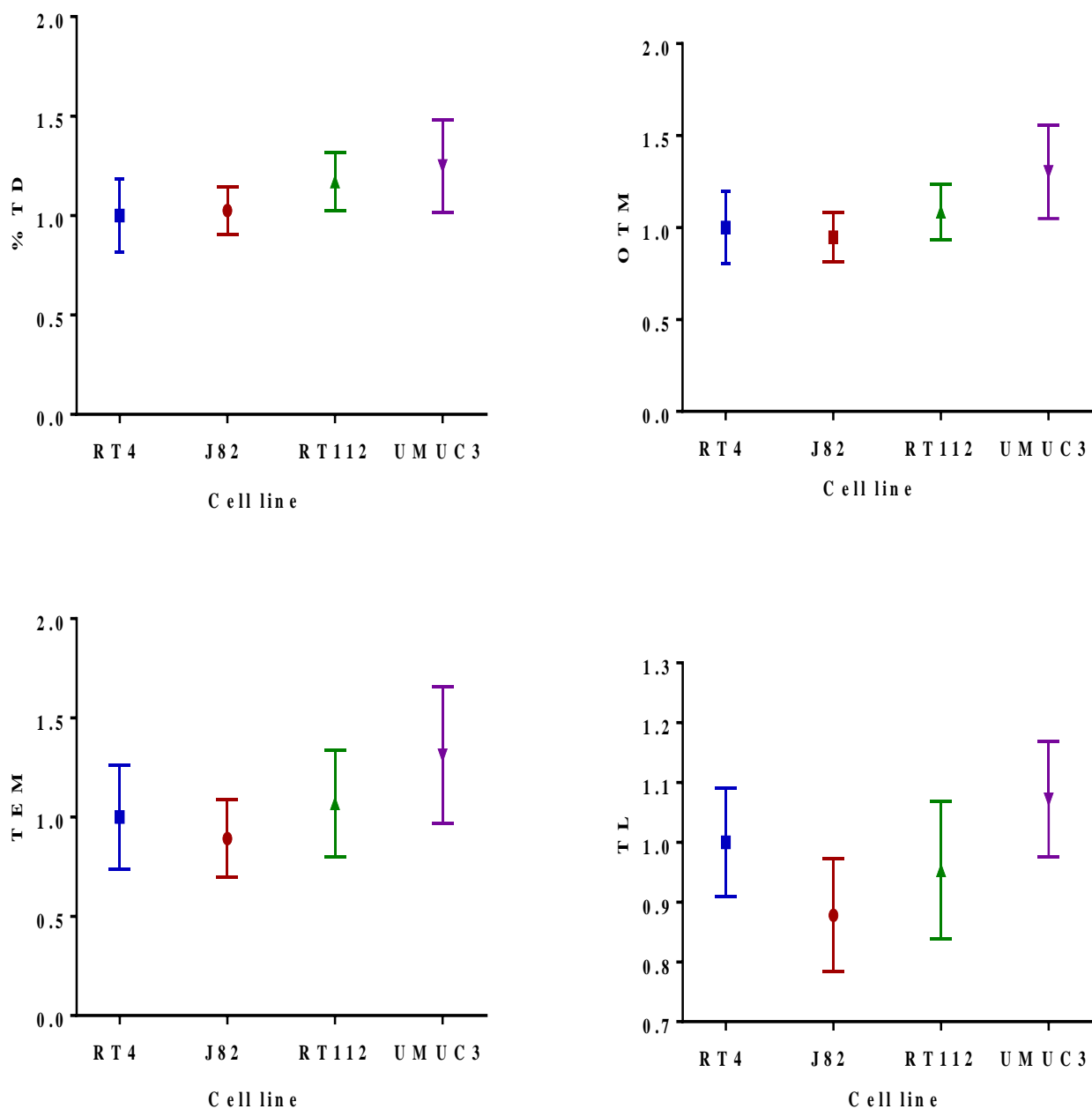
Two-way ANOVA with Tukey's multiple comparison test was used to investigate whether there was any significance in the comet formation observed between the four bladder cancer cell lines. Interestingly, %TD shows a significant IR-induced comet formation response between certain cell lines when a comparative analysis was conducted. For % TD, there was a significant increase in comet formation in UMUC3 cells compared to RT4 cells (ANOVA: \*\* $p=0.0011$ ), as well as for RT112 cells in comparison to RT4 cells (ANOVA: \* $p=0.0220$ ). UMUC3 cells also showed a significant increase in comet formation when compared to J82 cells (ANOVA: \*\* $p=0.0029$ ) post-radiation exposure. Therefore, the cell lines encompassed a range of comet formation response with UMUC3 and RT112 cells showing the highest comet formation response whilst RT4 and J82 cells showed the lowest comet formation response.

To further substantiate the above observations, when using OTM, a significant difference between UMUC3 and RT4 cells (ANOVA: \*\* $p=0.0039$ ), UMUC3 and J82 cells (ANOVA: \*\*\*  $p=0.0009$ ), and between UMUC3 and RT112 cells (ANOVA: \* $p=0.0397$ ) was observed. But, no significant differences were observable when comparative analysis was conducted between J82 and RT4 cells, between RT112 and RT4, and between RT112 and J82 cells.

Additionally, IR-induced comet formation was also analysed via the correlation between the four bladder cancer cell lines following exposure to IR doses as determined by the TEM

parameter. UMUC3 cells show scarcely a significant increase in comet formation (ANOVA:  $*p= 0.0113$ ) when compared to RT4 cells. However, when a comparative analysis was conducted between UMUC3 cells and J82 cells, UMUC3 cells shows a significant increase in comet formation response (ANOVA:  $***p= 0.0009$ ) compared to J82 cells. On the contrary, no significant differences in IR-induced comet responses were evident during the comparative analysis between UMUC3 and RT112 cells, R112 and RT4 cells, and between J82 and RT4 cells. When considering TL, the bladder cancer cell lines encompass a range of radio-responses. UMUC3 cells showed the highest level of comet formation, followed by RT112 cells then RT4 cells, and J82 cells exhibiting the lowest comet formation response. UMUC3 exhibited a significantly higher level of comet formation in comparison to J82 cells (ANOVA:  $***p= 0.0001$ ), and more prominent levels of comet formation noted in J82 than in RT4 cells (ANOVA:  $**p= 0.0074$ ), and in UMUC3 compared to RT112 cells (ANOVA:  $**p= 0.0092$ ). On the other hand, no significant differences in IR-induced comet responses was revealed between UMUC3 and RT4 cells, RT112 and RT4 cells, and between RT112 and J82 cells.

In summary, in using %TD, OTM TEM, to assess IR-induced comet formation, RT4 and J82 cancer cells were consistently shown to exhibit the lowest level of comet formation in comparison to RT112 and UMUC3 bladder cancer cell lines. In contrast, UMUC3 cell line consistently showed the highest level of comet formation following radiation exposure. Indeed, the rank order of comet formation for the four cell lines, according to the results in Figures 3.8, ranging from the lowest to highest comet formation response with TL exception was  $RT4 \geq J82 > RT112 > UMUC3$ .



**Figure 3.8 Comparison of the relative comet formation response, in bladder cancer cell lines exposed to IR** as determined by %TD, OTM, TEM, and TL by using the ACA. The relative comet formation responses for each individual cell were then averaged and plotted  $\pm$  SD. (Figure adapted from figure 3.6a & b). Significance was analysed with two-way ANOVA and with Tukey's multiple comparison test were used to compare the average relative comet formation between the four bladder cancer cell lines post IR exposure (see text above for details).

### **3.2.4 Comparison of IR-induced comet formation response for the four bladder cancer cell lines as determined by ACA, following the subtraction of background/basal levels of DNA damage**

To better assess actual intrinsic cell damage sensitivity, analysis of the above data was again undertaken for the four-bladder cancer cell lines but following the subtraction of background/basal levels of DNA damage; the corresponding dose response data are shown in Figure 3.9a&b.

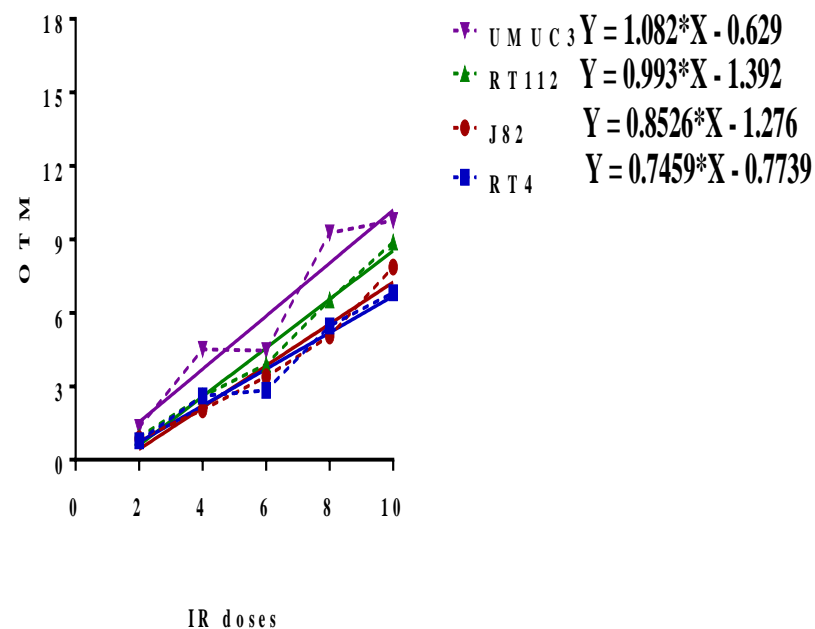
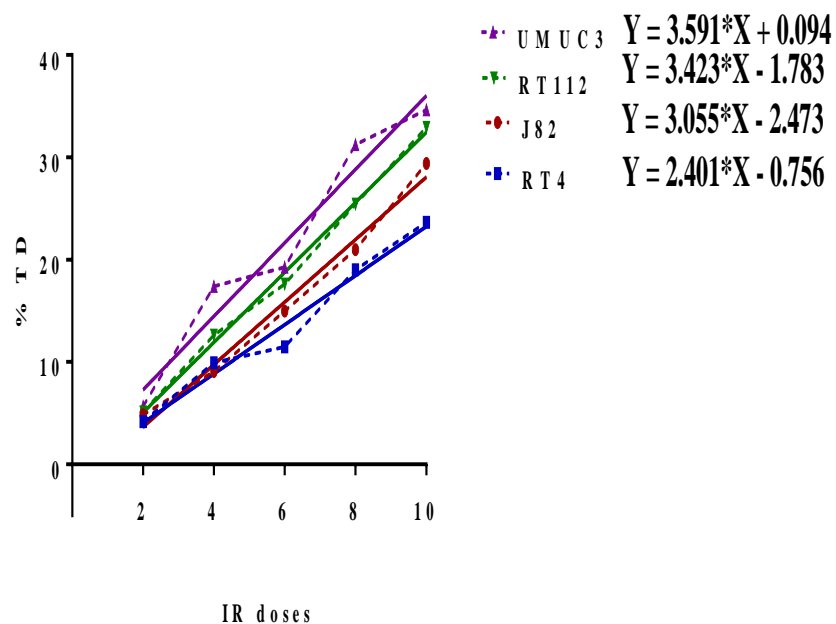
The finding revealed that the level of comet formation compared to un-irradiated controls, as determined by %TD, was not significantly different when the cell lines were exposed to 2, 4, and 6 Gy. However, DNA damage resulting in comet formation was significantly detectable at 8 Gy in UMUC3 cells when compared to RT4 cells (ANOVA:  $**p=0.0080$ ), and significant difference was detected between UMUC3 and J82 cells (ANOVA:  $*p=0.0250$ ). Yet, no significantly different IR-induced comet formation response was observed between UMUC3 and RT112 cells, between RT112 and J82 cells, between RT112 and RT4 cells, and between J82 and RT4 cells following radiation exposure of 8 Gy. Furthermore, a comparative analysis was conducted between the four bladder cancer cell lines at 10 Gy of IR dose. The results showed that RT4 cells exhibited the lowest comet formation response which was significantly lower than the levels of comet formation response noted for UMUC3 cells (ANOVA:  $*p=0.0166$ ) and RT112 cells (ANOVA:  $*p=0.0438$ ).

For OTM parameter, the results revealed that there was no significant difference at 2, 4, 6, nor 10 Gy. However, 8 Gy showed a significant difference between UMUC3 and J82 cells (ANOVA:  $**p=0.0061$ ), as well as between UMUC3 and RT4 cells (ANOVA:  $*p=0.0123$ ). Even so, no significant response was observed between UMUC3 and RT112 cells, RT112 and J82 cells, RT112 and RT4 cells and between J82 and RT4 cells.

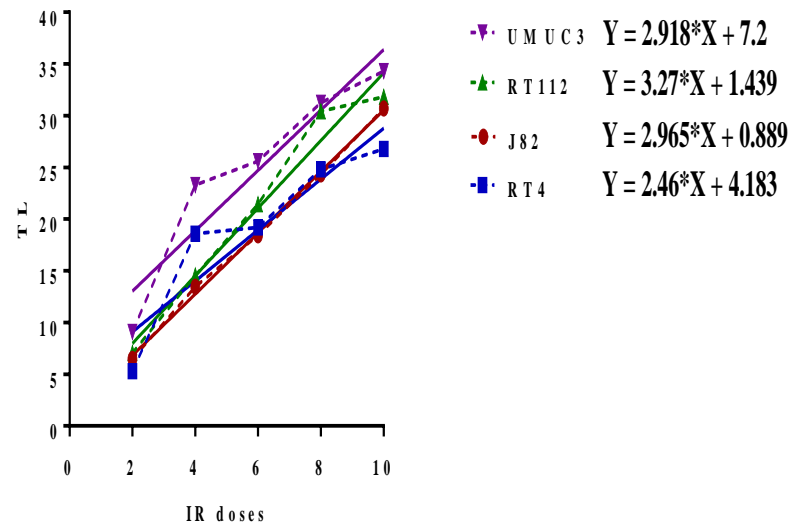
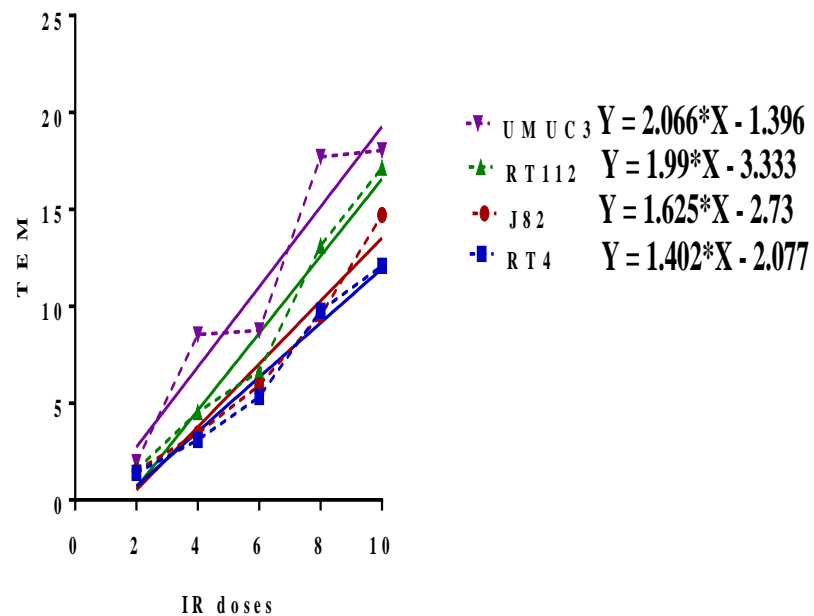
For TEM shows a comparative analysis of IR-induced comet formation observed in the four bladder cancer cell lines over a dose range of 0–10 Gy. The data exhibited a significant response when comparing UMUC3 and RT4 cells (ANOVA:  $*p=0.0124$ ), and UMUC3 and J82 cells (ANOVA:  $*p=0.0102$ ) following 8 Gy. However, the comparisons revealed that

there was no significance in the mean of comet formation response between the four bladder cancer cell lines post radiation exposure with 2, 4, 6, and 10 Gy.

Finally, in Figure 3.9, showing the evaluation of IR-induced comet formation of the four bladder cancer cell lines over a dose range of 0–10 Gy when recording the TL parameter, the result showed that there was no significant response in the four bladder cancer cell lines; with exception of exposure to 4 Gy, which exhibited a significant response between UMUC3 and J82 cells (ANOVA:  $*p=0.0247$ ), and between UMUC3 and RT112 cells (ANOVA:  $*p=0.0476$ ). However, it is known that the TL parameter has limited applicability at high doses, as TL gradually plateaus at higher doses. Therefore, it can be speculated that TL in the four bladder cancer cells was nearly the same, and the plot revealed no clear differences in the dose response curves for the four bladder cancer cells following exposure to 0, 2, 6, 8, and 10 Gy of IR.



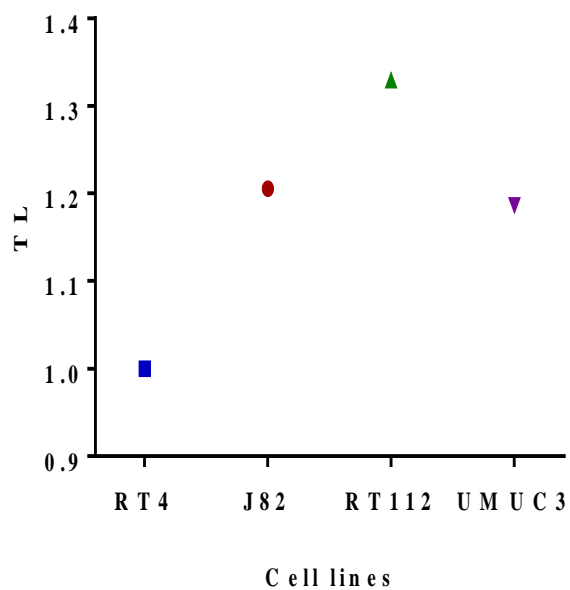
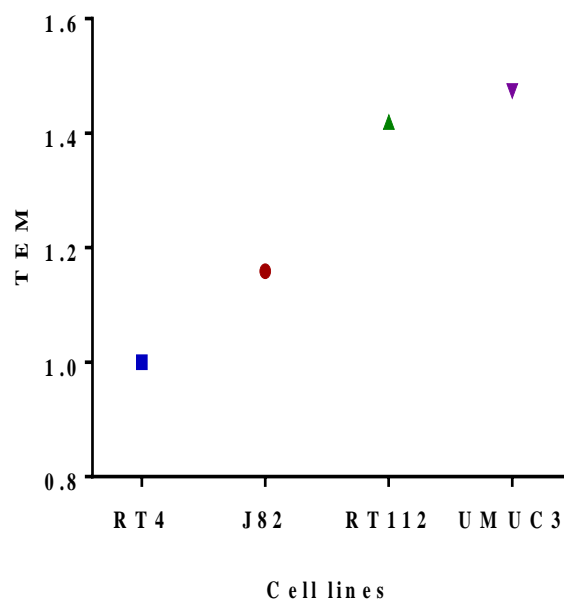
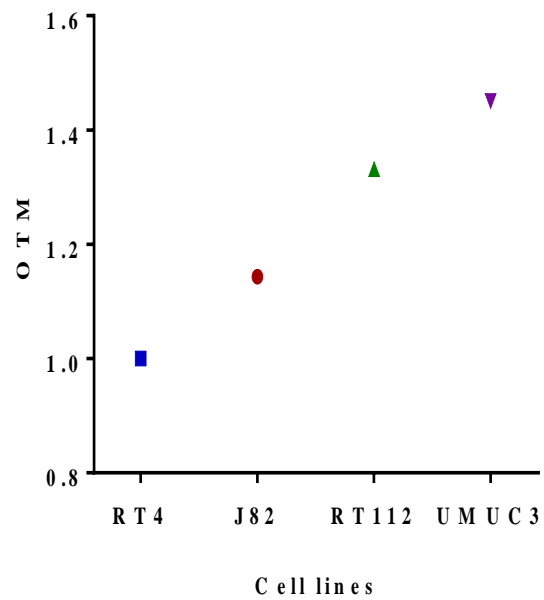
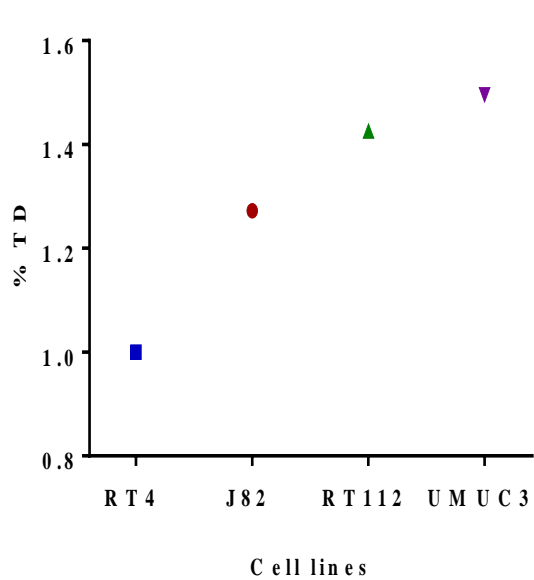
**Figure 3.9a IR-induced comet formation response, measured by alkaline comet assay, for UMUC3, RT112, J82, and RT4 bladder cancer cells.** The cells were exposed to 2, 4, 6, 8, and 10 Gy, the endogenous damage result was subtracted from each cell line separately. Each data point represents the mean of %TD and OTM pooled from three independent experiments. A two-way ANOVA was used for statistical analysis (see text for details).



**Figure 3.9b IR-induced comet formation response, measured by alkaline comet assay, for UMUC3, RT112, J82, and RT4 bladder cancer cells.** The cells were exposed to 2, 4, 6, 8, and 10 Gy, the endogenous damage result was subtracted from each cell line separately. Each data point represents the mean of TEM and TL pooled from three independent experiments. A two-way ANOVA was used for statistical analysis (see text for details).

In Figure 3.10, the graphs show the relative increase in comet formation as assessed by the relative dose response gradient of the four comet parameters, relative to the lowest responding cell line RT4 as assessed by alkaline comet assay after subtracting the endogenous damage result, for RT4, J82, RT112 and UMUC3 bladder cancer cell lines. RT4 cancer cells were consistently shown to exhibit the lowest level of comet formation in comparison to the other bladder cancer cell lines. In contrast, UMUC3 cell line consistently showed the highest level of comet formation following radiation exposure with exclusion of TL parameter. Nevertheless, the rank order of comet formation depending on %TD, OTM, TEM for the four cell lines, from the lowest to highest comet formation response was RT4 > J82 > RT112 > UMUC3.





**Figure 3.10** shows the relative increase in comet formation as assessed by the relative dose response gradient of the four comet parameters, relative to the lowest responding cell line RT4, as assessed by %TD, OTM, TEM, and TL using the ACA.

### **3.2.5 Further evaluation the relative comet formation response for the four bladder cancer cell lines after radiation exposure, as determined by the ACA, with subtraction of background/basal levels of DNA damage**

Again, to further analyse the data and to better resolve the differential effects of IR doses on the four bladder cancer cell lines, the following analysis was undertaken. For the RT4 cells (the lowest responding cell line) each individual parameter, following exposure to each individual radiation dose, was noted. Then, for each other cell line, the relative comet response increase noted at the exact same doses was determined relative to the RT4 cell line. The relative responses for each individual cell were averaged and values present as the mean  $\pm$  standard deviation (Mean  $\pm$  SD) (Figure 3.11).

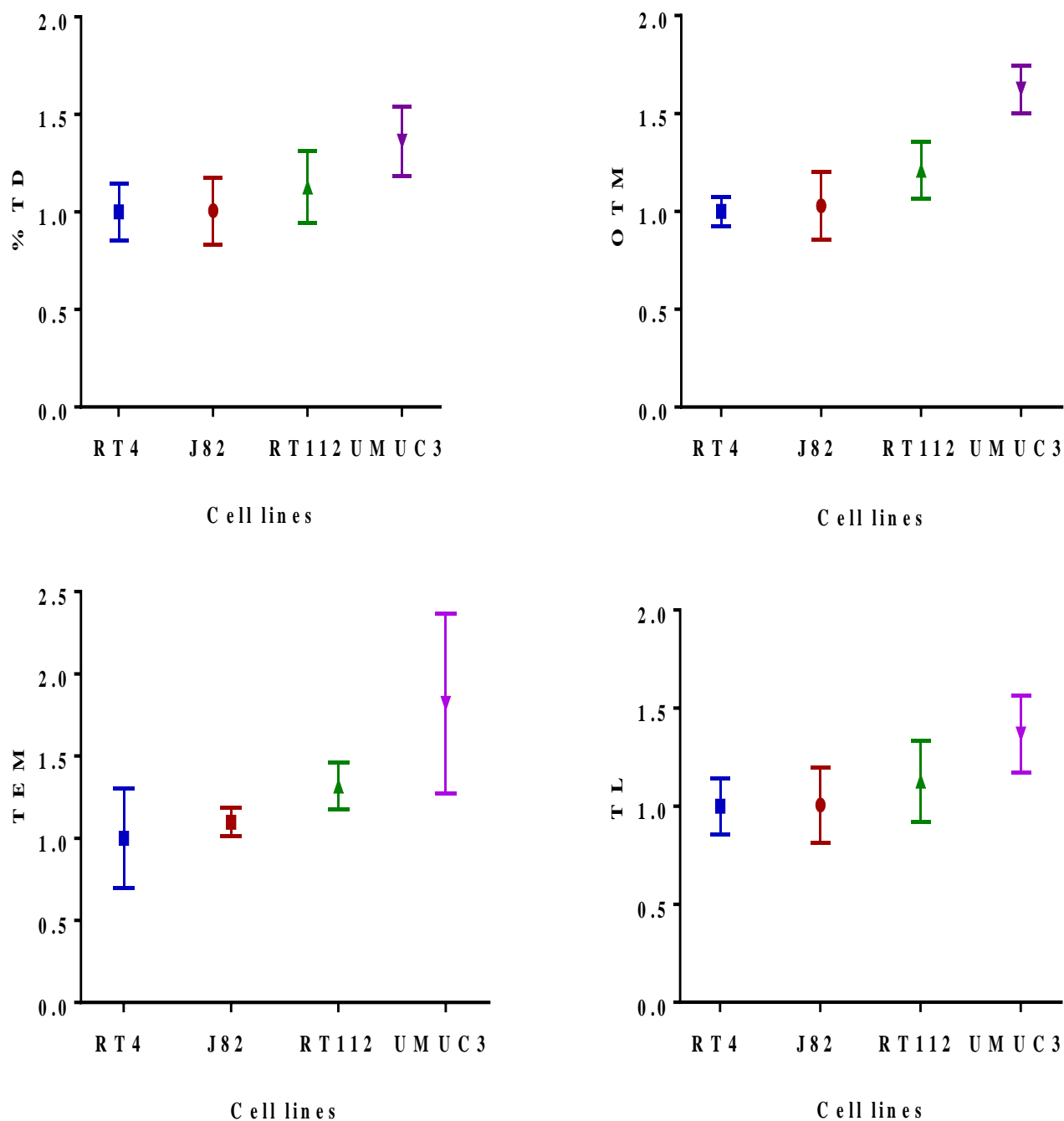
Two-way ANOVA with Tukey's multiple comparison test was used to assess any significant differences in the IR-induced comet formation between the four bladder cancer cell lines. The analysis revealed a clear differential response between the cells as measured by %TD. UMUC3 cells exhibited a significant response in comparison to RT4 cells (ANOVA: \*\*\* $p=0.0007$ ), J82 cells (ANOVA: \*\*\* $p=0.0008$ ), and RT112 cells (ANOVA: \* $p=0.0178$ ). Yet, Tukey's multiple comparison tests showed no observable significant differences between RT112 and J82 cells, RT112 and RT4 cells and between J82 and RT4 cells respectively. Data obtained from % TD parameter revealed the rank order for those cancer cell lines ranging from the lowest comet formation response to IR: RT4 > J82 > RT112 > UMUC3.

Furthermore, the extent of IR-induced comet formation response was measured via the OTM parameter. The result demonstrated that the response increased very significantly (ANOVA: \*\*\*\*  $p<0.0001$ ) following IR exposure for UMUC3 compared to RT4 cells, as well as UMUC3 compared to J82 cells (ANOVA: \*\*\* $p=0.0001$ ), and UMUC3 compared to RT112 cells (ANOVA: \*\* $p=0.0028$ ). However, the Tukey's multiple comparison tests showed no significant responses during comparative analysis between RT112 and RT4 cells, RT112 and J82 cells and between J82 and RT4 cells.

To further validate the above data, using TEM the UMUC3 cells exhibited significantly greater levels of comet formation response in contrast to RT112 cells (ANOVA: \* $p=0.0371$ ), J82 cells (ANOVA: \*\* $p=0.0034$ ) and RT4 cells (ANOVA: \*\* $p=0.0012$ ). Additionally, based

on the data obtained from the mean of TL parameter, there is a clear indication that RT4 cells had a less significant response to IR than UMUC3 cells (ANOVA: \*\*\* $p=0.0004$ ). A comparable situation was observed between UMUC3 and J82 cells (ANOVA: \*\*\* $p=0.0005$ ), and a significant comet formation response was observed via comparing UMUC3 and RT112 cells (ANOVA: \*\* $p=0.0122$ ).

**Overall**, these results indicated that RT4 cells had the least response, whilst UMUC3 cells showed the highest response to IR to induce comet formation. For %TD, TEM, OTM, and TL, the rank order for the four bladder cancer cell lines from lowest response to highest response to IR was as follows: RT4 > J82 > RT112 > UMUC3.

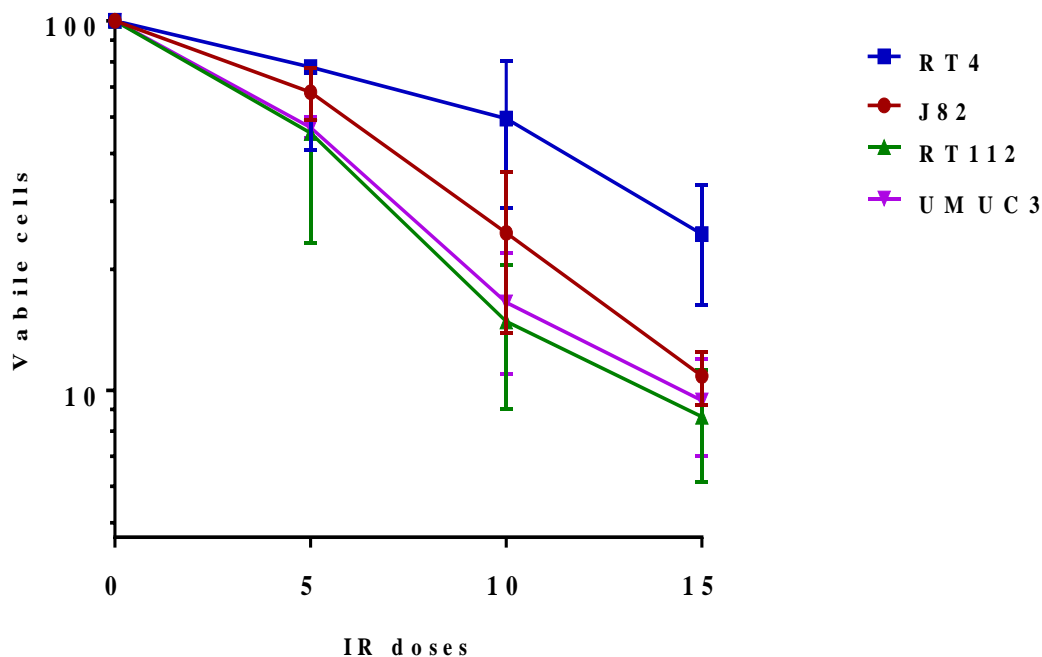


**Figure 3.11 Relative comet formation responses in bladder cancer cells after eliminating background/basal levels of DNA damage from each cell lines separately using ACA as assessed by (A) % TD, (B) OTM, (C) TEM, and (D) TL. Two-way ANOVA test was used to compare the average of relative comet formation response to IR doses between the four bladder cancer cell lines with the Tukey's multiple comparison tests (see text for further details).**

### 3.2.6 Assessment of RT4, J82, RT112 and UMUC3 bladder cancer cells viability following IR exposure by trypan blue exclusion assay

A brief separate study of cell viability was assessed by the trypan blue assay 7 days after exposure to 0, 5, 10, and 15 Gy of IR (Fig. 3.12). In each experiment, the effects of IR doses were compared with control sample cells (non-irradiated cells + complete medium). The trypan blue exclusion assay was used to calculate viable and dead cells in the irradiated bladder cancer cells. The trypan blue assay was performed in the next steps as indicated in Materials and Methods chapter.

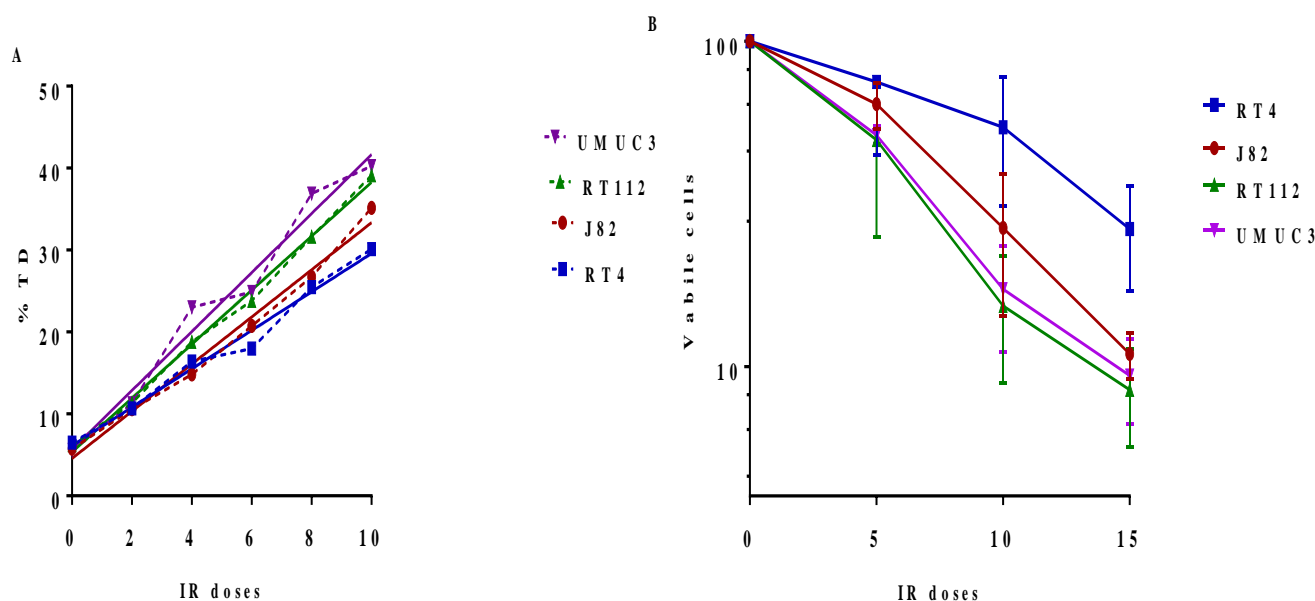
The effect of high IR doses (15 Gy) was more pronounced in UMUC3 and RT112 cells, which decreased cell numbers to below detectable limits. Nevertheless, there was no significant difference in meaning of cell growth in the four cell line. Overall, this assay reveals RT4 and J82 cancer cells to be the most radioresistant and UMUC3 plus RT112 cancer cells to be the most radiosensitive.



**Figure 3.12** The viable cell curve responses for the four bladder cancer cell lines investigated, over a dose range of 0–15 Gy, 7 days post irradiation as determined by trypan blue assay. Cell viability was determined % live vs dead cells following X-ray exposure.

### 3.2.7 Radiosensitivity in bladder cancer as assessed by Comet Assay and Trypan blue exclusion assay

With respect to the data observed in this chapter, additional analysis was performed on the above data, to study the effect of IR-induced DNA damage in UMUC3, RT112, J82, and RT4 cells. Simply, data from ACAs with the data from Trypan blue exclusion assay were used to compare SSBs (TD %) versus DSBs (cells viability) (Figure 3.13). Data clearly shows the difference in the quality of the DNA damage induced by ionising radiation. Analysis of the data demonstrates that IR-induced DNA DSBs formation, was entirely proportional to the level of IR-induced DNA SSBs. Interestingly, the cells with the highest amounts of DNA damages as assessed by %TD have lower levels of viable cells as assessed by cells viability assay and vice versa (Figure 3.13).



**Figure 3.13** (A) The extent of initial comet formation, as measured by mean %TD, for the four bladder cancer cell lines, over a dose range of 0–10 Gy, as determined by ACA. (B) The radiation cell viable curve responses for the four bladder cancer cell lines investigated, over a dose range of 0–15 Gy, as determined by trypan blue exclusion assay. For (A and B) each data point is the mean of three independent experiments.

### 3.3 Discussion

#### 3.3.1 ACA for evaluation DNA damage response (comet formation) in the four bladder cancer cell lines

The DNA molecule is the most important cellular target for the deleterious biological effects of ionising radiation. A wide variety of DNA lesions are formed post ionising radiation exposure (Jackson and Bartek, 2009a), such as SSBs and ALSSs. Several methods have been used to assess DNA damage post irradiation. ACA is widely used to measure DNA damage at the level of single cells (Collins, 2009). The ACA has several positive features that enables it to assess and predict radiation damage sensitivity in relation to cell radiosensitivity. For instance, it is simple and rapid to perform, and this assay does not require clonogenic cell growth; as it is carried out on single-cell suspensions from primary tumours and effects can be measured in the clinically relevant dose range (0–6 Gy). Thus, without doubt, these features are essential for this assay to be utilised within a clinical context (McKeown et al., 2003). Investigation of the utility of the ACA for determining tumour cell radiosensitivity has been limited to a few studies. Previously, studies of cell lines derived from transitional cell carcinoma (TCC) of the bladder cells were conducted to demonstrate that the ACA, in measuring DNA damage, is a good measurement of bladder cancer cells radiosensitivity *in vitro*, with both studies showing a strong inverse correlation between initial measures of comet formation and clonogenic survival (Moneef et al., 2003; McKeown et al., 2003).

Previously, using 6 bladder TCC cell lines (RT112, UMUC3, HT1376, J82, T24, and RT4), results have shown a strong, direct correlation between clonogenic cell death and radiation-induced DNA damage as assessed by the ACA (as illustrated in Figure 1.10), with a greater ACA response being noted in radiosensitive cells. The studied cell lines exhibit a range of radiogenic sensitivities, with J82 being the most sensitive to radiation-induced cell killing, and RT4 and HT1376 being the most resistant. Therefore, the rank order for initial comet formation matches the rank order of cell killing for all six cell lines ( $J82 > T24 > RT112 > UMUC3 > HT1376 > RT4$ ) (Moneef et al., 2003). This supported the hypothesis that the ACA might be useful in predicting radiosensitivity of individual cancer cell lines. Consequently, to estimate the level of radiation-induced comet formation in individual cells, without extracting the DNA, the ACA was implemented in this study (Singh et al., 1988).

Thus, to confirm the previous results, four bladder cancer cell lines (UMUC3, RT112, J82, RT4) were studied as culture cells models, following exposure to ionising radiation over a dose range (2, 4, 6, 8, and 10 Gy), and the non-irradiated sample (0 Gy) served for each cell line individually as the control. The ACA was used to assess bladder cancer cells damage sensitivity response to IR, as determined by the different comet parameters (%TD, OTM, TEM, and TL). The entire procedure was conducted is described in the Materials and Method (Chapter 2).

### **3.3.2 The effect of IR doses in the four bladder cancer cell lines as assessed via ACA**

The comet formation induced by IR significantly increased with increasing IR doses for the four individual bladder cancer cell lines (UMUC3, RT112, J82, RT4). With certain cell lines exhibiting increased comet formation measures, and others lower measures of comet formation, as determined by the ACA parameters %TD, OTM, TEM, and TL. Analysis of the data has shown that there was a significant response of immediate comet formation for the four bladder cancer cell lines which were evaluated as determined by %TD, OTM, TEM and TL over a dose range of 2, 4, 6, 8, and 10 Gy when compared with the non-irradiated control sample independently, as shown in Figures 3.1, 3.2, 3.3 and 3.4. This response confirmed that the level of comet formation for the four bladder cancer cell lines increased progressively when these cell lines were exposed to increasing IR doses (Figure 3.5).

In Figure 3.6, a linear relationship between comet formation and the IR doses was independently identified for each parameter of the comet assay (% TD, OTM, TEM, and TL) over a dose range of 0-10 Gy. The results illustrated a clear dose response in terms of the induced comet formation in the four bladder cancer cell lines. All the results indicated that the level of IR-induced comet formation was highest in the UMUC3 cell line whilst RT4 cell line showed the lowest levels of comet formation.

The level of IR-induced comet formation was measured with the endogenous response excluded from each IR dose result for the four bladder cancer cell lines. The results were then plotted to illustrate the differences. The results confirmed the previous finding in



Figures 3.6a & b and 3.9a & b, as the measures of mean %TD, OTM, TEM increased with dose due to the dose dependency of radiation-induced comet formation responses. Since the DNA damage response is directly proportional to the radiation dose, any changes in radiation dose should be reflected in the comet measurement (Kumaravel et al., 2009). Based on the data obtained within the present study, it is apparent that UMUC3 cancer cells are more susceptible to IR-induced comet formation.

The initial results of IR-induced comet formation with exclusion of the endogenous DNA response results in the four bladder cell lines suggested that the level of IR-induced comet formation observed in RT112 and UMUC3 bladder cancer cells was higher than that in J82 and RT4 bladder cancer cells. These findings are important as these differences may reflect actual differences in tumour cell radiosensitivity; with the observation of higher degrees of comet formation in the UMUC3 cell line and lower comet formation in RT4 cell line as detected by the ACA.

It was evident that the UMUC3 cell line showed a higher level of IR-induced comet formation, which was depicted from the four comet parameters recorded, compared with RT4, J82, and RT112 cell lines and RT4 cell line was revealed to be the cell line displaying the lowest comet formation response post radiation exposure (as shown in Figures 3.6a&b, 3.8, and 3.9a&b, and 3.11).

This study indicated the ACA to be an efficient measure of bladder cancer cell radiosensitivity *in vitro* and shows the assay's potential to be implemented within clinical tests; as this assay requires a small number of cells and results can be available within a few hours (Fairbairn et al., 1995). Interestingly, further studies also showed similar trends for chemo sensitivity, with greater ACA measurement of cisplatin and MMC-induced crosslinks correlating with higher bladder cancer cell chemo sensitivity, as determined by both clonogenic and MTT assays (Bowman et al., 2012).

The results are supported by two independent studies investigating bladder tumour cells. McKeown et al. (2003) and Moneef et al. (2003) shown that the induction and repair of radiation-induced DNA damage, as measured by the ACA, correlates bladder cancer cell radiosensitivity *in vitro* with the extent of comet formation. In addition, cells from human bladder tumour biopsies revealed a wide range of predicted radiosensitivities as determined

by ACA (Colquhoun et al., 2003; Moneef et al., 2003; Bowman et al., 2012). Additionally, this result has been confirmed by other studies on colorectal tumour cells (Dunne et al., 2003) suggesting that the ACA is vital and can be used in different tumour types and different laboratories. Overall, these studies demonstrated ACA to be a good predictive measure of bladder cancer cell radiosensitivity at clinically relevant doses, with potential clinical application (Bowman et al., 2014).

However, it has previously been shown that some constants in the ACA protocol, such as the concentration of low melting point agarose and time of the electrophoresis, seem to have an important impact on the results of the experiment (Möller et al., 2010; Azqueta et al., 2011). McKeown et al., (2003) recommended that since radiation-induced DNA damage is repaired very rapidly, the prepared cells need to be irradiated embedded in gels on slides on ice and then be placed in ice-cold lysis solution immediately following irradiation. Furthermore, it is noted that some DNA repair does occur if cells are embedded in warm agarose following irradiation, and even if pre-embedded cells are irradiated at room temperature, in comparison to those on ice, and a smaller amount of damage is obtained. Thus, every effort must be made to minimise DNA damage repair process during radiation exposure, and up to the time of lysis. It is therefore critical that cells are pre-embedded and cooled on ice for any study analysis using the ACA to measure initial/immediate radiation-induced DNA damage (McKeown et al., 2003). For this reason, all the experiments which belong to this protocol were done and repeated under the exact laboratory condition, and with the same equipment to avoid or minimise variations in the results as much as possible.

The finding of this study clearly demonstrated that the ACA would be a good predictive measure of bladder cancer cell sensitivity which may distinguish the response range between the bladder cancer cell lines' radiosensitivity (Moneef et al., 2003; Bowman et al., 2012).

The length of DNA migration, referred to as the TL which is measured from the center of the head or the end of the head to the end of the tail, was the first comet measurement outcome used to quantify DNA response (Kumaravel et al., 2009). Tail Length determines how far the damaged DNA has migrated out of the cell. Therefore, TL is directly related to the loops of released DNA or the size of DNA fragments, and it can be associated to the amounts of strand breakage and alkali-labile sites (Collins et al., 1997). Smaller DNA

fragments move furthest, thus, TL is determined by the size of the DNA fragments which are produced during the alkaline unwinding step of the comet assay protocol. Exposure of DNA to alkaline conditions at pH greater than 13.0 cleaves alkali-labile sites as DNA strand-breaks (Singh et al., 1988), this in turn releases fragments of broken DNA as well as relaxes the loops of super-coiled DNA near the sites of cleavage. During electrophoresis, the DNA fragments, as well as relaxed DNA loops, move towards the anode producing the tail of the comet. The DNA fragments tend to move freely during the electrophoresis, whereas the relaxed DNA loops are pulled out of the nuclear head due to unwinding of the supercoiled DNA, these can present slow mobility during electrophoresis. Variations in these relaxed DNA loops are therefore not detected when TL is used as the sole comet measurements. Moreover, the small fragments of DNA tend to accumulate and therefore, no additional increase in DNA length can occur during elevated levels of DNA damage (Kumaravel and Jha, 2006). Thus, in Figures 3.6 and 3.9, the TL was limited at high radiation dose, as the curves started quite steep but then gradually plateau at higher doses. Subsequently, it can be speculated that TL in the four bladder cancer cells was nearly the same, and the plot revealed less clear differential dose response curves for the four bladder cancer cells, when the cell lines were exposed to IR over a dose range of 0, 2, 6, 8 and even at 10 Gy. This observation of less of a differential effect being noted for TL (compared to the dose responses noted for the other parameters) tends to support the first theory/hypothesis for the differential measurements of comet formation: in that, the actual differential measures of comet formation reflect actual differences in DNA damage formation between the four bladder cancer cells; if more adjacent loops were released this should lead to longer tails in the more Comet assay responsive cells.

Robust Comet assay data and interpretation depend on good and optimum slide staining, adoption of robust image analysis practices and use of reliable and meaningful Comet Assay measurement (e.g. % Tail DNA or OTM). As OTM values can differ widely between laboratories and/or with different software packages, % Tail DNA is considered appropriate for regulatory or inter-laboratory comparison studies. Moreover, for all studies that involve multiple electrophoresis runs, it is recommended that % Tail DNA be used to reduce variability in the results. It is generally accepted that visual scoring is as comparable as image analysis; however, image analysis can provide additional information (e.g. determination of

the cell cycle status of cells by measuring their DNA content) that may be important in the characterisation of the genotoxicity of some compounds (Kumaravel et al., 2009)

### **3.3.3 Evaluation of IR-induced DNA damage formation through counting cells viability**

Data obtained from this experiment revealed that RT4 and J82 bladder cancer cells exhibit a substantially higher level of viable cells in contrast with RT112 and UMUC3 bladder cancer cells (Figure 3.12). Data obtained by this method agrees with the results obtained using the ACA. Thus, the cells with the highest amounts of DNA damages as assessed by %TD have lower levels of viable cells as assessed by cells viability assay and vice versa. Thus, the rank order for initial comet formation matches the rank order of cell killing for all four cell lines ( $UMUC3 \geq RT112 > J82 > RT4$ ).

However, to substantiate this observation, further analysis was done to confirm this finding. The ACA results were compared with an analytical method such as liquid chromatography-tandem mass spectrometry (LC-MS/MS), pulsed field gel electrophoresis (PFGE) and  $\gamma$ -H2AX to assess bladder cancer cell lines' damage sensitivity. If an equivalent differential response noted for these assays is identified, this indicates that the comet assay indeed measured differences in induced DNA damage between the bladder cancer cell lines (Hypothesis 1). However, an absence of a differential effect for the analytical methods might indicate that the differential effect noted from the comet assay measures was possibly due to the additional release of the adjacent/contiguous loops of DNA (Hypothesis 2).

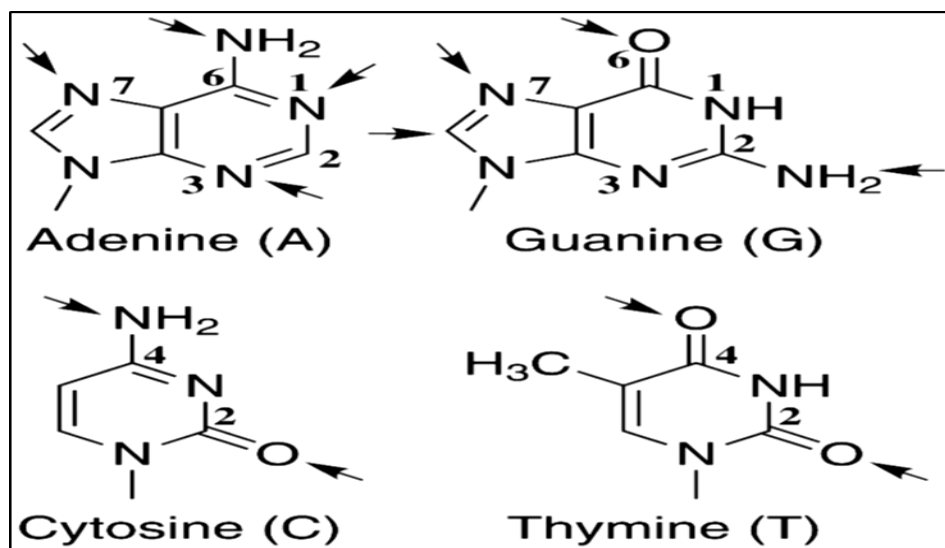
## **Chapter 4**

### **Liquid chromatography-tandem mass spectrometry (LC-MS/MS) for determination of ionising radiation-induced 8-oxodG in bladder cancer cell**

## 4.1 Introduction

### 4.1.1 Formation of DNA base adducts

Structural modifications of nucleobases in DNA of living cells can be induced following their exposure to endogenous and exogenous genotoxic agents and can result in DNA adduct formation (Kriaucionis and Heintz, 2009; Jin et al., 2011). Such structural DNA base modifications can include alkylation, oxidation, deamination and cross-linking, all of which can occur at various sites on the nucleobases. Such sites include the N-7, O-6, C-8 and N-2 of guanine, the N-1 and N-3 and the N-7 of adenine and the O-2 and O-4 of thymine and of cytosine (Singer and Grunberger, 2012), as illustrated in Figure 4.1. A large body of evidence demonstrates that DNA adducts are useful markers of radiation and another carcinogen exposure (Pernot et al., 2012b). Consequently, DNA adducts have been widely measured in human biological samples as markers of possible cancer risk. The most commonly studied DNA adduct biomarker for oxidative stress is 8-oxo-7, 8-dihydro-2'-deoxyguanosine (8-oxodG) (Bauchinger, 1997) and 8-oxo-7, 8-dihydro-2'-deoxyadenosine (8-oxodA) (Kamiya et al., 1995b).



**Figure 4.1** An illustration of the various DNA sites frequently modified by carcinogens and their metabolites (Tretyakova et al., 2013).

Humans are consistently exposed to the genotoxic carcinogens throughout their lives (Wogan et al., 2004; Luch, 2005); primarily through occupational exposure to genotoxic carcinogens or via diet and environmental pollution (Thier and Bolt, 2001). Carcinogens play a fundamental role in the initiation of carcinogenesis via the formation of mutagenic DNA adducts. These DNA adducts may lead to a myriad of alterations and cellular end-points, including, but are not limited to, cell death, mutations in the genome and aberrant cell cycle control. For instance, the types of mutations induced by polycyclic aromatic hydrocarbons (PAHs) in the p53 tumour suppressor gene in bronchial epithelial cells match the main mutations observed in smoking-induced human lung cancers, which suggests that PAHs are involved in lung carcinogenesis (Denissenko et al., 1996, Smith et al., 2000). In addition, increases in the level of environmental air pollution in industrial cities can induce genotoxic carcinogenesis, by means of polycyclic aromatic hydrocarbons (PAHs) (Perera et al., 1992; Schoket, 1999). Moreover, tobacco smoke, which contains ~4,000 chemicals of which ~60 are classified as carcinogens in humans and animals, significantly increases human exposure to genotoxic carcinogens (Wiencke, 2002; Phillips, 2002; Hecht, 2003). Thus, determination of the nature and extent of DNA adduct formation, together with (if possible) the position of these adducts within the DNA structure, may play a role in the assessment of carcinogenic hazards and possibly the risks (Singh and Farmer, 2006). Therefore, DNA adducts can be reliable markers for identification of carcinogens exposure, including for example, radiation exposure (Pernot et al., 2012b). Dipple (1995) reported that several genotoxic carcinogens can impact the DNA directly, but most of them require metabolic activation to form the electrophilic reactive species that covalently bind to nucleophilic sites in the DNA. However, the existence of DNA adducts may not trigger an immediate mutation, as these lesions are often subjected to repair processes before cell division (Dipple, 1995). Nonetheless, if DNA adducts are not accurately repaired, the result can play a crucial role in inducing cancer formation (Singh and Farmer, 2006).

#### **4.1.2 Oxidative DNA damage**

ROS can be generated in response to both endogenous and exogenous oxidising sources (Ushio-Fukai and Nakamura, 2008; Galaris et al., 2008). DNA adduct damage can result endogenously from ROS originating from cellular metabolism and inflammatory responses

(Cadet et al., 2003b), or by exposure to exogenous agents such as mineral fibres and IR (Frenkel, 1992; Loft and Poulsen, 1996). ROS can also act as signalling molecules to facilitate cell growth, migration, and differentiation under physiological concentrations (Valko et al., 2006). However, under continued environmental stress (derived from long-term chronic exogenous exposure), ROS can be continuously produced, and their effects can accumulate over time leading to a significant level of damage. This may occur within the cell structure and disrupt its functions including signal transduction, cellular proliferation, differentiation and apoptosis (Chandra et al., 2000; Valko et al., 2006), and such disruption in function can induce somatic mutations and initiate neoplastic transformation (Fang et al., 2009; Khandrika et al., 2009). Indeed, due to increasing DNA mutations in critical genes, such as those involved in the regulation of cellular growth, cancer can develop (Visconti and Grieco, 2009). Oxidative damage is linked to several human diseases (Franco et al., 2008; Valko et al., 2006), however, at high levels DNA mutations can also induce cell death (Chandra et al., 2000; Valko et al., 2006).

The DNA adduct biomarkers are typically used to study for oxidative stress. The formation of DNA adducts results from the covalent interaction of genotoxic carcinogens with DNA. The formation of 8-oxodG can lead to chromosomal aberrations and the induction of mutations, which primarily involves GC to TA transversions (Grollman and Moriya, 1993). The formation of 8-oxodA can induce mutations that involves TA to GC transversions (Kamiya et al., 1995; Tan et al., 1999). The DNA repair systems are responsible for eliminating nucleobase lesions. The main repair pathway for 8-oxodG and 8-oxodA adducts in DNA involves glycosylase repair enzymes which remove the modified base by excision following cleavage of the N-glycosidic bond (Klungland and Bjelland, 2007). Accordingly, DNA adduct structure and formation levels or the location of adducts within the DNA structure have a key role in the chemical carcinogenesis. As DNA adducts are characterised as critical biomarkers of carcinogen exposure (Tretyakova et al., 2013, Singh and Farmer, 2006), DNA adducts can be utilised to evaluate carcinogenic risks (Singh and Farmer, 2006).



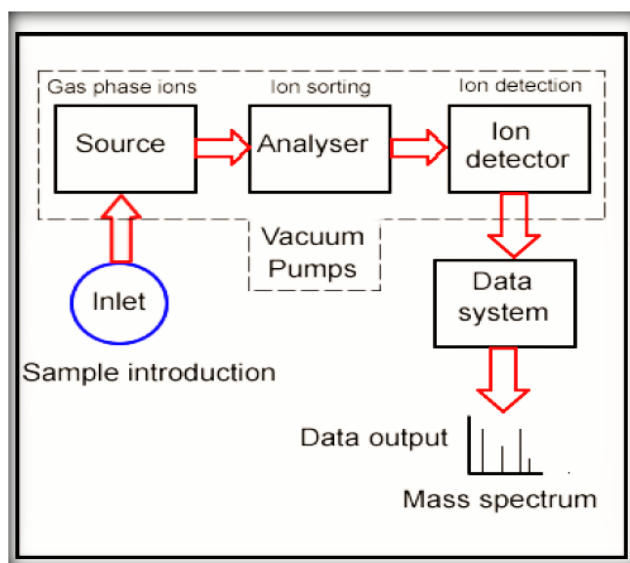
### **4.1.3 Liquid chromatography/mass spectrometry in the analysis of DNA adducts**

Recently, the development of liquid chromatography (LC) coupled to a mass spectrometer (MS) and its application for the identification of new DNA adducts or for detection and measurement of previously identified DNA adduct has been described within many comprehensive studies as a useful method for the quantification of DNA adducts level in animal and human samples post exposure to exogenous and endogenous genotoxic compounds (Farmer et al., 1988; Esmans et al., 1998; Andrews et al., 1999; Griffiths et al., 2001; Doerge et al., 2002; Koc and Swenberg, 2002; Watson et al., 2003; Lim and Lord, 2002; Banoub et al., 2005). Mass spectrometers operate by converting the analyte molecules to a charged (ionised) state, with subsequent analysis of the ions and any fragment ions that are produced during the ionisation process, based on the mass to charge ratio ( $m/z$ ) (Pitt, 2009a).

#### **4.1.3.1 Instrumentation of mass spectrometric detection**

A mass spectrometer (MS) is a device that is used to measure the mass-charge ratio of charged particles ( $m/z$ ). The basic mass spectrometry processes and instrumentation consist of: (1) the inlet system for sample introduction; the sample that is loaded can be a solid or liquid that is vaporised or indeed it can be a vapour. (2) The sample components are then ionised by one of several available methods to create ions; (3) the ions are then sorted in an analyser according to their  $m/z$  ratios through the use of electromagnetic fields; (4) the ions then pass through a detector where the ion flux is converted into a proportional electrical current; and finally (5) the magnitude of the ion/electrical signals is converted into a mass spectrum for data output (Watson and Sparkman, 2007; Grebe and Singh, 2011b; Madeira and Florêncio, 2012), as illustrated in Figure 4.2. Apart from these major components, the mass spectrometer requires two fundamental supplementary components. Firstly, a device that can bring samples in a suitable form to the inlet/vaporiser. Secondly, a device for signal processing/data reduction of detector signals, in the form of analogue-digital converter (usually part of the mass spectrometer) and a combination of firmware and computer software for data reduction, display, analysis, and quantification of detection events (Pitt,

2009a; Grebe and Singh, 2011b). The MS technique has both qualitative and quantitative uses. These include identifying unknown compounds, determining the isotopic composition of elements in a molecule, and determining the structure of a compound by observing its fragmentation. The focus of this project was to detect DNA adducts by LC-MS/MS, and tandem mass spectrometry will now be explained further.



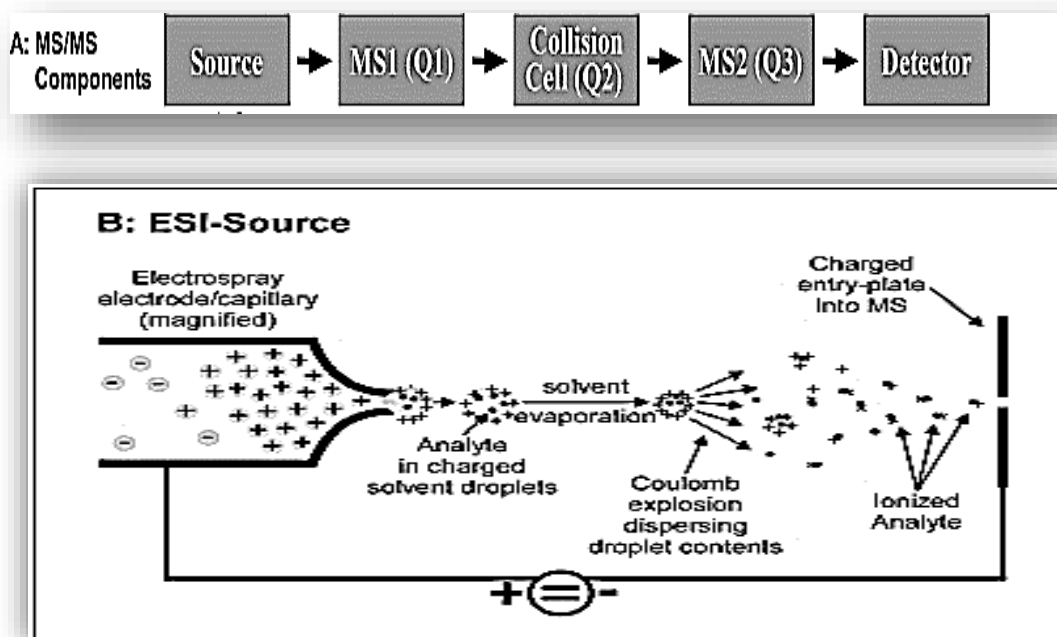
**Figure 4.2** Simplified diagram and function of instrumentation of typical mass spectrometry (Madeira and Florêncio, 2012).

#### 4.1.3.2 Tandem mass spectrometry (MS/MS)

LC-MS/MS is used for the evaluation of oxidative DNA damage. The LC-MS/MS is used to detect levels of DNA adducts at the level of 0.1–1 adducts per  $10^8$  unmodified DNA bases using low microgram amounts of DNA. This involves the use of multiple mass analysers which are used in DNA adduct analysis. Commonly used are triple quadrupole linear ion-trap mass spectrometers which allows for quantitative data to be obtained (Hopfgartner et al., 2004).

A LC-MS/MS instrument consists of an atmospheric pressure ionisation source (Figure 4.3A), typically an ESI source (Figure 4.3B) or an atmospheric pressure chemical ionisation (APCI) source, coupled by an ion-inlet and focusing component (Q0) which provides both transition from atmospheric pressure to vacuum and ion-focusing. This leads into a first mass-filtering device (Q1), which leads into a collision chamber (Q2) that can be filled with

low-pressure gas for collision-induced dissociation (CID) of an ionised molecule which leads to reproducible fragmentation. This is followed by a second mass-filtering device (Q3), and finally an ion-impact detector (electron multiplier) (Figure 4.3A) (Roboz, 2002; De Hoffmann and Stroobant, 2007; Grebe and Singh, 2011b).

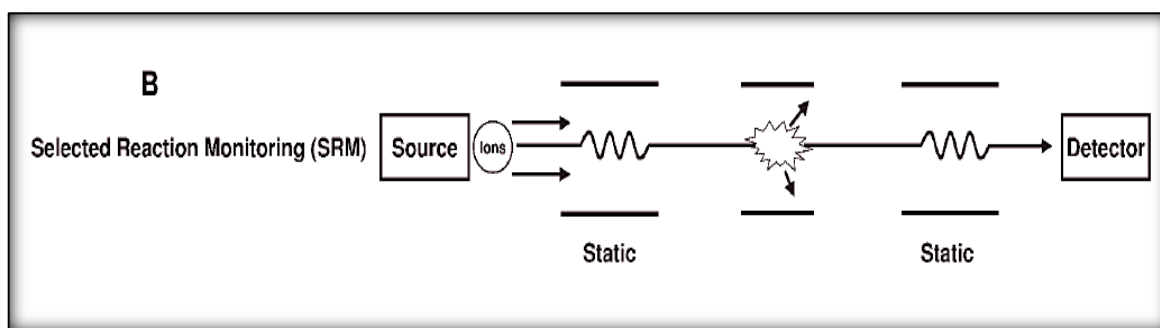


**Figure 4.3 Principal components of a tandem mass spectrometer.** (A) The sample is ionised in the source, and passes into the 1<sup>st</sup> mass filter (Q1), then into the collision cell (Q2), followed by the 2<sup>nd</sup> mass filter (Q3), and finally the detector (Grebe and Singh, 2011b) (B) The ionisation method (electrospray ionisation (ESI)) which is used in current clinical LC-MS/MS instruments.

In electrospray ionisation (ESI), the solvent-analyte flow from the LC passing into the source through a positively charged, very narrow capillary, and gets nebulised as microscopic, positively charged solvent-analyte droplets. These droplets fly towards the negatively-charged faceplate, with solvent evaporating on the way, until they disintegrate in a Coulomb explosion when the repulsive charge of their ionised components exceeds their surface tension. The individual ionised analyte molecules then pass through the faceplate entry hole into the mass spectrometer (Grebe and Singh, 2011b).

#### 4.1.4 The detection method for determination of DNA adducts

The selected reaction monitoring detection method (SRM) which is also referred to as multiple reaction monitoring (MRM) (Figure 4.4) can enhance levels of sensitivity and allow for greater specificity. The LC-MS/MS (SRM) method utilises online column-switching valve technology for the determination of DNA adduct biomarkers of oxidative stress allowing the direct analysis of enzymatically hydrolysed DNA samples (Brink et al., 2006; Chao et al., 2008). This method allows for fully automated sample clean-up and a reduction in ion suppression from matrix components which can interfere with the analysis (Doerge et al., 2000; Koc and Swenberg, 2002).



**Figure 4.4** Schematic representation of the main detection modes of a triple quadrupole mass spectrometer that have been used to study DNA adducts (Singh and Farmer, 2006).

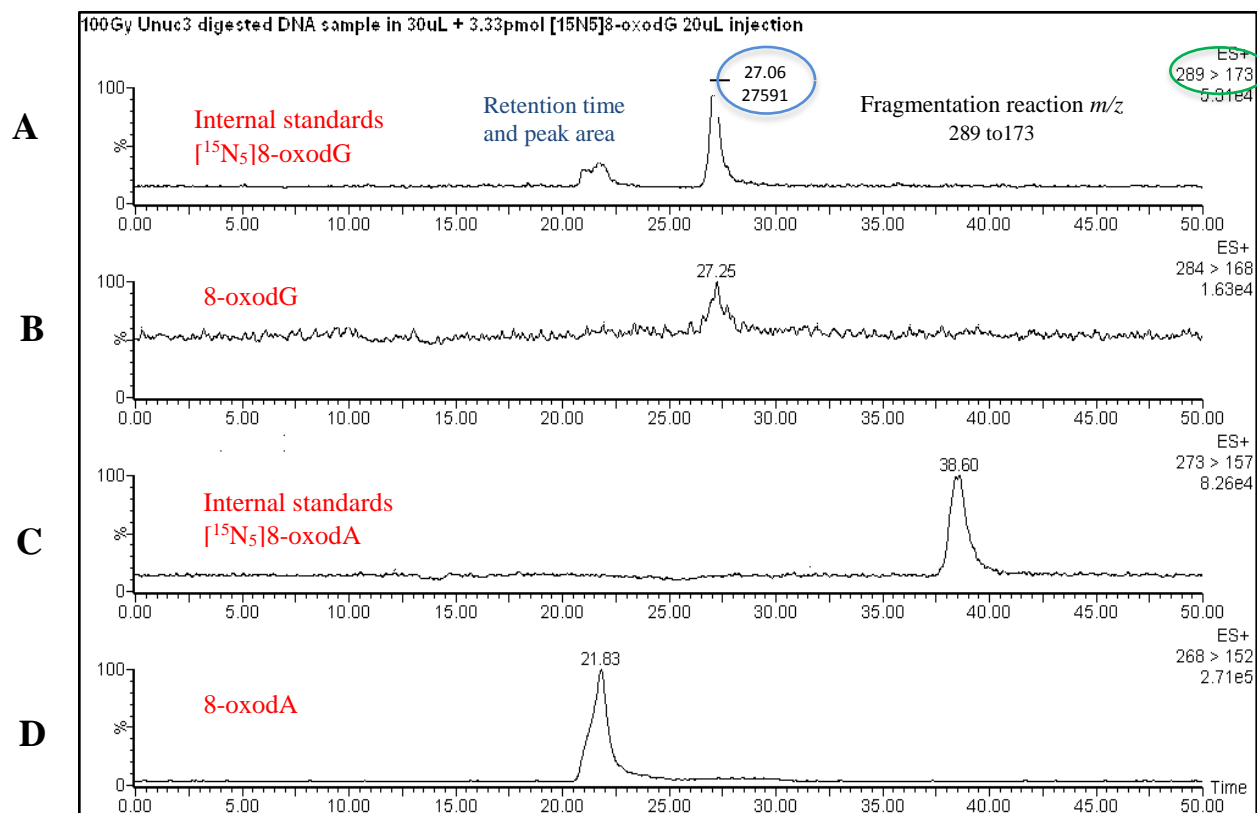
##### 4.1.4.1 Online column-switching system

Incorporating online column-switching into the method can help in improving the sensitivity by retaining the analyte of interest on a trap column while impurities are washed to waste. Then, when the switching valve reverses the flow, the analyte gets back-flushed and transferred onto the analytical column for separation, as illustrated in Chapter two (Figure 2.3) (Roboz, 2002; De Hoffmann and Stroobant, 2007).

For the present study, the 8-oxodG and 8-oxodA adducts are collected on a trap column while unmodified 2'-deoxynucleosides are eluted to waste. The switching valve then diverts the flow from the trap column into the analytical column, which is connected to the mass spectrometer allowing the direct analysis of the 8-oxodG and 8-oxodA adducts by LC/MS/MS SRM. This approach increases sample amount while reducing matrix effects and ionisation suppression.

### 4.1.5 General information about the chromatograms

Figure 4.5 shows typical chromatograms for analysis of the 8-oxodG and 8-oxodA adducts using LC-MS/MS SRM. The information that can be taken from a chromatogram is shown and aids the understanding of chromatograms presented in this chapter.



**Figure 4.5** Typical chromatogram obtained for the analysis of the 8-oxodG and 8-oxodA and its labelled standard using LC-MS/MS SRM. Details that can be taken from LC-MS/MS SRM chromatograms presented in this chapter. The presented LC-MS/MS SRM chromatograms reflects one sample injection by LC-MS to give the 4 monitored channels where the red labelling explains what compound is detected in this channel, blue states the peaks retention time (top value in circle) and area (bottom value in circle) and the green label points out which fragmentation is being monitored. LC-MS/MS SRM chromatogram A represents the channel monitoring the internal standard  $[^{15}\text{N}_5]$  8-oxodG. LC-MS/MS SRM chromatogram B monitors the 8-oxodG fragmentation reaction  $m/z$  284 to 168 which is used to quantify the adduct. LC-MS/MS SRM chromatogram C represents the channel monitoring the internal standard of  $[^{15}\text{N}_5]$ 8-oxodA. Finally, LC-MS/MS SRM chromatogram D monitors the 8-oxodG fragmentation reaction  $m/z$  268 to 152 which is used to quantify the adduct

To allow an accurate quantification of 8-oxodG and 8-oxodA adducts, known amounts of the corresponding synthesised [ $^{15}\text{N}_5$ ]-labelled stable isotope internal standards were added prior to the enzymatic hydrolysis of the DNA treated samples from the four bladder cancer cell lines (UMUC3, RT112, J82 and RT4) to 2'-deoxynucleosides. The LC-MS/MS protocol used requires between 10 and 40 $\mu\text{g}$  of hydrolysed DNA on-column for the analysis, and the limit of detection for both 8-oxodG and 8-oxodA adducts was 5fmol. The level of 8-oxodG and 8-oxodA adducts within each DNA sample was determined from the ratio of peak areas of the internal standards for [ $^{15}\text{N}_5$ ]8-oxodG and [ $^{15}\text{N}_5$ ]8-oxodA adducts to the peak areas of the analyte, respectively.

## **4.2 Aim**

The aim of this Chapter is to compare the relative differential measures of radiation-induced comet formation as determined by ACA for the four bladder cancer cells lines (reported in Chapter 3) with analogous analytical measure of radiation-induced 8-oxodG adduct formation as determined by LC-MS/MS. If the differential measures observed by the Comet assay are matched by those of LC-MS/MS analysis then it can be deduced that the differential extent of radiation-induced comet formation noted between the four bladder cancer cell lines indeed reflects distinct levels of DNA damage. However, if the differences in the comet measure are not reflected in the analytical LC-MS/MS measures (with LC-MS/MS showing equal levels of radiation-induced 8oxodG adducts between the different bladder cancer cell lines), this would indicate that the same level of DNA damage is induced in the bladder cancer cell lines. Within this context, it can be speculated that the greatest extent of comet formation was simply due to a greater electrophoretic release and migration of nucleoid DNA from comet head to the tail of the comet.

## **4.3 Summary of the techniques/approach**

Each of the four bladder cancer cell lines were exposed to various IR doses, after which the genomic DNA was purified. Following preliminary comparative experiments for the consideration of the quantity and quality of the DNA recovered, all future work was undertaken using the Maxwell 16 cell DNA purification kit to extract and purify the DNA.

The concentration of the extracted DNA was measured, then the extracted DNA was treated with digestion enzymes. The hydrolysed DNA samples were centrifuged, and the supernatant solution from each sample was transferred to HPLC vials containing low volume inserts for analysis by online column-switching LC-MS/MS for the detection of DNA adducts (Chao et al., 2008; Brink et al., 2006). This method was applied for the detection of 8-oxodG and 8-oxodA adducts in enzymatically hydrolysed DNA samples obtained from the bladder cancer cell lines (UMUC3, RT112, J82 and RT4). LC-MS/MS technique utilises full automated sample clean-up leading to a reduction in ion suppression from matrix components that could undoubtedly interfere with the analysis (Doerge et al., 2000, Koc and Swenberg, 2002). The materials and methods used for this Chapter have been described in detail in Chapter 2.

## **4.4 Results**

### **4.4.1 The analysis of the prepared DNA bladder cancer cell samples that exposed to (0, 20 and 100 Gy of ionising radiation doses)**

#### **4.4.1.1 Optimised method for the genomic DNA extraction**

Three different methods were used for DNA extraction from the four bladder cancer cell lines to acquire the accurate amount of genomic DNA, and to achieve an accurate degree of results:

- DNA extraction by Maxwell 16 Cell DNA Purification.
- DNA extraction by Qiagen Blood & Cell culture DNA Kit.
- DNA extraction by Wako DNA Extractor.

However, for the use of Wako DNA Extractor and Qiagen Blood & Cell culture DNA Kits no consistent or appropriate amount of the extracted DNA was obtained by these two methods, which needed to be at least to 30µg in total for each individual sample. On the other hand, using the Maxwell 16 Cell DNA Purification for DNA extraction, enough DNA was obtained by this procedure, within a brief timeframe (~35mins in total), to be able to analyse the samples in triplicates during each trial to achieve enough DNA for analysis (though this did require repeated extractions and pooling of the samples for analysis). Thus, conclusive results were achieved via use of the Maxwell 16 Cell DNA Purification method. (For information: the methods for the Wako DNA Extractor and Qiagen Blood & Cell culture DNA Kits are provided in an Appendix at the end of this thesis.)

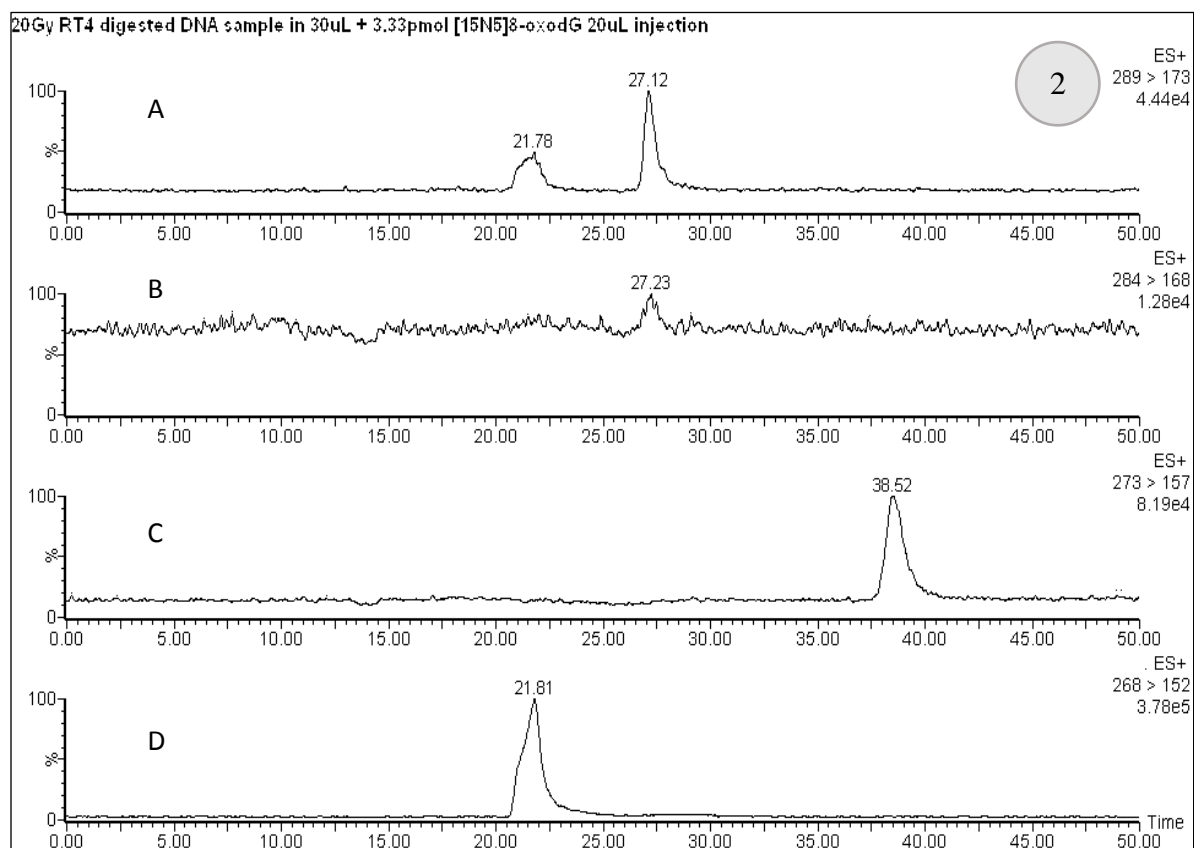
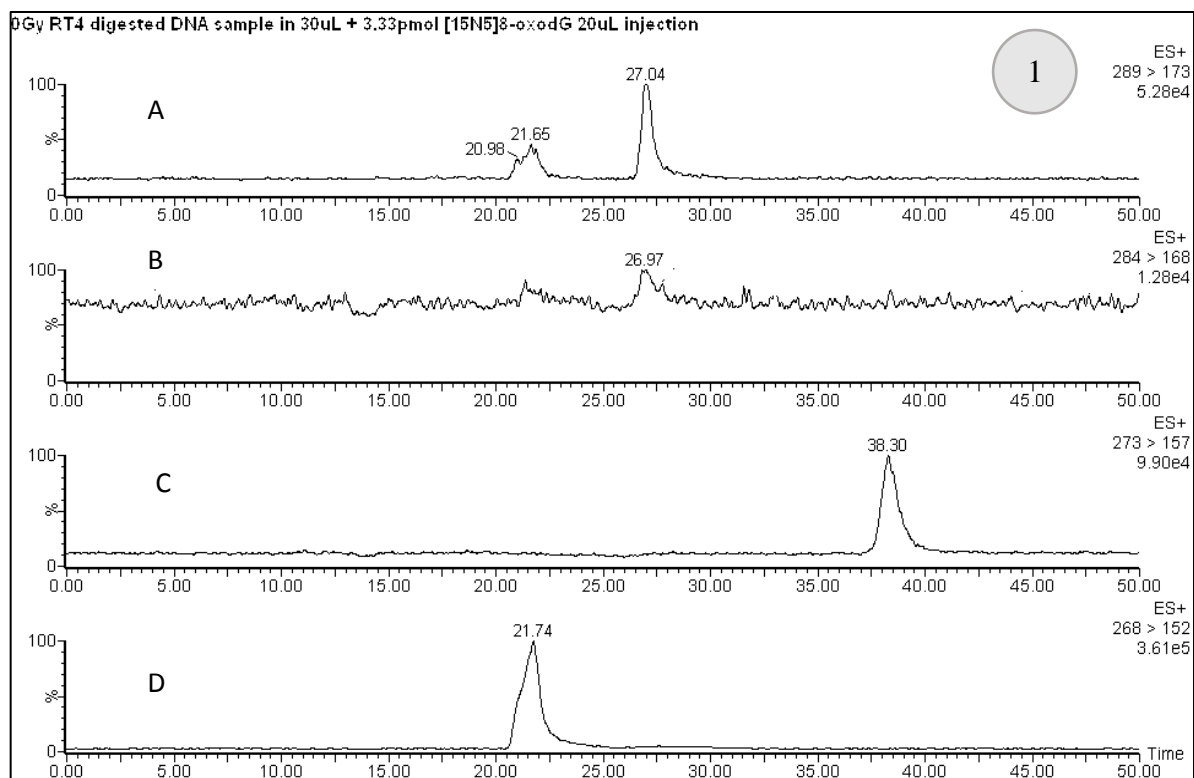
#### **4.4.1.2 Standards**

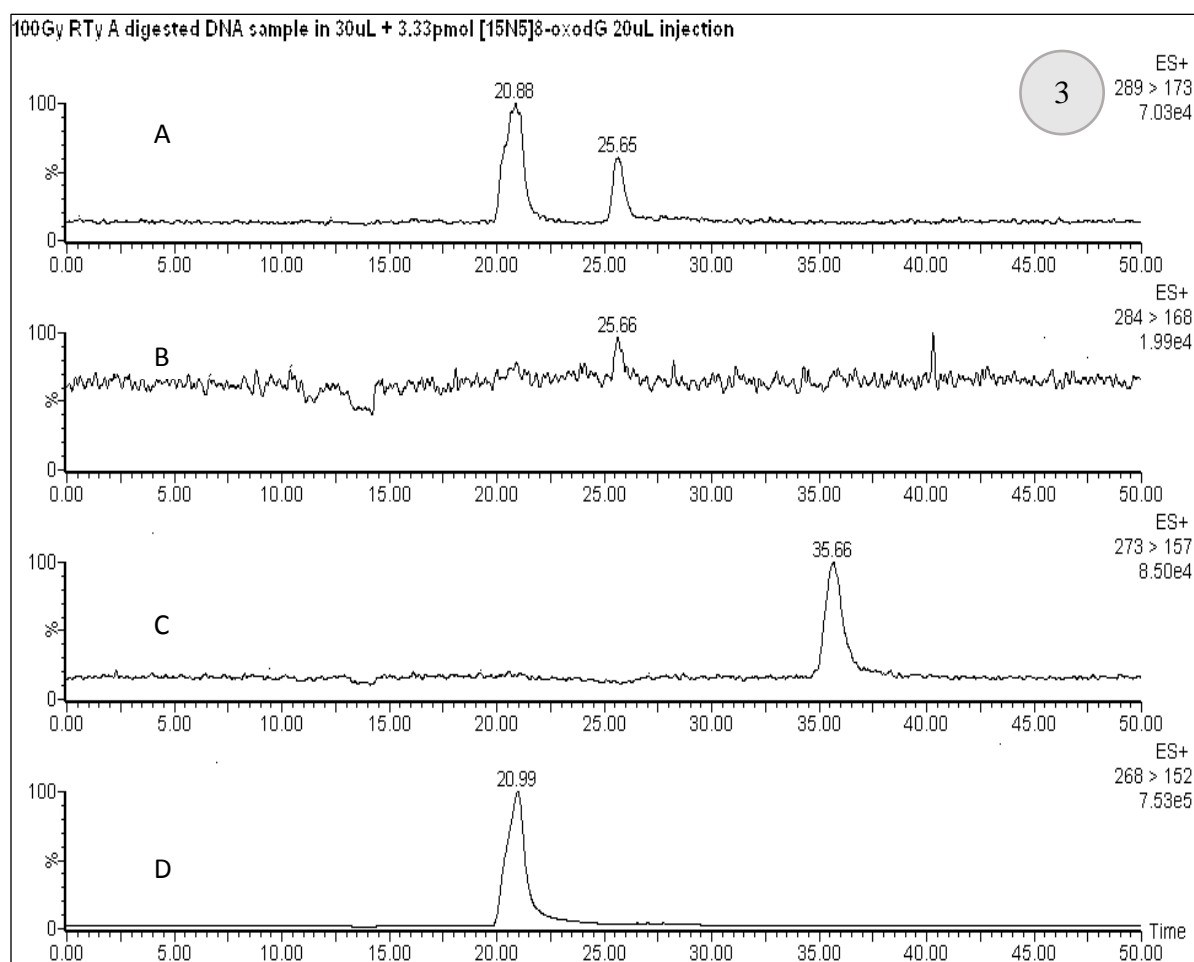
5 µL (5.0pmol) of each stable isotope internal standards [<sup>15</sup>N<sub>5</sub>]8-oxodG and [<sup>15</sup>N<sub>5</sub>]8-oxodA (each at 1pmol/µL) were added to 30µg of each prepared DNA sample, obtained from the four bladder cancer cell lines, to account for any matrix effects. Each of the samples containing the standards was then subjected to the entire analytical procedure including enzymatic hydrolysis. The amount of [<sup>15</sup>N<sub>5</sub>]-labelled stable isotope internal standard DNA adduct per sample was 3.33pmol ( $3.33 \times 10^{-12}$  moles).



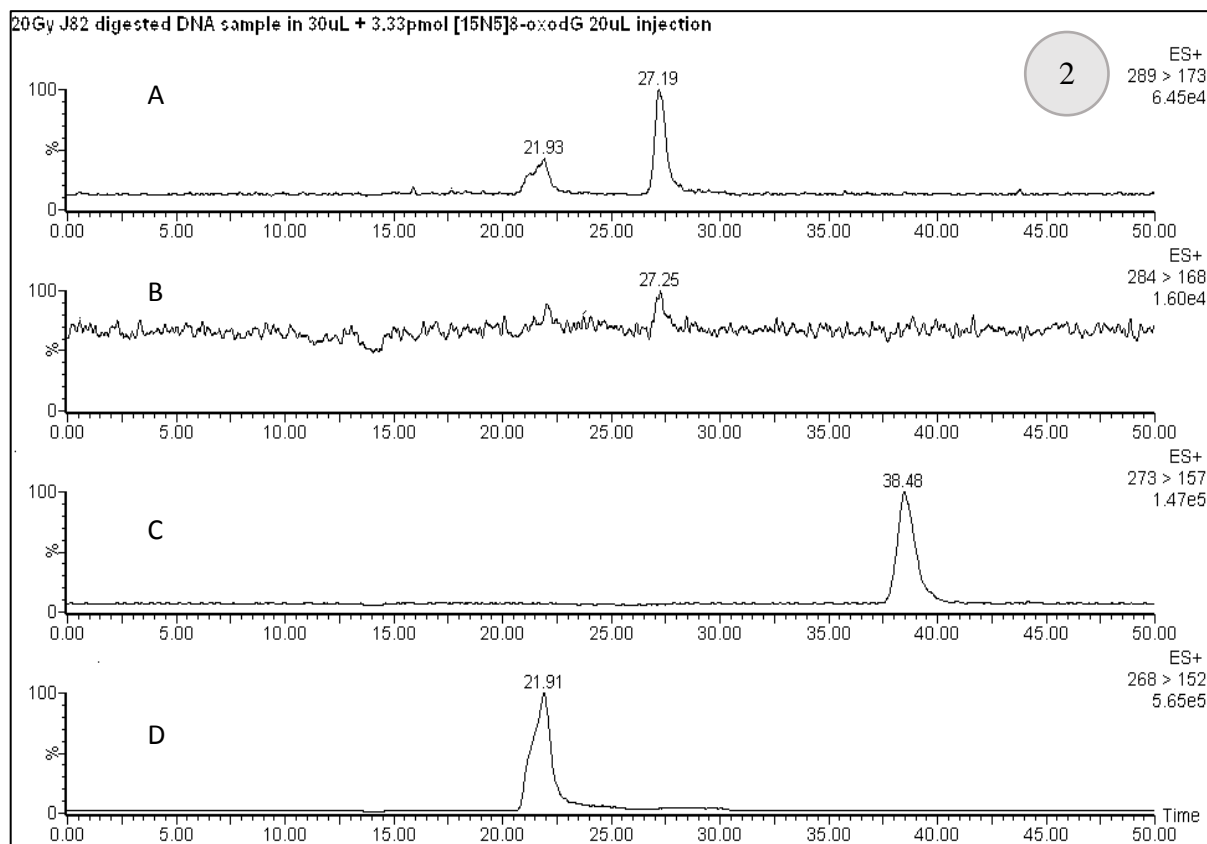
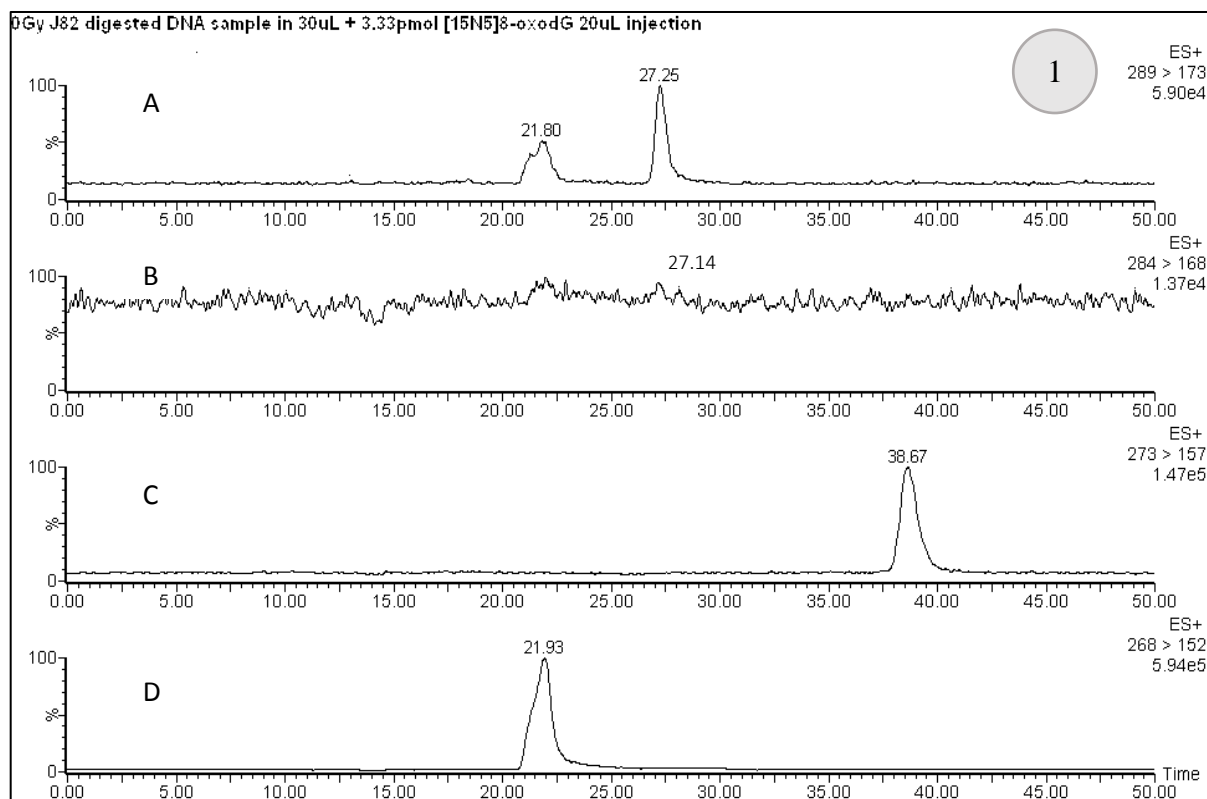
#### **4.4.1.3 Online column-switching LC-MS/MS SRM analysis**

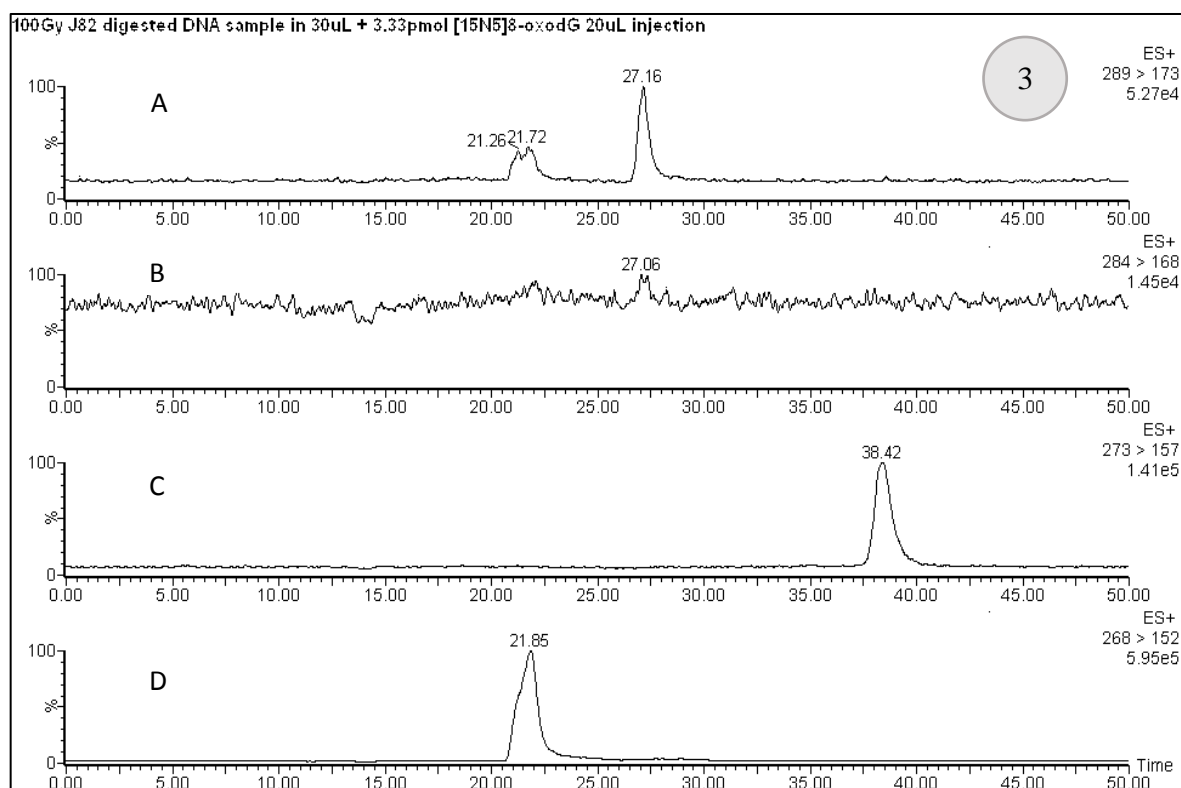
Typical online column-switching LC-MS/MS SRM ion chromatography was employed for the determination of the levels of radiation-induced 8-oxodG and 8-oxodA adducts within genomic DNA of UMUC3, RT112, J82 and RT4 bladder cancer cell lines following cell exposure to 0, 20 and 100 Gy, as shown in Figures 4.6a-d.



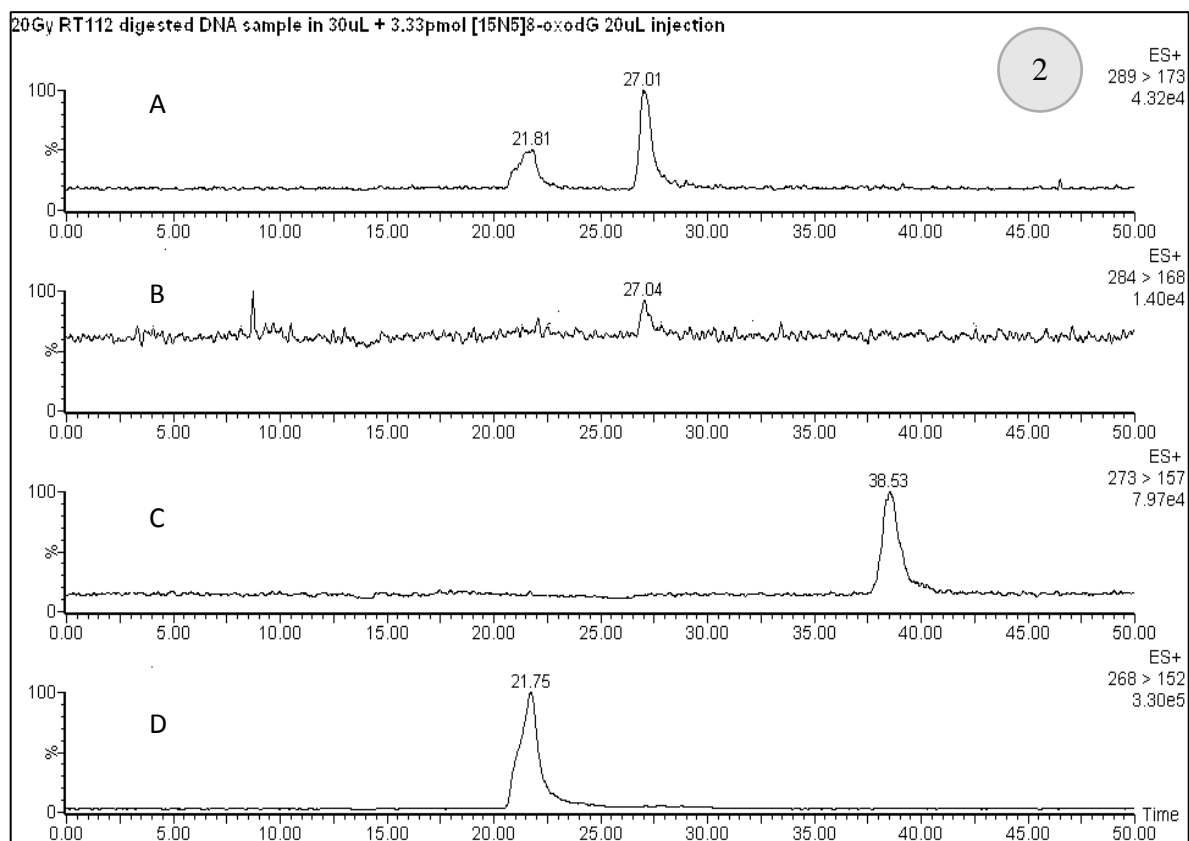
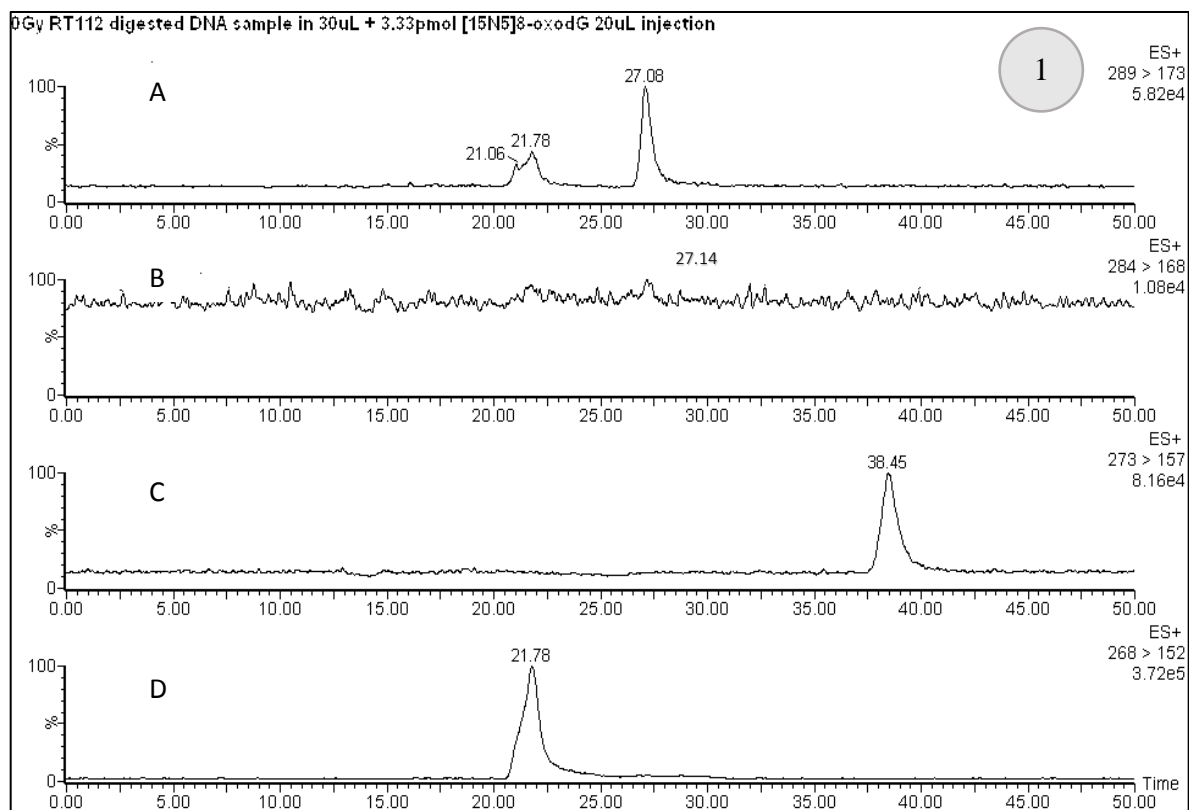


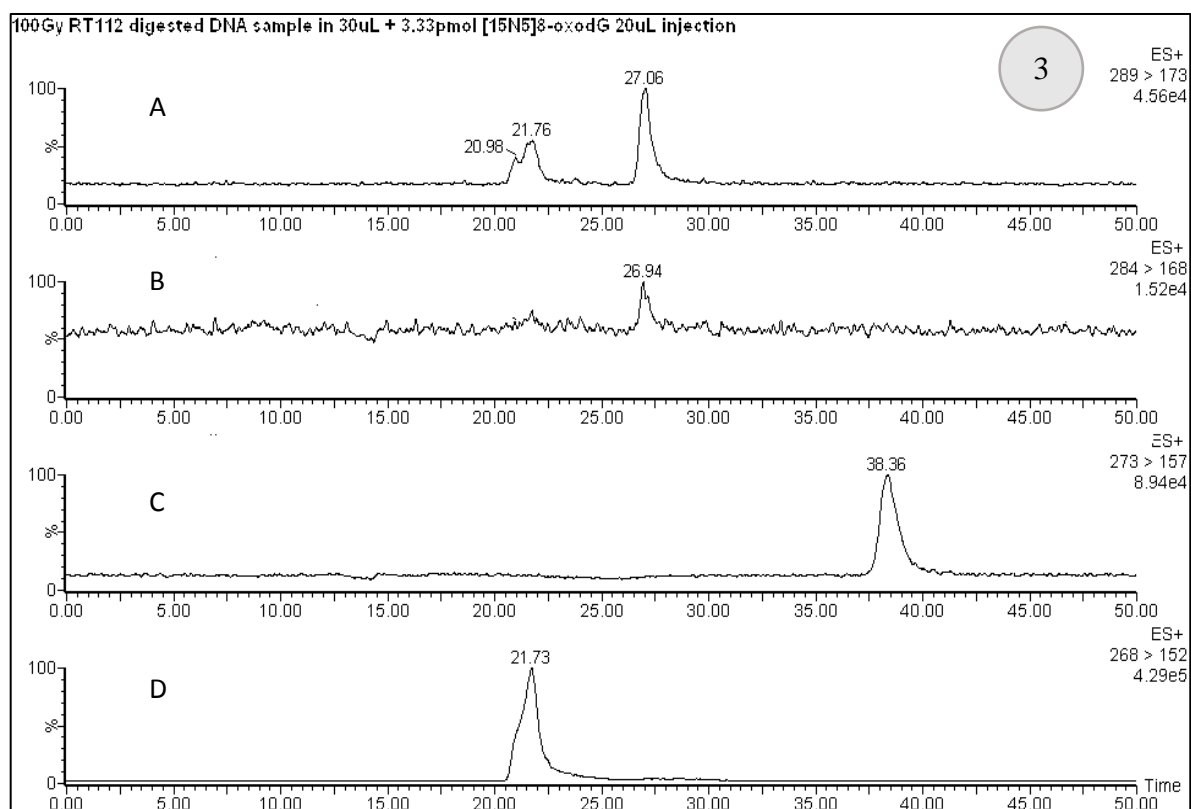
**Figure 4.6a** Typical chromatogram obtained for the analysis of the 8-oxo-dG and 8-oxo-dA adducts and its labelled standards using LC-MS/MS SRM. The presented LC-MS/MS SRM chromatograms reflect RT4 bladder cancer cells samples ([1] 0 Gy, [2] 20 Gy, and [3] 100 Gy) injected by LC-MS to give the 4 monitored channels where detected the peaks retention time in each channel. LC-MS/MS SRM chromatogram B and D monitor the 8-oxo-dG and 8-oxo-dA which are used to quantify DNA adduct. 30 µg DNA on column with SRM transitions monitoring the fragmentation of  $m/z$  289 to 173 for the labelled internal standard [<sup>15</sup>N<sub>5</sub>]8-oxodG adduct (A),  $m/z$  284 to 168 for the 8-oxo-dG adduct (B)  $m/z$  273 to 157 for the labelled internal standard [<sup>15</sup>N<sub>5</sub>]8-oxodA (C) and also  $m/z$  268 to 152 for the 8-oxo-dA adduct (D). Details that can be taken from LC-MS/MS SRM chromatograms for determination of the moles of DNA adduct detected on column and for calculation of the levels of the DNA adducts detected are mentioned in Materials and Methods Chapter (2.11.7 and 2.11.8).



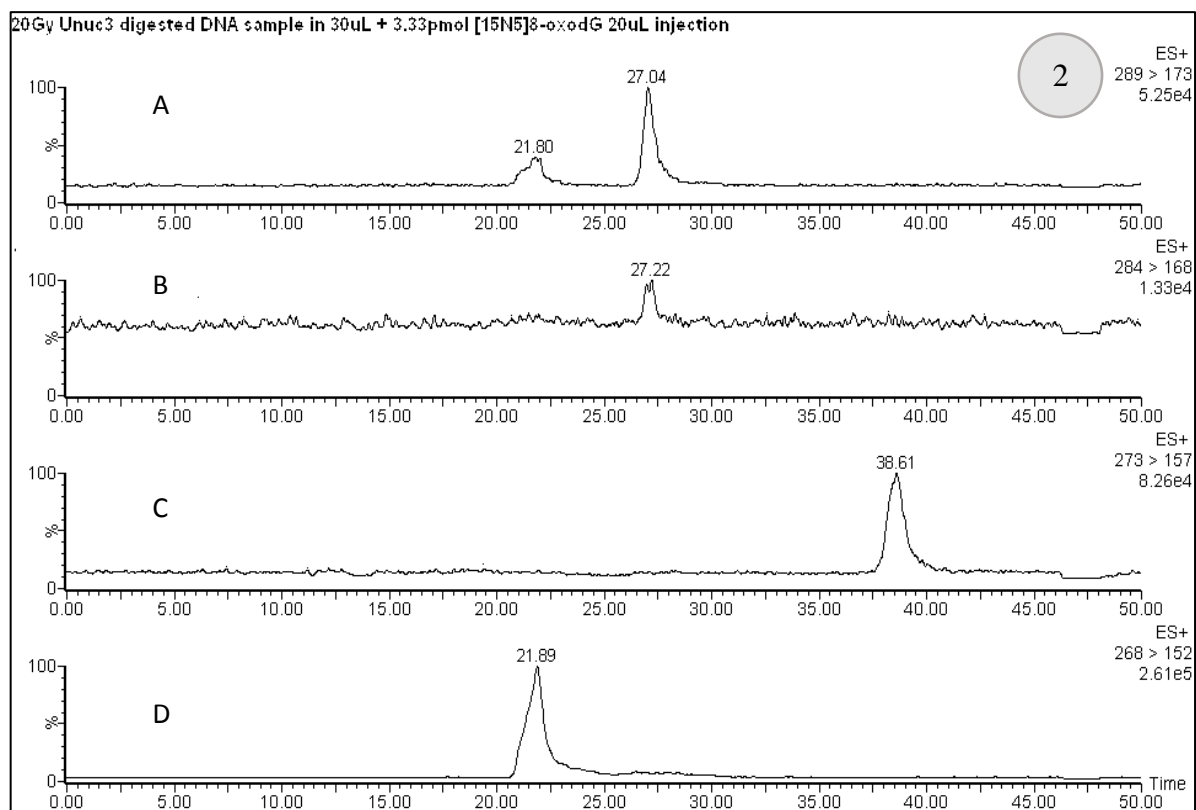
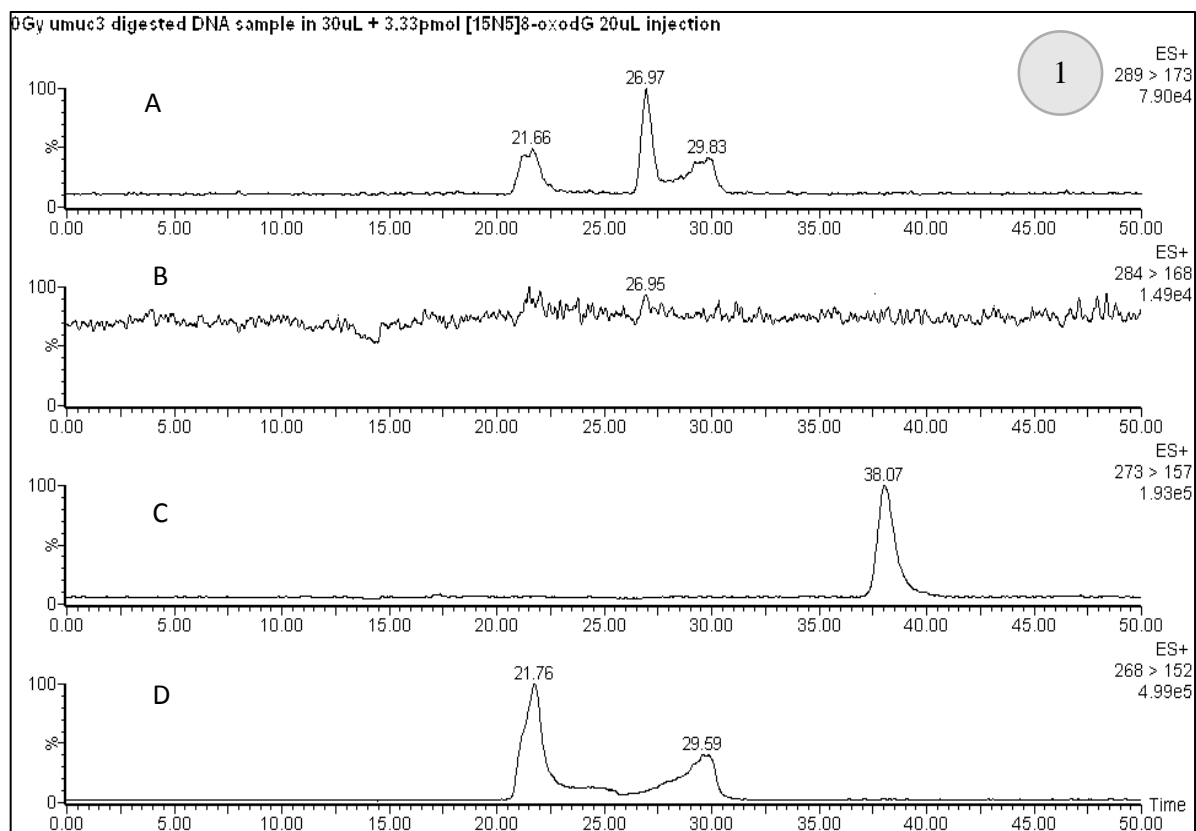


**Figure 4.6b** typical chromatogram obtained for the analysis of the 8-oxo-dG and 8-oxo-dA adducts and its labelled standards using LC-MS/MS SRM. The presented LC-MS/MS SRM chromatograms reflects J82 bladder cancer cells samples ([1] 0 Gy, [2] 20 Gy, and [3] 100 Gy) injected by LC-MS to give the 4 monitored channels where detected the peaks retention time in each channel. LC-MS/MS SRM chromatogram B and D monitor the 8-oxo-dG and 8-oxo-dA which are used to quantify DNA adduct. 30  $\mu\text{g}$  DNA on column with SRM transitions monitoring the fragmentation of  $m/z$  289 to 173 for the labelled internal standard [ $^{15}\text{N}_5$ ]8-oxodG adduct (A),  $m/z$  284 to 168 for the 8-oxo-dG adduct (B)  $m/z$  273 to 157 for the labelled internal standard [ $^{15}\text{N}_5$ ]8-oxodA (C) and also  $m/z$  268 to 152 for the 8-oxo-dA adduct (D). Details that can be taken from LC-MS/MS SRM chromatograms for determination of the moles of DNA adduct detected on column and for calculation of the levels of the DNA adducts detected are mentioned in Materials and Methods Chapter (2.11.7 and 2.11.8).

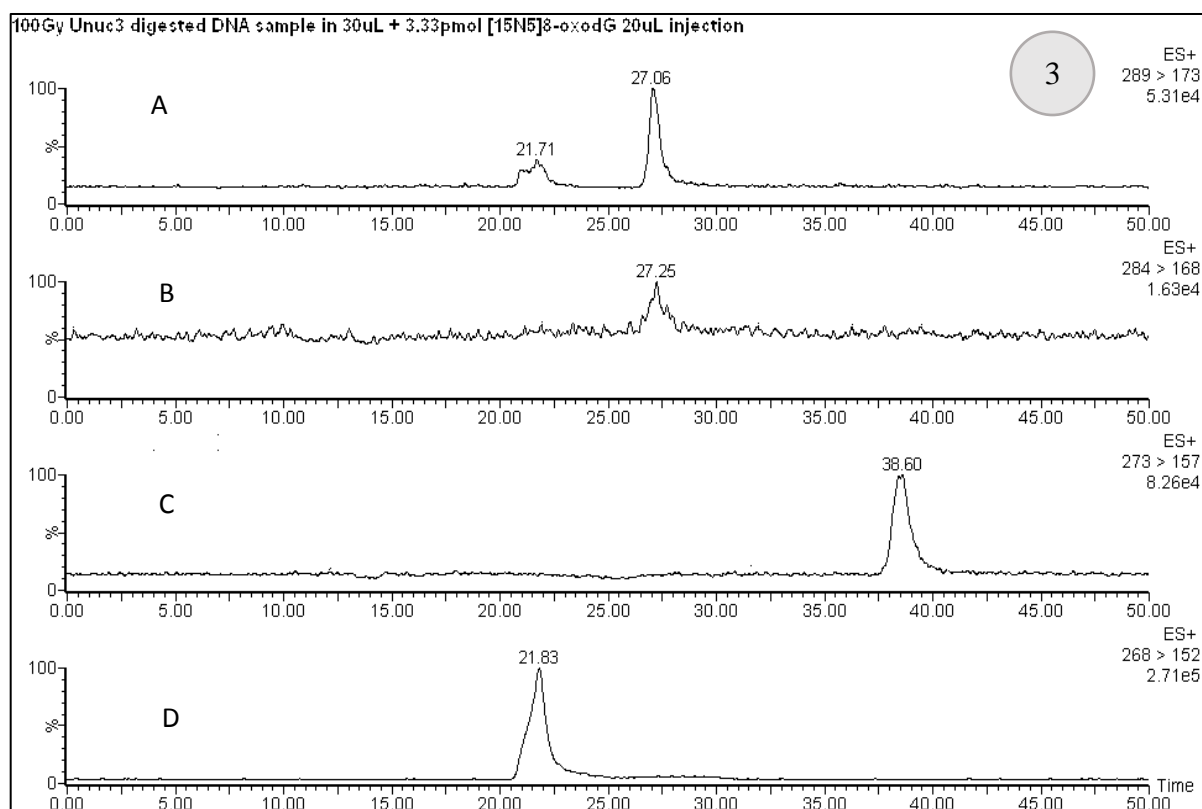




**Figure 4.6c** typical chromatogram obtained for the analysis of the 8-oxo-dG and 8-oxo-dA adducts and its labelled standards using LC-MS/MS SRM. The presented LC-MS/MS SRM chromatograms reflect RT112 bladder cancer cells samples ([1] 0 Gy, [2] 20 Gy, and [3] 100 Gy) injected by LC-MS to give the 4 monitored channels where detected the peaks retention time in each channel. LC-MS/MS SRM chromatogram B and D monitor the 8-oxo-dG and 8-oxo-dA which are used to quantify DNA adduct. 30  $\mu$ g DNA on column with SRM transitions monitoring the fragmentation of  $m/z$  289 to 173 for the labelled internal standard [ $^{15}\text{N}_5$ ]8-oxodG adduct (A),  $m/z$  284 to 168 for the 8-oxo-dG adduct (B)  $m/z$  273 to 157 for the labelled internal standard [ $^{15}\text{N}_5$ ]8-oxodA (C) and also  $m/z$  268 to 152 for the 8-oxo-dA adduct (D). Details that can be taken from LC-MS/MS SRM chromatograms for determination of the moles of DNA adduct detected on column and for calculation of the levels of the DNA adducts detected are mentioned in Materials and Methods Chapter (2.11.7 and 2.11.8).







**Figure 4.6d** typical chromatogram obtained for the analysis of the 8-oxo-dG and 8-oxo-dA adducts and its labelled standards using LC-MS/MS SRM. The presented LC-MS/MS SRM chromatograms reflect UMUC3 bladder cancer cells samples ([1] 0 Gy, [2] 20 Gy, and [3] 100 Gy) injected by LC-MS to give the 4 monitored channels where detected the peaks retention time in each channel. LC-MS/MS SRM chromatogram B and D monitor the 8-oxo-dG and 8-oxo-dA which are used to quantify DNA adduct. 30 µg DNA on column with SRM transitions monitoring the fragmentation of  $m/z$  289 to 173 for the labelled internal standard [ $^{15}\text{N}_5$ ]8-oxodG adduct (A),  $m/z$  284 to 168 for the 8-oxo-dG adduct (B)  $m/z$  273 to 157 for the labelled internal standard [ $^{15}\text{N}_5$ ]8-oxodA (C) and also  $m/z$  268 to 152 for the 8-oxo-dA adduct (D). Details that can be taken from LC-MS/MS SRM chromatograms for determination of the moles of DNA adduct detected on column and for calculation of the levels of the DNA adducts detected are mentioned in Materials and Methods Chapter (2.11.7 and 2.11.8).

An overall dose-dependent increase for the measures of radiation-induced 8-oxodG adduct in the genomic DNA was observed post radiation treatment of the four bladder cancer cell lines; with the ‘raw data’ (including the measured background/basal levels of 8-oxodG) shown in Table 4.1a and Figure 4.7a. Despite repeated attempts, there was no clear or evident dose response observable for 8-oxodA.

A range of background/basal 8-oxodG adduct was evident between the four bladder cancer cell lines; with the highest level (2.26 adducts per  $10^6$  2'-deoxynucleosides) being noted for the RT4 bladder cancer cell line and the lowest level (0.54 adducts per  $10^6$  2'-deoxynucleosides) being noted for the J82 bladder cancer cell line. This 4-5-fold variance in the basal background levels of DNA damage significantly contributed to the perceived induced damage levels. Consequently, the background basal levels of damage were subtracted from the induced damage levels and this data (of intrinsic damage sensitivity) is presented in the Table 4.1b and Figure 4.8b for the four radiation-treated bladder cancer cell lines. The rank order for damage sensitivity (from the most damage sensitive cell to the most damage resistant cell) as measured by radiation-induced 8oxodG damage levels was deduced as being  $UMUC3 \geq RT112 > RT4 \geq J82$  with the levels of radiation-induced 8-oxodG damage being most pronounced in the UMUC3 and RT112 cell lines, and the least in the RT4 and J82 cell lines.

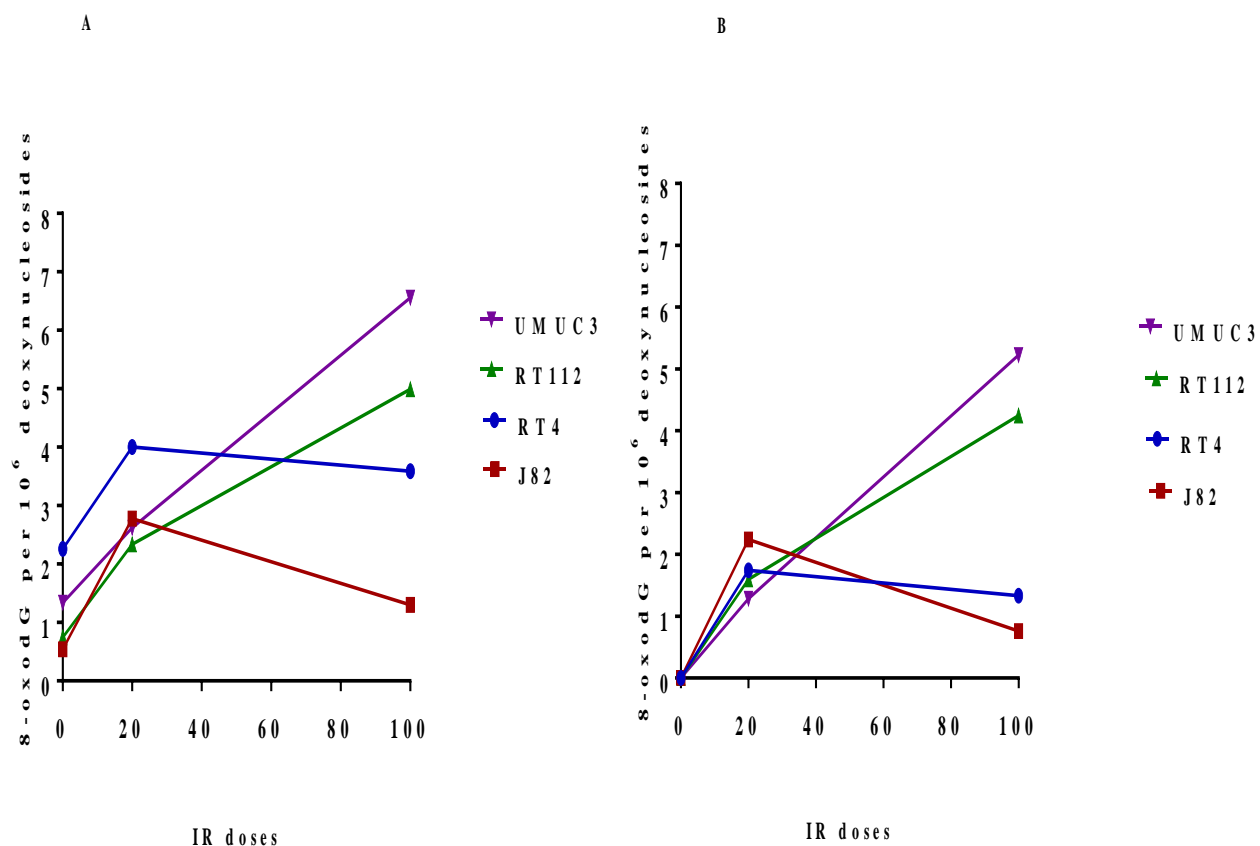
From Figures 4.7a and 4.7b, RT112 and UMUC3 cell lines are deduced as being the more damage sensitive cell lines. Whereas, J82 and RT4 cell lines are the most damage resistant. Overall, these results were broadly in-line with the Comet assay results whereby UMUC3 and RT112 cell lines displayed the highest measure of comet formation, and J82 and RT4 cell lines displayed the lowest extents of comet formation. Therefore, whilst not directly correlating, these data provide evidence in support of the first hypothesis (Model 1) that if the differential measures observed by Comet assay are matched by those of LC-MS/MS analysis, then it can be concluded that the differential extent of radiation-induced comet formation noted between the four bladder cancer cell lines indeed reflects distinct levels of DNA damage.

**Table 4.1a.** Formation of 8-oxodG following the treatment of the four bladder cancer cell lines DNA with different IR doses as determined by online column-switching LC-MS/MS SRM with background/basal damage. The results were obtained from one experiment.

Cell line	0Gy	20Gy	100Gy
<b>RT4</b>	2.26 adducts/10 <sup>8</sup> nucleotides	4.00 adducts/10 <sup>8</sup> nucleotides	3.6 adducts/10 <sup>8</sup> nucleotides
<b>J82</b>	0.54 adducts/10 <sup>8</sup> nucleotides	2.78 adducts/10 <sup>8</sup> nucleotides	1.30 adducts/10 <sup>8</sup> nucleotides
<b>RT112</b>	0.75 adducts/10 <sup>8</sup> nucleotides	2.34 adducts/10 <sup>8</sup> nucleotides	4.99 adducts/10 <sup>8</sup> nucleotides
<b>UMUC3</b>	1.34 adducts/10 <sup>8</sup> nucleotides	2.62 adducts/10 <sup>8</sup> nucleotides	6.56 adducts/10 <sup>8</sup> nucleotides

**Table 4.1b.** Formation of 8-oxodG following the treatment of the four bladder cancer cell lines DNA with different IR doses as determined by online column-switching LC-MS/MS SRM with subtracted background/basal damage (subtraction of 0 Gy results from 20 Gy, and 100 Gy IR results). The results were obtained from one experiment.

Cell line	0Gy	20Gy	100Gy
<b>RT4</b>	0.00 adducts/10 <sup>8</sup> nucleotides	1.74 adducts/10 <sup>8</sup> nucleotides	1.33 adducts/10 <sup>8</sup> nucleotides
<b>J82</b>	0.00 adducts/10 <sup>8</sup> nucleotides	2.24 adducts/10 <sup>8</sup> nucleotides	0.76 adducts/10 <sup>8</sup> nucleotides
<b>RT112</b>	0.00 adducts/10 <sup>8</sup> nucleotides	1.6 adducts/10 <sup>8</sup> nucleotides	4.25 adducts/10 <sup>8</sup> nucleotides
<b>UMUC3</b>	0.00 adducts/10 <sup>8</sup> nucleotides	1.28 adducts/10 <sup>8</sup> nucleotides	5.22 adducts/10 <sup>8</sup> nucleotides



**Figure 4.7 Formation of 8-oxodG following the treatment of the four bladder cancer cell lines DNA with different IR doses as determined by online column-switching LC-MS/MS SRM with (A) background/basal damage response and (B) with subtraction the background/basal damage.**

## 4.5 Discussion

DNA adduct levels are considered an effective marker of exposure to genotoxic carcinogens including ionising radiation (Pernot et al., 2012b). DNA adduct levels have been utilised to assess the industrial and environmental chemical carcinogen levels that can have a biological impact on human exposure (Koc and Swenberg, 2002; Swenberg et al., 2008). Thus, the presence of DNA adducts in human sources of DNA can be a useful measure for molecular epidemiological studies of cancer causation (Goggin et al., 2009; Goggin et al., 2011; Ishii et al., 2011).

Online column-switching valve technology allows enzymatically hydrolysed DNA samples to be analysed directly by LC-MS/MS. To allow for the accurate quantification of 8-oxodG and 8-oxodA and to account for signal variability of the mass spectrometer, the [<sup>15</sup>N<sub>5</sub>]8-oxodG and [<sup>15</sup>N<sub>5</sub>]8-oxodA labelled stable isotope internal standards of each adduct was added prior to enzymatic hydrolysis of the DNA samples (Singh et al., 2009).

The impact of radiation exposure on 8-oxodG DNA level in the genomic DNA of the four bladder cancer cell lines (UMUC3, RT112, J82 and RT4) was examined in the present study. The UMUC3, RT112, J82 and RT4 cells were treated with various IR doses (0, 20 and 100 Gy) to induce cellular oxidative stress. The DNA extraction were completed as outlined in Chapter 2. For each bladder cancer cell line, up to three separate DNA extraction procedures were undertaken to achieve the adequate amount of DNA for LC-MS/MS analysis to acquire an accurate degree of results. However, no accurate results were obtained from Wako and Qiagen Blood & Cell culture DNA Kits. Therefore, the conclusive results in this present study were obtained using the Maxwell 16 Cell DNA Purification method. This DNA extraction procedure was undertaken to achieve the adequate amount of the extracted genomic DNA within a brief timeframe (~35mins in total), and to be able to analyse the samples (though this did require repeated extractions and then pooling of the samples for analysis). Previous research evaluated the influence of the different DNA extraction procedures on the background levels of 8-oxodG (Ravanat et al., 2002) and differences in the levels of oxidative DNA adducts were observed due to variances in the quality and purity of DNA obtained from each DNA extraction procedure (Singh et al., 2009). Moreover, other factors, for instance the vacuum drying of DNA, can elevate the amount of 8-oxodG measured (Chao et al., 2008).

Although no meaningful data was observed for 8-oxodA, the amount of 8-oxodG DNA adducts was consistently elevated across all the bladder cancer cell lines examined in the present study following exposure to 20 Gy. In addition, UMUC3 and RT112 cell lines demonstrated an increased sensitivity to radiation-induced 8-oxodG DNA adducts formation when these cell lines were exposed to 100 Gy, with 4.25 8-oxodG DNA adducts being detected per 10<sup>6</sup> deoxynucleosides for RT112 and 5.22 adducts of 8-oxodG being detected per 10<sup>6</sup> deoxynucleosides for UMUC3 post exposure to 100 Gy. In contrast, the other cell

lines (J82 & RT4) were shown to be more damage resistant, having far lower levels of 8-oxodG post exposure to 100 Gy, with 1.33 adducts of 8-oxodG being detected per  $10^6$  deoxynucleosides for RT4 cells and 0.76 adducts of 8-oxodG per  $10^6$  deoxynucleosides being detected for J82 cells post exposure to 100 Gy (as illustrated in Table 4.1b with subtracted background/basal damage). The rank order for radiation-induced 8-oxodG DNA adducts in the four bladder cancer cell lines from the most damage sensitive to the most damage resistant is as follows: UMUC3  $\geq$  RT112  $>$  RT4  $\geq$  J82. Whilst not delivering an absolute sequential rank order, the rank order observed matched/approximated the rank order observed with the Comet assay (as outlined in Chapter 3) with UMUC3 and RT112 cells the most damage sensitive cell lines. Whereas, J82 and RT4 cells the most damage resistant cell lines.

Examining DNA adduct formation in human samples requires maximum sensitivity due to the trace levels of these analytes (1 adduct in  $10^6$ – $10^{10}$  nucleotides) in often limited amounts of available DNA (typically 1–100 $\mu$ g DNA) (Tretyakova et al., 2012; Villalta and Balbo, 2017). In human cells or animal models, sensitivity is critical due to the need to keep dose levels low to approximate human exposure (Tretyakova et al., 2012; Tretyakova et al., 2013). Several pilot experiments were undertaken in this study which used low IR doses; however, no DNA base adducts were detected from the four bladder cancer cell lines following exposure to low IR doses such as 5 Gy. Thus, high IR doses (20 Gy and 100 Gy) were used to achieve the IR dose responses from the four cell lines. High selectivity in DNA adduct identification is also needed to differentiate DNA adducts from the background signal present in biological samples. Therefore, due to the need to screen for multiple adducts often of unknown identity across large mass ranges or possibly due to the absence of the accurate concentration of isotopically labelled internal standards and the well characterised fragmentation patterns of the targeted DNA adduct analytes, the need for optimal sensitivity and selectivity is required for targeting DNA base adducts, (Tretyakova et al., 2012). Accurate complete quantification by LC-MS analysis requires the use of stable isotope-labelled internal standards of the analytes of interest. Yet, the use of stable isotope-labelled internal standards can cause several issues, including the variation of ionisation efficiency across analytes, and possibly the ion suppression/enhancement due to sample matrix components (Tretyakova et al., 2012; Tretyakova et al., 2013; Villalta and Balbo, 2017), as

matrix effects occur when molecules co-elute with the compounds of interest and alter the ionisation efficiency of the electrospray interface (King et al., 2000; Matuszewski et al., 2003).

The issue of reducing of the artefactual generation of 8-oxodG and 8-oxodA can be best achieved through the reduction of sample manipulation procedures during the protocol process (Singh et al., 2009). In addition, stable adducts can be emitted from the prepared DNA by increasing acid hydrolysis and thermal hydrolysis levels, as these factors can lead to the cleavage of unmodified DNA bases which are enormous in relation to the adducted bases. Therefore, a purification process would be required for ionisation and signal suppression resulting from the presence of the unmodified bases (Singh and Farmer, 2006). Consequently, identification and structural characterisation of DNA base adducts require many factors to be considered to acquire beneficial results such as differences in analytical goals (e.g., targeted or untargeted), the amounts of DNA available, DNA adduct levels, hydrophobic vs. hydrophilic adducts and instrument availability.

Overall, the achieved data of LC-MS/MS only tentatively supports the first hypothesis (Model 1): (that differential measures of the Comet assay do reflect actual differences in damage levels). Therefore, to seek further substantiation, it was decided to further investigate radiation-induced damage levels in the four bladder cancer cell lines using a common procedure for detection of DNA DSB formation, pulsed field gel electrophoresis (PFGE), and to assess this method's correlation with the previous noted differential measures of comet formation.

## **Chapter 5**

### **Estimation of IR-induced DNA DSBs damage by the Pulsed Field Gel Electrophoresis (PFGE)**



## **5.1 Introduction**

### **5.1.1 Analysis of IR-induced DNA DSBs damage by the Pulsed Field Gel Electrophoresis (PFGE)**

As mentioned previously, DNA is constantly being damaged by exogenous genotoxic agents such as ionizing radiation (IR) or drugs, or by endogenous agents such as ROS arising from cellular metabolism, immune responses, and inflammation (Kryston et al., 2011b). IR generates a wide variety of DNA damage including base lesions and both single and double strand breaks. DNA DSBs are IR-induced lesions which are responsible for radiogenic cell death. The persistence of unrepaired or mis-repaired DSBs leads to chromosomal abnormalities which can either cause cell death, or alternatively may subsequently contribute to the development of disorders including cancer (Jackson and Bartek, 2009b). Therefore, numerous studies have been undertaken to understand the mechanisms involved in the production and repair of DSBs (Vignard et al., 2013b).

### **5.1.2 Pulsed field gel electrophoresis (PFGE) technique**

The PFGE assay is one of the useful electrophoretic techniques utilised for fractionating high molecular-weight DNA of the size range 10kb to 10Mb (Orbach et al., 1988; Kuspa et al., 1989; Cooney, 1992). Using at least two alternating electrical fields at different angles within a flat agarose gel (Smith et al., 1988, Nasonova, 2008), the PFGE assay has the capability to separate and analyse large, normal, linear chromosomal DNA molecules from a variety of sources, including fragmented genomes of bacteria (Smith et al., 1986). In 1983, Schwartz *et al.* were the first to succeed in fractionating high-molecular-weight DNA by electrophoresis. They introduced the concept of separation of DNA of  $\geq 50$  kilobase (kb) pairs by applying two alternating electric fields.

In the PFGE assay, the DNA molecules, including Mb-size fragments, can be separated by a time-associated size-dependent reorientation of DNA migration which can be achieved by constantly pulsing the electric field in different directions. Thus, 24-point electrodes arrangements that are able to produce a highly uniform electrophoresis gradient, can cause the DNA molecules to reorient, typically over an angle of  $120^\circ$ . This subsequently can

provoke DNA migration to the left and right of the agarose gel centre resulting in straight vertical lanes of separation. The DNA fragments can move in an electric field due to the negatively charged phosphate backbone. The DNA fragments migrate toward the anode (the positively charged electrode) at a rate proportional to the molecules charge, which is an inverse measure of the size of DNA. Small pieces of DNA can move through a gel matrix in a straight path. Larger molecules need to migrate in a more indirect manner to find pores in the gel that are large enough to occupy.

The gel is a matrix that consists of agarose molecules (Townsend and Dawkins, 1993). DNA fragments will form a distinctive pattern of bands in the gel, which can be analysed both visually and electronically. However, this approach can encounter many factors which could interfere with the results, such as agarose gel concentration and thickness, buffer composition and the strength of the electric field (V/cm) (Birren and Lai, 2012, Goering, 2004, Struelens et al., 2001). Furthermore, cell lysis to release of the intact chromosomal DNA, and the separation of DNA fragments may also skew the results observed. Additionally, the resolution of the PFGE assay can be affected by the number and the configuration of the electrodes used, as these factors can alter the shape of the electrical field. Thus, for a good-resolution separation, the most beneficial electrode configurations enable reorientation angles of  $>110^\circ$  (Cantor et al., 1988). At the end of electrophoresis, the DNA fragments should form a characteristic pattern of bands in the gel (Goering, 2010).

Regarding DNA preparation, the PFGE assay initially requires the preparation of a cell suspension. Intact cells are embedded into agarose plugs where cells are enzymatically lysed and cellular proteins digested. The agarose plugs are washed and are introduced into the wells of the gel and electrophoresed under the desired conditions. Marker molecules are run alongside the experimental DNA serving as markers for identification of the various fragment sizes. Following electrophoresis (often 24 hours later), the gel is stained with a DNA binding dye such as ethidium bromide (Carter et al., 1994) and viewed with suitable image analysis software. Analysis of DNA fragment distribution in the gel is measured by image analysis (Gradzka and Iwanenko, 2005).

The implementation of the PFGE techniques for separating large DNA molecules has an important role within the study of chromosomal DNA molecules, the structure of genomes,

and the theory of electrophoresis (Smith et al., 1988). Consequently, several instruments have been developed to separate DNA molecules from a few kb to  $\geq 10$  megabase pairs (Mb) (Kaufmann et al., 1994).

#### **5.1.2.1 The basic equipment and features of the PFGE system**

The basic components of a PFGE system consist of a gel box with some means of temperature regulation, a switching unit for controlling the electric fields, a cooler and a power supply (Lai et al., 1989).

**A gel box** contains an immobilized gel within an arrangement of electrodes, and the electrophoresis buffer. The buffer is recirculated throughout the gel box using inlet and outlet ports (Carle and Olson, 1984, Birren et al., 1988).

**A switching unit** is used control the electric fields by providing a periodic switching of the electric field in different directions. This apparatus has the ability to control the reorientation angles between the electric fields. Most PFGE instruments use  $120^\circ$  as the applied angle of separation, but some have varying angles. Greater angles give higher resolution, however smaller angles enable higher speed/shorter run times. The PFGE conditions using smaller angles ( $90 < 120^\circ$ ) and lower agarose concentration ( $0.4 < 0.5$ ) are suitable for separating large DNA molecules such as  $\geq 2000\text{kb}$  (Kaewsawang, 2003, Zou et al., 2013).

**A cooler device.** DNA molecule migration is sensitive to temperature as it influences the DNA mobility. Therefore, a consistent temperature across the gel is necessary to ensure uniform DNA molecule migration in each of the lanes. Consequently, buffer temperature is typically maintained at  $14^\circ\text{C}$  throughout a typical run (Birren et al., 1988).

**A high voltage power supply.** The voltage is usually set at  $6\text{V/cm}$  for DNA fragments  $\leq 2000\text{kb}$ , but larger DNA fragment separation require lower-voltage grades and longer electrophoresis times (Lai et al., 1989).

### 5.1.2.2 Running conditions for the PFGE assay

PFGE separations are sensitive to a variety of different molecular and environmental variables. Although each PFGE system has its specific method and programming, the basic parameters are the same. There are several parameters that can affect molecule mobility and separation, including pulse time and its mode of switching, field strength, reorientation angle, run time, agarose concentration, buffer concentration and temperature (Nassonova, 2008).

**Pulse Time (switch time, switch interval):** is the time interval for switching the direction of the field. In PFGE, the DNA is subjected alternately to two electrical fields at different angles for a time called the pulse time. Each time the field is switched, the larger fractionated molecules take longer time to change direction and have less time to move during each pulse. Subsequently, these larger fractionated molecules migrate slower than smaller molecules. Thus, an optimal separation can be achieved by pulse times that are slightly longer than the time required for the largest DNAs to complete reorientation (Gurrieri et al., 1996). The change of pulse time during electrophoresis is called “ramping”. This parameter can be increased throughout a run either constantly or discontinuously over a range of discrete values (Nassonova, 2008).

**Field strength shape:** The area in the gel where effective DNA separation is achieved is called the “resolution zone”, or “resolution window.” Resolution is a function of both the pulse time and electric field strength. The resolution of the PFGE assay is affected by the number and configurations of the electrodes used. The most effective electrode configurations yield angles  $>110^\circ$ . Continually increasing the angle between the fields produces band sharpening that enhances the resolution. The angle between the alternate fields is always greater than  $90^\circ$ , where good resolution is observed. For best resolution, field angles typically range from  $120^\circ$  to  $150^\circ$  (Cantor et al., 1988).

**Electrical Field Strength:** As mentioned above, resolution is a function of both the pulse time and electric field strength. Higher field strength can lead to an increased rate of molecule migration. To separate molecules of less than 1Mb, the field strength applied is typically 6–10V/cm. A lower field strength can cause an elevation within the resolution. However, the

size range of separated molecules is narrower (Birren et al., 1988). An excessively high field strength ( $>10\text{V/cm}$ ) can cause poorer molecule separation, and the appearance of so-called “smears” (Mathew et al., 1988).

**Reorientation angle:** This parameter is fixed in some PFGE devices. Yet, in others, the reorientation angle can be varied from  $90^\circ$  to  $180^\circ$ . The alteration of the reorientation angle does not notably affect the migration of molecules of less than 1Mb. The mobility of larger molecules increases with a decrease of the reorientation angle (Clark et al., 1988); (Chu and Gunderson, 1991). Consequently, the best separation is achieved with an angle value of more than  $110^\circ$  (Cantor et al., 1988). Yet, most PFGE instruments use a fixed reorientation angle of  $120^\circ$ .

**Agarose concentration in gel:** The agarose concentration affects both the mobility and the separation of the DNA. At higher concentrations, bands become sharper, but only smaller DNA molecules can be resolved. Nevertheless, better resolution can be obtained for 1.2% agarose gels in comparison to 0.9% gels. To obtain high-band resolution, 1% agarose concentration can be used, but this requires a slower electrophoresis. Further increase in agarose concentration can decrease the mobility and, hence, increases the run time without improving the resolution (Mathew et al., 1988; Maule, 1998).

**Composition and temperature of electrophoresis buffer:** Buffers with high ionic strength, such as Tris-borate ( $0.5 \times \text{TBE}$ ) or Tris-acetate ( $1 \times \text{TAE}$ ), are frequently used for the PFGE assay. The temperature at which the gel is run affects both the migration rate and resolution (Mathew et al., 1988), and the PFGE assay is usually performed at over a temperature range of  $12\text{--}16^\circ\text{C}$  (Chu, 1990). At higher buffer temperatures, the bands become wide and diffuse. Therefore, the maintenance of the permanent temperature of the electrophoresis buffer is required for superior DNA molecule separation (Nassonova, 2008).

DNA molecules longer than 25kb are poorly resolved by standard agarose gel electrophoresis. These longer DNA molecules can be resolved using several techniques that periodically change the direction of the electric field in the gel. This describes the simplest and most useful of the pulsed-field techniques, field inversion electrophoresis, which can be tuned to resolve molecules ranging from 10 to 2000kb. To resolve molecules beyond this range of field inversion, it is necessary to use some sort of field-angle alternation

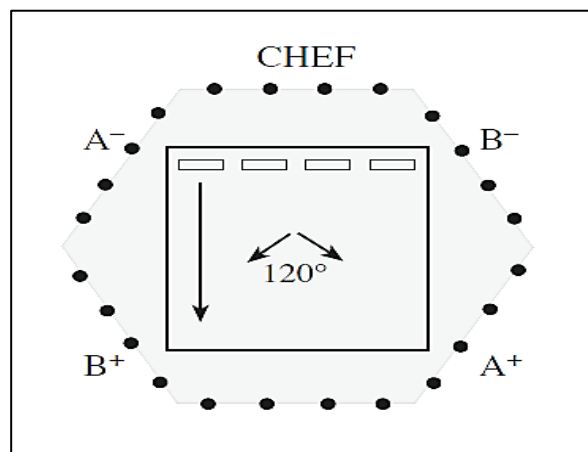
electrophoresis such as CHEF (contour-clamped homogeneous electric field) for evaluating the damaged DNA size distributions. A method is also provided for preparing high-molecular-weight DNA samples, and size markers embedded in agarose blocks (Finney, 2001). The CHEF instruments and protocols were developed to amplify the size resolution of both large and small DNA molecules (Chu et al., 1986; Basim et al., 1999). The CHEF instrument are now used within several laboratories. As such, the CHEF electrophoresis protocol has been used for the work described in this current study.

### **5.1.2.3 PFGE by Contour-Clamped Homogeneous Electric Fields (CHEF)**

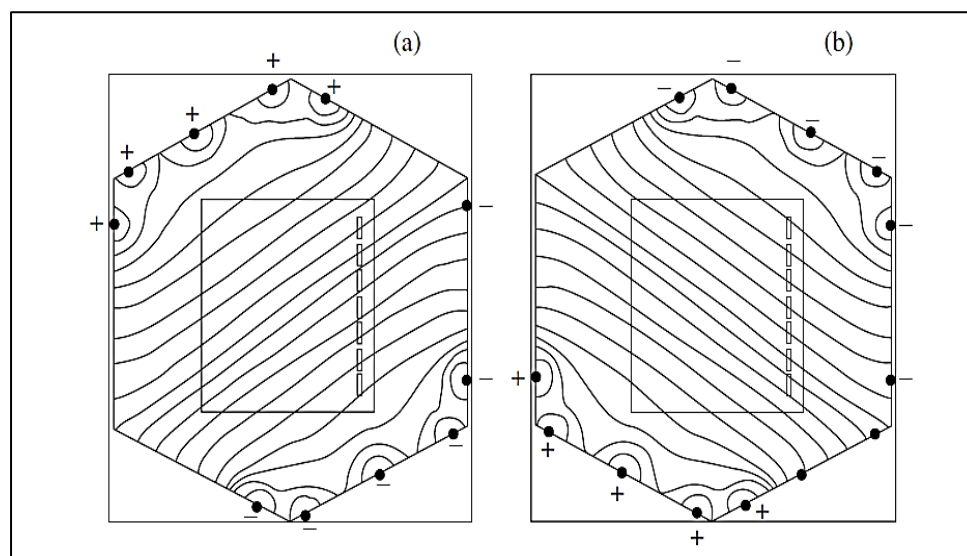
Chu and co-workers (Chu et al., 1986) developed the contour-clamped homogeneous electric field (CHEF) for PFGE which, offered a controlled homogeneous electric field. This system is considered as the gold standard apparatus within many laboratories. This instrument has 24-point electrodes (illustrated in Figure 5.1b) arranged equally spaced into six groups of four, aligned in a hexagonal orientation producing a highly uniform electrophoresis gradient. As a result, the DNA molecules reorient over an angle of  $120^\circ$  between adjacent electrode groups (as seen in Figure 5.1a) so all lanes of a gel run regularly (Nsofor, 2016). This generates a homogeneous gradient of electro-potential between the cathodes and anodes. With the CHEF system, it is possible to achieve straight lanes and stable DNA separation. This arrangement creates DNA migration to the left and right of the agarose gel centre causing the production of straight vertical lanes of separation (Birren and Lai, 2012, Struelens et al., 2001, Goering, 2004). In the CHEF system, there are no passive electrodes, and the best separation can be achieved for DNA fragments up to ~2000kb. Still, DNA molecules up to 12000kb can be separated by this device, through application of low temperature and longer electrophoresis times.

All the electrodes are connected to the main power supply through an external loop of devices which have the same resistance. The external loop is responsible of adjusting the voltages of all the hexagonal electrodes and can generate identical electric fields in each of the alternate switching positions. The CHEF system is affected by factors such as agarose gel concentration and thickness, buffer composition, and strength of the electric field (V/cm) (Goering, 2004; Birren and Lai, 2012). Still, the CHEF system is the most widely

implemented variants of electrophoresis using pulsed fields, as it is possible to achieve straight lanes and stable DNA separation. Moreover, it ensures the most effective fractionation of DNA molecules over a wide range of sizes. (Chu et al., 1986; Chu, 1989).



**Figure 5.1a. Schematic drawings showing CHEF (modified after (Lai et al., 1989; Mezhevaya et al., 1990)).** The CHEF system has a homogeneous electric field. The short thin arrows indicate the vectors of field strength of alternative electric fields; reorientation angle is shown inside. The wide arrow point to the net direction of migration. Symbols  $A^+$ ,  $A^-$ ,  $B^+$ , and  $B^-$  indicate positions of electrode pairs of alternative electric fields. Electrodes are indicated by dots within the CHEF system.



**Figure 5.1b. Homogeneous pulsed electric field in a CHEF instrument.** Electrodes generating the alternative electric fields (a & b) two alternative directions of the vectors of electric field strength (Nassanova, 2008).

As mentioned before, ionising radiation produces a wide variety of DNA lesions amongst which DSBs considered to be the major factor responsible for cell death. If unrepaired or improperly repaired, DSBs contribute to chromosomal aberrations, which may lead to human disorders including cancer (Bristow and Hill, 2008; Helleday et al., 2008; Jackson and Bartek, 2009a). The PGFE assay has been used to visualize DSB-broken DNA in mammalian cells post IR exposure (Ager et al., 1990).

The PFGE assay provides a vital platform for examination of DNA DSBs post exposure to ionising radiation, and appears applicable for the analysis of damage produced by any agent producing DSBs (Prise, 1998; Vignard et al., 2013a; Joshi and Grant, 2014). The PFGE assay exploits the nature that undamaged DNA (high molecular weight) is trapped in agarose plugs, and does not enter and migrate in an agarose gel. Whereas, damaged DNA (lower molecular weight) is able to do so. It is noteworthy that the fraction of migrating DNA has been demonstrated to correlate with the number of DSBs (Prise, 1998; Liu et al., 2008). Consequently, the PFGE assay has been implemented in this study to measure DNA DSBs induced by IR in the four bladder cancer cells investigated in this study.

## **5.2 Study Aims**

The investigations undertaken in this chapter were to determine the rank-order of the radiation-induced DNA damage sensitivity for the four bladder cancer cell lines (UMUC3, RT112, J82 and RT4) as assessed using the PFGE system using CHEF, and to assess the extent of any correlation with the differential measures of damage sensitivity reported by the ACA as described in Chapter 3. A noted correlation between the respective rank-orders would support the hypothesis that the differential measures noted by the ACA are due to actual differential damage (Model 1).

## **5.3 Summary of the technique/approach**

Four bladder cancer cell lines of transitional cells carcinoma (TCC) were used in this study (UMUC3, RT112, J82, RT4), and were exposed to ionising radiation over a dose range of 0-



50 Gy. Damage to DNA was assessed using PFGE using CHEF. The materials and methods used for this chapter have been described in Chapter 2

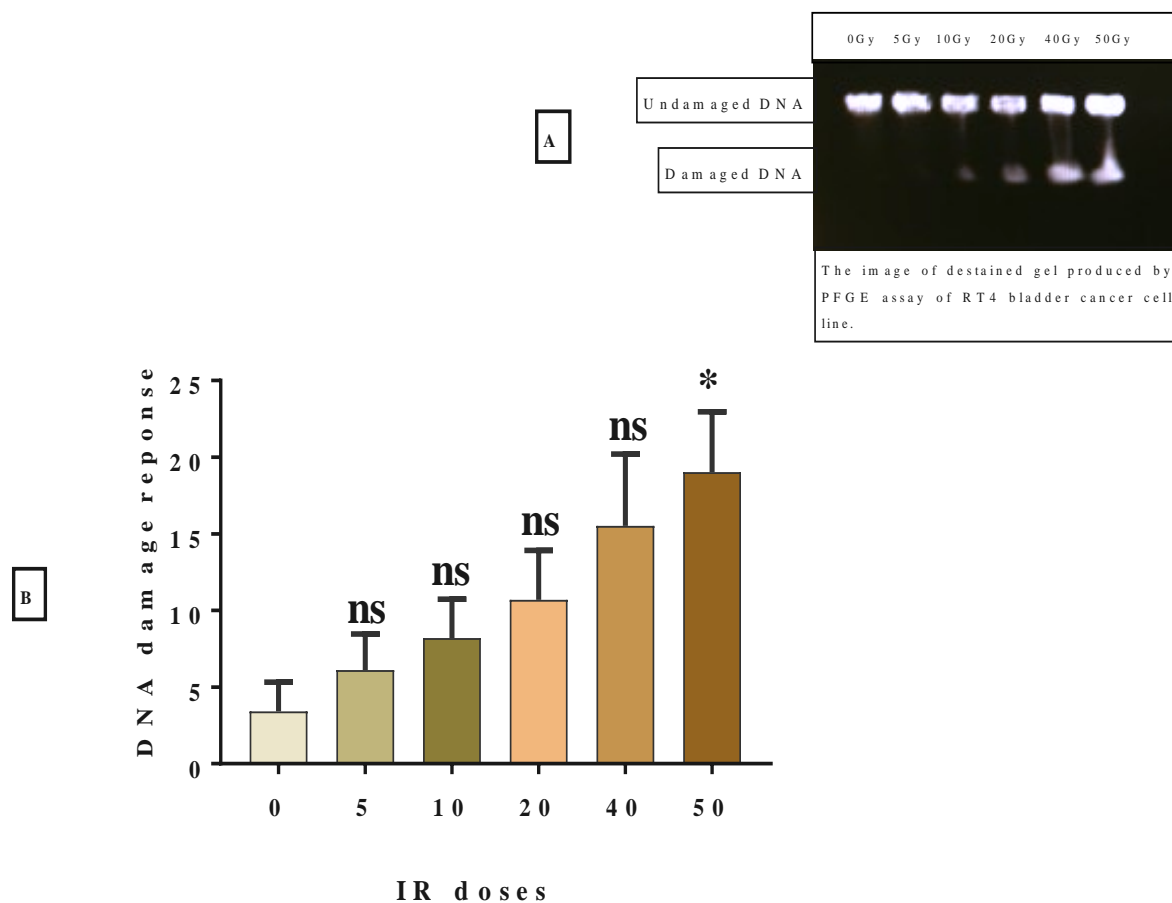
## **5.4 Results**

### **5.4.1 Assessment of IR-induced DNA damage formation in the four bladder cancer cell lines as assessed by PFGE/CHEF**

PFGE using CHEF was carried out on UMUC3, RT112, J82 and RT4 bladder cancer cells to examine and analyse the formation of IR-induced DNA damage in the form of DNA DSBs. The plugs were prepared according to the number of doses, in duplicate. The unirradiated control cell samples were prepared, and experimental samples were exposed to 5, 10, 20, 40 and 50 Gy of IR. All experimental steps were completed as outlined in the Materials and Methods (Chapter 2). Finally, the gel was stained, and the bands were visualised and analysed by SyngeneGeneSnap software (Syngene, Corston, UK). Results were expressed as Mean $\pm$ SEM of four independent experiments.

### **5.4.2 Evaluation of IR-induced DNA DSBs formation in the RT4 bladder cancer cell line**

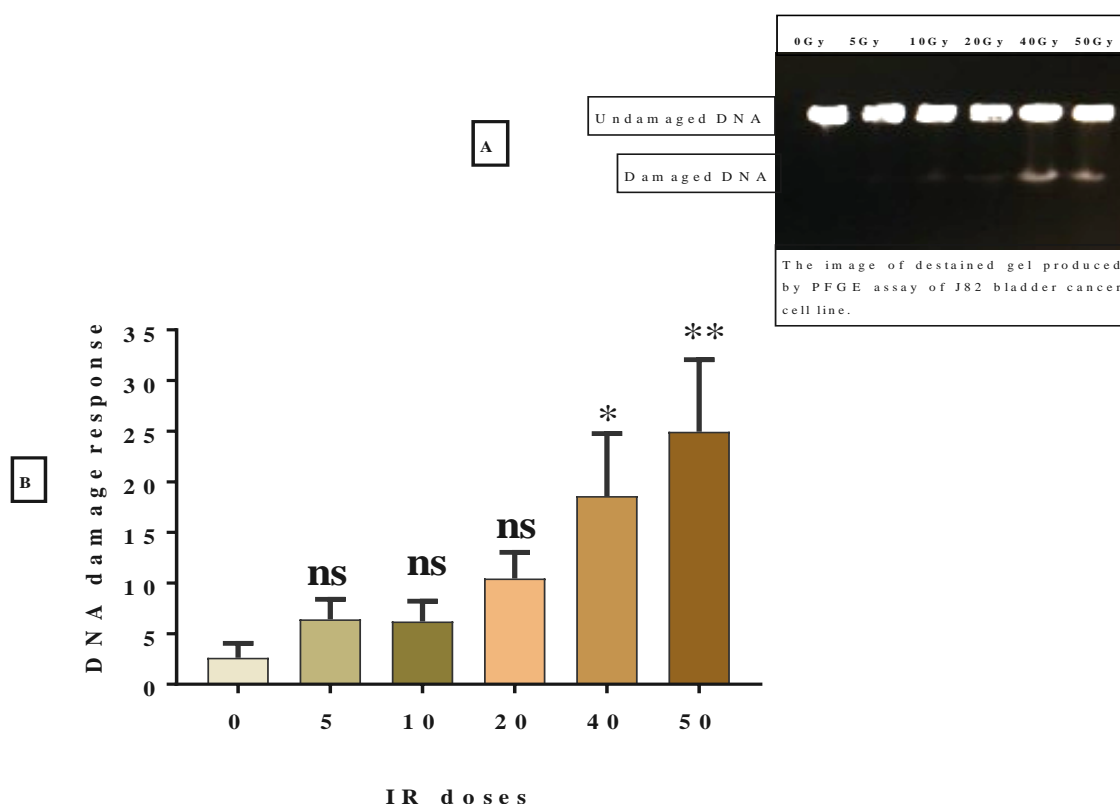
The DSB DNA damage induced by IR was firstly examined in RT4 bladder cancer cells using the PFGE assay. Figure 5.2 shows that the treatment with IR significantly increased DNA damage following radiation exposure of 50 Gy, in comparison to non-irradiated control samples (ANOVA,  $*p=0.0103$ ). Whilst exposure to 5, 10, 20 and 40 Gy exhibited a non-significant increase in DNA damage compared to the non-irradiated control samples.



**Figure 5.2 (A) Image of a de-stained gel produced by PFGE for RT4 bladder cancer cells. (B) DNA damage response for RT4 bladder cancer cell line after exposure to 5, 10, 20, 40 and 50 Gy of IR doses compared to control sample (non-irradiated cells) using PFGE assay. Results are expressed as Mean  $\pm$  SEM of four independent experiments. One-way ANOVA was used for statistical analysis between the IR treated samples and the control sample: Ns, non-significant; \* $p$ <0.05.**

### 5.4.3 Evaluation of IR-induced DNA DSBs formation in the J82 bladder cancer cell line

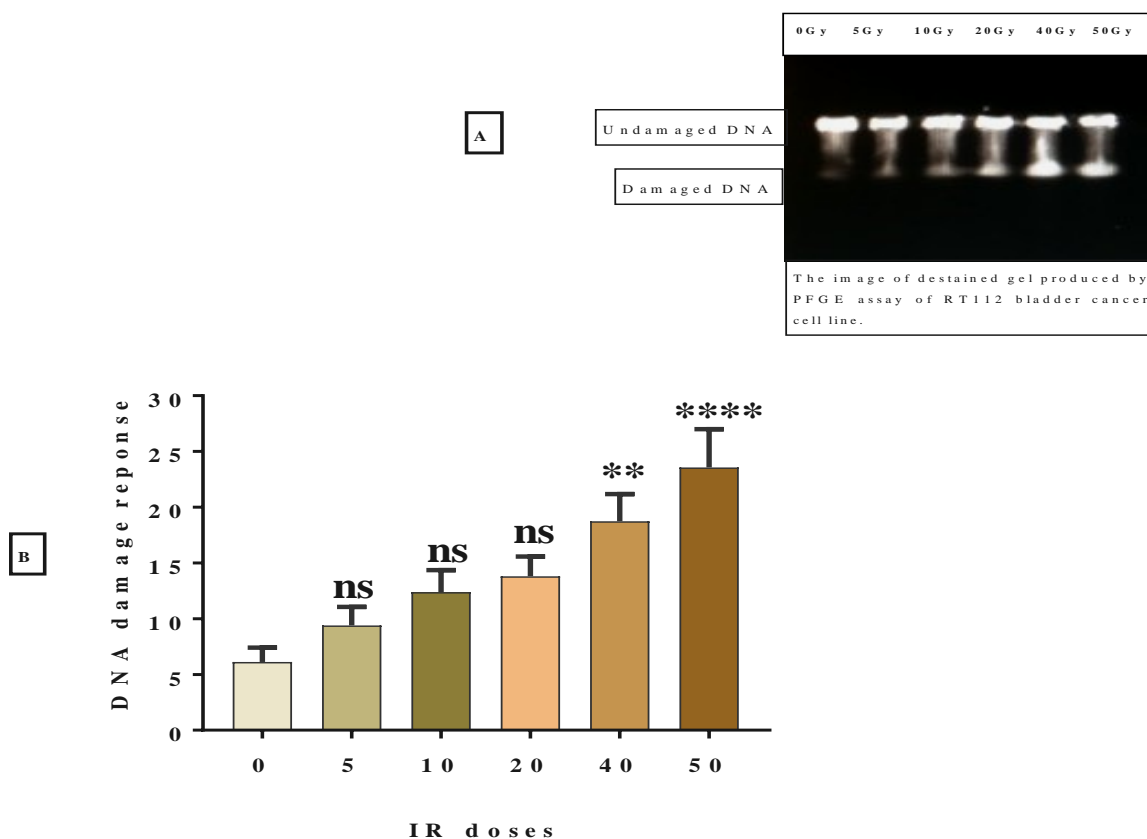
The J82 cells were prepared and treated under exact laboratory conditions. Figure 5.3 illustrates that the treatment with IR significantly increased DNA damage formation compared to non-irradiated control sample when cells were exposed to 40 and 50 Gy (ANOVA,  $*p=0.0498$  and  $**p=0.0041$ , respectively). Yet, similar to RT4 cells, a non-significant increase was observed between the untreated control sample and cells exposed to 5, 10 and 20 Gy.



**Figure 5.3 (A) Image of a de-stained gel produced by PFGE for J82 bladder cancer cells. (B) DNA damage response for J82 bladder cancer cell line after exposure to 5, 10, 20, 40 and 50 Gy of IR doses compared to control sample (non-irradiated cells) using PFGE assay. Results are expressed as Mean  $\pm$  SEM of four independent experiments. One-way ANOVA was used for statistical analysis between the IR treated samples and the control sample: Ns, non-significant;  $*p<0.05$ .**

#### 5.4.4 Evaluation of IR-induced DNA DSBs formation in the RT112 bladder cancer cell line

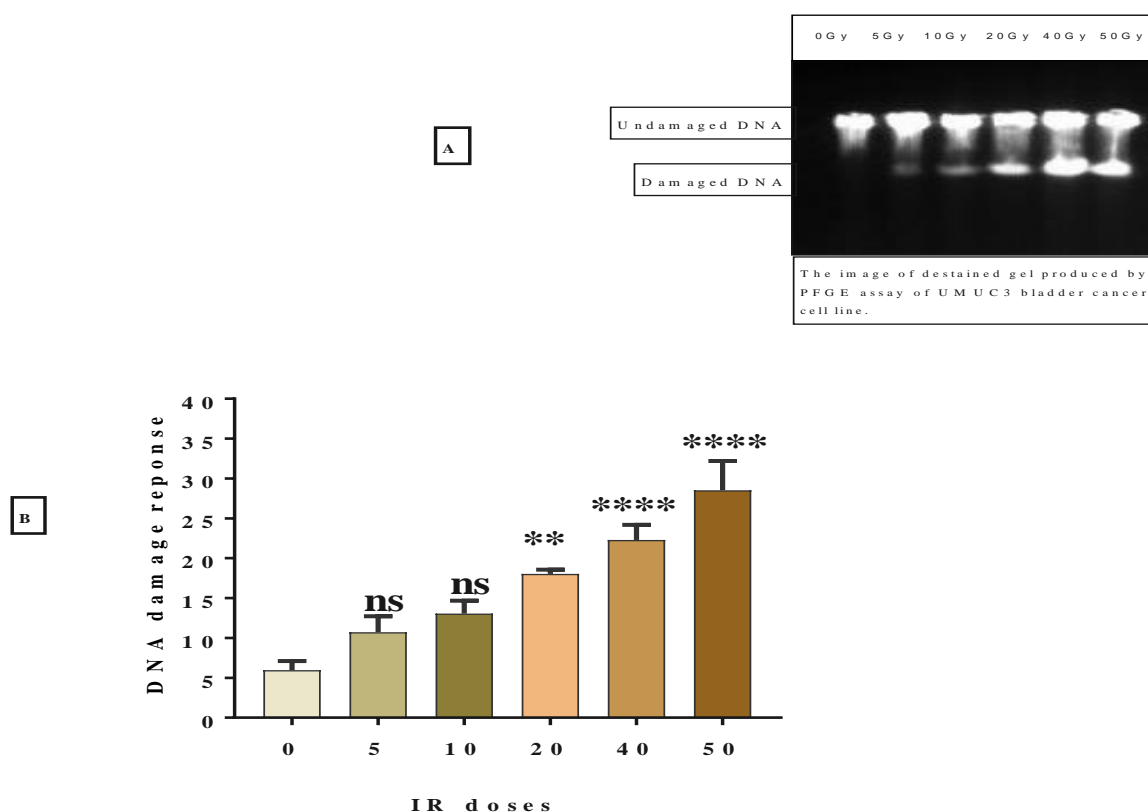
IR-induced DNA damage was further assessed in the RT112 bladder cancer cell line. These cells were treated and analysed under exact laboratory conditions as the previous cell lines. In Figure 5.4, increasing IR doses yielded a significant increase in DNA damage formation compared to non-irradiated control sample, when cells were exposed to 40 and 50 Gy (ANOVA,  $**p=0.0022$  and  $****p=0.0001$ , respectively). Yet, similarly to previous cell lines, exposure to 5, 10, and 20 Gy exhibited a non-significant increase in DNA damage compared to the non-irradiated control sample.



**Figure 5.4 (A) Image of a de-stained gel produced by PFGE for RT112 bladder cancer cells. (B) DNA damage response for RT112 bladder cancer cell line after exposure to 5, 10, 20, 40 and 50 Gy of IR doses compared to control sample (non-irradiated cells) using PFGE assay. Results are expressed as Mean  $\pm$  SEM of four independent experiments. One-way ANOVA was used for statistical analysis between the IR treated samples and the control sample: Ns, non-significant;  $**p<0.01$  and  $****p<0.0001$ .**

### 5.4.5 Evaluation of IR-induced DNA DSBs formation in the UMUC3 bladder cancer cell line

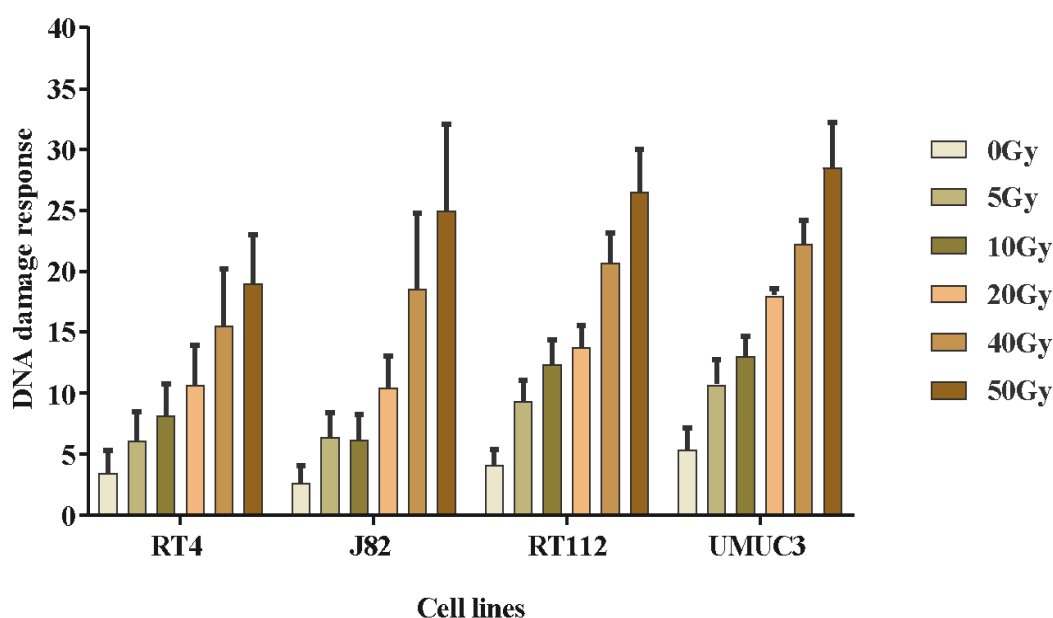
IR-induced DNA damage formation was assessed in UMUC3 bladder cancer cell line by utilising the PFGE assay, and the cells were prepared, treated and analysed under exact laboratory conditions as previously mentioned. Dunnett's multiple comparisons test showed that when cells were exposed to IR dose of 20, 40 and 50 Gy, there was a significant difference between the non-irradiated control sample and the irradiated cells (ANOVA,  $**p=0.0016$ ,  $****p=0.0001$ , and  $****p=0.0001$ , respectively). Still, similarly to previous cell lines, no significant DNA damage response was observed between the non-irradiated control sample and the cells were exposed to IR doses of 5 and 10 Gy, as depicted in Figure 5.5.



**Figure 5.5 (A) Image of a de-stained gel produced by PFGE for UMUC3 bladder cancer cells. (B) DNA damage response for UMUC3 bladder cancer cell line after exposure to 5, 10, 20, 40 and 50 Gy of IR doses compared to control sample (non-irradiated cells) using PFGE assay. Results are expressed as Mean  $\pm$  SEM of four independent experiments. One-way ANOVA was used for statistical analysis between the IR treated samples and the control sample: Ns, non-significant;  $**p<0.01$  and  $****p<0.0001$ .**

#### 5.4.6 The combined results for RT4, J82, RT112 and UMUC3 for estimation of the rank-order of IR-induced DNA DSB levels in these cell lines, as measured by the PFGE assay

Figure 5.6 compares the PFGE assay measurements of IR-induced DNA DSBs formation observed in the RT4, J82, RT112, and UMUC3 bladder cancer lines. Cells were exposed to IR over a dose range of 0, 5, 10, 20, 40, and 50 Gy, and assessed by the PFGE assay. From the results, a clear IR-induced DNA damage response was observed in the four bladder cancer cell lines, in which UMUC3 bladder cancer cells being the most damage sensitive, and RT4 cells being least damage sensitive to IR exposure.

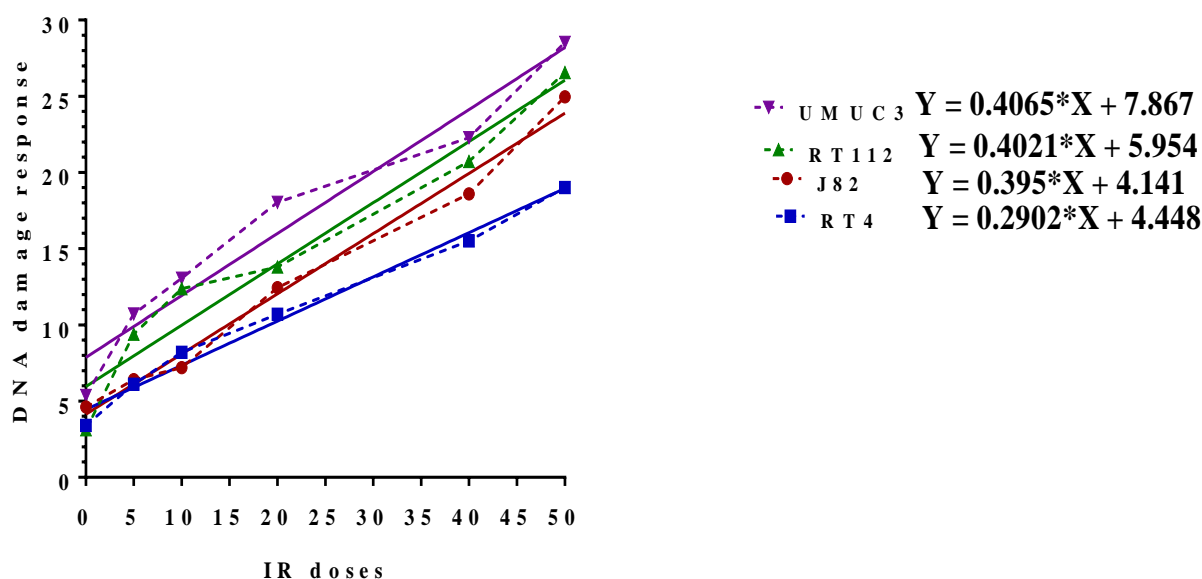


**Figure 5.6 IR-induced DNA damage in RT4, J82, RT112, and UMUC3 bladder cancer cell lines.** The percentage of DNA DSBs damage response was measured by the PFGE assay. Results were expressed as Mean  $\pm$  SEM of four independent experiments.

A further analysis was carried out on the data acquired for the four bladder cancer cell lines, as determined by the PFGE assay. Figure 5.7 shows a linear plot depicting the relationship between the level of induced DNA DSBs and IR dose. Each point represents mean of four

different readings from four independent experiments. Two-way ANOVA tests were conducted to test for significant differences between the damage levels observed. Tukey's multiple comparison test was conducted, which compared the overall mean obtained for each radiation dose with each specific measure at the same single dose for the four bladder cancer cell lines.

The data presented in Figure 5.7 revealed that UMUC3 cells and RT112 cells are the most damage sensitive cells, whilst J82 cells and RT4 cells are the most damage resistant. Analysis of data has shown that there were no significant differences in the level of IR-induced DNA DSBs obtained between the four bladder cancer cell lines after exposure to 0, 5 and 10 Gy with an exception being between UMUC3 cells and J82 cells (ANOVA,  $*p=0.0322$ ) post exposure to 10 Gy. The level of DNA DSBs formation was significantly increased between UMUC3 cells and RT4 cells when cells were exposed to 20 Gy (ANOVA,  $*p=0.0210$ ), however, no observable significant increase was found from the comparative analysis between other cell lines following exposure to 20 Gy. Additionally, significant enhancements in the level of IR-induced DNA DSBs formation was evident for comparative analysis between UMUC3 cells and RT4 cells when exposed to 40 Gy (ANOVA,  $*p=0.0343$ ). But, no notable significant differences in the level of IR-induced DNA DSBs formation was evident when comparative analysis was conducted between RT4 cells and J82 cells, RT4 cells and RT112 cells, J82 cells and RT112, J82 cells and UMUC3 cells, as well as between RT112 cells and UMUC3 cells post exposure to 40 Gy as revealed by Tukey's multiple comparison tests. Comparative analysis of UMUC3 cells and RT112 cells with RT4 cells revealed that the level of DNA DSBs formation induced by 50 Gy was significantly higher than that in RT4 cells (ANOVA,  $**p=0.0030$  and  $*p=0.0176$ , respectively). However, no significant differences in the level of DNA DSBs formation was observed when comparing the differences between any of the other cell lines.



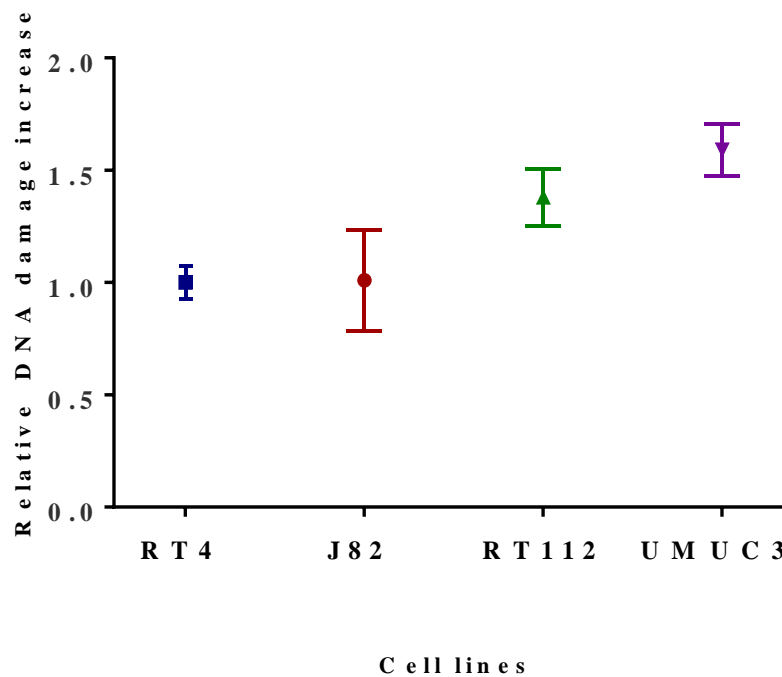
**Figure 5.7** The DNA DSBs damage response for four bladder cancer cell line after exposing to 0, 5, 10, 20, 40, and 50Gy of IR doses as assessed by PFGE assay. The data represent mean of four independent experiments. Two-way ANOVA was used for statistical analysis to compare between the four bladder cancer cells: Ns, non-significant, \* $p < 0.05$ , \*\* $p < 0.01$ , \*\*\* $p < 0.001$  and \*\*\*\* $p < 0.0001$  versus the damage induced by IR doses (See text for details).

#### 5.4.7 Measurement of the relative DNA DSB formation increase induced by IR in the four bladder cancer cell lines, as determined by the PFGE assay

To further substantiate the differential effects of IR on the levels of induced DNA DSBs formation in the four bladder cancer cell lines as measured by the PFGE assay, and to enable further statistical analysis, a further analysis was conducted. For this analysis (shown in Figure 5.8) each individual dose measure of the lowest responding cell line (RT4) was used to calculate the relative damage response increase noted from each other cell line at the same dose. Then, the relative DNA damage responses for each individual cell line were then averaged and plotted  $\pm$  SD. Two-way ANOVA with Tukey's multiple comparison tests was used to investigate significant differences between relative DNA damage responses of the



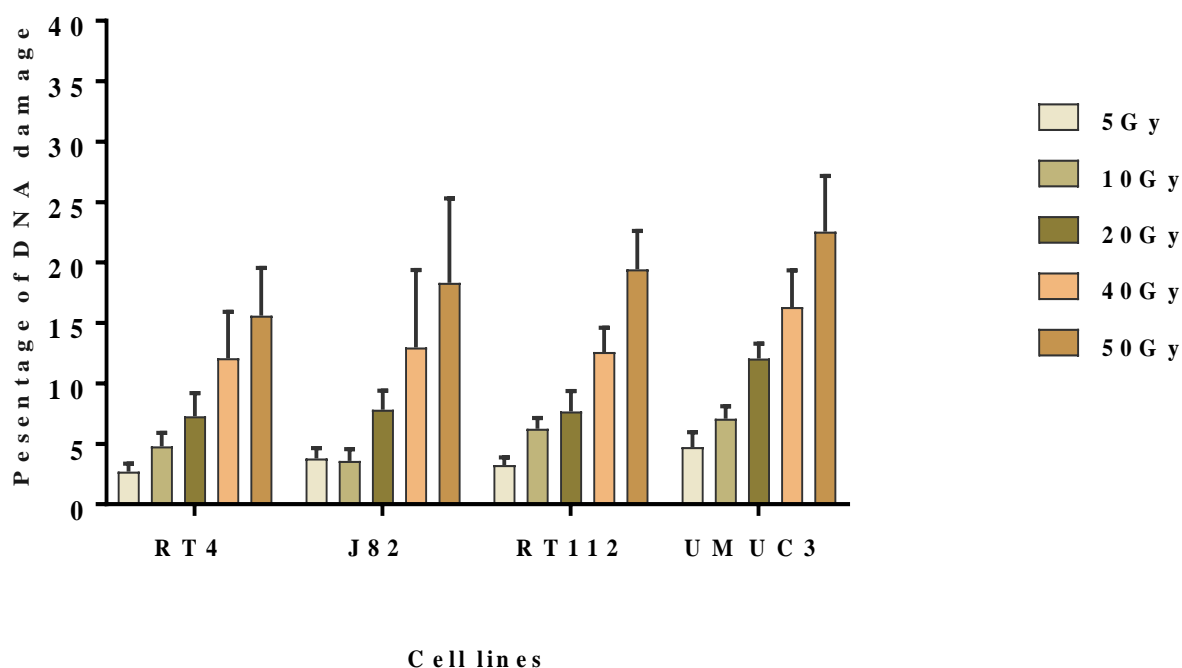
four bladder cancer cell lines. Interestingly, the relative levels of IR-induced DNA DSBs formation observed were significantly higher in UMUC3 cells in comparison to RT4 cells (ANOVA, \*\*\*\* $p < 0.0001$ ), also when UMUC3 cells were compared to J82 cells (ANOVA, \*\*\*\* $p < 0.0001$ ). Moreover, RT112 cells exhibited significantly higher relative level of IR-induced DNA DSBs formation in comparison to RT4 cells (ANOVA, \*\* $p = 0.0019$ ) and to J82 cells (ANOVA, \*\* $p = 0.0024$ ). Yet, there was no significant difference noted between RT4 cells and J82 cells, nor between RT112 cells and UMUC3 cells. Overall, these results indicated that the cells exhibited a wide range of damage response, with UMUC3 cells having the highest damage response, with RT112 cells having relatively less sensitive response to IR when compared to UMUC3 cells. RT4 cells and J82 cells exhibited the lowest DNA damage response.



**Figure 5.8** The relative of DNA damage increase for the four bladder cancer cell line, inclusive of the background/basal levels of damage, after exposure to 0, 5, 10, 20, 40 and 50 Gy of IR doses as measured by PFGE. Each bar represents Mean  $\pm$  SD of the relative damage increases. Two-way ANOVA test was used to analyse the mean of the four bladder cancer cell lines' responses. (See text for details).

#### 5.4.8 Investigation of the effect of IR-induced DNA DSBs formation response on the four bladder cancer cell lines following the subtraction of background/basal levels of DNA damage, as determined by PFGE

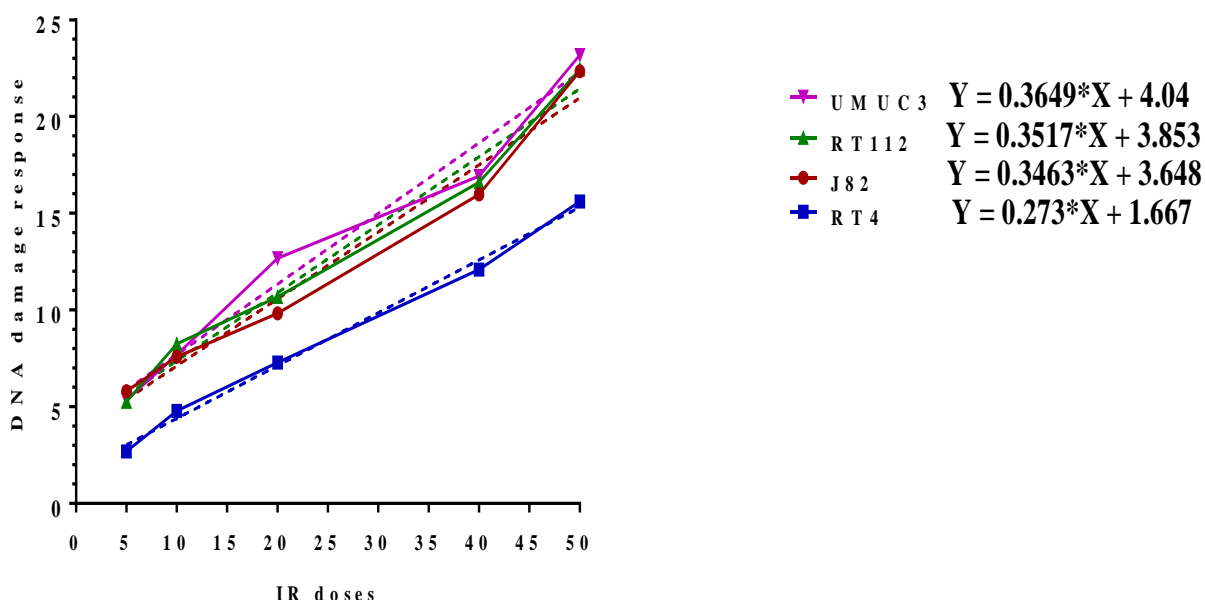
To further substantiate the above observations, analyses were repeated following the subtraction of the background/basal levels of DNA damage, so as to focus on the ‘truly’ induced levels of DNA DSBs formation in the four bladder cancer cell lines. Clear increases in IR-induced DNA damage for the RT4, J82, RT112, and UMUC3 bladder cancer cells were obtained which assisted in distinguishing the damage sensitivity of these cell lines (Figure depicted in 5.9).



**Figure 5.9** IR-induced DNA damage in RT4, J82, RT112, and UMUC3 bladder cancer cell lines after subtraction the background/basal levels of DNA damage following 5, 10, 20, 40 and 50 Gy of IR, as assessed by PFGE assay. Each bar represents Mean  $\pm$  SEM of four independent experiments.

Figure 5.10 reveals that the level of IR-induced DNA DSBs formation. Two-way ANOVA was used to investigate whether there were significant differences in DNA damage response occurring between the four bladder cancer cell lines. No significant difference was observed when the four bladder cancer cell lines were exposed to 5, 10 and 20 Gy. However, there was a significant difference in the comparative analysis of UMUC3 cells and RT4 cells at 20 Gy (ANOVA,  $*p=0.0130$ ), and DNA DSBs formation level was significantly detectable at 40 Gy when comparing the following cell lines: UMUC3 cells and RT4 cells (ANOVA,  $*p=0.0257$ ) and RT112 cells and RT4 cells (ANOVA,  $*p=0.0378$ ). Yet, the Tukey's multiple comparison tests showed no significant difference in the level of IR-induced DNA DSBs formation in comparative analysis between UMUC3 cells and J82 cells, RT112 cells and J82 cells, and UMUC3 cells and RT112 cells following 40 Gy. Finally, a significant increase in the level of IR-induced DNA DSBs formation was evident at 50 Gy in comparative investigations of the cancer cells lines (UMUC3, J82 and RT112) to RT4 cells; specifically, UMUC3 cells (ANOVA,  $**p=0.0010$ ), RT112 cells (ANOVA,  $**p=0.0023$ ) and J82 cells (ANOVA,  $**p=0.0026$ ). Still, the Tukey's multiple comparison tests showed no significant difference in the level of IR-induced DNA DSBs formation in comparative analysis between UMUC3 cells and J82 cells, RT112 cells and J82 cells, and UMUC3 cells and RT112 cells.

Based on the results outlined, with omission of the background/basal levels of DNA DSBs, the four bladder cancer cell lines revealed a considerably higher level of IR-induced DNA DSBs formation evident in UMUC3 cells followed by the RT112 cells, with the lowest level of DSBs formation being observed in the J82 cells and RT4 cells.

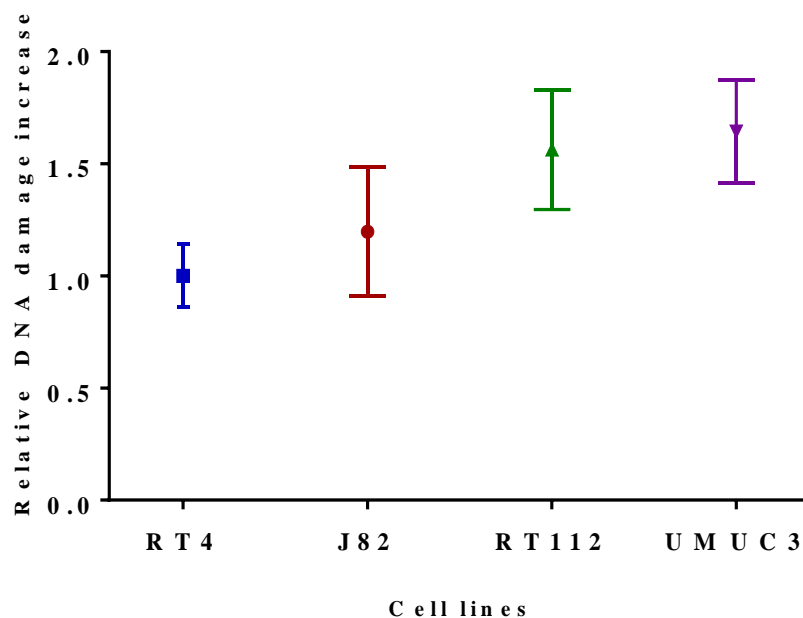


**Figure 5.10** The DNA damage (DSBs) for the four bladder cancer cell lines, after subtraction the endogenous damage, following 5, 10, 20, 40 and 50 Gy of IR as assessed by PFGE assay. The data represent mean of four independent experiments. Two-way ANOVA was used for statistical analysis to compare between the groups (see text for further details).

#### 5.4.9 Measurement of relative DNA DSBs formation level induced by IR in the four bladder cancer cell lines following the subtraction of background/basal levels

Following the encouraging results obtained and depicted in Figures 5.9 and 5.10, an additional investigation was carried out to compare the relative level of IR-induced DNA DSBs formation in the four bladder cancer cells lines. In Figure 5.11, after omission of the background/basal levels of DNA damage from the four cell lines individually, each individual dose measure of the lowest responding cell line (RT4) was used to calculate the relative damage-response increase noted from each other cell line at the same dose. The relative DNA damage responses for each individual cell were then averaged and plotted  $\pm$  SD. Two-way ANOVA with Tukey's multiple comparison tests were used to investigate significant differences between relative responses of the four bladder cancer cell lines. The

plot reveals a clear response as measured by the percentage of DNA damage response. UMUC3 cells exhibited signs of acquiring significant levels of IR-induced DNA DSBs formation when comparative analysis was undertaken between UMUC3 cells and RT4 cells (ANOVA,  $**p=0.0013$ ), UMUC3 cells and J82 cells (ANOVA,  $*p=0.0185$ ), and RT112 cells and RT4 cells (ANOVA,  $**p=0.0037$ ), as determined by the PFGE assay. Though, Tukey's multiple comparison tests showed non-significant differences in the meaning of measuring the relative DNA DSBs damage increase when comparing J82 cells to RT4 cells, RT112 cells to J82 cells, and UMUC3 cells to RT112 cells, respectively.



**Figure 5.11** The relative of DNA damage increase for the four bladder cancer cell lines, after subtraction the endogenous damage from 5, 10, 20, 40 and 50Gy of IR doses results, as assessed by PFGE assay. Each bar represents Mean  $\pm$  SD of four independent experiments. Two-way ANOVA test was used to compare the mean of the four bladder cancer cell lines (see text for further details).

#### **5.4.10 Correlation of total summation of IR-induced DNA SSBs damages as assessed by ACA with total summation of IR-induced DNA DSBs damages as assessed by PFGE assay in UMUC3, RT112, J82 and RT4 bladder cancer cell lines**

Figure 5.12a, shows a clear positive correlation between the total summation of IR-induced DNA SSBs damage as assessed by % TD and the total summation of IR-induced DNA DSBs damage as assessed by PFGE assay with inclusion of background/basal levels of DNA damage. Notably, UMUC3 and RT112 cells presented the highest level of DNA damage as measured by ACA and PFGE assay. In contrast, J82 and RT4 cells, presented a lowest level of DNA damage.

Moreover, a good correlation was observed between the total summation of IR-induced DNA SSBs damage as assessed by % TD and the total summation of IR-induced DNA DSBs damage as assessed by PFGE assay with subtraction of the background/basal levels of DNA damage. Again, UMUC3 and RT112 cells presented with the highest level of DNA damage sensitivity. In contrast, J82 and RT4 cells, presented a lowest level of DNA damage sensitivity (Figure 5.12b).

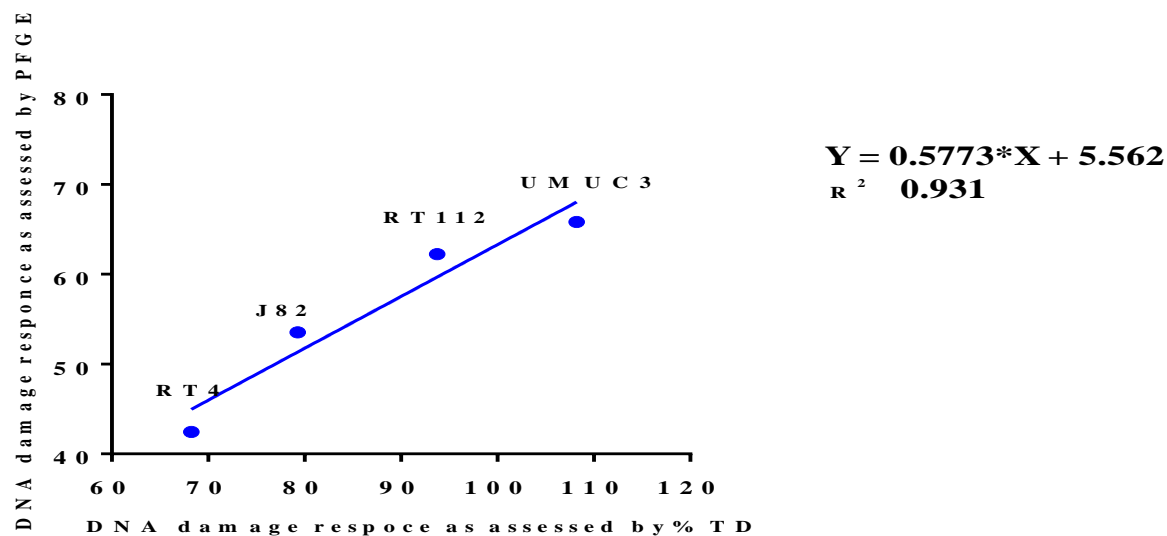
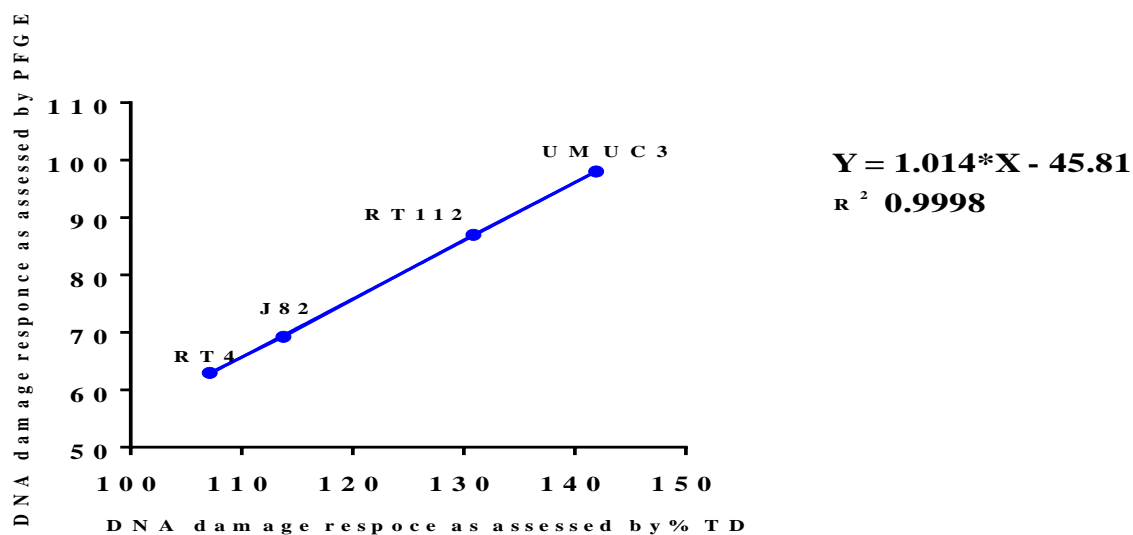


Figure 5.12a Relationship between total summation of IR-induced DNA damage as assessed by Comet assay %TD and the total summation of IR-induced DNA damage as assessed by PFGE assay; with inclusion of background/basal levels of DNA damage in UMUC3, RT112, J82 and RT4 cells



**Figure 5.12b** Relationship between total summation of IR-induced DNA damage as assessed by Comet assay %TD and the total summation of IR-induced DNA damage as assessed by PFGE assay; with subtraction of the background/basal levels of DNA damage.

Overall, following the promising results obtained as illustrated in Figures 5.7 to 5.12, UMUC3 cells showed the highest levels of IR-induced DNA DSBs formation. Accordingly, it can be concluded that the UMUC3 cells can be characterised as DNA damage sensitive to IR, followed by RT112 cells. In contrast, RT4 cells were shown to exhibit the lowest levels of DNA DSBs formation in comparison to the other bladder cancer cell lines. The rank order from the highest responding cells to the lowest responding cells, according to the results obtained, was UMUC3 > RT112 > J82 > RT4, matching the data obtained from the previous chapters; the comet assay and LC-MS/MS results Chapters.

## **5.5 Discussion**

Ionising radiation generates a wide variety of DNA damage through both direct ionisation and indirect damage to the DNA macromolecule with IR-induced DNA DSBs being the lesions responsible for radiation-induced cell killing mechanism (Jackson and Bartek, 2009b). The level of DNA damage in the four bladder cancer cell lines was measured following exposing the cells to different radiation doses and DSB levels were assessed using the PFGE assay. The analysis of the PFGE data showed that the level of IR-induced DNA DSBs formation increased with higher radiation dose. Results revealed that the rank order of differential IR-induced DNA DSBs formation as determined by the PFGE assay matched the rank order of damage sensitivity determined by ACA.

The PFGE assay has been shown to be a powerful method for genomic analysis (Grądzka and Iwaneńko, 2005; Goering, 2010) this method has been constantly developed, with various modifications being introduced. Yet, the most commonly used protocol, and the one implemented in this project, is the contour-clamped homogeneous electric field electrophoresis (CHEF) system (Chu et al., 1986), as it has the potential to enhance DNA separation by changing the reorientation angle between the two run directions, the pulse length, as well as the strength of the electric field.

Within the present study, RT4, J82, RT112, and UMUC3 cells were studied by the PFGE/CHEF assay to evaluate the levels of IR-induced DNA DSB damage to distinguish between damage sensitive and damage resistant bladder cancer cell lines. The cells were



irradiated whilst embedded in agarose gel plugs, and the procedure was undertaken as described in the Materials and Methods chapter (Chapter 2).

The results showed that irradiation the doses used caused a considerable level of induced DNA DSBs that positively correlated with the increasing doses of IR for all four bladder cancer cell lines. The results overall demonstrated an increase in DSBs formation at all the doses studied, with a consistent and significantly higher level of IR-induced DSBs being observed in the UMUC3 cells and RT112 cells compared with lower levels of IR-induced DSBs observed in the RT4 cells and J82 cells. This was irrespective of the nature of the data analysis undertaken: correlated dose-response, calculated relative damage increases and the Correlation between the total summation SSBs damages as assessed by ACA with total summation of DSBs damages as assessed by PFGE assay in UMUC3, RT112, J82 and RT4 bladder cancer cell lines. Indeed, taking all the data together, the rank-order of damage sensitivity as determined by PFGE assessment of IR-induced DSB formation is: UMUC3 > RT112 > J82 > RT4; as determined by dose response in Figures 5.6, 5.7, 5.9, 5.10, and 5.12 for the four bladder cancer cells lines.

The effects of IR-induced DNA DSBs formation in the bladder cancer cell lines, as shown in Figures 5.8 and 5.11, were calculated to measure the relative damage increase noted for each of the more damage sensitive cells, relative to RT4, at the same dose. The relative responses for each individual cell line were then averaged and plotted  $\pm$  SD. The relative damage increase data also indicated that UMUC3 cells were substantially more sensitive to IR dose effects compared with RT4 cells and J82 cells. Thus, based on the data presented in the current study for the four bladder cancer cells, it can be speculated that UMUC3 cells and RT112 cells are more damage sensitive to IR effects in contrast to RT4 cells and J82 cells which exhibited a more damage resistant response to IR effects.

Nevertheless, the PFGE method has some limitations. One key limitation is background damage in un-irradiated human cells. Background damage levels are often quite high, especially when measurements are taken from primary patient samples. Therefore, this effect must be controlled for during any DNA damage evaluation, as background damage levels can skew the sensitivity of the data which subsequently can influence the nonlinearity of the dose-response curves (McMillan et al., 2001). Another limitation for this assay is

arrangement of the agarose slices. For optimal electrophoresis the agarose plugs have to be uniformly aligned in the wells to allow for the consistent migration of the DNA. In addition, the presence of skewed lanes may result from uneven gel thickness due to uneven surface during gel casting or faulty electrodes (Goering, 2004). However, more recent protocols can be completed in two days by the direct addition of lytic enzyme(s) to the agarose mixture before the blocks are cast and high temperature short-term washes (50–55°C) which improve in facilitating the extraction of unwanted compounds (Goering and Winters, 1992; Ribot et al., 2006; Halpin et al., 2010).

Data obtained from the present study suggests that UMUC3 cells and RT112 cells are more susceptible to IR-induced DNA damage in comparison to RT4 cells and J82 cells. This observation is consistent with previous research (McKeown et al., 2003; Moneef et al., 2003) which indicated that UMUC3 cells are more damage sensitive and RT4 cells are more damage resistant when exposed to varying IR doses. More importantly, based on the results shown in Figure 5.9, and 5.10, after omission of the background/basal levels of DNA damage occurring within the four bladder cancer cell lines, permits the evaluation of the radiogenic induced damage sensitivities of these bladder cancer cell lines. UMUC3 cells were more susceptible to DNA damage post exposure to IR dose range. Consequently, UMUC3 cells yielded the highest radiogenic sensitivity followed by RT112 cells, with J82 and RT4 cells revealing the lowest level of radiogenic sensitivity.

Thus, these findings corresponded with the data analysed in previous chapters (Chapters 3 & 4). Therefore, the results obtained and analysed here support the first hypothesis (Model 1), that differential measurements of comet formation between the four bladder cancer cell lines reflect actual differences in DNA damage levels.

## **Chapter 6**

**Estimation of IR-induced DNA DSBs damage in the four  
bladder cancer cells using the  $\gamma$ -H2AX assay**

## **6.1 Introduction**

### **6.1.1 Estimation of IR-induced DNA DSBs damage in the four bladder cancer cells using the $\gamma$ -H2AX assay**

The genomic DNA is primary cellular target for the biological effects of ionizing radiation, with DNA DSBs being considered to be the most lethal lesions induced. However, DNA DSBs also occur during normal cellular processes, including DNA replication, cellular senescence, and exposure to reactive oxygen species (Myung et al., 2008). DSBs in DNA may lead to genetic instability and gene mutation resulting in reduced integrity of the genome and reduced survival of the organism (Olive, 1998; Svetlova et al., 2010).

Radiation-induced changes in DNA damage signaling factors, such as formation of  $\gamma$ -H2A histone family member X ( $\gamma$ -H2AX), contribute to the key cellular responses to ionising radiation. These responses consist of the induction of genes for proteins that are involved in DNA repair processes, cell cycle arrest and cell division or apoptosis. An early response to DNA DSBs in the cell is the phosphorylation of the C-terminal of the core histone protein H2AX (termed  $\gamma$ -H2AX when phosphorylated) (Rogakou et al., 1998; Savic et al., 2009; Ban  th et al., 2010). The histone protein H2AX is rapidly phosphorylated at serine 139 of its C-terminal tail by DNA kinases such as ATM, ATR, and DNA-PK to form  $\gamma$ -H2AX (Kinner et al., 2008). The phosphorylation of histone H2AX occurs extensively about the DNA DSB site forming foci at the sites of DSB damage (Rothkamm et al., 2015); the foci are in turn responsible for recruiting further DNA repair proteins (Srivastava et al., 2009; Rothkamm and Horn, 2009; Scully and Xie, 2013).

There are several different terms in use for DNA damage foci, such as (ionizing) radiation-induced foci (IRIF or RIF) or DNA repair foci. In general, they all refer to local accumulations of DNA damage response proteins that form at the sites of DNA DSBs (Rothkamm et al., 2015). The phosphorylated histone  $\gamma$ -H2AX, which involves a remarkable number of histone modifications, that can be visualized microscopically as spots after immunostaining (Stiff et al., 2004) and has been exploited for its usefulness as a marker of DSBs in multiple settings, including, making it a sensitive biomarker for radiation exposure (Rothkamm and Horn, 2009). Further details of bio-sampling, foci staining, detection and quantification have been discussed extensively (Olive, 2004; Nakamura et al., 2006;

Rothkamm and Horn, 2009; Löbrich et al., 2005; Ivashkevich et al., 2011; Redon et al., 2011; Barnard et al., 2013; Vignard et al., 2013a; Pouliliou and Koukourakis, 2014).

Exposure to ionising radiation leads to numerous types of DNA lesions. the absorption of a single unit of X-ray dose, termed a Gy (1 Gy = 1 joule/kg), corresponds to about 50,000–100,000 ionisations in a mammalian cell nucleus, which in turn induces about 2,000 base lesions (BL) per cell, about 1,000 single-strand breaks (SSB) and about 30 DSB (Dikomey et al., 2016). To repair some of these lesions, including DSB lesions, the DDR is initiated at the site of DNA damage (Ward and Chen, 2004; Sharpless and DePinho, 2007) whereby multiple factors involved in DNA repair and chromatin re-modelling accumulate at the broken site leading to the formation of  $\gamma$ -H2AX foci (Rogakou et al., 1999). The role of  $\gamma$ -H2AX is to activate DDR proteins and ensure the retention of repair proteins in the DNA DSB sites (Paull et al., 2000; Celeste et al., 2003). Phosphorylation of H2AX is an important step in the DDR process (Furuta et al., 2003; Lou et al., 2006; Bhogal et al., 2009). IR-induced  $\gamma$ -H2AX foci formation and loss have been extensively investigated (Madigan et al., 2002; Roch-Lefevre et al., 2010; Scully and Xie, 2013).

Detection of  $\gamma$ -H2AX has been used to measure DSBs in basic research, as a cancer biomarker (Keimling et al., 2012; Fernández et al., 2013) and as a means to measure radiation exposure (Muslimovic et al., 2012; Garty et al., 2015). The phosphoinositide 3-kinase-related protein kinase (PIKK) family which includes Ataxia Telangiectasia Mutated (ATM), Ataxia Telangiectasia and Rad3-related protein (ATR) and DNA protein kinase catalytic subunit (DNA-PKcs) are the major kinases that phosphorylate H2AX following DNA damage (Redon et al., 2002; Kinner et al., 2008). However, ATM is considered as the main kinase for H2AX phosphorylation in response to DSBs under normal physiological conditions and when a cell is exposed to ionising radiation, such as  $\gamma$ -radiation (Burma et al., 2001; Redon et al., 2002).

$\gamma$ -H2AX foci analysis is an assay that exploits this early step in the damage response (Paull et al., 2000; Rothkamm and Löbrich, 2003). Foci of  $\gamma$ -H2AX form within minutes after irradiation in a dose-dependent manner and typically peak between 30min and one – several hours post-irradiation; but then these foci are rapidly lost returning to baseline levels within one to several days, depending on the dose received (Goodarzi and Jeggo, 2012). Indeed, there are two main types of  $\gamma$ -H2AX foci in cells; first, the transient  $\gamma$ -H2AX foci which are

associated with rapid DSB repair and dephosphorylation of  $\gamma$ -H2AX to H2AX. These foci are usually activated within minutes to hours. Second are the residual  $\gamma$ -H2AX foci that tend to persist for days to months. The residual  $\gamma$ -H2AX foci has been also termed “excess  $\gamma$ -H2AX” foci (Löbrich et al., 2005; Moroni et al., 2013). Excess  $\gamma$ -H2AX foci suggest that DNA DSBs may exist for prolonged periods of time or can probably remain permanently unrepaired due to cellular senescence (Torudd et al., 2005; Fumagalli et al., 2012).

An antibody was generated to recognize  $\gamma$ -H2AX phosphorylated at the serine at position 139. Individual  $\gamma$ -H2AX can be observed by fluorescence microscopy by immunostaining cells with primary  $\gamma$ -H2AX antibodies coupled with fluorescent labeled secondary antibodies (Hamasaki et al., 2007; Siddiqui et al., 2015). The microscope counting of  $\gamma$ -H2AX foci (manual and automated) is the preferred method of quantitation, as it permits the detecting of very low doses of radiation and enables an estimate of dose even 24 h after irradiation (Horn et al., 2011). The  $\gamma$ -H2AX foci counting method is used in numerous studies as there is a close correlation between  $\gamma$ -H2AX foci and DSB numbers and between the rate of foci loss and DSB repair, providing a sensitive assay to monitor DSB repair in individual cells using physiological doses (Löbrich et al., 2010; Lassmann et al., 2010; Siddiqui et al., 2015). In radiation biology the number of DSBs positively correlates with  $\gamma$ -H2AX foci formation (Sedelnikova et al., 2002).

After DSB repair, the  $\gamma$ -H2AX molecules are dephosphorylated by protein phosphatase 2A (PP2A) and foci are no longer observable (Stiff et al., 2004). The kinetics of DNA DSBs repair follows two distinctive phases: a fast phase generally lasting a few hours followed by a slower phase that may continue for several hours or days and may extend to several months. The majority of DSBs (~80%) are repaired during the first phase of the repair process and the remaining portion (~20%) are repaired by slower phase (Riballo et al., 2004; Löbrich et al., 2010). Measuring DSBs which remain unrepaired several hours after an initial radiation exposure, may be predictive of individual radiosensitivity to complex DNA lesions which can be lethal to the cell (Banáth et al., 2010; Djuzenova et al., 2013). Also, the rate of  $\gamma$ -H2AX foci loss and the presence of residual foci has also been correlated with cellular radiosensitivity and absorbed radiation dose (Jeggo et al., 2011; Paris et al., 2011). In the present study, the  $\gamma$ -H2AX immunoassay was utilised for the detection of  $\gamma$ -H2AX foci in cells after x-ray radiation treatment with the foci being microscopically counted.

## **6.2 Summary of the techniques/approach**

To seek further substantiation of the findings of the previous Chapters, in which both LC-MS/MS and the PFGE assay indicated the bladder cancer cell lines UMUC3 and RT112 cells to be more damage sensitive than J82 and RT4 cells, it was decided to further investigate radiation-induced damage levels in the four cell lines using the often-used  $\gamma$ -H2AX assay. The different cells were exposed to IR at different doses and were then incubated for different time points prior to the analysis of  $\gamma$ -H2AX foci formation as markers of DNA DSB formation and repair. The materials and methods used for this chapter have been described in Chapter 2.

## **6.3 Aim**

The aim of this Chapter is to compare the relative differential measures of IR-induced comet formation as determined by ACA for the four bladder cancer cells lines (reported in Chapter 3), with  $\gamma$ -H2AX assay as a measure of IR-induced DNA DSBs formation, as determined by the number of foci. If an equivalent differential response is noted for the  $\gamma$ -H2AX assay, this would strongly suggest that the Comet assay does indeed measure differences in induced DNA damage between cell lines (so supporting Model 1); whilst the absence of a differential effect for the  $\gamma$ -H2AX assay would indicate that the differential effect noted by the Comet assay is possibly due to the additional release of the adjacent/contiguous loops of DNA to form a more extensive tail (Model 2). The number of foci per nucleus were measured for the four bladder cancer cell lines with both increasing dose and time post-irradiation. These experiments would help to establish the previous chapter's findings and so help establish the rank order of the bladder cell lines in terms of their damage sensitivity.

## **6.4 Results**

### **6.4.1 Optimisation the $\gamma$ -H2AX assay**

The number of foci per DAPI-stained nucleus needed to be optimised to enable the assessment a consistent number of foci for each treatment of the four bladder cancer cell lines.

In order to examine the effect of IR-induced DNA DSBs damages on the formation  $\gamma$ -H2AX foci, an Olympus Cytological imaging system was used to take images of the four cell lines after treatment with different IR doses and after different incubation times. The number of foci per DAPI-stained nuclei was measured for the four bladder cancer cell lines by using two different software programs (Data base program and Velocity program). In the Data base program, an automated meta-system was used to assess 4slides from each time point. 125 DAPI per slide were counted automatically and chosen for analysis by the Fiji software (WCIF Image J version 1.42, available from research services branch NIH) for each cell lines with duplicate. Images of clear  $\gamma$ -H2AX foci were captured using a 485 $\mu$ M filter, whereas the number of DAPI-stained nuclei were captured using a DAPI filter.  $\gamma$ -H2AX foci and nuclei numbers were counted automatically. After exclusion of cells with more than one nucleus, the average number of  $\gamma$ -H2AX foci per cell (DAPI nuclei) were obtained by dividing the total number of  $\gamma$ -H2AX foci by the total number of the counted cells. In the velocity program, Images were visualised using Velocity 6.3 software together with an upright Olympus BX16 automated fluorescent microscope (40x oil immersion objective) and Hamamatsu ORCA-R2 digital camera (pixel size 6.45 x 6.45 $\mu$ m). Images of nuclei stained with DAPI (Narrow-band UV filter: exciter filter B360-370, beam splitter DM400, barrier filter BA420) and  $\gamma$ H2AX foci (Narrow-band green filter: exciter filter BP530-550, beam splitter DM570, barrier filter BA590), 16 field images were captured manually from each cover slip and the same two filters were used to display  $\gamma$ -H2AX foci and the cell's nucleus. Then these 16 fields of view per slide were analysed by the Fiji software which obtained different numbers of DAPI per field. The actual numbers of  $\gamma$ -H2AX foci per cell (DAPI nuclei) were obtained by dividing the total number of  $\gamma$ -H2AX foci by the total number of cells per field.

After comparison of the two systems, the results of this Chapter were obtained using the Data base program software as it was able to obtain a consistent number of DAPI-stained nuclei for each dose and experiment. Moreover, this software was programmed to count the foci per nucleus automatically which reduced the counting time. (For information: Examples of some results obtained via Velocity program are given in an Appendix at the end of this thesis.)



#### **6.4.2 IR-induced DNA DSBs damage (foci formation) as assessed via $\gamma$ -H2AX assay in RT4, J82, RT112 and UMUC3 cells**

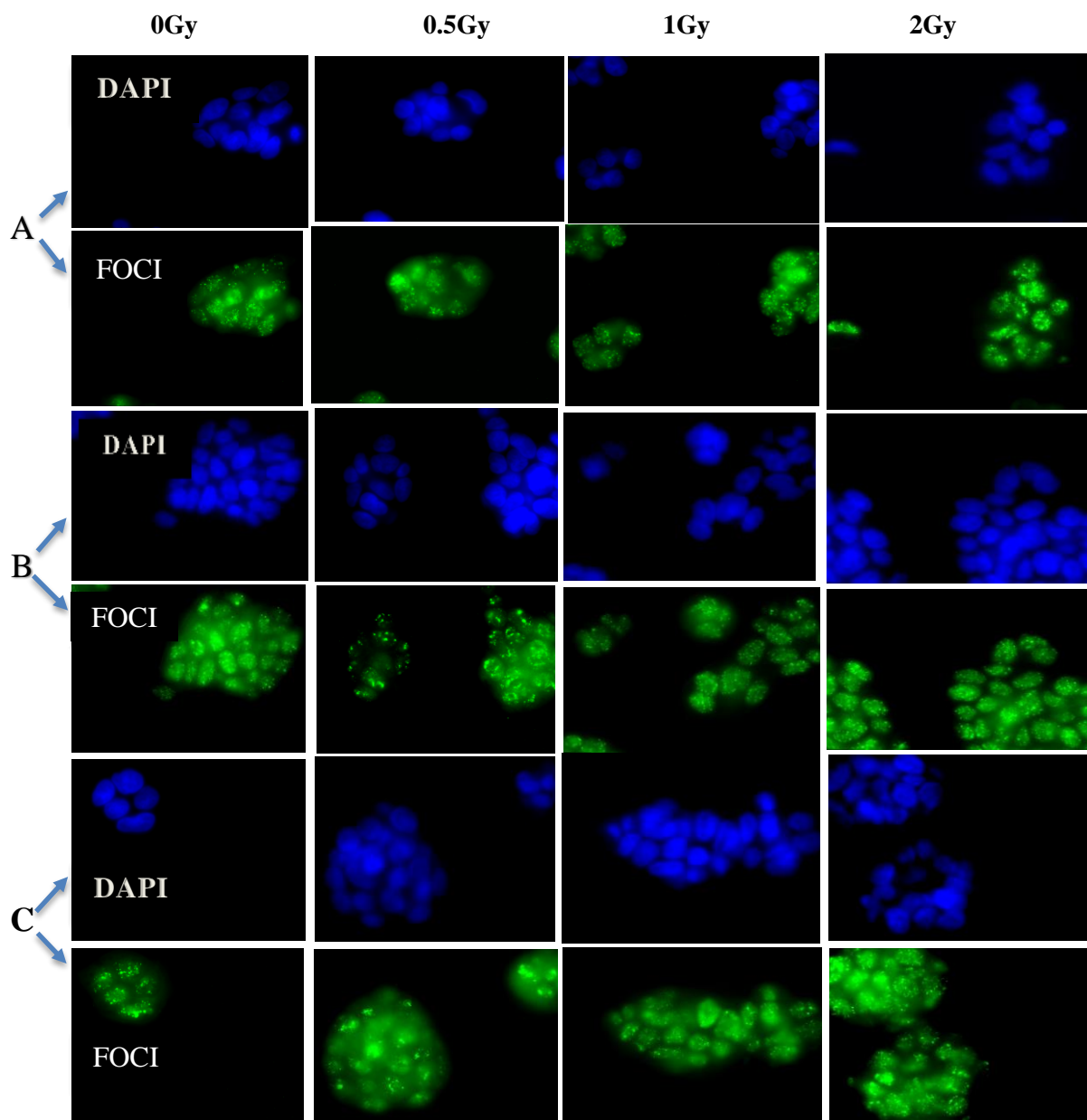
The effect of IR-induced DSBs was investigated in the four bladder cancer cell lines (RT4, J82, RT112, and UMUC3). The  $\gamma$ -H2AX immunoassay was used for the detection of  $\gamma$ -H2AX foci in cells after treatment. RT4, J82, RT112 and UMUC3 cells were seeded on coverslips in six-well plates at a density of 50,000 cells for each well, supplemented with 2ml of growth medium and left to grow overnight in a tissue culture incubator at 37°C, 5% CO<sub>2</sub> to enable 100,000 cells per well on the day of fixation. Separate six-well plates were required for each dose of IR used (0, 0.5, 1 and 2 Gy). The use of lower doses of IR, than those used in the Comet assay, was to avoid oversaturation of the cells with foci which may give false results as determined by the image analysis software (e.g. ImageJ and Fiji); as at higher doses, overlapping of foci leads to underestimation of foci number (Moquet et al., 2014). Runge et al. (2013) showed that the visual and automated scoring of  $\gamma$ -H2AX foci formation in rat thyroid cells demonstrated a direct correlation between  $\gamma$ -H2AX foci and radiation dose but that this was restricted up to 1 Gy of IR. Following exposure of cells to a dose of 5 Gy, visual scorers were unable to score  $\gamma$ -H2AX foci due to high density of DSBs which lead to  $\gamma$ H2AX foci overlap (diffuse foci). Thus, one of the main issues when scoring multiple foci after exposure to a high radiation dose is the phenomenon of foci overlap that makes it more difficult to distinguish  $\gamma$ -H2AX as discrete entities (foci) (Willitzki et al., 2013). The number of  $\gamma$ -H2AX foci per nucleus were assessed at different time points (30 mins, 2 hrs, 6 hrs, 16 hrs and 24 hrs). The number of foci per nucleus was measured for the four bladder cancer cell lines by using an Olympus Cytological imaging system together with the Data base program software.

##### **6.4.2.1 Estimation of DNA DSBs damage levels induced by ionising radiation in RT4 bladder cancer cells as assessed by $\gamma$ -H2AX foci counting**

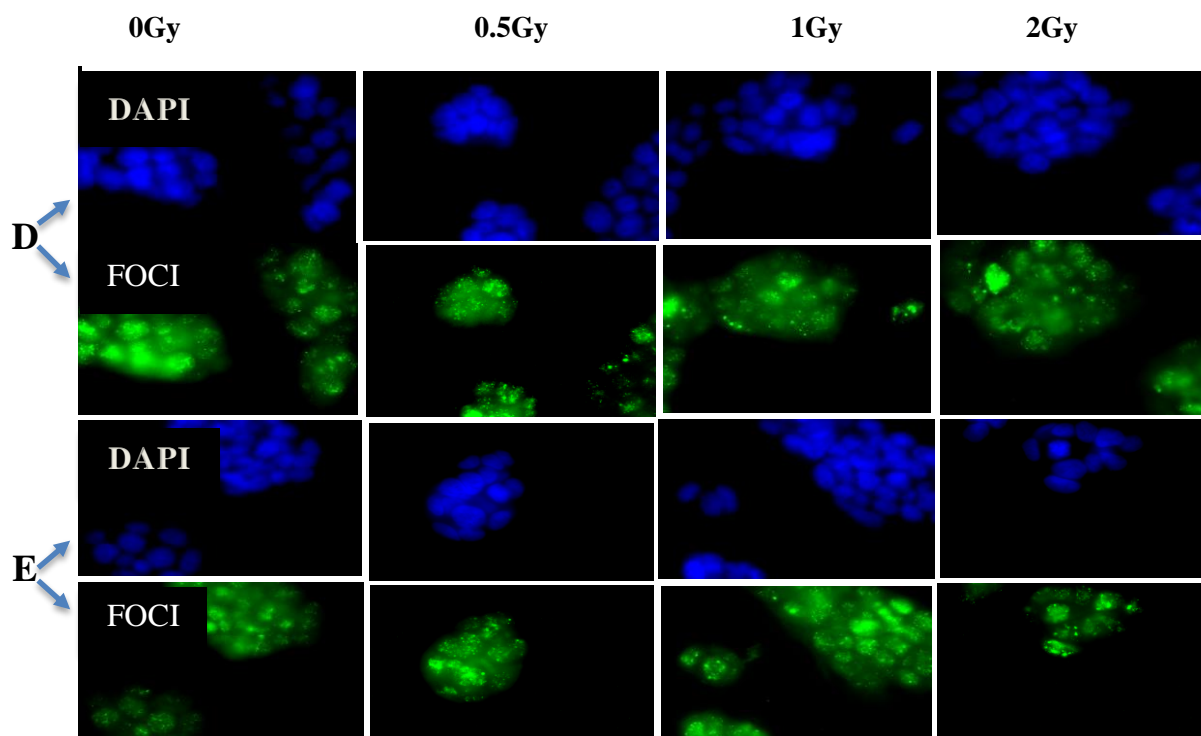
RT4 cells were first tested for  $\gamma$ -H2AX foci formation after exposure to IR (Figures 6.1a-c). The number of  $\gamma$ -H2AX foci induced by IR was significantly higher following 1 and 2 Gy (mean foci/cell:  $140.1 \pm 10.9$ ,  $*p= 0.0195$  &  $165.3 \pm 9.5$ ,  $****p<0.0001$ , ANOVA, respectively) detected after 30 mins of incubation time, when compared with the control

sample (non-irradiated cells). However, there was no significant difference in the number of foci detected between treated and non-treated cells when exposed to 0.5 Gy of IR. After 2hrs incubation post-irradiation, there was a significant increase in the number of DNA foci after 2 Gy and compared to the control sample (mean foci/cell:  $185.6 \pm 14.27$ ,  $*p= 0.0109$ , ANOVA), but no significant increase was seen for cells treated with 0.5 and 1 Gy compared to control sample cells. At 6 hrs post-irradiation with 1 and 2 Gy, the number of induced foci reached to the highest level (mean foci/cell:  $195.1 \pm 10.94$ ,  $**p= 0.0020$  &  $233.7 \pm 20.67$ ,  $***p<0.0001$ , respectively, ANOVA) but there was no significant increase in the number of foci after 0.5 Gy. Sixteen hours post-irradiation, the number of foci had declined, with the only significant difference being noted for cells irradiated with 2 Gy (mean foci/cell:  $157.5 \pm 9.319$ ,  $**p= 0.0059$ , ANOVA) compared to control cells. Twenty-four hours post-irradiation there is a significant difference in the DNA foci present following 1 and 2 Gy irradiation (mean foci/cell:  $148.8 \pm 9.8$ ,  $*p= 0.0326$  &  $151.5 \pm 7.2$ ,  $*p= 0.0169$ , respectively, ANOVA). It is clear that there are less numbers of foci after 16hrs and 24hrs of incubation compared to cells that were incubated for 6hrs. This was probably due to repair occurring in the RT4 cells with the highest level of foci being formed after 6hrs of incubation time. One-way ANOVA did reveal significant increases after exposure to the highest doses following 16 hrs and 24 hrs of incubation time, but overall there is a clear decline in the number of foci/cells.

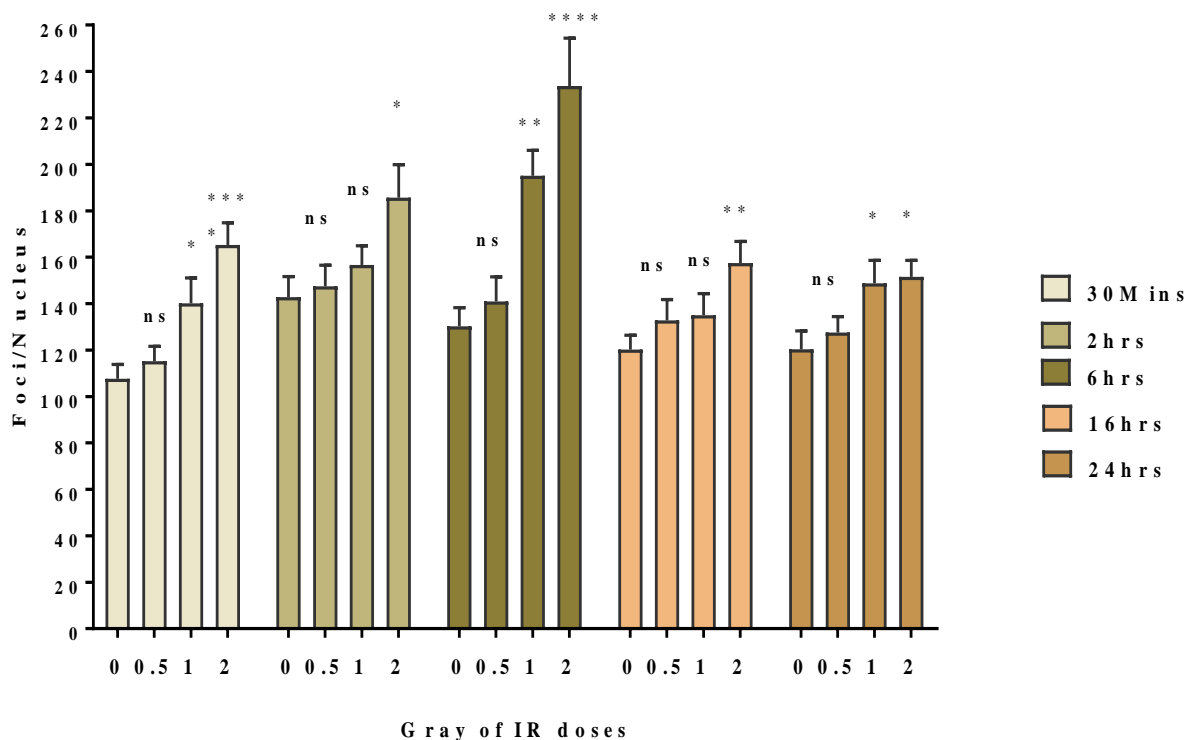
Interestingly, in these cells (and in the other cells – see below), high number of foci/cell were present even in the control samples. This is possibly due to high levels of endogenous DNA damage and/or ongoing instability, which could be possibly because they are cancerous cells.



**Figure 6.1a** Examples of DNA damage foci in Bladder cancer cells. Immunofluorescence staining for  $\gamma$ -H2AX (green) and DNA counterstaining with Dapi (blue) in RT4 bladder cancer cell line after exposing to 0, 0.5, 1 and 2 Gy of IR doses and incubated for (A) 30 mins (B) 2 hrs and (C) 6 hrs post irradiation. The fluorescence microscopy images were visualised at 40 x objective and captured using data base software program.



**Figure 6.1b** Examples of DNA damage foci in Bladder cancer cells. Immunofluorescence staining for  $\gamma$ -H2AX (green) and DNA counterstaining with Dapi (blue) in RT4 bladder cancer cell line after exposing to 0, 0.5, 1 and 2 Gy of IR doses and incubated for (D) 16 hrs and (E) 24 hrs post irradiation. The fluorescence microscopy images were visualised at 40 x objective and captured using data base software program.



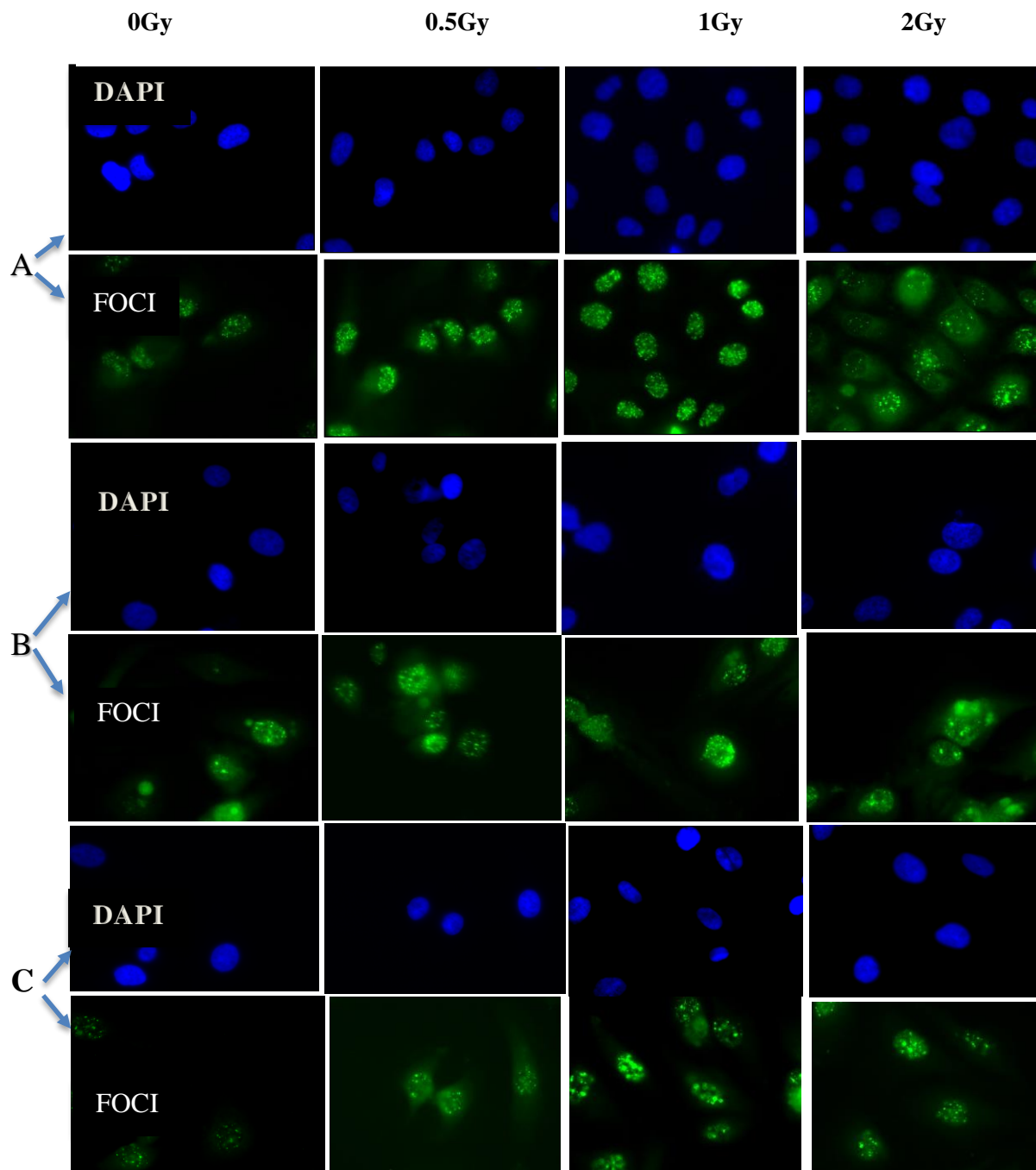
**Figure 6.1c IR-induced DNA DSBs formation and repair as presented by the number of foci per cell in RT4 bladder cancer cell line.** DNA DSB formation and repair were analysed using the  $\gamma$ -H2AX assay after exposure to 0.5, 1, and 2 Gy of IR doses and incubation for different times. Results are expressed as Mean  $\pm$  SEM of two independent experiments (approximately 240 nuclei). One-way ANOVA test was used to compare the mean of the non-irradiated control samples and with the DSB-foci of RT4 bladder cancer cell after different incubation times: ns = non-significant, \* $p$ <0.05, \*\* $p$ <0.01, \*\*\* $p$ <0.001 and \*\*\*\* $p$ <0.0001 compared to control samples.

#### 6.4.2.2 Estimation of DNA DSBs damage levels induced by ionising radiation in the J82 bladder cancer cell line as assessed by $\gamma$ -H2AX foci counting

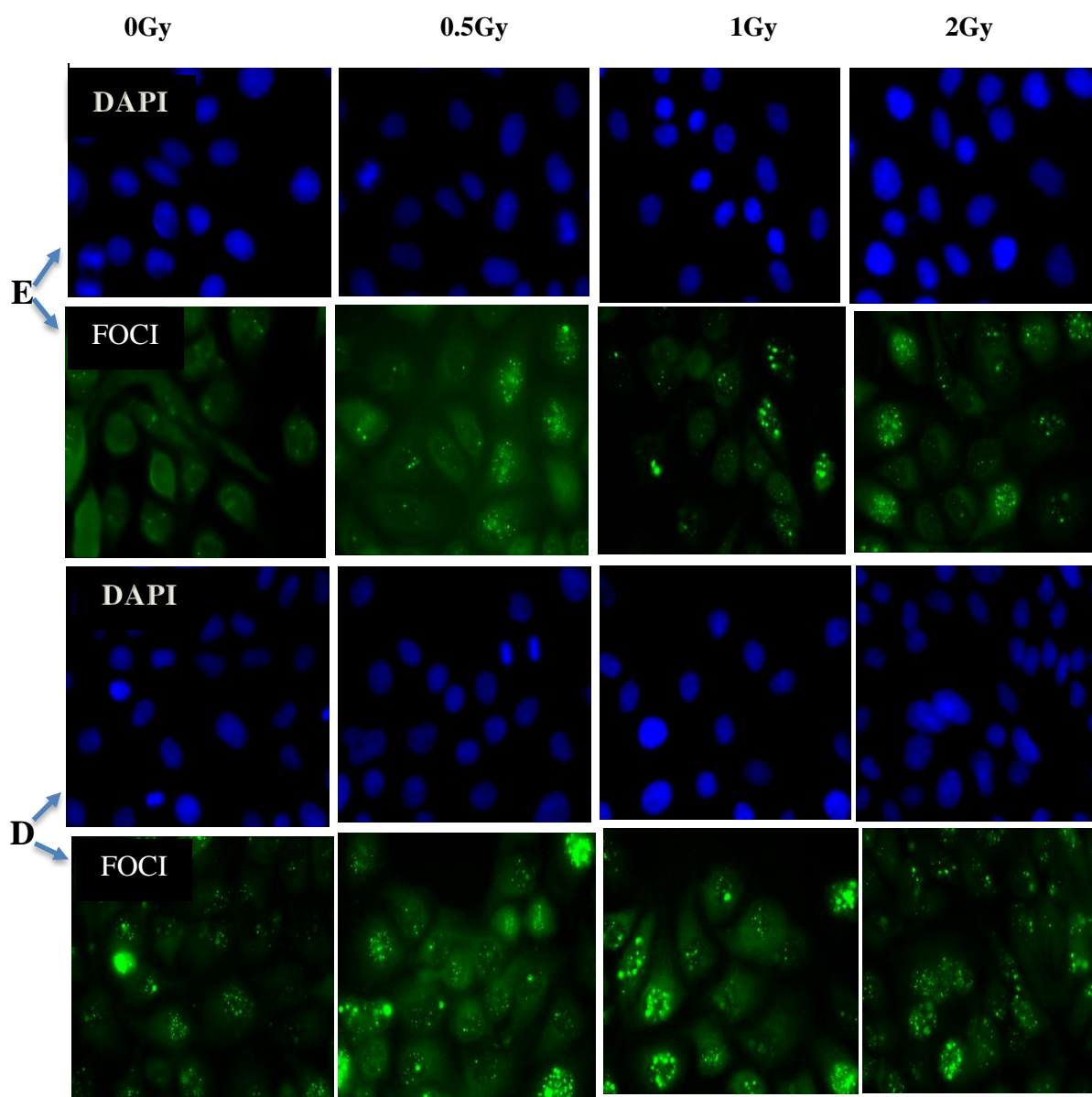
The effect of IR-induced DNA DSBs foci formation was next investigated in the J82 bladder cancer cell line (Figures 6.2a-c). As in the previous  $\gamma$ -H2AX experiments, the cells were prepared and then exposed to 0.5, 1, 2 Gy of IR doses and compared with the control sample (non-irradiated cells), after incubation for 30 mins, 2 hrs, 6 hrs, 16 hrs, and 24 hrs post irradiation. As can be seen from Figure 6.2, the highest number of foci was observed after

2hrs of incubation when the cells were exposed to 1 and 2 Gy of IR doses (mean foci/cell:  $148.1 \pm 4.922$ , \*\*\* $p=0.001$ ;  $191 \pm 10.11$ , \*\*\*\* $p=0.0001$ , ANOVA, respectively).

The number of IR-induced DNA DSBs started to decline by 6hrs of incubation time, although foci numbers were still significantly increased when were compared to the control sample after they were exposed to 0.5, 1, and 2 Gy of IR doses (mean foci/cell:  $127.8 \pm 4.828$ , \*\*\*\* $p= 0.0001$ ,  $109.6 \pm 3.13$ , \*\* $p= 0.0056$  &  $107 \pm 3.013$ , \* $p= 0.0257$ , ANOVA, respectively). However, whilst analysis revealed significant differences in the number of foci when cells were irradiated and incubated for 16 hrs but there is a clear decline in the number of foci per cells at doses 2 Gy (mean foci/cell:  $95.49 \pm 4.191$ , \*\*\*\* $p= 0.0001$ , ANOVA); and there was clearly less numbers of foci after 24 hrs compared to control, but they were still significantly increased compared to control at doses of 0.5, 1, 2 Gy of IR doses (mean of foci/cell:  $79.15 \pm 2.06$ , \*\*\*\* $p= 0.0001$ ,  $71.95 \pm 2.082$ , \* $p= 0.0120$  &  $72.98 \pm 2.719$ , \*\* $p= 0.0040$ , ANOVA, respectively). Taken together, these results suggest that, the DNA foci numbers dropped, and repair increased with extended periods of incubation after treatment, probably because the cells are repairing the DSBs, which in turn causes a reduction in the number of foci.

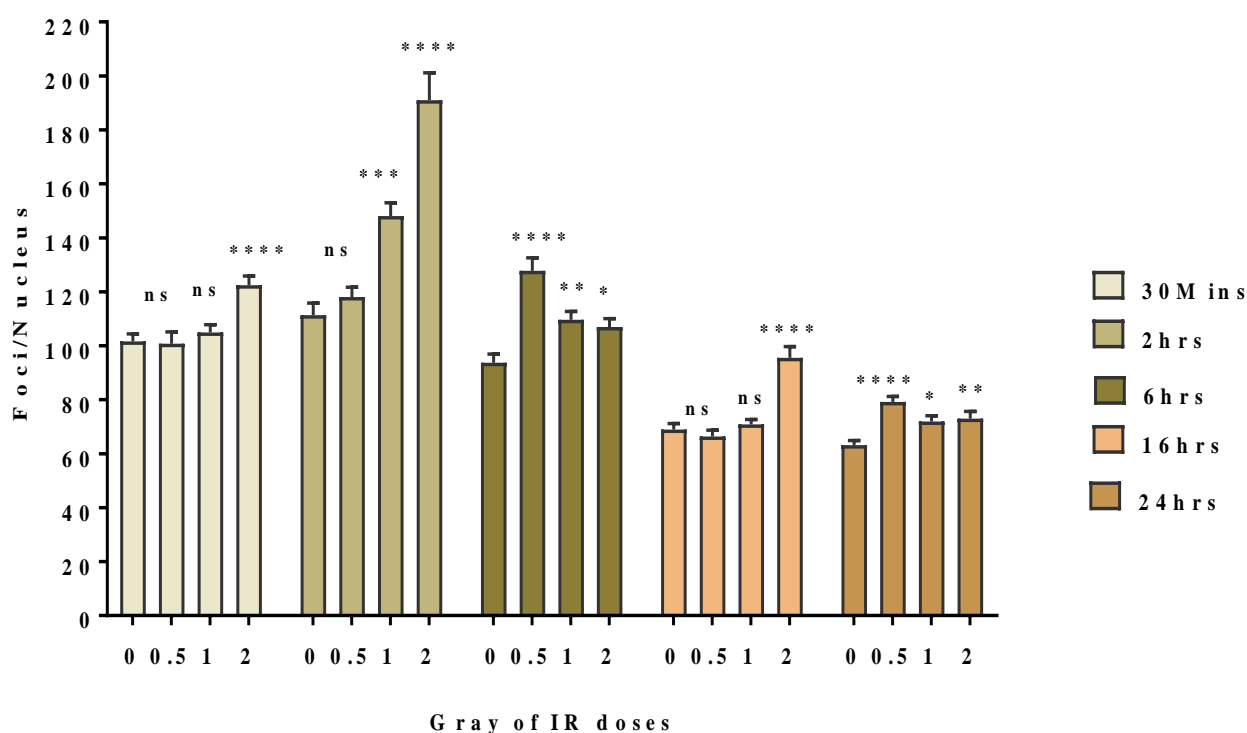


**Figure 6.2a** Examples of DNA damage foci in bladder cancer cells. Immunofluorescence staining for  $\gamma$ -H2AX (green) and DNA counterstaining with Dapi (blue) in J82 bladder cancer cell line after exposing to 0, 0.5, 1 and 2 Gy of IR doses and incubated for (A) 30 mins (B) 2 hrs and (C) 6 hrs post irradiation. The fluorescence microscopy images were visualised at 40 x objective and captured using data base software program.



**Figure 6.2b** Examples of DNA damage foci in bladder cancer cells. Immunofluorescence staining for  $\gamma$ -H2AX (green) and DNA counterstaining with Dapi (blue) in J82 bladder cancer cell line after exposing to 0, 0.5, 1 and 2 Gy of IR doses and incubated for (D) 16 hrs and (E) 24 hrs post irradiation. The fluorescence microscopy images were visualised at 40 x objective and captured using data base software program.



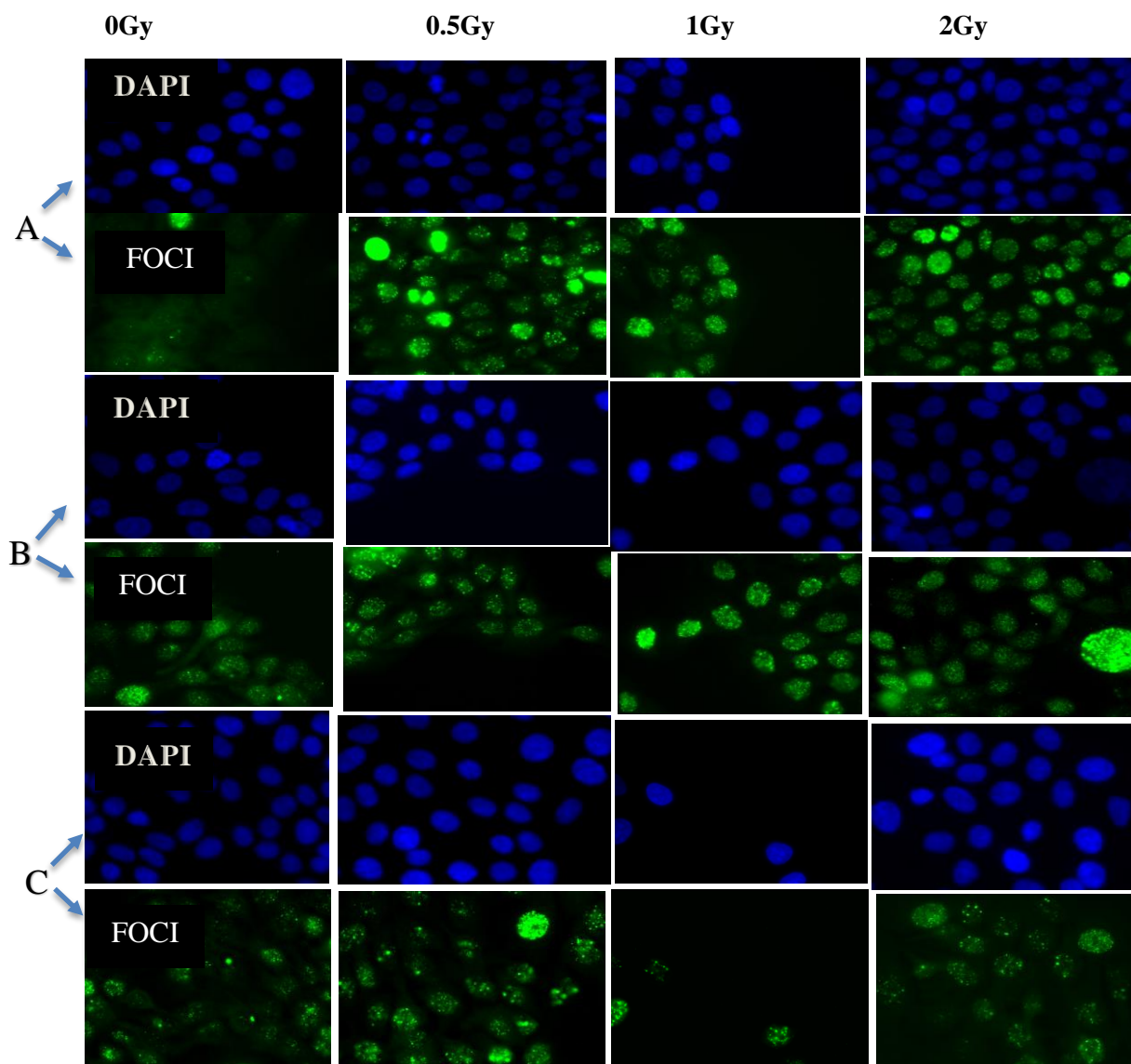


**Figure 6.2c IR-induced DNA DSBs formation and repair as presented by the number of foci per cell in J82 bladder cancer cell line.** DNA DSB formation and repair were analysed using the  $\gamma$ -H2AX assay after exposure to 0.5, 1, and 2 Gy of IR doses and incubation for different times. Results are expressed as Mean  $\pm$  SEM of two independent experiments ( $\sim$ 240 nuclei). One-way ANOVA test was used to compare the mean of the non-irradiated control samples and with the DSB-foci of J82 bladder cancer cell after different incubation times: ns=non-significant, \* $p$ <0.05, \*\* $p$ <0.01, \*\*\* $p$ <0.001 and \*\*\*\* $p$ <0.0001 compared to control samples.

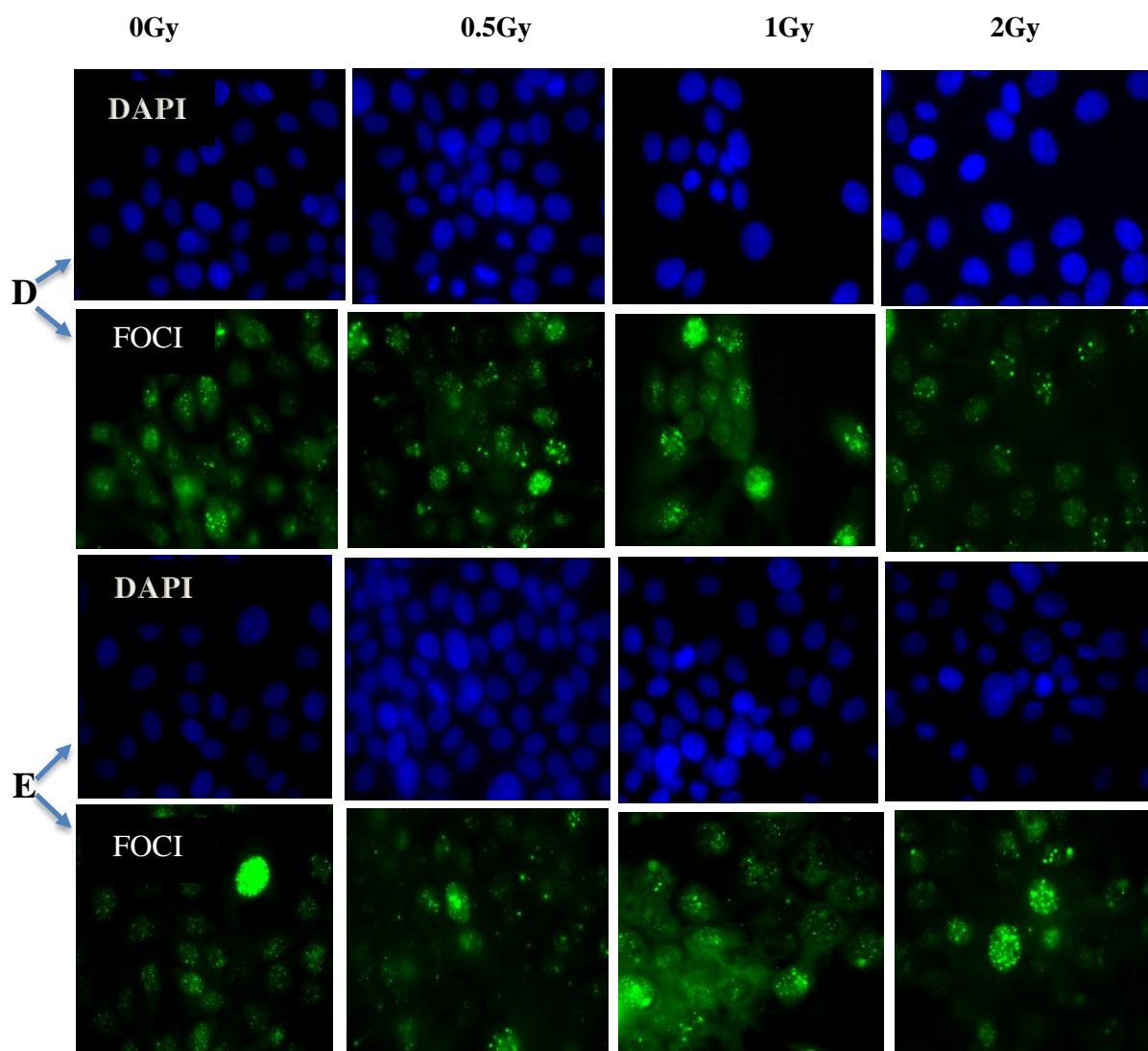
#### 6.4.2.3 Estimation of DNA DSBs damage levels induced by ionising radiation in the RT112 bladder cancer cell line as assessed by $\gamma$ -H2AX foci counting

IR-induced DNA DSBs foci formation were next assessed in the RT112 bladder cancer cells. As shown in Figures 6.3a-c, the highest significant level of DNA foci was observed after 2hrs of incubation time when the cells were exposed to 0.5, 1 and 2 Gy of IR doses compared to the control sample (mean foci/cell:  $103.6 \pm 2.531$ , \*\*\* $p$ = 0.0001,  $109.2 \pm 2.773$ , \*\*\* $p$ = 0.0001 &  $124.4 \pm 3.333$ , \*\*\*\* $p$ = 0.0001, ANOVA, respectively). Despite the reduction in

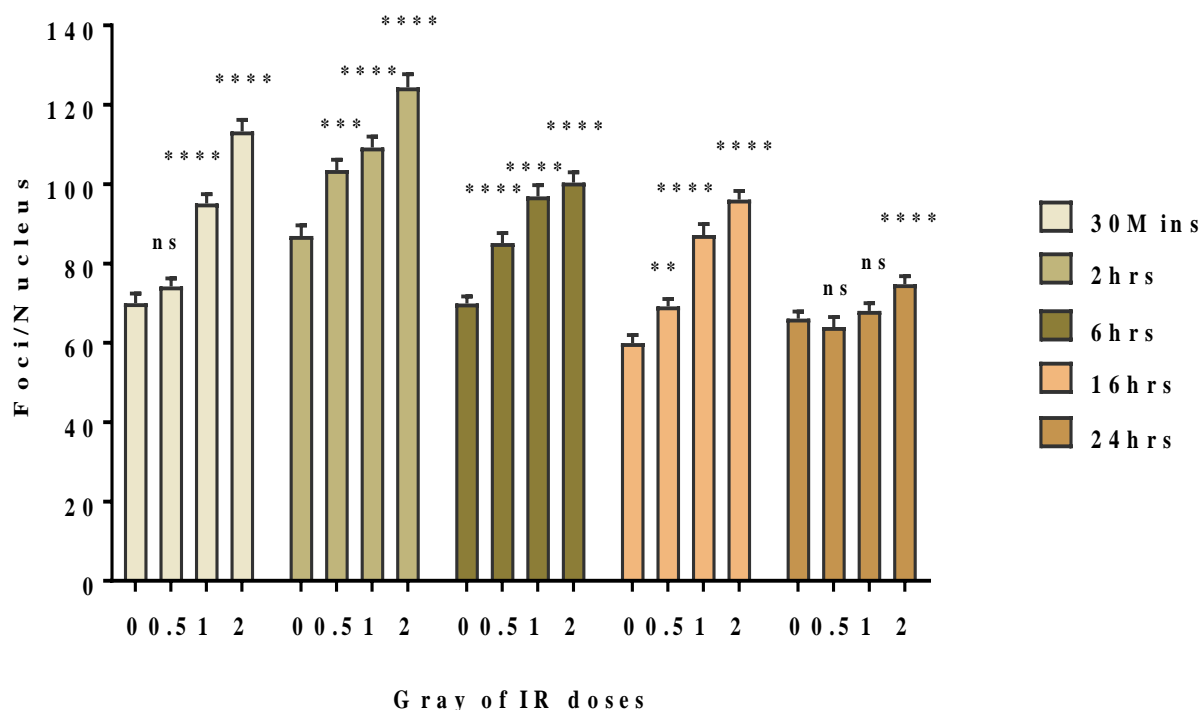
number of foci after 6hrs, 16hrs and 24hrs, the number of foci induced by IR was still significantly increased compared to control (non-irradiated cells) for several time points. However, in RT112 cells, the enhancement of IR-induced DNA DSBs foci formation was less effective reaching a maximum of <130 foci/cell.



**Figure 6.3a** Examples of DNA damage foci in bladder cancer cells. Immunofluorescence staining for  $\gamma$ -H2AX (green) and DNA counterstaining with Dapi (blue) in RT112 bladder cancer cell line after exposing to 0, 0.5, 1 and 2 Gy of IR doses and incubated for (A) 30 mins (B) 2 hrs and (C) 6 hrs post irradiation. The fluorescence microscopy images were visualised at 40 x objective and captured using data base software program.



**Figure 6.3b** Examples of DNA damage foci in bladder cancer cells. Immunofluorescence staining for  $\gamma$ -H2AX (green) and DNA counterstaining with Dapi (blue) in RT112 bladder cancer cell line after exposing to 0, 0.5, 1 and 2 Gy of IR doses and incubated for (D) 16 hrs and (E) 24 hrs post irradiation. The fluorescence microscopy images were visualised at 40 x objective and captured using data base software program.

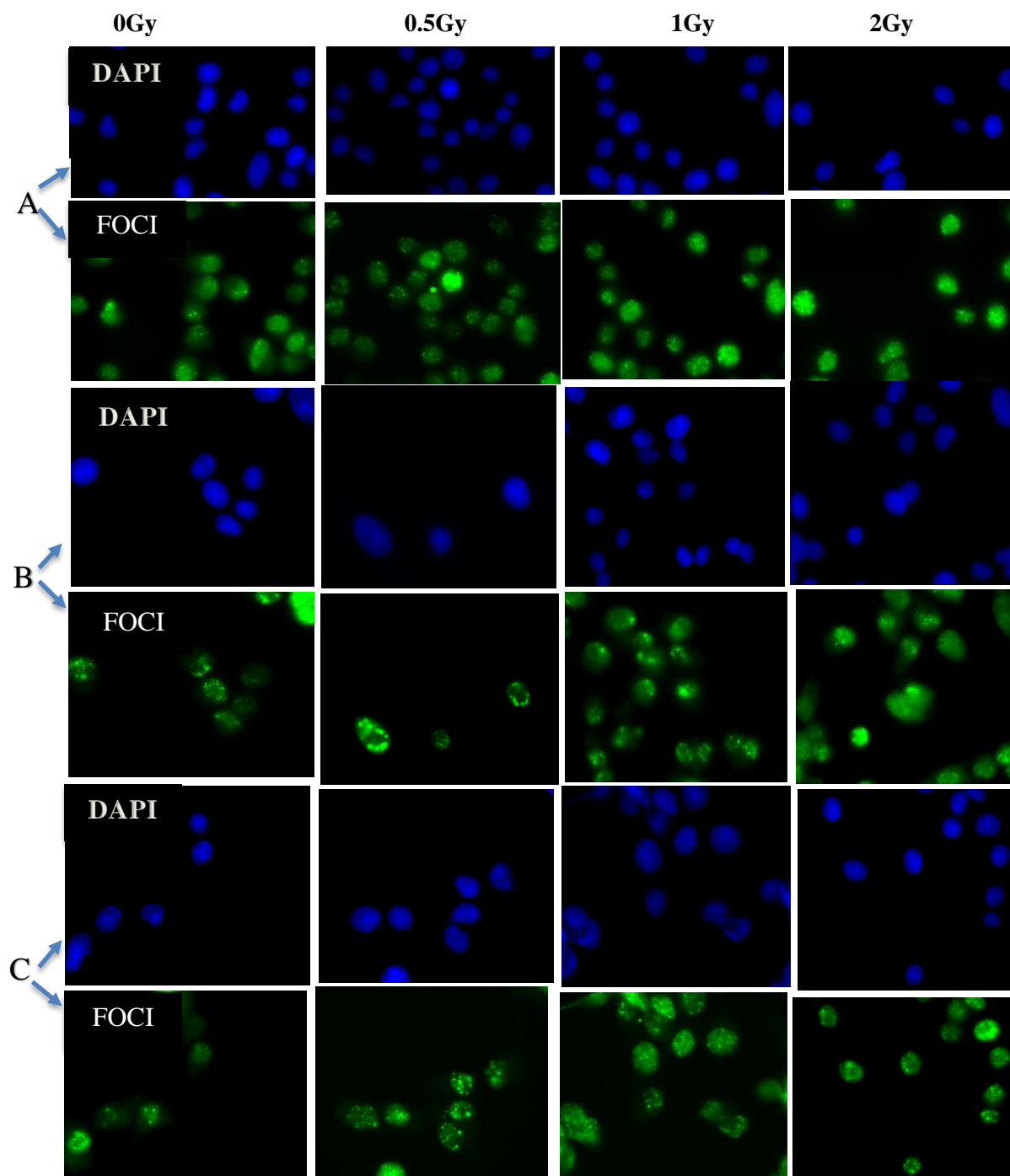


**Figure 6.3c IR-induced DNA formation and repair as presented by the number of foci per cell in RT112 bladder cancer cell line.** DNA DSB formation and repair were analysed using the  $\gamma$ -H2AX assay after exposure to 0.5, 1, and 2 Gy of IR doses and incubation for different times. Results are expressed as Mean  $\pm$  SEM of two independent experiments ( $\sim$ 240 nuclei). One-way ANOVA test was used to compare the mean of the non-irradiated control samples and with the DSB-foci of RT112 bladder cancer cell after different incubation times: ns=non-significant, \* $p$ <0.05, \*\* $p$ <0.01, \*\*\* $p$ <0.001 and \*\*\*\* $p$ <0.0001 compared to control samples.

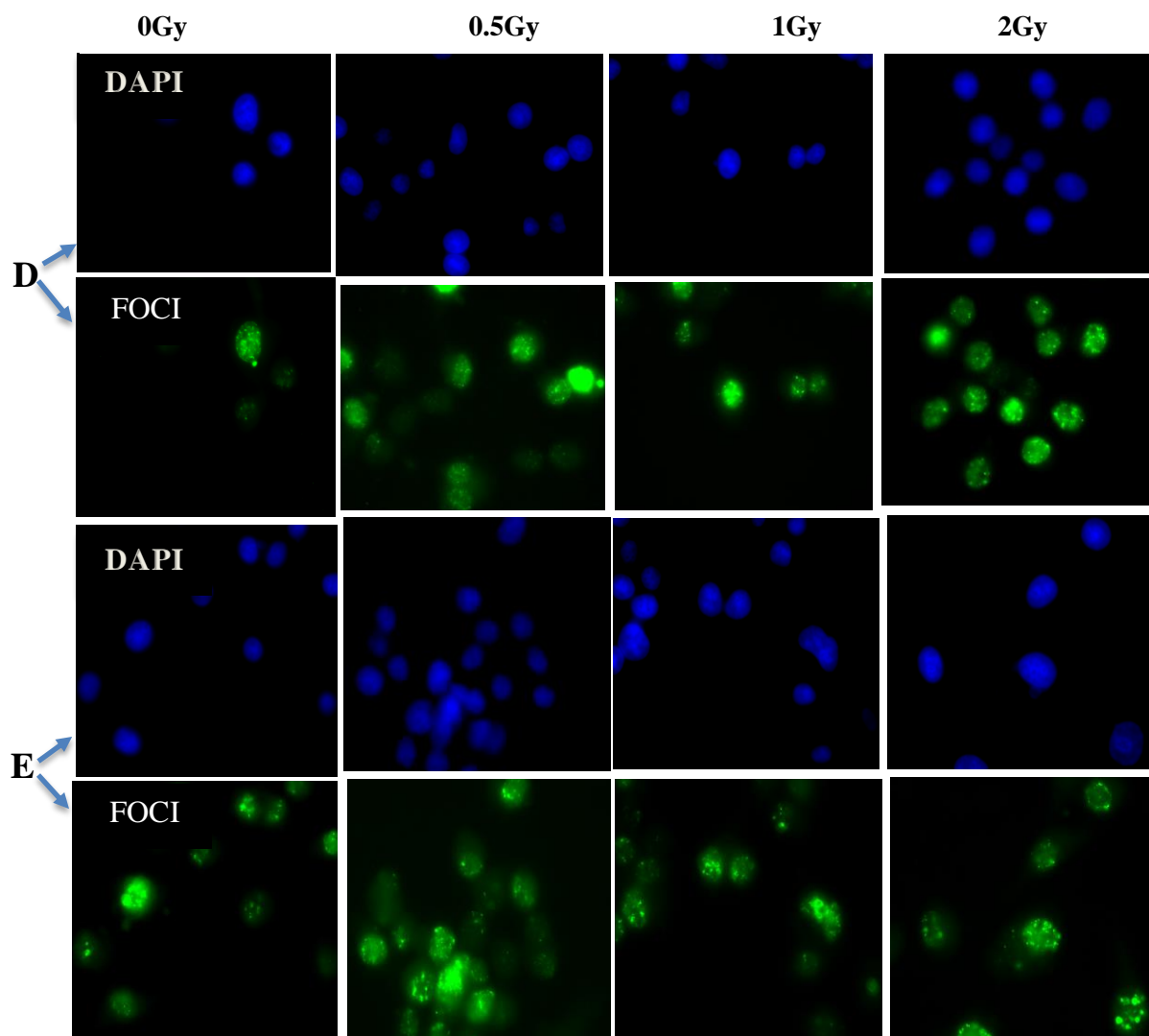
#### 6.4.2.4 Estimation of DNA DSBs damage levels induced by ionising radiation in UMUC3 bladder cancer cell line as assessed by $\gamma$ -H2AX foci counting

The effect of IR-induced DNA DSBs foci formation was also investigated in the UMUC3 bladder cancer cells line (Figures 6.4a-c). UMUC3 cells were exposed to 0.5, 1 and 2 Gy IR doses then incubated for 30 mins, 2 hrs, 6 hrs, 16 hrs, and 24 hrs post-irradiation. Cells were treated and analysed as were the previous cells lines. Notably, the DNA DSBs, as estimated by the number of  $\gamma$ -H2AX foci after exposing to IR, was increased significantly after 30mins, 2 hrs, and reaching a maximum at 6 hrs post-IR time compared with the control samples exposed to 1 and 2 Gy of IR doses (mean foci/cell 30 mins post irradiation:  $110.4 \pm 2.926$ ,

\*\*\*\* $p=0.0001$  &  $117.2 \pm 2.749$ , \*\*\*\* $p=0.0001$ , ANOVA, respectively), (mean foci/cell 2 hrs post irradiation:  $123.2 \pm 4.325$ , \*\*\*\* $p=0.0001$  &  $134.5 \pm 3.388$ , \*\*\*\* $p=0.0001$ , ANOVA, respectively) and (mean foci/cell 6 hrs post irradiation:  $150.7 \pm 5.054$ , \*\*\* $p=0.0008$  &  $164.2 \pm 5.563$ , \*\*\*\* $p=0.0001$ , ANOVA, respectively) when compared to control samples. However, after 16hrs and 24hrs there were an obvious decline in the number of foci per nucleus. One-way ANOVA revealed little of no significant increase in the number of foci overall after 16 hrs and 24 hrs of incubation time at high dose and there was a considerable decline in the number of foci compared to their control sample.

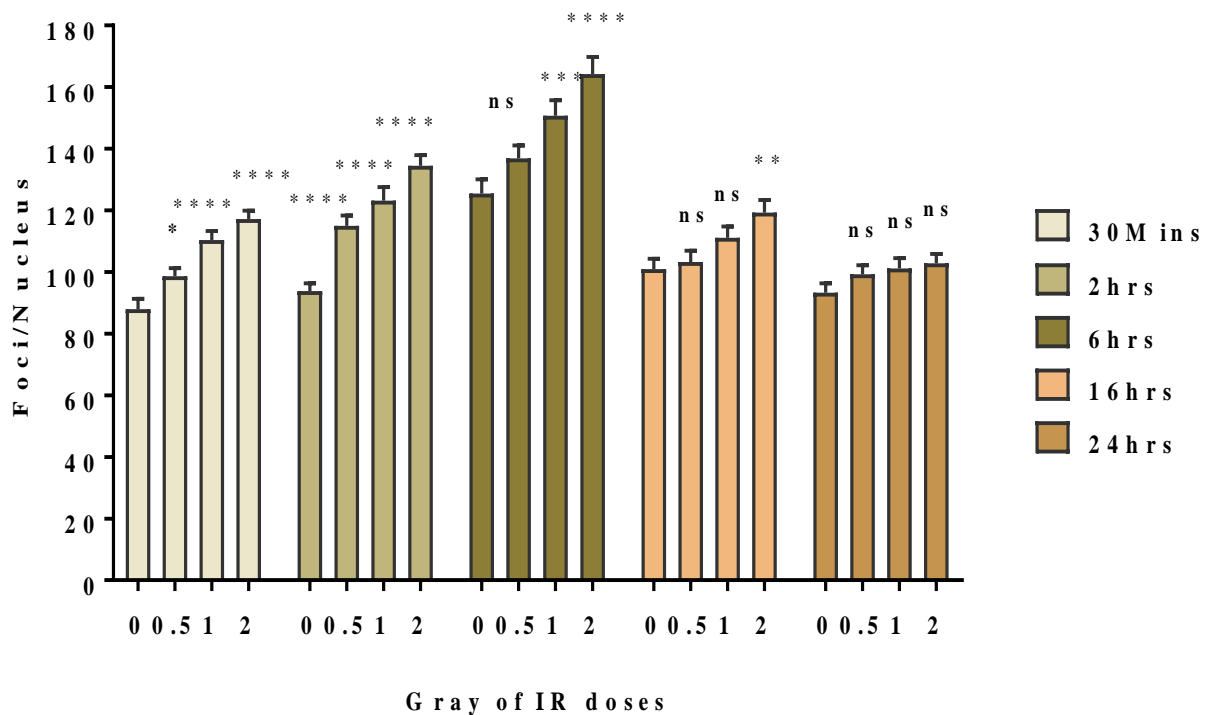


**Figure 6.4a** Examples of DNA damage foci in bladder cancer cells. Immunofluorescence staining for  $\gamma$ -H2AX (green) and DNA counterstaining with Dapi (blue) in UMUC3 bladder cancer cell line after exposing to 0, 0.5, 1 and 2 Gy of IR doses and incubated for (A) 30 mins (B) 2 hrs and (C) 6 hrs post irradiation. The fluorescence microscopy images were visualised at 40 x objective and captured using data base software program.



**Figure 6.4b** Examples of DNA damage foci in bladder cancer cells. Immunofluorescence staining for  $\gamma$ -H2AX (green) and DNA counterstaining with Dapi (blue) in UMUC3 bladder cancer cell line after exposing to 0, 0.5,1 and 2 Gy of IR doses and incubated for (D) 16 hrs and (E) 24 hrs post irradiation. The fluorescence microscopy images were visualised at 40 x objective and captured using data base software program.





**Figure 6.4c IR-induced DNA DSBs formation and repair as presented by the number of foci per cell in UMUC3 bladder cancer cell line.** DNA DSB formation and repair were analysed using the  $\gamma$ -H2AX assay after exposure to 0.5, 1, and 2 Gy of IR doses and incubation for different times. Results are expressed as Mean  $\pm$  SEM of two independent experiments (~240 nuclei). One-way ANOVA test was used to compare the mean of the non-irradiated control samples and with the DSB-foci of UMUC3 bladder cancer cell after different incubation times: ns=non-significant, \* $p$ <0.05, \*\* $p$ <0.01, \*\*\* $p$ <0.001 and \*\*\*\* $p$ <0.0001 compared to control samples.

### 6.4.3 Assessment of IR-induced DNA DSBs (foci formation) for the four bladder cancer cell lines over the five different time points post-irradiation, including background/basal levels of DNA foci, via $\gamma$ -H2AX assay

Cell radiosensitivity is determined by the amount of DNA damage resulting from exposure, and by the cells ability to repair these damages. In this regard, it is important to not only assess the DSB level arising from a given IR dose, but also to consider the extent of DSB persistence and repair over time, which might fluctuate considerably between these four bladder cancer cells. Therefore, an analysis was conducted by plotting the kinetics of damage

repair over time of each incubation for each cell line time. This cumulative analysis takes account of the fact that both the extent and time of foci formation and repair varied for the cell lines, with some cells forming foci relatively earlier and whilst other had more persistent foci. Two-way ANOVA followed up by Tukey's multiple comparison tests was used to test for significant differences between the means of DNA DSBs damage (foci numbers) for each incubation time post irradiation of the four bladder cancer cell lines after exposing to either 0.5, 1 or 2 Gy of IR (Figure 6.5).

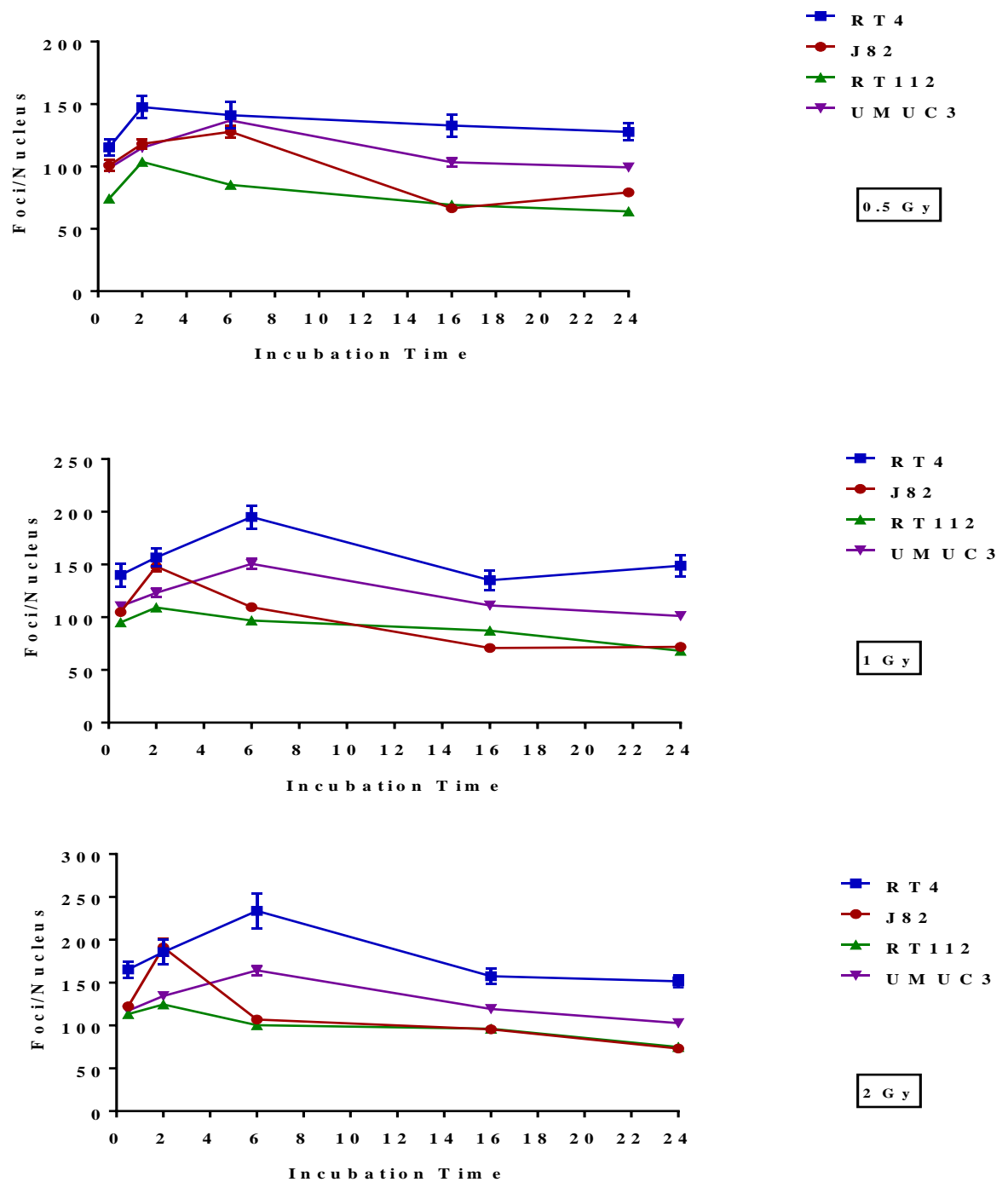
Following irradiation with 0.5 Gy, There was no considerable difference between the four bladder cancer cells after 30 mins, and 2 hrs of incubation time post irradiation. Highly significant levels of damage being observed in RT4 cells compared to RT112 cells after 6 hrs post irradiation (\* $p=0.0212$ ), RT112 cells compared to UMUC3 cells (\* $p=0.0330$ ). However, no significant difference was found in the mean of foci formation between, RT4 cells and J82 cells, RT4 cells and UMUC3 cells, J82 cells and RT112 cells and J82 cells and UMUC3 cells. Additionally, after 16 hrs of incubation time post irradiation, there was a significant high level of damage being observed in RT4 cells compared to J82 cells (\*\* $p=0.0067$ ) and when compared to RT112 cells (\*\* $p=0.0091$ ). Nevertheless, no significant differences were found with the rest of the bladder cancer cells. During the 24 hrs of incubation post irradiation with 0.5 Gy, a considerable significant different in the mean of DNA DSBs (foci formation) was noticed between RT4 and J82 cells (\* $p=0.0469$ ) and also RT4 verses RT112 cells (\*\* $p=0.0091$ ) but no substantial differences were found between the remaining cells. Thus, the rank order of damage sensitivity was revealed as RT4 > UMUC3 > J82 > RT112

In Figure 6.5, following irradiation with 1Gy, there was no considerable difference between the four bladder cancer cells after 30 mins, 2 hrs and 16 hrs of incubation time. However, the graph exhibits the highest number of IR induced DNA DSBs (foci formation) in RT4 cells compared to J82 cells (\* $p=0.0131$ ), RT4 cells compared to RT112 cells (\*\* $p=0.0050$ ) after 6 hrs post irradiation, while no significance difference in the meaning of DNA damage was obtained between J82 cells and RT112 cells, J82 cells and UMUC3 cells and finally between RT112 cells and UMUC3 cells. Finally, Data obtained from this experiment revealed that RT4 cells exhibit a substantially higher level of DNA DSBs than J82 cells and RT112 cells

(\* $p=0.0254$ ; \* $p=0.0188$ ) respectively. Therefore, the rank order of damage sensitivity was determined as  $RT4 > UMUC3 > J82 \geq RT112$ .

A similar situation was observed in Figure 6.5, after exposure to 2 Gy of IR. The rank order of damage sensitivity was shown as  $RT4 > UMUC3 > J82 \geq RT112$  with significantly higher levels of damage being observed in RT4 cells compared to J82 cells (\* $p=0.0123$ ), RT4 cells compared to RT112 cells (\*\* $p=0.0088$ ) after 6 hrs post irradiation. In contrast, no significant responses were seen during the comparison analysis between the four bladder cancer cells, after exposing to 30mins, 2hrs, 16 hrs, and 24 hrs post irradiation.

Overall, these results indicated that the cells exhibited a wide range of DNA DSB foci formation, with RT4 cells having the highest damage with the remaining cells exhibiting approximately equal levels of lower damage. Therefore, the rank order according to the damage sensitivity was determined as  $RT4 > UMUC3 > J82 \geq RT112$ .



**Figure 6.5** The level of DNA DSBs (foci formation) for the five time points post-irradiation (30 mins, 2 hrs, 6 hrs, 16 hrs, and 24 hrs) for the four bladder cancer cell lines after exposure to 0, 0.5 Gy, 1 Gy, and 2 Gy of IR doses as measured by  $\gamma$ -H2AX assay. Each bar represents Mean  $\pm$  SEM of two independent experiments. Two-way ANOVA test was used to analyse the mean of the four bladder cancer cell lines (see text for details).

## 6.5 Discussion

IR produces a wide variety of DNA lesions among them DSBs. DNA DSBs are critical lesions that can promote genomic instability and cell killing. If unrepaired or improperly repaired, DSBs can lead to chromosomal aberrations, which in turn, can activate several detrimental cellular responses and end-points, including carcinogenesis (Jackson and Bartek, 2009a; Vignard et al., 2013a).

DNA repair foci have been used extensively as markers of DNA damage and repair in human population studies (Valdiglesias et al., 2013). Indeed, the most prominently studied protein partaking in foci formation at the site of DSBs is the phosphorylated histone variant H2AX (termed  $\gamma$ -H2AX). Chromosomal DSBs induce a significant early response, adjusting chromatin surrounding an unrepaired DSB, which is characterised by phosphorylation of histone H2AX on serine 139 of its C-terminal tail to create “ $\gamma$ -H2AX” by DNA kinases such as ATM, ATR, and DNA-PK to form  $\gamma$ -H2AX. Studies have helped to clarify a strong, quantitative correlation between  $\gamma$ -H2AX foci formation and DNA DSBs induced by IR exposure (Rothkamm and Löbrich, 2003; Barnard et al., 2013).

The  $\gamma$ -H2AX assay has emerged as a useful measurement for estimation of ionising radiation dose exposure (Siddiqui et al., 2015).  $\gamma$ -H2AX assay is readily able to detect DSBs induced by ionising radiation (Kuo and Yang, 2008) which then leads on to DSB repair (Scully and Xie, 2013). In the present study,  $\gamma$ -H2AX assay attempted to focus on DNA DSBs that took place after ionising radiation.

To compare with the results of ACA,  $\gamma$ -H2AX assay was used to assess the level of DNA foci formation formed by IR over a dose range of 0, 0.5, 1 and 2 Gy. For this reason, DNA DSBs produced by IR UMUC3, RT112, J82 and RT4 cells were assessed using the  $\gamma$ -H2AX assay. All treated cells were analysed under the same laboratory conditions.

The number of foci per nucleus increased as a consequence of high amount of DSBs after being exposed to IR, which means that cells with higher foci numbers are more damage sensitive to IR and considerable range of DNA damage response between the four cell lines was observed. Notably, according to the data obtained from the Figures 6.1c, 6.2c, 6.3c and 6.4c, it can be observed that as the dose of the radiation increased, there was an increase in

the number of foci with a higher number of DNA foci formation was observed RT4 and J82 cells compared to RT112 and UMUC3 cells. The effect of various incubation time post irradiation in the four bladder cancer cells were investigated in this study. RT4 cells reached to the highest level of DNA foci formation after 6 hrs post-irradiation, whereas J82 cells reached to the highest number of DNA foci repair after 2 hrs of incubation. However, UMUC3 cells reached a maximum number of DNA foci repair after 6 hrs of incubation, compared to RT112 cells which were reached to the highest level of foci just 2 hrs of incubation time. As can be seen in Figures 6.3, and 6.4 for RT112 and UMUC3 cells the number of foci was lower than those in RT4 and J82 cells (Figures 6.1c, and 6.2c).

The background levels of  $\gamma$ -H2AX foci in this study are high and this could be due to (1) a high background genomic instability in the cancer cells or alternatively (2) due to an inappropriate threshold setting resulting in an overly high levels of supposed foci being counted. In support of (1) many cancers have increased numbers of cellular DSBs and therefore high basal foci levels. However, the levels of induced foci recorded in the present study were in line with the expected level of radiation-induced DSB (20-40 per Gy). It should be noted that there is a variable background level of  $\gamma$ H2AX signals also associated with DNA replication and expressed mostly in S-phase cells (MacPhail et al., 2003).

Analysis, as shown in Figure 6.5, was undertaken to estimate the level of DNA DSBs (foci formation) for the five different incubation time points post-irradiation (30 mins, 2 hrs, 6 hrs, 16 hrs, and 24 hrs); this initial analysis included the background/basal levels of DNA foci after exposure to 0.5 Gy, 1 Gy, and 2 Gy. The graphs exhibited that the highest number of IR induced  $\gamma$ -H2AX foci was found in RT4 and UMUC3 with approximately equivalent levels of foci being noted in J82 and RT112.

Data obtained from this result revealed the rank order according to the damage sensitivity was determined as  $RT4 > UMUC3 > J82 \geq RT112$ . However, in comparing these findings with the data analysed in previous chapters (Chapters 3, 4 and 5) the rank order obtained with the  $\gamma$ -H2AX assay was not what was expected. The rank order for the four cell lines according to their damage sensitivity as assessed by  $\gamma$ -H2AX assay was determined as  $RT4 > UMUC3 > J82 \geq RT112$  while the rank order of damage sensitivity for the four bladder

cancer cell lines as evaluated by ACA, LC-MS/MS and PFGE was determined as UMUC3 > RT112 > J82 > RT4.

Here are several reasons why these results don't match the previous Chapters' results. Perhaps most significantly is the fact that the  $\gamma$ -H2AX assay is 'indirect' method, reliant on the functionality of a cell's relevant DNA damage sensing and signalling pathways that are involved in foci formation and removal after ionising radiation; and in many instances it has been shown that such responses in cancer cells are compromised or non-existent. Other reasons as to why the  $\gamma$ -H2AX assay results failed to match the results from the other assays might be to do with known limitations of the  $\gamma$ -H2AX assay. For instance, the position of a DSB within the nucleus affects the way of its repair. DSBs located at the nuclear membrane or in the centre of the nucleus, may lose their ability to activate DDR and they possibly be repaired by alternative end joining (Lemaître et al., 2014). Recent electron microscopic studies have provided a more detailed picture of repair proteins arrangements within foci structures (Lorat et al., 2012). DNA damage signaling and distinctive pattern of foci distribution can be varied considerably according to DSBs location in different chromatin environments such as heterochromatin and euchromatin (Goodarzi et al., 2010; Chiolo et al., 2013). Due to the structural compaction of heterochromatin and presence of heterochromatic-specific non-histone proteins might prevent the ATM complex from phosphorylating histone H2AX. Therefore, this situation can impact on the DSB repair because the repair process takes longer to proceed in heterochromatin compared to euchromatin (Goodarzi et al., 2010)

Furthermore, other research suggests that IR-induced DNA DSBs (foci formation) tend to move and combine with each other in repair domains when they are situated 1 to 2 $\mu$ m apart (Neumaier et al., 2012), which could lead to an underestimation of true DSB yields at high doses (Vadhavkar et al., 2014). Besides, although the continuous phosphorylation of  $\gamma$ -H2AX occurs, mediated by the DNA damage kinases ATM, DNA-PK and ATR, at the site of DSBs, this does not necessarily mean that the underlying DSBs are not repaired with the existing foci not being dephosphorylated (Rothkamm et al., 2015). The highly dynamic changes of foci number and foci size over time after treatment with radiation can make the visual scoring ineffective and may possibly involve fluorescence bleaching due to extended

evaluation time (Siddiqui et al., 2015). As already mentioned, one of the main issues when scoring multiple foci after exposure to a high radiation dose is the phenomenon of foci overlap that makes it more difficult to distinguish  $\gamma$ -H2AX as separate spots (foci) therefore,  $\gamma$ -H2AX foci method is sensitive and accurate after exposure to low doses (Willitzki et al., 2013). Over time, the total  $\gamma$ -H2AX fluorescence signal would be expected to decrease rapidly, leaving only residual  $\gamma$ -H2AX levels by 24–48hrs. While it is considered that in this situation the  $\gamma$ -H2AX yield would no longer be representative of the initial radiation dose received (Andrievski and Wilkins, 2009). Additionally, it is important to consider that the functional relevance of DNA damage foci in DSB repair is not always clear, particularly in the case of factors that induce mainly non-DSB lesions (Revet et al., 2011; Cleaver, 2011). However, improvements have been made to reduce processing time (Moquet et al., 2014), analysis speed and time required to access dose in case of radiological emergencies using the  $\gamma$ -H2AX assay (Turner et al., 2010). However, it must be stressed that despite all these problems and inadequacies,  $\gamma$ -H2AX foci is generally considered to be a useful measurement and much experimental work has been already used  $\gamma$ -H2AX foci as DSB biomarker of DNA damage or repair (Valdiglesias et al., 2013). The assay continues to be broadly exploited in various applications, to monitor DSB formation and repair, including radiosensitivity (Martin et al., 2011; Menegakis et al., 2011)

Returning to Chapter 3, 4, and 5, it was evident that all the four cell lines (UMUC3, RT112, J82 and RT4) have nearly the same rank order in terms of damage sensitivity as determined by ACA, LC-MS/MS and PFGE. Therefore, the rank order from damage sensitive cells to damage resistant cells was  $UMUC3 > RT112 > J82 \geq RT4$ . However, a further hypothesis can be considered that may help rationalise the differing results observed in this Chapter. Whilst  $\gamma$ -H2AX foci are markers of DSB (Rothkamm et al., 2015) this can be further refined to state that they are markers of DSB ‘marked’ for repair; indeed, it is well established that  $\gamma$ -H2AX foci formation is an early part/player of the DSB DNA damage repair response (Löbrich et al., 2010; Lassmann et al., 2010; Siddiqui et al., 2015). Thus, the high number of foci per nucleus can possibly be associated with enhanced/heightened repair processes for DNA DSBs in more resistant cells which could increase the survive rate of these cells. Therefore, if the number of foci per nucleus is increased due to enhanced repair processes for DNA DSBs in the more resistant bladder cancer cells, this may explain why at least RT4



cells were shown to have the higher number of DNA foci formation after exposing to IR for the different incubation time points. Indeed, RT4 has been shown to be one of the most radioresistant of bladder cancer cells (Moneef et al., 2003)

In summary, the  $\gamma$ -H2AX analysis showed the highest level DSB formation to occur in RT4 cells peaking at 6 hrs post-irradiation with the remaining cells having more equivalent levels of damage. This seemingly highest level of damage in RT4 cells was not in keeping with the results obtained using ACA (Chapter 3), LC-MS/MS (Chapter 4) and PFGE (Chapter 5); all of which indicated RT4 cells to be highly damage resistant. However,  $\gamma$ -H2AX foci formation has been shown to precede the DNA-repair mechanism and has been deemed essential for DNA damage repair (Paull et al., 2000). Therefore, if the number of foci per nucleus is increased due to enhanced repair processes for DNA DSBs in the more resistant bladder cancer cells, this could explain why at least RT4 cells were shown to have a higher number of DNA foci formation after exposing to IR for the different incubation time points. Indeed, RT4 has been shown to be one of the most radioresistant of bladder cancer cells (Moneef et al., 2003) and this may be due to enhanced DNA DSB repair.

## **Chapter 7**

### **General Discussion and Thesis Summary**

## 7.1 Final Discussion

Radiation can cause damage to every molecule in an exposed cell. However, the collected findings of radiobiological studies show that DNA is the critical target for the biologic effects of ionising radiation. DNA damage occurs when cells are exposed to ionising radiation through both direct and indirect effects, the latter effect being mediated mostly by diffusible ROS free radicals. IR kills cancer cells by extensively damaging their DNA. IR generates a wide variety of DNA damage, with DNA DSBs being considered to be the lesions which are mostly responsible for the radiogenic cell death (Jackson and Bartek, 2009a). Many of the cytotoxic and mutagenic (gene mutation and chromosome aberration) effects of IR can occur as consequences of radiation-induced DNA lesions leading to cellular transformation, carcinogenesis and finally cell death (Price and D'Andrea, 2013). Indeed, it is the cytotoxic effects of IR are employed in the eradication of cancer cells via radiotherapy (Lawrence et al., 2008).

Numerous methods have used to assess DNA damage in both studies of cancer causation and cancer treatment. ACA has become a standard method for detection of DNA damage and repair, both *in vitro* and *in vivo* (Dhawan et al., 2009). It is a sensitive method which is used to estimate the SSBs and ALSs, and other types of damage (Azqueta et al., 2009; Collins, 2009). The Comet assay is a straightforward method for assessing DNA damage formation and repair at the level of individual cells (Singh et al, 1988; Singh, 1996), and is particularly suitable for the measurement of radiogenic damage (Olive, 1999). The assay is inexpensive, data are available within 24hrs and only low numbers of cells are required, allowing results to be generated from small clinical biopsies. This technique is therefore ideal for translational studies and clinical application (Ward, 1988; Singh, 1996; Azqueta et al., 2009; Collins, 2009).

To examine the effect of ionising radiation on cancerous cells, a panel of four bladder cancer cell lines (UMUC3, RT112, J82 and RT4) have been used in this study to measure their DNA damage sensitivity to ionising radiation exposure. Previously, two studies were conducted to demonstrate that ACA in measuring radiation-induced DNA damage is a good measurement of bladder cancer cells' radiosensitivity *in vitro*, with both studies showing a strong inverse correlation between initial measures of comet formation and clonogenic survival (Moneef et

al., 2003; McKeown et al., 2003). However, no research has been published as to reason for differential measures of comet formation associated with the effects of IR on cancer cells, such as bladder cancer.

In the above studies, for an individual cell-sample, measures of increased comet formation are due to the straightforward dose-dependency of induced damage formation. However, a further factor, which may influence the extent of comet formation, is the nature of the DNA anchoring to the nuclear NM via MARs, with weaker MARs allowing for the additional release and electrophoretic-migration of adjacent/contiguous loops of damaged DNA. Therefore, a key question is (I) do differential measures of comet formation between cells truly reflect differential damage or alternatively, or (II) whether the extent of the comet formation is the consequence of additional release of DNA sequences/loops from the comet head (the nucleoids), resulting in larger comet tails at the same level of DNA damage.

To determine which scenario occurs, cell lines, which exhibited differential ACA responses, were examined using alternate DNA damage assays including LC-MS/MS, PFGE &  $\gamma$ -H2AX. The implications of these findings with respect to the validity of DNA damage measures as markers of cancer cell treatment sensitivity will now be discussed.

### **7.1.1 Assessment of IR-induced DNA damage response (comet formation) for the four bladder cancer cells via ACA**

The extent of comet formation induced by IR increased considerably with increasing IR doses for the four bladder cancer cell lines (UMUC3, RT112, J82 and RT4) (Figure 3.5), as determined by the ACA parameters %TD, OTM, TEM, and TL. It was evident that the UMUC3 cell line showed a higher level of IR-induced comet formation compared with the RT4, J82, and RT112 cell lines. Furthermore, the RT4 cell line was revealed to be the cell line displaying the lowest comet formation response post radiation exposure (as shown in Figures 3.6, 3.7, 3.8, 3.9, 3.10, 3.11, 3.12 and 3.13). Indeed, the rank order for the four bladder cancer cells from the most damage sensitive to most damage resistant cells, as determined by comet formation response, was UMUC3 > RT112 > J82 > RT4.

However, one of the potential mechanisms that could render one cell's DNA more damage sensitive than a different second cell could be due to differences in the relative ratio of heterochromatin vs. euchromatin within the two cell types. DNA in the more open euchromatin structure is more accessible hence more damage sensitive (particularly resulting from the indirect effects of ionising radiation exposure) than the DNA in the closed, more tightly packed structure of heterochromatin. Therefore a cell with relatively more euchromatin would have more DNA damage induced than a cell with more heterochromatin for the same level of radiation exposure (Caron et al., 2001; Falk et al., 2008).

### **7.1.2 Measurement of 8-oxodG DNA adducts in bladder cancer cell lines after ionising radiation treatment using LC-MS/MS**

DNA adduct levels are considered to be effective markers of ionising radiation exposure and other genotoxic carcinogens (Pernot et al., 2012b). The presence of DNA adducts in human sources of DNA can be a useful measure for molecular epidemiological studies of cancer causation (Goggin et al., 2009; Goggin et al., 2011; Ishii et al., 2011). The levels of IR-induced 8-oxodG DNA in the genomic DNA of the four bladder cancer cell lines (UMUC3, RT112, J82 and RT4) was examined in the present study using LC-MS/MS. The amount of 8-oxodG DNA adducts was consistently elevated across all the bladder cancer cell lines examined in the present study following exposure to 20 Gy, but with the UMUC3 and RT112 cell lines demonstrating an increased sensitivity to radiation-induced 8-oxodG DNA adducts formation when these cell lines were exposed to 100 Gy. In contrast, the other cell lines (J82 & RT4) were shown to be more damage resistant, having far lower levels of 8-oxodG post exposure to 100 Gy (as illustrated in Figure 4.6). The rank order for radiation-induced 8-oxodG DNA adducts in the four bladder cancer cell lines from the most damage sensitive to the most damage resistant is as follows:  $UMUC3 \geq RT112 > RT4 \geq J82$ . Whilst not delivering an absolute sequential rank order, the rank order observed approximated the rank order observed with the Comet assay (as outlined in Chapter 3) with UMUC3 and RT112 cells the most damage sensitive cell lines and J82 and RT4 cells the most damage resistant cell lines.

### **7.1.3 Investigation of the effect of IR-induced DNA DSBs formation response on the four bladder cancer cell lines as determined by the PFGE assay**

UMUC3, RT112, J82 and RT4 cells were studied by the PFGE assay to evaluate the levels of IR-induced DNA DSB damage and to distinguish between damage sensitive and damage resistant bladder cancer cell lines. The results showed that irradiation with the doses used caused a considerable level of induced DNA DSBs that positively correlated with the increasing doses of IR for all four bladder cancer cell lines. The results overall demonstrated an increase in DSBs formation at all the doses studied, with a consistent and significantly higher levels of IR-induced DSBs being observed in the UMUC3 cells and RT112 cells compared with lower levels of IR-induced DSBs observed in the J82 and RT4 cells. This was irrespective of the nature of analysis undertaken: correlated dose-response, area under the curve, or calculated relative damage increases. Indeed, taking all the data together, the rank-order of damage sensitivity as determined by PFGE assessment of IR-induced DSB formation is: UMUC3 > RT112 > J82 > RT4; as determined by dose response (Figures 5.6, 5.7, 5.10, and 5.11), by area under the curve analysis (Figures 5.8 and 5.12) and relative damage increases (Figures 5.9 and 5.13) for the four bladder cancer cells lines. Thus, these findings corresponded with the data analysed in previous chapters (Chapters 3 & 4). Therefore, these results obtained and analysed here supported the first theory of the differential measurements of comet formation response between the four bladder cancer cell lines (Model1); whereby differential comet measures do reflect actual variances in DNA damage levels.

### **7.1.4 Assessment of IR-induced DNA DSBs damage via the $\gamma$ -H2AX assay in UMUC3, RT112, J82 and RT4 bladder cancer cells**

The  $\gamma$ -H2AX assay has emerged as a useful measurement for estimation of ionising radiation dose exposure (Siddiqui et al., 2015).  $\gamma$ -H2AX assay is readily able to detect DSBs induced by ionising radiation (Kuo and Yang, 2008) and their repair (Scully and Xie, 2013). In the present study,  $\gamma$ -H2AX assay was used to focus on DNA DSB induction and repair that took place after ionising radiation.

To compare with the results of ACA,  $\gamma$ -H2AX assay was used to assess the level of DNA foci formation formed by IR over a dose range of 0, 0.5, 1 and 2 Gy. All treated cells were analysed under the same laboratory conditions.

According to the results in Figures 6.5 and 6.6 the highest number of IR induced  $\gamma$ -H2AX foci formation (determined as the number of foci/nucleus), was found in RT4 with approximate equal measures being noted in the other cell lines (RT4 > J82 = UMUC3 = RT112). This was in stark contrast with the data obtained in the previous chapters (Chapters 3, 4 & 5). This rank order was not what was expected with the rank order of damage sensitivity for the four bladder cancer cell lines as evaluated by ACA, LC-MS/MS and PFGE determined as UMUC3 > RT112 > J82 > RT4.

There are several reasons why these results do not match the previous Chapters' results. Perhaps most significantly is the fact that the  $\gamma$ -H2AX assay is 'indirect' method, reliant on the functionality of a cell's relevant DNA damage sensing and signalling pathways that are involved in foci formation and removal after ionising radiation (Bonner et al., 2008). Other reasons as to why the  $\gamma$ -H2AX assay results failed to match the results from the other assays might be associated with known limitations of the  $\gamma$ -H2AX assay such as:

- The heterogeneous distribution of the H2AX histone in the nucleus (Bewersdorf et al., 2006)
- Low formation in/expulsion of foci from heterochromatin (Jakob et al., 2011)
- Noted delays between DSB induction and visible foci formation (Rothkamm and Horn, 2009)
- Coalescence of multiple foci in close proximity into one (Neumaier et al., 2012)

Initially in this study,  $\gamma$ -H2AX level was used as an indicator of DNA damage (Redon et al., 2012); with high a number of foci per nucleus indicating a high amount of DSBs after IR exposure, meaning that cells are more damage sensitive to IR. However, as  $\gamma$ -H2AX stimulates accumulation of repair proteins at the site of DNA damage (Stiff et al., 2004), a further hypothesis can be considered that may help rationalize the differing results observed between Chapter 6 and Chapters 3, 4 & 5. Whilst  $\gamma$ -H2AX foci are markers of DSB (Rothkamm et al., 2015) this can be further refined to state that  $\gamma$ -H2AX foci are in fact

markers of DSB ‘*marked*’ for repair. Therefore, cells with an increased number of foci, can possibly indicate a greater ability/capacity to repair DNA DSBs and so increase their ability to survive, deeming them more radioresistant.

Consequently, two different hypotheses can be proposed to explain the impact of  $\gamma$ -H2AX foci formation post-IR exposure.

- Firstly, the number of foci per nucleus could be increased due to high amounts of DSBs post-IR exposure, which means that cells with higher levels of IR-induced foci are more damage sensitive towards IR.
- Secondly, a possible alternative hypothesis is that if the number of foci increased, the cells may have a greater ability to repair DNA DSBs and so increase their ability to survive, indicating these cells to be more radioresistant.

In the present study RT4 cells were shown to have a higher number of DNA foci formation after exposing to IR for the different incubation time points. If indeed the number of foci per nucleus is increased due to an enhanced repair processing of DSBs, this may explain why at least RT4 cells were shown to have the higher number of DNA foci formation, as RT4 has been shown to be one of the most radioresistant of bladder cancer cells (Moneef et al., 2003; McKeown et al., 2003).

In summary, many studies have successfully demonstrated how the Comet assay can be applied to the analysis of cells derived from a variety of different human tissues, lending considerable weight to the suggestion that this assay could benefit many areas of clinical investigation by providing valuable information about the intrinsic DNA characteristics of individual cells and their responses to various external factors, such as radiation, chemicals and drugs. This type of information would prove particularly relevant in the diagnosis, prognosis and treatment of cancer. Readily available accurate and informative data are fundamental to the successful management of tumours with the ultimate aim of achieving a positive outcome for the patient. From a practical point of view, the Comet assay would be eminently suitable for use in a clinical setting since it is a relatively simple and inexpensive technique, which requires only a few cells and results can be obtained within a matter of hours (McKenna et al., 2008).



## 7.2 Conclusion

Alkaline comet assay (ACA) is an often-used method for assessing DNA damage. Previously, two independent studies with panels of bladder cancer cells has shown that ACA measures of radiation-induced DNA damage correlate cell radiosensitivity *in vitro* (Al Moneef et al., 2003; McKeown et al., 2003). Furthermore, it has been shown that modified-ACA measures of cisplatin and mitomycin-C-induced crosslinks correlate chemo sensitivity *in vitro* with higher bladder cancer cell chemo sensitivity (Bowman et al., 2014). Moreover, the analysis of bladder tumour biopsies reveals a wide range of ACA responses (Al Moneef et al., 2003). These studies indicate ACA to be good measure of bladder cancer cell radiosensitivity.

In the above studies, for individual samples, measures of increased comet formation are due to the straightforward dose-dependency of induced damage formation. However, a further factor, which may influence the extent of comet formation, is the nature of the DNA anchoring to the nuclear matrix (NM) via matrix-associated regions (MARs), with weaker MARs allowing for the additional release and electrophoretic-migration of adjacent/contiguous loops of damaged DNA. Therefore, a key question is (I) do differential measures of comet formation between cells truly reflect differential damage or alternatively (II) do differential comet measures reflect differing extents to which DNA is released from the nucleoids for similar damage levels. To determine which scenario occurs, cell lines, which exhibited differential ACA responses, were examined using alternate DNA damage assays including LC-MS/MS,  $\gamma$ -H2AX & PFGE.

The agreement of the determined rank order of damage sensitivity as determined by ACA, LC-MS/MS and PFGE (all assays that directly measure DNA damage) supports the proposed model (Model 1) that the differential measures of initial comet formation actually reflects differential measures of DNA damage between cells.

This project also suggests a further new insight regarding  $\gamma$ -H2AX foci formation. The  $\gamma$ -H2AX assay is classed as an indirect method of assessing DNA damage, in that it relies on the functionality of a cell's relevant DNA damage sensing and signalling pathways that are involved in foci formation and removal. In addition,  $\gamma$ -H2AX foci formation has been shown

to precede the DNA-repair mechanism and has been deemed essential for DNA damage repair (Paull et al., 2000). Therefore, whilst  $\gamma$ -H2AX foci are markers of DSB (Rothkamm et al., 2015), this can be further refined to state that  $\gamma$ -H2AX foci are in fact markers of DSB ‘marked’ for repair (Löbrich et al., 2010; Lassmann et al., 2010; Siddiqui et al., 2015). Despite this caveat, DNA damage foci, and especially  $\gamma$ -H2AX, have already been used extensively as markers of DNA damage or repair in human population studies (reviewed in Valdiglesias et al., 2013), and this trend will most certainly continue in the coming years.

### **7.3 Future Work / The Next Project**

Taking together the previous studies with the finding of this study, it can be speculated that the nuclear DNA's sensitivity towards induced damage is a key factor in determining bladder cancer cell sensitivity towards radiation. Consequently, factors that modulate DNA damage sensitivity will be expected to increase bladder cancer cell radiosensitivity. Furthermore, epigenetic modulation of chromatin structure by reversible covalent modification of histones is an important control mechanism for co-ordination of processes such as transcription and DNA repair. Histones can undergo multiple types of covalent modification (De Ruijter et al., 2003) and of direct relevance to this work, as it can be modified pharmacologically, is histone acetylation. Histone acetylation status is controlled by the opposing actions of histone acetyltransferases (HATs) and histone deacetylases (HDACs). Acetylation of histones results in neutralization of their positive charge, decreasing their interaction with DNA, leading to a more 'relaxed', 'open' chromatin conformation (Marks et al., 2000) which is proposed to be more damage sensitive. Histone acetylation also plays multiple functions in DSB repair, not only by allowing physical access of repair proteins to DNA, but also by direct interaction between selected repair proteins and acetylated histones, so affecting radiation response (Munshi et al, 2005; Munshi et al, 2006; Camphausen et al, 2004a). The enhancement of cell radiosensitivity, by treatment with several chemical classes of HDAC inhibitors (HDIs), has been reported in the literature, although the mechanistic details are not fully understood (Camphausen et al., 2004a; Camphausen et al., 2004b; Camphausen et al., 2005; Banuelos et al., 2007). However, studies with a variety of HDIs have reported increased levels of initial radiogenic damage (as measured by  $\gamma$ -H2AX foci) and/or inhibition of repair (Camphausen et al., 2004a; Munshi et al., 2005; Karagiannis et al., 2005).

Given that it has shown DNA damage sensitivity to be a key factor in determining bladder cancer cell radiosensitivity, HDAC inhibition represents a promising target to achieve enhanced bladder cancer cell radiosensitisation.

## References

- AGER D.D., DEWEY W.C., GARDINER K., HARVEY W., JOHNSON R.T., WALDREN C.A. 1990. Measurement of radiation-induced DNA double-strand breaks by pulsed-field gel electrophoresis. *Radiation Oncology*, 122,181–7.
- AHMAD, K. A., ISKANDAR, K. B., HIRPARA, J. L., CLEMENT, M.-V. & PERVAIZ, S. 2004. Hydrogen peroxide-mediated cytosolic acidification is a signal for mitochondrial translocation of Bax during drug-induced apoptosis of tumor cells. *Cancer research*, 64, 7867-7878.
- AHMAD, S. S., DUKE, S., JENA, R., WILLIAMS, M. V. & BURNET, N. G. 2012. Advances in radiotherapy. *BMJ-British Medical Journal*, 345, e7765.
- AIKEN, C. T., KAAKE, R. M., WANG, X. & HUANG, L. 2011. Oxidative stress-mediated regulation of proteasome complexes. *Molecular & Cellular Proteomics*, 10, R110.006924.
- AKBARI, M. & KROKAN, HE. 2008. Cytotoxicity and mutagenicity of endogenous DNA base lesions as potential cause of human aging. *Mech Ageing Dev*, 129,353–65.
- AL-SALMANI, K. K. S. 2017. *A Pre-Clinical Investigation of the Anti-Cancer Effects of the Frankincense Constituent AKBA on Ovarian Cancer Cells*. Department of Cancer Studies & Molecular Medicine.
- AL AHMAD, M., MILHEM, R. M., PANICKER, N. G., RIZVI, T. A. & MUSTAFA, F. 2016. Electrical characterization of DNA supported on nitrocellulose membranes. *Scientific reports*, 6, 29089.
- AL MONEEF, M., SHERWOOD, B. T., BOWMAN, K. J., KOCKELBERGH, R. C., SYMONDS, R. P., STEWARD, W. P., MELLON, J. K. & JONES, G. D. D. 2003. Measurements using the alkaline comet assay predict bladder cancer cell radiosensitivity. *British Journal of Cancer*, In Press.
- ALBERTS, B., JOHNSON, A., LEWIS, J., RAFF, M., ROBERTS, K. & WALTER, P. 2002. The structure and function of DNA.
- ALBERTS, B., JOHNSON, A., WALTER, P., LEWIS, J., RAFF, M. & ROBERTS, K. 2008. Molecular cell biology. *New York and London: Garland Science*, 4.

- ALMEIDA, C. A. & BARRY, S. A. 2011. *Cancer: basic science and clinical aspects*, John Wiley & Sons.
- ANDREWS, C. L., VOUIROS, P. & HARSCH, A. 1999. Analysis of DNA adducts using high-performance separation techniques coupled to electrospray ionization mass spectrometry. *J Chromatogr A*, 856, 515-26.
- ANDRIEVSKI, A. & WILKINS, R. C. 2009. The response of gamma-H2AX in human lymphocytes and lymphocytes subsets measured in whole blood cultures. *International journal of radiation biology*, 85, 369-376.
- AZQUETA, A., GUTZKOW, K. B., BRUNBORG, G. & COLLINS, A. R. 2011. Towards a more reliable comet assay: optimising agarose concentration, unwinding time and electrophoresis conditions. *Mutation Research/Genetic Toxicology and Environmental Mutagenesis*, 724, 41-45.
- AZQUETA, A., SHAPOSHNIKOV, S. & COLLINS, A. R. 2009. DNA oxidation: investigating its key role in environmental mutagenesis with the comet assay. *Mutation Research/Genetic Toxicology and Environmental Mutagenesis*, 674, 101-108.
- AZZAM, E. I., JAY-GERIN, J.-P. & PAIN, D. 2012. Ionizing radiation-induced metabolic oxidative stress and prolonged cell injury. *Cancer letters*, 327, 48-60.
- BABJUK, M., OOSTERLINCK, W., SYLVESTER, R., KAASINEN, E., BÖHLE, A., PALOU-REDORTA, J. and ROUPRET, M. (2012) EAU guidelines on non-muscle-invasive urothelial carcinoma of the bladder, the 2011 update. *Actas Urológicas Españolas (English Edition)*, 36(7), pp. 389-402.
- BAJINSKIS, A., OLSSON, G. & HARMS-RINGDAHL, M. 2012. The indirect effect of radiation reduces the repair fidelity of NHEJ as verified in repair deficient CHO cell lines exposed to different radiation qualities and potassium bromate. *Mutation Research/Fundamental and Molecular Mechanisms of Mutagenesis*, 731, 125-132.
- BALABAN, R. S., NEMOTO, S. & FINKEL, T. 2005. Mitochondria, oxidants, and aging. *Cell*, 120, 483-495.
- BANÁTH, J. P., KLOKOV, D., MACPHAIL, S. H., BANUELOS, C. A. & OLIVE, P. L. 2010. Residual  $\gamma$ H2AX foci as an indication of lethal DNA lesions. *BMC cancer*, 10, 4.

- BANOUB, J. H., NEWTON, R. P., ESMANS, E., EWING, D. F. & MACKENZIE, G. 2005. Recent developments in mass spectrometry for the characterization of nucleosides, nucleotides, oligonucleotides, and nucleic acids. *Chem Rev*, 105, 1869-915.
- BANUELOS, C.A., BANATH, J.P., MACPHAIL, S.H., ZHAO, J., REITSEMA, T., & OLIVE, P.L. 2007. Radiosensitization by the Histone Deacetylase Inhibitor PCI-24781. *Clinical Cancer Research* 13:6816-6826.
- BARNARD, S., BOUFFLER, S. & ROTHKAMM, K. 2013. The shape of the radiation dose response for DNA double-strand break induction and repair. *Genome integrity*, 4, 1.
- BARNES, D. E. & LINDAHL, T. 2004. Repair and genetic consequences of endogenous DNA base damage in mammalian cells. *Annu. Rev. Genet.*, 38, 445-476.
- BARNETT, G. C., WEST, C. M., DUNNING, A. M., ELLIOTT, R. M., COLES, C. E., PHAROAH, P. D. & BURNET, N. G. 2009. Normal tissue reactions to radiotherapy: towards tailoring treatment dose by genotype. *Nature Reviews Cancer*, 9, 134.
- BASIM, H., STALL, R. E., MINSAVAGE, G. V. & JONES, J. B. 1999. Chromosomal Gene Transfer by Conjugation in the Plant Pathogen *Xanthomonas axonopodis* pv. *vesicatoria*. *Phytopathology*, 89, 1044-9.
- BASKAR, R. 2010. Emerging role of radiation induced bystander effects: Cell communications and carcinogenesis. *Genome integrity*, 1, 13.
- BASKAR, R., LEE, K. A., YEO, R. & YEOH, K.-W. 2012. Cancer and radiation therapy: current advances and future directions. *International journal of medical sciences*, 9, 193.
- BAUDAT, F. & DE MASSY, B. 2007. Regulating double-stranded DNA break repair towards crossover or non-crossover during mammalian meiosis. *Chromosome research*, 15, 565-577.
- BAUCHINGER, M. Cytogenetic effects as quantitative indicators of radiation exposure. Health Impacts of Large Releases of Radionuclides. Ciba Foundation Symposium, 1997. 188-204.
- BECKMAN, K. B. & AMES, B. N. 1998. The free radical theory of aging matures. *Physiological reviews*, 78, 547-581.

- BEGG, A. C., STEWART, F. A. & VENS, C. 2011. Strategies to improve radiotherapy with targeted drugs. *Nature Reviews Cancer*, 11, 239.
- BENTZEN, S. M. 2006. Preventing or reducing late side effects of radiation therapy: radiobiology meets molecular pathology. *Nature Reviews Cancer*, 6, 702.
- BENTZEN, S. M., CONSTINE, L. S., DEASY, J. O., EISBRUCH, A., JACKSON, A., MARKS, L. B., TEN HAKEN, R. K. & YORKE, E. D. 2010. Quantitative Analyses of Normal Tissue Effects in the Clinic (QUANTEC): an introduction to the scientific issues. *International Journal of Radiation Oncology• Biology• Physics*, 76, S3-S9.
- BEREZNEY, R. & COFFEY, D. S. 1975. Nuclear protein matrix: association with newly synthesized DNA. *Science*, 189, 291-293.
- BERNSTEIN, C., PRASAD, A. R., NFONSAM, V. & BERNSTEIN, H. 2013. DNA damage, DNA repair and cancer. *New Research Directions in DNA Repair*. InTech.
- BEWERSDORF, J., BENNETT, B. T. & KNIGHT, K. L. 2006. H2AX chromatin structures and their response to DNA damage revealed by 4Pi microscopy. *Proceedings of the National Academy of Sciences*, 103, 18137-18142.
- BOONSTRA, J. & POST, J. A. 2004. Molecular events associated with reactive oxygen species and cell cycle progression in mammalian cells. *Gene*, 337, 1-13.
- BHIDE, S. & NUTTING, C. 2010. Recent advances in radiotherapy. *BMC medicine*, 8, 25.
- BHOGAL, N., JALALI, F. & BRISTOW, R. G. 2009. Microscopic imaging of DNA repair foci in irradiated normal tissues. *International journal of radiation biology*, 85, 732-746.
- BICHLER, J., CAVIN, C., SIMIC, T., CHAKRABORTY, A., FERK, F., HOELZL, C., R., SCHULTE-HERMANN, A., M. KUNDI, D., G., HAIDINGER, A., K., ANGELIS, E., S., Knasmüller. 2007. Coffee consumption protects human lymphocytes against oxidative and 3-amino-1-methyl-5H-pyrido[4,3-b] indole acetate (Trp-P-2) induced DNA-damage: results of an experimental study with human volunteers. *Food and Chemical Toxicology*, 45, 1428–1436
- BIRREN, B. & LAI, E. 2012. *Pulsed field gel electrophoresis: a practical guide*, Academic Press.

- BIRREN, B. W., LAI, E., CLARK, S. M., HOOD, L. & SIMON, M. I. 1988. Optimized conditions for pulsed field gel electrophoretic separations of DNA. *Nucleic acids research*, 16, 7563-7582.
- BOWMAN, K., AL MONEEF, M., SHERWOOD, B., KOCKELBERGH, R., SYMONDS, R., STEWARD, W., COLQUHOUN, A., GODDARD, J., PAYNE, D. & SINGH, S. Measures of DNA damage and bladder cancer cell treatment response. MUTAGENESIS, 2012. OXFORD UNIV PRESS GREAT CLARENDON ST, OXFORD OX2 6DP, ENGLAND, 104-104.
- BOWMAN, K. J., AL- MONEEF, M. M., SHERWOOD, B. T., COLQUHOUN, A. J., GODDARD, J. C., GRIFFITHS, T., PAYNE, D., SINGH, S., BUTTERWORTH, P. C. & KHAN, M. A. 2014. Comet assay measures of DNA damage are predictive of bladder cancer cell treatment sensitivity in vitro and outcome in vivo. *International journal of cancer*, 134, 1102-1111.
- BRINK, A., LUTZ, U., VOLKEL, W. & LUTZ, W. K. 2006. Simultaneous determination of O6-methyl-2'-deoxyguanosine, 8-oxo-7,8-dihydro-2'-deoxyguanosine, and 1,N6-etheno-2'-deoxyadenosine in DNA using on-line sample preparation by HPLC column switching coupled to ESI-MS/MS. *J Chromatogr B Analyt Technol Biomed Life Sci*, 830, 255-61.
- BRISTOW, R. G. & HILL, R. P. 2008. Hypoxia and metabolism. Hypoxia, DNA repair and genetic instability. *Nat Rev Cancer*, 8, 180-92.
- BRIZEL, D. M. 2005. Strategies for protecting normal tissue in the treatment of head and neck cancer. *Squamous Cell Head and Neck Cancer*. Springer.
- BURMA, S., CHEN, B. P., MURPHY, M., KURIMASA, A. & CHEN, D. J. 2001. ATM phosphorylates histone H2AX in response to DNA double-strand breaks. *Journal of Biological Chemistry*, 276, 42462-42467.
- BURGER, M., CATTO, J. W., DALBAGNI, G., GROSSMAN, H. B., HERR, H., KARAKIEWICZ, P., KASSOUF, W., KIEMENEY, L. A., La VECCHIA, C. and SHARIAH, S. (2013) Epidemiology and risk factors of urothelial bladder cancer. *European urology*, 63(2), pp. 234-241.



- BURRELL, R. A., MCGRANAHAN, N., BARTEK, J. & SWANTON, C. 2013. The causes and consequences of genetic heterogeneity in cancer evolution. *Nature*, 501, 338.
- CADET, J., DOUKI, T., GASPARUTTO, D. & RAVANAT, J.-L. 2003a. Oxidative damage to DNA: formation, measurement and biochemical features. *Mutation Research/Fundamental and Molecular Mechanisms of Mutagenesis*, 531, 5-23.
- CADET, J., DOUKI, T., GASPARUTTO, D. & RAVANAT, J. L. 2003b. Oxidative damage to DNA: formation, measurement and biochemical features. *Mutat Res*, 531, 5-23.
- CALDECOTT, K. W. 2001. Mammalian DNA single- strand break repair: an X- ra (y) ted affair. *Bioessays*, 23, 447-455.
- CALDECOTT, K. W. 2007. Mammalian single-strand break repair: mechanisms and links with chromatin. *DNA repair*, 6, 443-453.
- CALDECOTT, K. W. 2008. Single-strand break repair and genetic disease. *Nature Reviews Genetics*, 9, 619.
- CAMPHAUSEN K, BURGAN W, CERRA M, OSWALD KA, TREPEL JB, LEE MJ *et al.* (2004a). Enhanced Radiation-Induced Cell Killing and Prolongation of  $\gamma$ H2AX Foci Expression by the Histone Deacetylase Inhibitor MS-275. *Cancer Research* **64**: 316–321.
- CAMPHAUSEN, K., SCOTT, T., SPROULL, M., and TOFILON, P.J. 2004b. Enhancement of xenograft tumor radiosensitivity by the histone deacetylase inhibitor MS-275 and correlation with histone hyperacetylation. *Clinical Cancer Research* 10:6066-6071.
- CAMPHAUSEN, K., CERRA, D., SCOTT, T., SPROULL, M., BURGA, W.E., CERRA, M.A., FINE H., and TOFILON, P.J. 2005. Enhancement of in vitro and in vivo tumor cell radiosensitivity by valproic acid. *Int Journal Cancer* 114:380-386
- CANTOR, C. R., GAAL, A. & SMITH, C. L. 1988. High-resolution separation and accurate size determination in pulsed-field gel electrophoresis of DNA. 3. Effect of electrical field shape. *Biochemistry*, 27, 9216-9221.
- CARON, H., SCHAIK, B., DER MEE, M., BAAS, F., RIGGINS, G., SIUIS, P., HERMUS, M.C., ASPEREN, R., BOON, K., VOUTE, P.A. and HEISTERKAMP, S., 2001. The human transcriptome map: clustering of highly expressed genes in chromosomal domains. *Science*, 291,1289-1292.

- CARLE, G. F. & OLSON, M. V. 1984. Separation of chromosomal DNA molecules from yeast by orthogonal-field-alternation gel electrophoresis. *Nucleic Acids Res*, 12, 5647-64.
- CARRANO, A., MINKLER, J., DILLEHAY, L. & THOMPSON, L. 1986. Incorporated bromodeoxyuridine enhances the sister-chromatid exchange and chromosomal aberration frequencies in an EMS-sensitive Chinese hamster cell line. *Mutation Research/Fundamental and Molecular Mechanisms of Mutagenesis*, 162, 233-239.
- CARTER, G. L., WILSON, L. J. & DUNN-COLEMAN, N. S. 1994. Molecular characterization of chromosomes by pulsed field electrophoresis. *Prog Ind Microbiol*, 29, 667-83.
- CELESTE, A., FERNANDEZ-CAPETILLO, O., KRUHLAK, M. J., PILCH, D. R., STAUDT, D. W., LEE, A., BONNER, R. F., BONNER, W. M. & NUSSENZWEIG, A. 2003. Histone H2AX phosphorylation is dispensable for the initial recognition of DNA breaks. *Nature cell biology*, 5, 675.
- CHANDRA, J., SAMALI, A. & ORRENIUS, S. 2000. Triggering and modulation of apoptosis by oxidative stress. *Free Radic Biol Med*, 29, 323-33.
- CHAO, M. R., YEN, C. C. & HU, C. W. 2008. Prevention of artifactual oxidation in determination of cellular 8-oxo-7,8-dihydro-2'-deoxyguanosine by isotope-dilution LC-MS/MS with automated solid-phase extraction. *Free Radic Biol Med*, 44, 464-73.
- CHAPMAN, J. R., TAYLOR, M. R. & BOULTON, S. J. 2012. Playing the end game: DNA double-strand break repair pathway choice. *Molecular cell*, 47, 497-510.
- CHENG, L., LOPEZ-BELTRAN, A. and BOSTWICK, D. G. (2012) *Bladder pathology*, John Wiley & Sons.
- CHIOLO, I., TANG, J., GEORGESCU, W. & COSTES, S. V. 2013. Nuclear dynamics of radiation-induced foci in euchromatin and heterochromatin. *Mutation Research/Fundamental and Molecular Mechanisms of Mutagenesis*, 750, 56-66.
- CHU, G. 1989. Pulsed field electrophoresis in contour-clamped homogeneous electric fields for the resolution of DNA by size or topology. *Electrophoresis*, 10, 290-295.
- CHU, G. & GUNDERSON, K. 1991. Separation of large DNA by a variable-angle contour-clamped homogeneous electric field apparatus. *Anal Biochem*, 194, 439-46.

- CHU, G., VOLLRATH, D. & DAVIS, R. W. 1986. Separation of large DNA molecules by contour-clamped homogeneous electric fields. *Science*, 234, 1582-5.
- CICCIA, A. & ELLEDGE, S. J. 2010. The DNA damage response: making it safe to play with knives. *Molecular cell*, 40, 179-204.
- CLARK, S. M., LAI, E., BIRREN, B. W. & HOOD, L. 1988. A novel instrument for separating large DNA molecules with pulsed homogeneous electric fields. *Science*, 241, 1203-5.
- CLEAVER, J. E. 2011.  $\gamma$ H2Ax: biomarker of damage or functional participant in DNA repair “all that glitters is not gold!”. *Photochemistry and photobiology*, 87, 1230-1239.
- COLLINS, A. 2002. The comet assay. Principles, applications, and limitations. *Methods in molecular biology (Clifton, NJ)*, 203, 163.
- COLLINS, A., DUŠINSKÁ, M., FRANKLIN, M., SOMOROVSKÁ, M., PETROVSKÁ, H., DUTHIE, S., FILLION, L., PANAYIOTIDIS, M., RAŠLOVÁ, K. & VAUGHAN, N. 1997. Comet assay in human biomonitoring studies: reliability, validation, and applications. *Environmental and molecular mutagenesis*, 30, 139-146.
- COLLINS, A. R. 2004. The comet assay for DNA damage and repair: principles, applications, and limitations. *Mol Biotechnol*, 26, 249-61.
- COLLINS, A. R. 2009. Investigating oxidative DNA damage and its repair using the comet assay. *Mutation Research/Reviews in Mutation Research*, 681, 24-32.
- COLLIS, S. J., DEWEESE, T. L., JEGGO, P. A. & PARKER, A. R. 2005. The life and death of DNA-PK. *Oncogene*, 24, 949.
- COLQUHOUN, A. J., JONES, G. D., MONEEF, M. A., BOWMAN, K. J., KOCKELBERGH, R. C., SYMONDS, R. P., STEWARD, W. P. & MELLON, J. K. 2003. Improving and predicting radiosensitivity in muscle invasive bladder cancer. *The Journal of urology*, 169, 1983-1992.
- COMPTON, S. A., ÖZGÜR, S. & GRIFFITH, J. D. 2010. Ring-shaped Rad51 paralog protein complexes bind Holliday junctions and replication forks as visualized by electron microscopy. *Journal of Biological Chemistry*, 285, 13349-13356.
- COOK, P. & BRAZELL, I. 1976. Conformational constraints in nuclear DNA. *Journal of cell science*, 22, 287-302.

- COOKE, P., DUNN, J., LATIEF, T., BATHERS, S., JAMES, N. and WALLACE, D. 2000. Long-Term Risk of Salvage Cystectomy after Radiotherapy for Muscle-Invasive Bladder Cancer. *European urology*, 38(3), pp. 279-286.
- COONEY, C. A. 1992. Separation and Size Determination of DNA over a 10-, 200 kbp Range. *Methods Mol Biol*, 12, 31-7.
- DAHM-DAPHI, C. S., W. ALBERTI, J 2000. Comparison of biological effects of DNA damage induced by ionizing radiation and hydrogen peroxide in CHO cells. *International journal of radiation biology*, 76, 67-75.
- DALY, M. J., GAIDAMAKOVA, E. K., MATROSOVA, V. Y., VASILENKO, A., ZHAI, M., LEAPMAN, R. D., LAI, B., RAVEL, B., LI, S.-M. W. & KEMNER, K. M. 2007. Protein oxidation implicated as the primary determinant of bacterial radioresistance. *PLoS biology*, 5, e92.
- DAVID, S. S. 2005. Structural biology: DNA search and rescue. *Nature*, 434, 569.
- DE HOFFMANN, E. & STROOBANT, V. 2007. *Mass spectrometry: principles and applications*, John Wiley & Sons.
- DE MIGUEL, M. & CORDERO, M. D. 2012. Oxidative therapy against cancer. *Oxidative Stress and Diseases*. InTech.
- DE RUIJTER, A.J., VAN GENNIP, A.H., CARON, H.N., KEMP, S., & VAN KUIENBURG, A.B. (2003). Histone deacetylases (HDACs): characterization of the classical HDAC family. *Biochemistry journal*. **370**:737-749.
- DI PIERRO, G. B., GULIA, C., CRISTINI, C., FRAIETTA, G., MARINI, L., GRANDE, P., GENTILE, V. and PIERGENTILI, R. (2012) Bladder cancer: a simple model becomes complex. *Current genomics*, 13(5), pp. 395.
- DEANS, A. J. & WEST, S. C. 2011. DNA interstrand crosslink repair and cancer. *Nature Reviews Cancer*, 11, 467.
- DELANEY, G., JACOB, S., FEATHERSTONE, C. & BARTON, M. 2005. The role of radiotherapy in cancer treatment. *Cancer*, 104, 1129-1137.

- DENISSENKO, M. F., PAO, A., TANG, M. & PFEIFER, G. P. 1996. Preferential formation of benzo[a]pyrene adducts at lung cancer mutational hotspots in P53. *Science*, 274, 430-2.
- DEVITA JR, V. T., LAWRENCE, T. & ROSENBERG, S. A. 2012. *Cancer: Principles & Practice of Oncology: Annual Advances in Oncology*, Lippincott Williams & Wilkins.
- DHAWAN, A., BAJPAYEE, M. & PARMAR, D. 2009. Comet assay: a reliable tool for the assessment of DNA damage in different models. *Cell biology and toxicology*, 25, 5-32.
- DIANOV, G. L., O'NEILL, P. & GOODHEAD, D. T. 2001. Securing genome stability by orchestrating DNA repair: removal of radiation- induced clustered lesions in DNA. *Bioessays*, 23, 745-749.
- DICKEY, J. S., REDON, C. E., NAKAMURA, A. J., BAIRD, B. J., SEDELNIKOVA, O. A. & BONNER, W. M. 2009. H2AX: functional roles and potential applications. *Chromosoma*, 118, 683-692.
- DIKOMEY, E., BORGMANN, K., KÖCHER, S., KRIEGS, M., MANSOUR, W., PARPLYS, A., RIECKMANN, T. & ROTHKAMM, K. 2016. Radiation DNA damage and use in cancer/therapeutics-translation of radiation modifiers. *DNA Repair in Cancer Therapy (Second Edition)*. Elsevier.
- DIPPLE, A. 1995. DNA adducts of chemical carcinogens. *Carcinogenesis*, 16, 437-41.
- DIZDAROGLU, M. 1984. The use of capillary gas chromatography—mass spectrometry for identification of radiation-induced DNA base damage and DNA base—amino acid cross-links. *Journal of Chromatography A*, 295, 103-121.
- DJUZENOVA, C. S., ELSNER, I., KATZER, A., WORSCHKECH, E., DISTEL, L. V., FLENTJE, M. & POLAT, B. 2013. Radiosensitivity in breast cancer assessed by the histone  $\gamma$ -H2AX and 53BP1 foci. *Radiation oncology*, 8, 98.
- DOERGE, D. R., CHURCHWELL, M. I. & BELAND, F. A. 2002. Analysis of DNA adducts from chemical carcinogens and lipid peroxidation using liquid chromatography and electrospray mass spectrometry. *J Environ Sci Health C Environ Carcinog Ecotoxicol Rev*, 20, 1-20.

- DOERGE, D. R., CHURCHWELL, M. I., FANG, J. L. & BELAND, F. A. 2000. Quantification of etheno-DNA adducts using liquid chromatography, on-line sample processing, and electrospray tandem mass spectrometry. *Chem Res Toxicol*, 13, 1259-64.
- DOMENECH, H. 2017. Biological Effects of Ionizing Radiation. *Radiation Safety*. Springer.
- DOMÍNGUEZ, I., DAZA, P., NATARAJAN, A. & CORTES, F. 1998. A high yield of translocations parallels the high yield of sister chromatid exchanges in the CHO mutant EM9. *Mutation Research/Fundamental and Molecular Mechanisms of Mutagenesis*, 398, 67-73.
- DROUET, J., DELTEIL, C., LEFRANÇOIS, J., CONCANNON, P., SALLES, B. & CALSOU, P. 2005. DNA-dependent protein kinase and XRCC4-DNA ligase IV mobilization in the cell in response to DNA double strand breaks. *Journal of Biological Chemistry*, 280, 7060-7069.
- DUEZ, P., DEHON, G., KUMPS, A. & DUBOIS, J. 2003. Statistics of the Comet assay: a key to discriminate between genotoxic effects. *Mutagenesis*, 18, 159-166.
- DUNNE, A., PRICE, M., MOTHERSILL, C., MCKEOWN, S., ROBSON, T. & HIRST, D. 2003. Relationship between clonogenic radiosensitivity, radiation-induced apoptosis and DNA damage/repair in human colon cancer cells. *British journal of cancer*, 89, 2277.
- DURANTE, M. & LOEFFLER, J. S. 2010. Charged particles in radiation oncology. *Nature reviews Clinical oncology*, 7, 37.
- ECCLES, L. J., O'NEILL, P. & LOMAX, M. E. 2011. Delayed repair of radiation induced clustered DNA damage: friend or foe? *Mutation Research/Fundamental and Molecular Mechanisms of Mutagenesis*, 711, 134-141.
- ELCOCK, L. S. & BRIDGER, J. M. 2008. Exploring the effects of a dysfunctional nuclear matrix. Portland Press Limited.
- EMAMI, B., LYMAN, J., BROWN, A., COLA, L., GOITEIN, M., MUNZENRIDER, J., SHANK, B., SOLIN, L. & WESSON, M. 1991. Tolerance of normal tissue to therapeutic irradiation. *International Journal of Radiation Oncology• Biology• Physics*, 21, 109-122.

- ESMANS, E. L., BROES, D., HOES, I., LEMIERE, F. & VANHOUTTE, K. 1998. Liquid chromatography–mass spectrometry in nucleoside, nucleotide and modified nucleotide characterization. *Journal of Chromatography A*, 794, 109-127.
- EVANS, M. D., DIZDAROGLU, M. & COOKE, M. S. 2004. Oxidative DNA damage and disease: induction, repair and significance. *Mutation Research/Reviews in Mutation Research*, 567, 1-61.
- FAJKOVIC, H., HALPERN, J. A., CHA, E. K., BAHADORI, A., CHROMECKI, T. F., KARAKIEWICZ, P. I., BREINL, E., MERSEBURGER, A. S. and SHARIAT, S. F. (2011) Impact of gender on bladder cancer incidence, staging, and prognosis. *World journal of urology*, 29(4), pp. 457-463.
- FAIRBAIRN, D. W., OLIVE, P. L. & O'NEILL, K. L. 1995. The comet assay: a comprehensive review. *Mutation Research/Reviews in Genetic Toxicology*, 339, 37-59.
- FANG, J., SEKI, T. & MAEDA, H. 2009. Therapeutic strategies by modulating oxygen stress in cancer and inflammation. *Adv Drug Deliv Rev*, 61, 290-302.
- FARBER, J. M. 1996. An Introduction to the Hows and Whys of Molecular Typing. *Journal of Food Protection*, 59, 1091-1101.
- FARMER, P. B., LAMB, J. & LAWLEY, P. D. 1988. Novel uses of mass spectrometry in studies of adducts of alkylating agents with nucleic acids and proteins. *IARC Sci Publ*, 347-55.
- FERLAY, J., SHIN, H. R., BRAY, F., FORMAN, D., MATHERS, C. and PARKIN, D. M. 2010. Estimates of worldwide burden of cancer in 2008: *International Journal of Cancer*, 127, 2893-2917.
- FERNÁNDEZ, M. I., GONG, Y., YE, Y., LIN, J., CHANG, D. W., KAMAT, A. M. & WU, X. 2013.  $\gamma$ -H2AX level in peripheral blood lymphocytes as a risk predictor for bladder cancer. *Carcinogenesis*, 34, 2543-2547.
- FINKEL, T. & HOLBROOK, N. J. 2000. Oxidants, oxidative stress and the biology of ageing. *Nature*, 408, 239.
- FIORITI, D., PIETROPAOLO, V., DAL FORNO, S., LAURENTI, C., CHIARINI, F. and DEGENER, A. (2002) Urothelial bladder carcinoma and viral infections: different

- association with human polyomaviruses and papillomaviruses. *International journal of immunopathology and pharmacology*, 16, 283-288.
- FINNEY, M. 2001. Pulsed-field gel electrophoresis. *Curr Protoc Mol Biol*, Chapter 2, Unit2 5B.
- FISHER, A.E., BURKE, D., ROUTLEDGE, M.N. Can irradiation of rectal tumour cells from patient biopsy predict outcome of radiotherapy? Proceedings of the Genome Stability network/ United Kingdom Environmental Mutagen Society Joint Congress, University of Cardiff. 1 – 4 July 2007.
- FLOYD, R. A. 1999. Antioxidants, oxidative stress, and degenerative neurological disorders (44448). *Proceedings of the Society for Experimental Biology and Medicine*, 222, 236-245.
- FLOYD, R. A., WATSON, J. J. & WONG, P. K. 1984. Sensitive assay of hydroxyl free radical formation utilizing high pressure liquid chromatography with electrochemical detection of phenol and salicylate hydroxylation products. *Journal of biochemical and biophysical methods*, 10, 221-235.
- FONTES, F. L., PINHEIRO, D. M. L., DE OLIVEIRA, A. H. S., DE MEDEIROS OLIVEIRA, R. K., LAJUS, T. B. P. & AGNEZ-LIMA, L. F. 2015. Role of DNA repair in host immune response and inflammation. *Mutation Research/Reviews in Mutation Research*, 763, 246-257.
- FALK, M., LUKASOVA, E. and KOZUBEK, S., 2008. Chromatin structure influences the sensitivity of DNA to  $\gamma$ -radiation. *(BBA)-Molecular Cell Research*, 12, 2398-2414.
- FREEDMAN, N. D., SILVERMAN, D. T., HOLLENBECK, A. R., SCHATZKIN, A. and ABNET, C. C. 2011. Association between smoking and risk of bladder cancer among men and women. *JAMA: the journal of the American Medical Association*, 306, 737.
- FRENKEL, K. 1992. Carcinogen-mediated oxidant formation and oxidative DNA damage. *Pharmacol Ther*, 53, 127-66.
- FUMAGALLI, M., ROSSIello, F., CLERICI, M., BAROZZI, S., CITTARO, D., KAPLUNOV, J. M., BUCCI, G., DOBREVA, M., MATTI, V. & BEAUSEJOUR,



- C. M. 2012. Telomeric DNA damage is irreparable and causes persistent DNA-damage-response activation. *Nature cell biology*, 14, 355.
- FURUTA, T., TAKEMURA, H., LIAO, Z.-Y., AUNE, G. J., REDON, C., SEDELNIKOVA, O. A., PILCH, D. R., ROGAKOU, E. P., CELESTE, A. & CHEN, H. T. 2003. Phosphorylation of histone H2AX and activation of Mre11, Rad50, and Nbs1 in response to replication-dependent DNA double-strand breaks induced by mammalian DNA topoisomerase I cleavage complexes. *Journal of Biological Chemistry*, 278, 20303-20312.
- GALARIS, D., SKIADA, V. & BARBOUTI, A. 2008. Redox signaling and cancer: the role of "labile" iron. *Cancer Lett*, 266, 21-9.
- GALLUZZI, L., PIETROCOLA, F., BRAVO- SAN PEDRO, J. M., AMARAVADI, R. K., BAEHRECKE, E. H., CECCONI, F., CODOGNO, P., DEBNATH, J., GEWIRTZ, D. A. & KARANTZA, V. 2015. Autophagy in malignant transformation and cancer progression. *The EMBO journal*, 34, 856-880.
- GARAJ-VRHOVAC, V. & KOPJAR, N. 2003. The alkaline Comet assay as biomarker in assessment of DNA damage in medical personnel occupationally exposed to ionizing radiation. *Mutagenesis*, 18, 265-271.
- GARTY, G., BIGELOW, A. W., REPIN, M., TURNER, H. C., BIAN, D., BALAJEE, A. S., LYULKO, O. V., TAVERAS, M., YAO, Y. L. & BRENNER, D. J. 2015. An automated imaging system for radiation biodosimetry. *Microscopy research and technique*, 78, 587-598.
- GAUTHIER, M. G. & BECHHOEFER, J. 2009. Control of DNA replication by anomalous reaction-diffusion kinetics. *Physical review letters*, 102, 158104.
- GENESTRA, M. 2007. Oxyl radicals, redox-sensitive signalling cascades and antioxidants. *Cellular signalling*, 19, 1807-1819.
- GENOIS, M.-M., PAQUET, E. R., LAFFITTE, M.-C. N., MAITY, R., RODRIGUE, A., OUELLETTE, M. & MASSON, J.-Y. 2014. DNA repair pathways in trypanosomatids: from DNA repair to drug resistance. *Microbiology and Molecular Biology Reviews*, 78, 40-73.
- GEORGAKILAS, A. G. 2008. Processing of DNA damage clusters in human cells: current status of knowledge. *Molecular BioSystems*, 4, 30-35.

- GEORGAKILAS, A. G., BENNETT, P. V. & SUTHERLAND, B. M. 2002. High efficiency detection of bi-stranded abasic clusters in  $\gamma$ -irradiated DNA by putrescine. *Nucleic acids research*, 30, 2800-2808.
- GEORGAKILAS, A. G., BENNETT, P. V., WILSON III, D. M. & SUTHERLAND, B. M. 2004. Processing of bistranded abasic DNA clusters in  $\gamma$ -irradiated human hematopoietic cells. *Nucleic acids research*, 32, 5609-5620.
- GETZENBERG, R. H., KONETY, B. R., OELER, T. A., QUIGLEY, M. M., HAKAM, A., BECICH, M. J. & BAHNSON, R. R. 1996. Bladder cancer-associated nuclear matrix proteins. *Cancer Research*, 56, 1690-1694.
- GHARDI, M., MOREELS, M., CHATELAIN, B., CHATELAIN, C. & BAATOUT, S. 2012. Radiation-induced double strand breaks and subsequent apoptotic DNA fragmentation in human peripheral blood mononuclear cells. *International journal of molecular medicine*, 29, 769-780.
- GIBELLINI, L., PINTI, M., NASI, M., DE BIASI, S., ROAT, E., BERTONCELLI, L. & COSSARIZZA, A. 2010. Interfering with ROS metabolism in cancer cells: the potential role of quercetin. *Cancers*, 2, 1288-1311.
- GLUCH, A., VIDAKOVIC, M. & BODE, J. 2008. Scaffold/matrix attachment regions (S/MARs): relevance for disease and therapy. *Protein-Protein Interactions as New Drug Targets*. Springer.
- GOERING, R. & WINTERS, M. 1992. Rapid method for epidemiological evaluation of gram-positive cocci by field inversion gel electrophoresis. *Journal of clinical microbiology*, 30, 577-580.
- GOERING, R. V. 2004. Pulsed-field gel electrophoresis. *Molecular microbiology: diagnostic principles and practice*. ASM Press, Washington, DC, 185-196.
- GOERING, R. V. 2010. Pulsed field gel electrophoresis: a review of application and interpretation in the molecular epidemiology of infectious disease. *Infection, Genetics and Evolution*, 10, 866-875.
- GOGGIN, M., SANGARAJU, D., WALKER, V. E., WICKLIFFE, J., SWENBERG, J. A. & TRETYAKOVA, N. 2011. Persistence and repair of bifunctional DNA adducts in tissues of laboratory animals exposed to 1,3-butadiene by inhalation. *Chem Res Toxicol*, 24, 809-17.

- GOGGIN, M., SWENBERG, J. A., WALKER, V. E. & TRETYAKOVA, N. 2009. Molecular dosimetry of 1,2,3,4-diepoxybutane-induced DNA-DNA cross-links in B6C3F1 mice and F344 rats exposed to 1,3-butadiene by inhalation. *Cancer Res*, 69, 2479-86.
- GOODARZI, A. A., JEGGO, P. & LOBRICH, M. 2010. The influence of heterochromatin on DNA double strand break repair: Getting the strong, silent type to relax. *DNA repair*, 9, 1273-1282.
- GOODARZI, A. A. & JEGGO, P. A. 2012. Irradiation induced foci (IRIF) as a biomarker for radiosensitivity. *Mutation Research/Fundamental and Molecular Mechanisms of Mutagenesis*, 736, 39-47.
- GOODHEAD, D. T. 1994. Initial Events in the Cellular Effects of Ionizing Radiations: Clustered Damage in DNA. *International Journal of Radiation Biology*, 65, 7-17.
- GOODHEAD, D. T. 1999. Mechanisms for the biological effectiveness of high-LET radiations. *Journal of radiation research*, 40, S1-S13.
- GOODISON, S., ROSSER, C. J. and URQUIDI, V. 2013. Bladder cancer detection and monitoring: assessment of urine-and blood-based marker tests. *Molecular diagnosis & therapy*, 17, 71-84.
- GRADZKA, I. & IWANENKO, T. 2005. A non-radioactive, PFGE-based assay for low levels of DNA double-strand breaks in mammalian cells. *DNA Repair (Amst)*, 4, 1129-39.
- GRĄDZKA, I. & IWANEŃKO, T. 2005. A non-radioactive, PFGE-based assay for low levels of DNA double-strand breaks in mammalian cells. *DNA repair*, 4, 1129-1139.
- GREBE, S. K. & SINGH, R. J. 2011a. LC-MS/MS in the clinical laboratory—where to from here? *The Clinical Biochemist Reviews*, 32, 5.
- GREBE, S. K. & SINGH, R. J. 2011b. LC-MS/MS in the Clinical Laboratory - Where to From Here? *Clin Biochem Rev*, 32, 5-31.
- GRIFFITHS, W. J., JONSSON, A. P., LIU, S., RAI, D. K. & WANG, Y. 2001. Electrospray and tandem mass spectrometry in biochemistry. *Biochem J*, 355, 545-61.
- GROLLMAN, A. P. & MORIYA, M. 1993. Mutagenesis by 8-oxoguanine: an enemy within. *Trends Genet*, 9, 246-9.

- GU, J., LU, H., TIPPIN, B., SHIMAZAKI, N., GOODMAN, M. F. & LIEBER, M. R. 2007. XRCC4: DNA ligase IV can ligate incompatible DNA ends and can ligate across gaps. *The EMBO journal*, 26, 1010-1023.
- GUADAGNOLO, B. A., LIAO, K.-P., ELTING, L., GIORDANO, S., BUCHHOLZ, T. A. & SHIH, Y.-C. T. 2013. Use of radiation therapy in the last 30 days of life among a large population-based cohort of elderly patients in the United States. *Journal of Clinical Oncology*, 31, 80.
- GURRIERI, S., SMITH, S. B., WELLS, K. S., JOHNSON, I. D. & BUSTAMANTE, C. 1996. Real-Time Imaging of the Reorientation Mechanisms of YOYO-Labelled DNA Molecules during 90° and 120° Pulsed Field Gel Electrophoresis. *Nucleic Acids Research*, 24, 4759-4767.
- HADA, M. & GEORGAKILAS, A. G. 2008. Formation of clustered DNA damage after high-LET irradiation: a review. *Journal of radiation research*, 49, 203-210.
- HALFORD, S. E. & MARKO, J. F. 2004. How do site- specific DNA- binding proteins find their targets? *Nucleic acids research*, 32, 3040-3052.
- HALL, E. J. 2007. Cancer caused by x-rays—a random event? *The Lancet Oncology*, 8, 369-370.
- HALLIWELL, B. & CROSS, C. E. 1994. Oxygen-derived species: their relation to human disease and environmental stress. *Environmental health perspectives*, 102, 5.
- HALLIWELL, B. 2007. Biochemistry of oxidative stress. Portland Press Limited.
- HALL, E. J. & GIACCIA, A. J. 2006. *Radiobiology for the Radiologist*, Lippincott Williams & Wilkins Philadelphia:.
- HALPIN, J. L., GARRETT, N. M., RIBOT, E. M., GRAVES, L. M. & COOPER, K. L. 2010. Re-evaluation, optimization, and multilaboratory validation of the PulseNet-standardized pulsed-field gel electrophoresis protocol for *Listeria monocytogenes*. *Foodborne pathogens and disease*, 7, 293-298.
- HAMASAKI, K., IMAI, K., NAKACHI, K., TAKAHASHI, N., KODAMA, Y. & KUSUNOKI, Y. 2007. Short- term culture and  $\gamma$ H2AX flow cytometry determine differences in individual radiosensitivity in human peripheral T lymphocytes. *Environmental and molecular mutagenesis*, 48, 38-47.
- HANAHAN, D. & WEINBERG, R. A. 2000. The hallmarks of cancer. *cell*, 100, 57-70.

- HANAHAN, D. & WEINBERG, R. A. 2011. Hallmarks of cancer: the next generation. *cell*, 144, 646-674.
- HARRISON, L., HATAHET, Z. & WALLACE, S. S. 1999. In vitro repair of synthetic ionizing radiation-induced multiply damaged DNA sites1. *Journal of molecular biology*, 290, 667-684.
- HECHT, S. S. 2003. Tobacco carcinogens, their biomarkers and tobacco-induced cancer. *Nat Rev Cancer*, 3, 733-44.
- HELLEDAY, T., PETERMANN, E., LUNDIN, C., HODGSON, B. & SHARMA, R. A. 2008. DNA repair pathways as targets for cancer therapy. *Nature Reviews Cancer*, 8, 193.
- HERR, H. W. (1992) Intravesical BCG: Current results, natural history and implicants for urothelial cancer prevention. *Journal of Cellular Biochemistry*, 50(S16I), pp. 112-119.
- HERSKIND, C. & WENZ, F. 2014. Radiobiological aspects of intraoperative tumour-bed irradiation with low-energy X-rays (LEX-IORT). *Translational Cancer Research*, 3, 3-17.
- HIGGINS, G. C., BEART, P. M., SHIN, Y. S., CHEN, M. J., CHEUNG, N. S. & NAGLEY, P. 2010. Oxidative stress: emerging mitochondrial and cellular themes and variations in neuronal injury. *Journal of Alzheimer's Disease*, 20, S453-S473.
- HOEIJMAKERS, J. H. 2001. Genome maintenance mechanisms for preventing cancer. *nature*, 411, 366.
- HOEIJMAKERS, J. H. 2009. DNA damage, aging, and cancer. *New England Journal of Medicine*, 361, 1475-1485.
- HOPFGARTNER, G., VARESIO, E., TSCHAPPAT, V., GRIVET, C., BOURGOGNE, E. & LEUTHOLD, L. A. 2004. Triple quadrupole linear ion trap mass spectrometer for the analysis of small molecules and macromolecules. *J Mass Spectrom*, 39, 845-55.
- HORN, S., BARNARD, S. & ROTHKAMM, K. 2011. Gamma-H2AX-based dose estimation for whole and partial body radiation exposure. *PloS one*, 6, e25113.
- IORNS, E., LORD, C. J., GRIGORIADIS, A., MCDONALD, S., FENWICK, K., MACKAY, A., MEIN, C. A., NATRAJAN, R., SAVAGE, K. & TAMBER, N. 2009.

- Integrated functional, gene expression and genomic analysis for the identification of cancer targets. *PloS one*, 4, e5120.
- ISHII, Y., SUZUKI, Y., HIBI, D., JIN, M., FUKUHARA, K., UMEMURA, T. & NISHIKAWA, A. 2011. Detection and quantification of specific DNA adducts by liquid chromatography-tandem mass spectrometry in the livers of rats given estragole at the carcinogenic dose. *Chem Res Toxicol*, 24, 532-41.
- ISMAIL, I. H., WADHRA, T. I. & HAMMARSTEN, O. 2007. An optimized method for detecting gamma-H2AX in blood cells reveals a significant interindividual variation in the gamma-H2AX response among humans. *Nucleic acids research*, 35, e36.
- IVASHKEVICH, A. N., MARTIN, O. A., SMITH, A. J., REDON, C. E., BONNER, W. M., MARTIN, R. F. & LOBACHEVSKY, P. N. 2011.  $\gamma$ H2AX foci as a measure of DNA damage: a computational approach to automatic analysis. *Mutation Research/Fundamental and Molecular Mechanisms of Mutagenesis*, 711, 49-60.
- JACKSON, S. P. & BARTEK, J. 2009a. The DNA-damage response in human biology and disease. *Nature*, 461, 1071.
- JACKSON, S. P. & BARTEK, J. 2009b. The DNA-damage response in human biology and disease. *Nature*, 461, 1071-8.
- JÄKEL, O. 2008. The relative biological effectiveness of proton and ion beams. *Zeitschrift für Medizinische Physik*, 18, 276-285.
- JAKOB, B., SPLINTER, J., CONRAD, S., VOSS, K.-O., ZINK, D., DURANTE, M., LÖBRICH, M. & TAUCHER-SCHOLZ, G. 2011. DNA double-strand breaks in heterochromatin elicit fast repair protein recruitment, histone H2AX phosphorylation and relocation to euchromatin. *Nucleic acids research*, 39, 6489-6499.
- JAMES, N. D., HUSSAIN, S. A., HALL, E., JENKINS, P., TREMLETT, J., RAWLINGS, C., CRUNDWELL, M., SIZER, B., SREENIVASAN, T., HENDRON, C., LEWIS, R., WATERS, R. and HUDDART, R. A. (2012) Radiotherapy with or without chemotherapy in muscle-invasive bladder cancer. *N Engl J Med*, 366(16), pp. 1477-88.
- JEFFREY, G. A. & SAENGER, W. 2012. *Hydrogen bonding in biological structures*, Springer Science & Business Media.

- JEGGO, P. & LÖBRICH, M. 2007. DNA double-strand breaks: their cellular and clinical impact? *Oncogene*, 26, 7717.
- JEGGO, P. A., GEUTING, V. & LÖBRICH, M. 2011. The role of homologous recombination in radiation-induced double-strand break repair. *Radiotherapy and Oncology*, 101, 7-12.
- JEMAL, A., CENTER, M. M., DESANTIS, C. & WARD, E. M. 2010. Global patterns of cancer incidence and mortality rates and trends. *Cancer Epidemiology and Prevention Biomarkers*, 19, 1893-1907.
- JEMAL, A., BRAY, F., CENTER, M. M., FERLAY, J., WARD, E. and FORMAN, D. (2011) Global cancer statistics. *CA: a cancer journal for clinicians*, 61(2), pp. 69-90.
- JIN, S. G., WU, X., LI, A. X. & PFEIFER, G. P. 2011. Genomic mapping of 5-hydroxymethylcytosine in the human brain. *Nucleic Acids Res*, 39, 5015-24.
- JIRICNY, J. 2006. The multifaceted mismatch-repair system. *Nature reviews Molecular cell biology*, 7, 335.
- JOSHI, N. & GRANT, S. G. 2014. Pulsed-field gel electrophoresis analysis of multicellular DNA double-strand break damage and repair. *Methods Mol Biol*, 1105, 193-202.
- KAESAWANG, T. 2003. *Comparative Study of DNA Patterns of Salmonella Enteritidis Isolated from Human Patients and Chicken Meat in Thailand by Pulsed-Field Gel Electrophoresis*. Chulalongkorn University.
- KAMIYA, H., MIURA, H., MURATA-KAMIYA, N., ISHIKAWA, H., SAKAGUCHI, T., INOUE, H., SASAKI, T., MASUTANI, C., HANAOKA, F., NISHIMURA, S. & ET AL. 1995. 8-Hydroxyadenine (7,8-dihydro-8-oxoadenine) induces misincorporation in in vitro DNA synthesis and mutations in NIH 3T3 cells. *Nucleic Acids Res*, 23, 2893-9.
- KARAGIANNIS, T.C., KN, H. & EL-OSTA A. (2005). The histone deacetylase inhibitor, Trichostatin A, enhances radiation sensitivity and accumulation of gammaH2AX. *Cancer Biology Ther* 4: 787–793.
- KASSIE, F., PARZEFALL, W. & KNASMÜLLER, S. 2000. Single cell gel electrophoresis assay: a new technique for human biomonitoring studies. *Mutation Research/Reviews in Mutation Research*, 463, 13-31.

- KAUFMANN, M., PITT, T. & CHART, H. 1994. Methods in practical laboratory bacteriology. *Methods in Practical Laboratory Bacteriology*.
- KAVANAGH, J. N., REDMOND, K. M., SCHETTINO, G. & PRISE, K. M. 2013. DNA double strand break repair: a radiation perspective. *Antioxidants & redox signaling*, 18, 2458-2472.
- KEIMLING, M., DENIZ, M., VARGA, D., STAHL, A., SCHREZENMEIER, H., KREIENBERG, R., HOFFMANN, I., KÖNIG, J. & WIESMÜLLER, L. 2012. The power of DNA double-strand break (DSB) repair testing to predict breast cancer susceptibility. *The FASEB Journal*, 26, 2094-2104.
- KHALED, S. & HELD, K. D. 2012. Radiation biology: a handbook for teachers and students. Taylor & Francis.
- KHANDRIKA, L., KUMAR, B., KOUL, S., MARONI, P. & KOUL, H. K. 2009. Oxidative stress in prostate cancer. *Cancer Lett*, 282, 125-36.
- KIM, J.-S., KRASIEVA, T. B., KURUMIZAKA, H., CHEN, D. J., TAYLOR, A. M. R. & YOKOMORI, K. 2005. Independent and sequential recruitment of NHEJ and HR factors to DNA damage sites in mammalian cells. *J Cell Biol*, 170, 341-347.
- KING, R., BONFIGLIO, R., FERNANDEZ-METZLER, C., MILLER-STEIN, C. & OLAH, T. 2000. Mechanistic investigation of ionization suppression in electrospray ionization. *Journal of the American Society for Mass Spectrometry*, 11, 942-950.
- KINNER, A., WU, W., STAUDT, C. & ILIAKIS, G. 2008.  $\gamma$ -H2AX in recognition and signaling of DNA double-strand breaks in the context of chromatin. *Nucleic acids research*, 36, 5678-5694.
- KLUNGLAND, A. & BJELLAND, S. 2007. Oxidative damage to purines in DNA: role of mammalian Ogg1. *DNA Repair (Amst)*, 6, 481-8.
- KNOWLES, M. A. and HUREST, C. D. 2015. Molecular biology of bladder cancer: new insights into pathogenesis and clinical diversity. *Nature Reviews Cancer*, 15, 25-41.
- KOC, H. & SWENBERG, J. A. 2002. Applications of mass spectrometry for quantitation of DNA adducts. *J Chromatogr B Analyt Technol Biomed Life Sci*, 778, 323-43.
- KOHN, K. W. & BOHR, V. A. 2002. Genomic instability and DNA repair. *The cancer handbook*.



- KOTWAL, S., CHOUDHURY, A., JOHNSTON, C., PAUL, A. B., WHELAN, P. and KILTIE, A. E. 2008. Similar treatment outcomes for radical cystectomy and radical radiotherapy in invasive bladder cancer treated at a United Kingdom specialist treatment center. *International Journal of Radiation Oncology\* Biology\* Physics*, 70(2), pp. 456-463.
- KOTURBASH, I., KUTANZI, K., HENDRICKSON, K., RODRIGUEZ-JUAREZ, R., KOGOSOV, D. & KOVALCHUK, O. 2008. Radiation-induced bystander effects in vivo are sex specific. *Mutation Research/Fundamental and Molecular Mechanisms of Mutagenesis*, 642, 28-36.
- KRIAUCIONIS, S. & HEINTZ, N. 2009. The nuclear DNA base, 5-hydroxymethylcytosine is present in brain and enriched in Purkinje neurons. *Science (New York, N.y.)*, 324, 929-930.
- KRYSTON, T. B., GEORGIEV, A. B., PISSIS, P. & GEORGAKILAS, A. G. 2011a. Role of oxidative stress and DNA damage in human carcinogenesis. *Mutation Research/Fundamental and Molecular Mechanisms of Mutagenesis*, 711, 193-201.
- KRYSTON, T. B., GEORGIEV, A. B., PISSIS, P. & GEORGAKILAS, A. G. 2011b. Role of oxidative stress and DNA damage in human carcinogenesis. *Mutat Res*, 711, 193-201.
- KUMARAVEL, T. & JHA, A. N. 2006. Reliable Comet assay measurements for detecting DNA damage induced by ionising radiation and chemicals. *Mutation Research/Genetic Toxicology and Environmental Mutagenesis*, 605, 7-16.
- KUMARAVEL, T.S. & BRISTOW, R., G. 2005. Detection of genetic instability at HER-2/neu and p53 loci in breast cancer cells using Comet-FISH. *Breast Cancer Res Treat*, 91, 89-93.
- KUMARAVEL, T., VILHAR, B., FAUX, S. P. & JHA, A. N. 2009. Comet assay measurements: a perspective. *Cell biology and toxicology*, 25, 53-64.
- KUO, L. J. & YANG, L.-X. 2008.  $\gamma$ -H2AX-a novel biomarker for DNA double-strand breaks. *In vivo*, 22, 305-309.

- KUSPA, A., VOLLRATH, D., CHENG, Y. & KAISER, D. 1989. Physical mapping of the *Myxococcus xanthus* genome by random cloning in yeast artificial chromosomes. *Proc Natl Acad Sci U S A*, 86, 8917-21.
- KUZMINOV, A. 2001. Single-strand interruptions in replicating chromosomes cause double-strand breaks. *Proceedings of the National Academy of Sciences*, 98, 8241-8246.
- LAI, E., BIRREN, B. W., CLARK, S. M., SIMON, M. I. & HOOD, L. 1989. Pulsed field gel electrophoresis. *Biotechniques*, 7, 34-42.
- LANGIE, S. A., AZQUETA, A. & COLLINS, A. R. 2015. The comet assay: past, present, and future. *Frontiers in genetics*, 6, 266.
- LASSMANN, M., HÄNSCHEID, H., GASSEN, D., BIKO, J., MEINEKE, V., REINERS, C. & SCHERTHAN, H. 2010. In vivo formation of  $\gamma$ -H2AX and 53BP1 DNA repair foci in blood cells after radioiodine therapy of differentiated thyroid cancer. *Journal of Nuclear Medicine*, 51, 1318-1325.
- LAWRENCE, T. S., TEN HAKEN, R. K. & GIACCIA, A. 2008. Principles of radiation oncology. *Cancer: principles and practice of oncology. 8th ed. Philadelphia: Lippincott Williams and Wilkins.*
- LEHNERT, S. 2007. *Biomolecular action of ionizing radiation*, CRC Press.
- LEMAÎTRE, C., GRABARZ, A., TSOUROULA, K., ANDRONOV, L., FURST, A., PANKOTAI, T., HEYER, V., ROGIER, M., ATTWOOD, K. M. & KESSLER, P. 2014. Nuclear position dictates DNA repair pathway choice. *Genes & development*, 28, 2450-2463.
- LI, P., DU, C.-R., XU, W.-C., SHI, Z.-L., ZHANG, Q., LI, Z.-B. & FU, S. 2013. Correlation of dynamic changes in  $\gamma$ -H2AX expression in peripheral blood lymphocytes from head and neck cancer patients with radiation-induced oral mucositis. *Radiation Oncology*, 8, 155.
- LIAUW, S. L., CONNELL, P. P. & WEICHSELBAUM, R. R. 2013. New paradigms and future challenges in radiation oncology: an update of biological targets and technology. *Science translational medicine*, 5, 173sr2-173sr2.

- LIEBER, M. R. 2010. The mechanism of double-strand DNA break repair by the nonhomologous DNA end-joining pathway. *Annual review of biochemistry*, 79, 181-211.
- LIM, C. K. & LORD, G. 2002. Current developments in LC-MS for pharmaceutical analysis. *Biol Pharm Bull*, 25, 547-57.
- LINDAHL, T. & WOOD, R. D. 1999. Quality control by DNA repair. *Science*, 286, 1897-1905.
- LINDGREN, D., LIEBERG, F., ANDERSSON, A., CHEBIL, G., GUDJONSSON, S., BORG, Å., MANSSON, W., FIORETOS, T. and HÖGLIND, M. (2006) Molecular characterization of early-stage bladder carcinomas by expression profiles, FGFR3 mutation status, and loss of 9q. *Oncogene*, 25(18), pp. 2685-2696.
- LITTLE, J. B. 2003. Genomic instability and bystander effects: a historical perspective. *Oncogene*, 22, 6978.
- LIU, S. K., OLIVE, P. L. & BRISTOW, R. G. 2008. Biomarkers for DNA DSB inhibitors and radiotherapy clinical trials. *Cancer and Metastasis Reviews*, 27, 445-458.
- LÖBRICH, M., RIEF, N., KÜHNE, M., HECKMANN, M., FLECKENSTEIN, J., RÜBE, C. & UDER, M. 2005. In vivo formation and repair of DNA double-strand breaks after computed tomography examinations. *Proceedings of the National Academy of Sciences of the United States of America*, 102, 8984-8989.
- LÖBRICH, M., SHIBATA, A., BEUCHER, A., FISHER, A., ENSMINGER, M., GOODARZI, A. A., BARTON, O. & JEGGO, P. A. 2010.  $\gamma$ H2AX foci analysis for monitoring DNA double-strand break repair: strengths, limitations and optimization. *Cell cycle*, 9, 662-669.
- LOEFFLER, J. S. & DURANTE, M. 2013. Charged particle therapy—optimization, challenges and future directions. *Nature reviews Clinical oncology*, 10, 411.
- LOFT, S. & POULSEN, H. E. 1996. Cancer risk and oxidative DNA damage in man. *Journal Molecular Medicine (Berl)*, 74, 297-312.
- LOMAX, M., FOLKES, L. & O'NEILL, P. 2013. Biological consequences of radiation-induced DNA damage: relevance to radiotherapy. *Clinical oncology*, 25, 578-585.

- LONGHESE, M. P., BONETTI, D., GUERINI, I., MANFRINI, N. & CLERICI, M. 2009. DNA double-strand breaks in meiosis: checking their formation, processing and repair. *DNA repair*, 8, 1127-1138.
- LOPEZ-LÁZARO, M. 2007. Dual role of hydrogen peroxide in cancer: possible relevance to cancer chemoprevention and therapy. *Cancer letters*, 252, 1-8.
- LORAT, Y., SCHANZ, S., SCHULER, N., WENNEMUTH, G., RÜBE, C. & RÜBE, C. E. 2012. Beyond repair foci: DNA double-strand break repair in euchromatic and heterochromatic compartments analyzed by transmission electron microscopy. *PloS one*, 7, e38165.
- LOU, Z., MINTER-DYKHOUSE, K., FRANCO, S., GOSTISSA, M., RIVERA, M. A., CELESTE, A., MANIS, J. P., VAN DEURSEN, J., NUSSENZWEIG, A. & PAULL, T. T. 2006. MDC1 maintains genomic stability by participating in the amplification of ATM-dependent DNA damage signals. *Molecular cell*, 21, 187-200.
- LOVEJOY, C. A. & CORTEZ, D. 2009. Common mechanisms of PIKK regulation. *DNA repair*, 8, 1004-1008.
- LUCH, A. 2005. Nature and nurture - lessons from chemical carcinogenesis. *Nat Rev Cancer*, 5, 113-25.
- MACPHAIL, S.H., BANATH, J.P., YU, Y., CHU, E., OLIVE. 2003. Cell cycle-dependent expression of phosphorylated histone H2AX: reduced expression in un-irradiated but not X-irradiated G1-phase cells. *Radiat Res.*, 159,759–767.
- MADEIRA, P.J.A. and FLORÊNCIO, M.H., 2012. Applications of Tandem Mass Spectrometry: From Structural Analysis to Fundamental Studies. In *Tandem Mass Spectrometry-Applications and Principles*. InTech.
- MADIGAN, J. P., CHOTKOWSKI, H. L. & GLASER, R. L. 2002. DNA double- strand break- induced phosphorylation of Drosophila histone variant H2Av helps prevent radiation- induced apoptosis. *Nucleic acids research*, 30, 3698-3705.
- MAH, L., EL-OSTA, A. & KARAGIANNIS, T. 2010.  $\gamma$ H2AX: a sensitive molecular marker of DNA damage and repair. *Leukemia*, 24, 679.
- MAIER, P., WENZ, F. & HERSKIND, C. 2014. Radioprotection of normal tissue cells. *Strahlentherapie und Onkologie*, 190, 745-752.

- MCKENNA, D.J., RAJAB, N.F., MCKEOWN, S.R., MCKERR, G., MCKEVEY-MARTIN, V.J. 2003. Use of the comet-FISH assay to demonstrate repair of the TP53 gene region in two human bladder carcinoma cell lines. *Radiat Res*, 159, 49–56.
- MCKENNA, D.J., MCKEOWN, S.R., MCKELVEY-MARTIN, V.J. 2008. Potential use of the comet assay in the clinical management of cancer. *Mutagenesis*, 23,183-90
- MALYAPA, R. S., WRIGHT, W. D. & ROTI, J. L. R. 1994. Radiation sensitivity correlates with changes in DNA supercoiling and nucleoid protein content in cells of three Chinese hamster cell lines. *Radiation research*, 140, 312-320.
- MALYAPA, R. S., WRIGHT, W. D. & ROTI, J. L. R. 1996. DNA supercoiling changes and nucleoid protein composition in a group of L5178Y cells of varying radiosensitivity. *Radiation research*, 145, 239-242.
- MALYARCHUK, S., BRAME, K. L., YOUNGBLOOD, R., SHI, R. & HARRISON, L. 2004. Two clustered 8-oxo-7, 8-dihydroguanine (8-oxodG) lesions increase the point mutation frequency of 8-oxodG, but do not result in double strand breaks or deletions in *Escherichia coli*. *Nucleic acids research*, 32, 5721-5731.
- MARKS, P.A., RICHON, V.M. & RIFKIND RA. (2000). Histone deacetylase inhibitors: inducers of differentiation or apoptosis of transformed cells. *Journal Natl Cancer Institution* **92**: 1210–1216.
- MARTIN, N. T., NAHAS, S. A., TUNUGUNTLA, R., FIKE, F. & GATTI, R. A. 2011. Assessing ‘radiosensitivity ’with kinetic profiles of  $\gamma$ -H2AX, 53BP1 and BRCA1 foci. *Radiotherapy and oncology*, 101, 35-38.
- MASHIMA, R., WITTING, P. K. & STOCKER, R. 2001. Oxidants and antioxidants in atherosclerosis. *Current opinion in lipidology*, 12, 411-418.
- MATHEW, M. K., SMITH, C. L. & CANTOR, C. R. 1988. High-resolution separation and accurate size determination in pulsed-field gel electrophoresis of DNA. 1. DNA size standards and the effect of agarose and temperature. *Biochemistry*, 27, 9204-10.
- MATUSZEWSKI, B., CONSTANZER, M. & CHAVEZ-ENG, C. 2003. Strategies for the assessment of matrix effect in quantitative bioanalytical methods based on HPLC–MS/MS. *Analytical chemistry*, 75, 3019-3030.
- MAULE, J. 1998. Pulsed-field gel electrophoresis. *Molecular Biotechnology*, 9, 107-26.

- MCKEOWN, S. R., ROBSON, T., PRICE, M. E., HO, E. T., HIRST, D. G. & MCKELVEY-MARTIN, V. J. 2003. Potential use of the alkaline comet assay as a predictor of bladder tumour response to radiation. *Br Journal cancer*, 89, 2264-70.
- MCKINNON, P. J. & CALDECOTT, K. W. 2007. DNA strand break repair and human genetic disease. *Annu. Rev. Genomics Hum. Genet.*, 8, 37-55.
- MCMILLAN, T. J., TOBI, S., MATEOS, S. & LEMON, C. 2001. The use of DNA double-strand break quantification in radiotherapy. *International Journal of Radiation Oncology• Biology• Physics*, 49, 373-377.
- MENEGAKIS, A., EICHELER, W., YAROMINA, A., THAMES, H. D., KRAUSE, M. & BAUMANN, M. 2011. Residual DNA double strand breaks in perfused but not in unperfused areas determine different radiosensitivity of tumours. *Radiotherapy and Oncology*, 100, 137-144.
- MEZHEVAYA, E.V., STEPAOVA, V.P., YAROVOY, B.F., BERITASHVILI, D.R. and ZAKHAROV, I.A., 1990. Pulsed field gradient electrophoresis study of pYF91 plasmid integration into yeast chromosomes. *Biopolymers and Cell*, 6(3), pp.90-94.
- MISTELI, T. & SPECTOR, D. L. 1998. The cellular organization of gene expression. *Current opinion in cell biology*, 10, 323-331.
- MODING, E. J., KASTAN, M. B. & KIRSCH, D. G. 2013. Strategies for optimizing the response of cancer and normal tissues to radiation. *Nature reviews Drug discovery*, 12, 526.
- MØLLER, P., MÖLLER, L., GODSCHALK, R. W. & JONES, G. D. 2010. Assessment and reduction of comet assay variation in relation to DNA damage: studies from the European Comet Assay Validation Group. *Mutagenesis*, 25, 109-111.
- MONEEF, M., SHERWOOD, B., BOWMAN, K. J., KOCKELBERGH, R., SYMONDS, R., STEWARD, W., MELLON, J. & JONES, G. 2003. Measurements using the alkaline comet assay predict bladder cancer cell radiosensitivity. *British journal of cancer*, 89, 2271.
- MOQUET, J., BARNARD, S. & ROTHKAMM, K. 2014. Gamma-H2AX biodosimetry for use in large scale radiation incidents: comparison of a rapid '96 well lyse/fix' protocol with a routine method. *PeerJ*, 2, e282.

- MORONI, M., MAEDA, D., WHITNALL, M. H., BONNER, W. M. & REDON, C. E. 2013. Evaluation of the gamma-H2AX assay for radiation biodosimetry in a swine model. *International journal of molecular sciences*, 14, 14119-14135.
- MOSTAFA, M. H., SHEWEITA, S. and O'CONNOR, P. J. (1999) Relationship between schistosomiasis and bladder cancer. *Clinical Microbiology Reviews*, 12(1), pp. 97-111.
- MUNSHI A, KURLAND JF, NISHIKAWA T, TANAKA T, HOBBS ML, TUCKER SL *et al.* (2005). Histone deacetylase inhibitors radiosensitize human melanoma cells by suppressing DNA repair activity. *Clinical cancer research* **11**: 4912–4922.
- MUNSHI A, TANAKA T, HOBBS ML, TUCKER SL, RICHON, V.M., and MEYN, R.E. 2006. Vorinostat, a histone deacetylase inhibitor, enhances the response of human tumor cells to ionizing radiation through prolongation of gamma-H2AX foci. *Molecular Cancer Ther* 5:1967-1974
- MUSLIMOVIC, A., JOHANSSON, P. & HAMMARSTEN, O. 2012. Measurement of H2AX phosphorylation as a marker of ionizing radiation induced cell damage. *Current topics in ionizing radiation research*. InTech.
- MYUNG, N.-H., ZHU, X., KRUMAN, I. I., CASTELLANI, R. J., PETERSEN, R. B., SIEDLAK, S. L., PERRY, G., SMITH, M. A. & LEE, H.-G. 2008. Evidence of DNA damage in Alzheimer disease: phosphorylation of histone H2AX in astrocytes. *Age*, 30, 209-215.
- NAEGELI, H. & SUGASAWA, K. 2011. The xeroderma pigmentosum pathway: decision tree analysis of DNA quality. *DNA repair*, 10, 673-683.
- NAKAMURA, A., SEDELNIKOVA, O. A., REDON, C., PILCH, D. R., SINOGEVA, N. I., SHROFF, R., LICHTEN, M. & BONNER, W. M. 2006. Techniques for gamma-H2AX detection. *Methods in enzymology*, 409, 236-250.
- NASSONOVA, E. 2008. Pulsed field gel electrophoresis: Theory, instruments and application. *Cell and Tissue Biology*, 2, 557.
- NEGRINI, S. GORGOULIS, VG. HALAZONETIS, TD.2010. Genomic instability—an evolving hallmark of cancer. *Nat Rev Mol Cell Biol*, 11,220–8.
- NEUMAIER, T., SWENSON, J., PHAM, C., POLYZOS, A., LO, A. T., YANG, P., DYBALL, J., ASAITHAMBY, A., CHEN, D. J. & BISSELL, M. J. 2012. Evidence

- for formation of DNA repair centers and dose-response nonlinearity in human cells. *Proceedings of the National Academy of Sciences*, 109, 443-448.
- NIKITAKI, Z., HELLWEG, C. E., GEORGAKILAS, A. G. & RAVANAT, J.-L. 2015. Stress-induced DNA damage biomarkers: applications and limitations. *Frontiers in chemistry*, 3, 35.
- NIKJOO, H., O'NEILL, P., WILSON, W. & GOODHEAD, D. 2001. Computational approach for determining the spectrum of DNA damage induced by ionizing radiation. *Radiation research*, 156, 577-583.
- NIKJOO S. UEHARA WE WILSON M. HOSHI DT GOODHEAD, H. 1998. Track structure in radiation biology: theory and applications. *International journal of radiation biology*, 73, 355-364.
- NSOFOR, C. A. 2016. Pulsed-Field Gel Electrophoresis (PFGE): Principles and Applications in Molecular Epidemiology: A Review. *Int. J. Curr. Res. Med. Sci*, 2, 38-51.
- OLIVE, P. 1999. DNA damage and repair in individual cells: applications of the comet assay in radiobiology. *International journal of radiation biology*, 75, 395-405.
- OLIVE, P. L. 1998. The role of DNA single-and double-strand breaks in cell killing by ionizing radiation. *Radiation research*, 150, S42-S51.
- OLIVE, P. L. 2004. Detection of DNA damage in individual cells by analysis of histone H2AX phosphorylation. *Methods in cell biology*. Elsevier.
- OLIVE, P. L., BANÁTH, J. P. & DURAND, R. E. 1990. Heterogeneity in radiation-induced DNA damage and repair in tumor and normal cells measured using the "comet" assay. *Radiation research*, 122, 86-94.
- ORBACH, M. J., VOLLRATH, D., DAVIS, R. W. & YANOFSKY, C. 1988. An electrophoretic karyotype of *Neurospora crassa*. *Mol Cell Biol*, 8, 1469-73.
- OSTLING, O. & JOHANSON, K.J. (1984) Microelectrophoretic Study of Radiation-Induced DNA Damages in Individual Mammalian Cells. *Biochemical and Biophysical Research Communications*, 123, 291-298.
- PARIS, L., CORDELLI, E., ELEUTERI, P., GROLLINO, M. G., PASQUALI, E., RANALDI, R., MESCHINI, R. & PACCHIEROTTI, F. 2011. Kinetics of  $\gamma$ -H2AX



- induction and removal in bone marrow and testicular cells of mice after X-ray irradiation. *Mutagenesis*, 26, 563-572.
- PANG, K. H. and CATTO, J. W. 2013. Bladder cancer. *Surgery (Oxford)*, 31(10), pp. 523-529.
- PAULL, T. T., ROGAKOU, E. P., YAMAZAKI, V., KIRCHGESSNER, C. U., GELLERT, M. & BONNER, W. M. 2000. A critical role for histone H2AX in recruitment of repair factors to nuclear foci after DNA damage. *Current Biology*, 10, 886-895.
- PERERA, F. P., HEMMINKI, K., GRYZBOWSKA, E., MOTYKIEWICZ, G., MICHALSKA, J., SANTELLA, R. M., YOUNG, T. L., DICKEY, C., BRANDT-RAUF, P., DE VIVO, I. & ET AL. 1992. Molecular and genetic damage in humans from environmental pollution in Poland. *Nature*, 360, 256-8.
- PERNOT, E., HALL, J., BAATOUT, S., BENOTMANE, M. A., BLANCHARDON, E., BOUFFLER, S., EL SAGHIRE, H., GOMOLKA, M., GUERTLER, A. & HARMS-RINGDAHL, M. 2012a. Ionizing radiation biomarkers for potential use in epidemiological studies. *Mutation Research/Reviews in Mutation Research*, 751, 258-286.
- PERNOT, E., HALL, J., BAATOUT, S., BENOTMANE, M. A., BLANCHARDON, E., BOUFFLER, S., EL SAGHIRE, H., GOMOLKA, M., GUERTLER, A., HARMS-RINGDAHL, M., JEGGO, P., KREUZER, M., LAURIER, D., LINDHOLM, C., MKACHER, R., QUINTENS, R., ROTHKAMM, K., SABATIER, L., TAPIO, S., DE VATHAIRE, F. & CARDIS, E. 2012b. Ionizing radiation biomarkers for potential use in epidemiological studies. *Mutat Res*, 751, 258-86.
- PHILLIPS, D. H. 2002. Smoking-related DNA and protein adducts in human tissues. *Carcinogenesis*, 23, 1979-2004.
- PIENTA, K., GETZENBERG, R. & COFFEY, D. 1991. Cell structure and DNA organization. *Critical reviews in eukaryotic gene expression*, 1, 355-385.
- PIENTA, K. J. & COFFEY, D. S. 1984. A structural analysis of the role of the nuclear matrix and DNA loops in the organization of the nucleus and chromosome. *J Cell Sci*, 1984, 123-135.

- PIENTA, K. J. & COFFEY, D. S. 1992. Nuclear- Cytoskeletal interactions: Evidence for physical connections between the nucleus and cell periphery and their alteration by transformation. *Journal of cellular biochemistry*, 49, 357-365.
- PITT, J. J. 2009a. Principles and applications of liquid chromatography-mass spectrometry in clinical biochemistry. *Clin Biochem Rev*, 30, 19-34.
- PITT, J. J. 2009b. Principles and Applications of Liquid Chromatography-Mass Spectrometry in Clinical Biochemistry. *The Clinical Biochemist Reviews*, 30, 19-34.
- PLO, I., LIAO, Z.-Y., BARCELÓ, J. M., KOHLHAGEN, G., CALDECOTT, K. W., WEINFELD, M. & POMMIER, Y. 2003. Association of XRCC1 and tyrosyl DNA phosphodiesterase (Tdp1) for the repair of topoisomerase I-mediated DNA lesions. *DNA repair*, 2, 1087-1100.
- POLO, S. E. & JACKSON, S. P. 2011. Dynamics of DNA damage response proteins at DNA breaks: a focus on protein modifications. *Genes & development*, 25, 409-433.
- POULILIOU, S. & KOUKOURAKIS, M. I. 2014. Gamma histone 2AX ( $\gamma$ -H2AX) as a predictive tool in radiation oncology. *Biomarkers*, 19, 167-180.
- PRICE, B. D. & D'ANDREA, A. D. 2013. Chromatin remodeling at DNA double-strand breaks. *Cell*, 152, 1344-1354.
- PRISE, K. 1998. A review of dsb induction data for varying quality radiations. *International journal of radiation biology*, 74, 173-184.
- PRISE, K. M. 2006. New advances in radiation biology. *Occupational Medicine*, 56, 156-161.
- PURKAYASTHA, S., MILLIGAN, J. R. & BERNHARD, W. A. 2007. On the chemical yield of base lesions, strand breaks, and clustered damage generated in plasmid DNA by the direct effect of X rays. *Radiation research*, 168, 357-366.
- RAJSKI, S. R. & WILLIAMS, R. M. 1998. DNA Cross-Linking Agents as Antitumor Drugs. *Chem Rev*, 98, 2723-2796.
- R. BOREHAM, D., DOLLING, J., R. MAVES, S., SIWARUNGSUN, N. & EJ MITCHEL, R. 2000. Dose-rate effects for apoptosis and micronucleus formation in gamma-irradiated human lymphocytes. *Radiation research*, 153, 579-586.
- RAVANAT, J.-L. 2012. Chromatographic methods for the analysis of oxidatively damaged DNA. *Free radical research*, 46, 479-491.

- RAVANAT, J. L., DOUKI, T., DUEZ, P., GREMAUD, E., HERBERT, K., HOFER, T., LASSERRE, L., SAINT-PIERRE, C., FAVIER, A. & CADET, J. 2002. Cellular background level of 8-oxo-7,8-dihydro-2'-deoxyguanosine: an isotope based method to evaluate artefactual oxidation of DNA during its extraction and subsequent work-up. *Carcinogenesis*, 23, 1911-8.
- RAY, K., HUDAK, K., CITRIN, D. & STICK, M. 2014. Biomarkers of radiation injury and response. *Biomarkers in Toxicology*. Elsevier.
- RAZIN, S. V. 1999. Chromosomal DNA loops may constitute basic units of the eukaryotic genome organization and evolution. *Critical Reviews<sup>TM</sup> in Eukaryotic Gene Expression*, 9.
- REBOIS, R. V. & RAY, K. 2012. Ionizing radiation and radioactive materials in health and disease. *Veterinary Toxicology (Second Edition)*. Elsevier.
- REDON, C., PILCH, D., ROGAKOU, E., SEDELNIKOVA, O., NEWROCK, K. & BONNER, W. 2002. Histone H2a variants H2AX and H2AZ. *Current opinion in genetics & development*, 12, 162-169.
- REDON, C. E., NAKAMURA, A. J., SORDET, O., DICKEY, J. S., GOULIAEVA, K., TABB, B., LAWRENCE, S., KINDERS, R. J., BONNER, W. M. & SEDELNIKOVA, O. A. 2011.  $\gamma$ -H2AX detection in peripheral blood lymphocytes, splenocytes, bone marrow, xenografts, and skin. *DNA Damage Detection In Situ, Ex Vivo, and In Vivo*. Springer.
- REDON, C. E., WEYEMI, U., PAREKH, P. R., HUANG, D., BURRELL, A. S. & BONNER, W. M. 2012.  $\gamma$ -H2AX and other histone post-translational modifications in the clinic. *Biochimica et Biophysica Acta (BBA)-Gene Regulatory Mechanisms*, 1819, 743-756.
- RENE, N., CURY, F. and SOUTAMI, L. (2009) Conservative treatment of invasive bladder cancer. *Current Oncology*, 16(4), pp. 36.
- REVET, I., FEENEY, L., BRUGUERA, S., WILSON, W., DONG, T. K., OH, D. H., DANKORT, D. & CLEAVER, J. E. 2011. Functional relevance of the histone  $\gamma$ H2Ax in the response to DNA damaging agents. *Proceedings of the National Academy of Sciences*, 108, 8663-8667.

- RIBALLO, E., KÜHNE, M., RIEF, N., DOHERTY, A., SMITH, G. C., RECIO, M. A.-J., REIS, C., DAHM, K., FRICKE, A. & KREMPLER, A. 2004. A pathway of double-strand break re-joining dependent upon ATM, Artemis, and proteins locating to  $\gamma$ -H2AX foci. *Molecular cell*, 16, 715-724.
- RIBOT, E. M., FAIR, M., GAUTOM, R., CAMERON, D., HUNTER, S., SWAMINATHAN, B. & BARRETT, T. J. 2006. Standardization of pulsed-field gel electrophoresis protocols for the subtyping of Escherichia coli O157: H7, Salmonella, and Shigella for PulseNet. *Foodborne Pathogens & Disease*, 3, 59-67.
- RICH, T., ALLEN, R. L. & WYLLIE, A. H. 2000. Defying death after DNA damage. *Nature*, 407, 777.
- ROBOZ, J. 2002. *Mass spectrometry in cancer research*, CRC Press.
- ROCH-LEFÈVRE, S., MANDINA, T., VOISIN, P., GAËTAN, G., MESA, J. E. G., VALENTE, M., BONNESOEUR, P., GARCÍA, O., VOISIN, P. & ROY, L. 2010. Quantification of  $\gamma$ -H2AX foci in human lymphocytes: a method for biological dosimetry after ionizing radiation exposure. *Radiation research*, 174, 185-194.
- ROGAKOU, E. P., BOON, C., REDON, C. & BONNER, W. M. 1999. Megabase chromatin domains involved in DNA double-strand breaks in vivo. *The Journal of cell biology*, 146, 905-916.
- ROGAKOU, E. P., PILCH, D. R., ORR, A. H., IVANOVA, V. S. & BONNER, W. M. 1998. DNA double-stranded breaks induce histone H2AX phosphorylation on serine 139. *Journal of biological chemistry*, 273, 5858-5868.
- ROJAS, E., LOPEZ, M. & VALVERDE, M. 1999. Single cell gel electrophoresis assay: methodology and applications. *Journal of Chromatography B: Biomedical Sciences and Applications*, 722, 225-254.
- ROOS, W. P., THOMAS, A. D. & KAINA, B. 2016. DNA damage and the balance between survival and death in cancer biology. *Nature Reviews Cancer*, 16, 20.
- ROTHKAMM, K., BARNARD, S., MOQUET, J., ELLENDER, M., RANA, Z. & BURDAK- ROTHKAMM, S. 2015. DNA damage foci: Meaning and significance. *Environmental and molecular mutagenesis*, 56, 491-504.
- ROTHKAMM, K. & HORN, S. 2009. gamma-H2AX as protein biomarker for radiation exposure. *Ann Ist Super Sanita*, 45, 265-271.

- ROTHKAMM, K., KRÜGER, I., THOMPSON, L. H. & LÖBRICH, M. 2003. Pathways of DNA double-strand break repair during the mammalian cell cycle. *Molecular and cellular biology*, 23, 5706-5715.
- ROTHKAMM, K. & LÖBRICH, M. 2003. Evidence for a lack of DNA double-strand break repair in human cells exposed to very low x-ray doses. *Proceedings of the National Academy of Sciences*, 100, 5057-5062.
- SAENGER, W. 1984. Dna structure. *Principles of Nucleic Acid Structure*. Springer.
- SAGE, E. & SHIKAZONO, N. 2017. Radiation-induced clustered DNA lesions: Repair and mutagenesis. *Free Radical Biology and Medicine*, 107, 125-135.
- SAHA, G. B. 2012. *Physics and radiobiology of nuclear medicine*, Springer Science & Business Media.
- SANCAR, A., LINDSEY-BOLTZ, L. A., ÜNSAL-KAÇMAZ, K. & LINN, S. 2004. Molecular mechanisms of mammalian DNA repair and the DNA damage checkpoints. *Annual review of biochemistry*, 73, 39-85.
- SAVIC, V., YIN, B., MAAS, N. L., BREDEMEYER, A. L., CARPENTER, A. C., HELMINK, B. A., YANG-IOTT, K. S., SLECKMAN, B. P. & BASSING, C. H. 2009. Formation of dynamic gamma-H2AX domains along broken DNA strands is distinctly regulated by ATM and MDC1 and dependent upon H2AX densities in chromatin. *Mol Cell*, 34, 298-310.
- SCHÄRER, O. D. 2005. DNA Interstrand Crosslinks: Natural and Drug- Induced DNA Adducts that Induce Unique Cellular Responses. *ChemBioChem*, 6, 27-32.
- SCHIPLER, A. & ILIAKIS, G. 2013. DNA double-strand-break complexity levels and their possible contributions to the probability for error-prone processing and repair pathway choice. *Nucleic acids research*, 41, 7589-7605.
- SCHOKET, B. 1999. DNA damage in humans exposed to environmental and dietary polycyclic aromatic hydrocarbons. *Mutat Res*, 424, 143-53.
- SCULLY, R. & XIE, A. 2013. Double strand break repair functions of histone H2AX. *Mutation Research/Fundamental and Molecular Mechanisms of Mutagenesis*, 750, 5-14.
- SEDELNIKOVA, O. A., REDON, C. E., DICKEY, J. S., NAKAMURA, A. J., GEORGAKILAS, A. G. & BONNER, W. M. 2010. Role of oxidatively induced

- DNA lesions in human pathogenesis. *Mutation Research/Reviews in Mutation Research*, 704, 152-159.
- SEDELNIKOVA, O. A., ROGAKOU, E. P., PANYUTIN, I. G. & BONNER, W. M. 2002. Quantitative detection of 125IdU-induced DNA double-strand breaks with  $\gamma$ -H2AX antibody. *Radiation research*, 158, 486-492.
- SEIWERT, T. Y., SALAMA, J. K. & VOKES, E. E. 2007. The chemoradiation paradigm in head and neck cancer. *Nature Reviews Clinical Oncology*, 4, 156.
- SEMENENKO, V. & STEWART, R. 2004. A fast Monte Carlo algorithm to simulate the spectrum of DNA damages formed by ionizing radiation. *Radiation research*, 161, 451-457.
- SHARIAT, S. F., SFAKIANOS, J. P., DROLLER, M. J., KARAKIEWICZ, P. I., MERYN, S. and BOCHNER, B. H. (2010) The effect of age and gender on bladder cancer: a critical review of the literature. *BJU international*, 105(3), pp. 300-308.
- SHARPLESS, N. E. & DEPINHO, R. A. 2007. How stem cells age and why this makes us grow old. *Nature reviews Molecular cell biology*, 8, 703.
- SHIMIZU, I., YOSHIDA, Y., SUDA, M. & MINAMINO, T. 2014. DNA damage response and metabolic disease. *Cell metabolism*, 20, 967-977.
- SHRIVASTAV, M., DE HARO, L. P. & NICKOLOFF, J. A. 2008. Regulation of DNA double-strand break repair pathway choice. *Cell research*, 18, 134.
- SIDDIQUI, M. S., FRANÇOIS, M., FENECH, M. F. & LEIFERT, W. R. 2015. Persistent  $\gamma$ H2AX: a promising molecular marker of DNA damage and aging. *Mutation Research/Reviews in Mutation Research*, 766, 1-19.
- SMITH, A.J.O., ALMEIDA, G.M., THOMAS, A.L., JONES, G.D. Comet assay measures of irinotecan-induced DNA damage in vitro and in vivo. Proceedings of the Genome Stability network/United Kingdom Environmental Mutagen Society Joint Congress University of Cardiff, 1 – 4 July 2007.
- SINGER, B. & GRUNBERGER, D. 2012. *Molecular biology of mutagens and carcinogens*, Springer Science & Business Media.
- SINGH, N. P. 1996. Microgel electrophoresis of DNA from individual cells. *Technologies for detection of DNA damage and mutations*. Springer.

- SINGH, N. P., MCCOY, M. T., TICE, R. R. & SCHNEIDER, E. L. 1988. A simple technique for quantitation of low levels of DNA damage in individual cells. *Experimental cell research*, 175, 184-191.
- SINGH, R. & FARMER, P. B. 2006. Liquid chromatography-electrospray ionization-mass spectrometry: the future of DNA adduct detection. *Carcinogenesis*, 27, 178-96.
- SINGH, R., TEICHERT, F., VERSCHOYLE, R. D., KAUR, B., VIVES, M., SHARMA, R. A., STEWARD, W. P., GESCHER, A. J. & FARMER, P. B. 2009. Simultaneous determination of 8- oxo- 2'- deoxyguanosine and 8- oxo- 2'- deoxyadenosine in DNA using online column- switching liquid chromatography/tandem mass spectrometry. *Rapid Communications in Mass Spectrometry*, 23, 151-160.
- SJAKSTE, N., SJAKSTE, T. & VIKMANIS, U. 2004. Role of the nuclear matrix proteins in malignant transformation and cancer diagnosis. *Exp Oncol*, 26, 170-178.
- SMITH, C., COOTE, J. & PARTON, R. 1986. R-plasmid-mediated chromosome mobilization in *Bordetella pertussis*. *Microbiology*, 132, 2685-2692.
- SMITH, L. E., DENISSENKO, M. F., BENNETT, W. P., LI, H., AMIN, S., TANG, M. & PFEIFER, G. P. 2000. Targeting of lung cancer mutational hotspots by polycyclic aromatic hydrocarbons. *J Natl Cancer Inst*, 92, 803-11.
- SMITH, N., KLCO, S. & CANTOR, C. R. 1988. Pulsed-Field Gel Electrophoresis and Methods of Work with Large DNA Molecules. Oxford: IRL Press.
- SØRENSEN, B. S., OVERGAARD, J. & BASSLER, N. 2011. In vitro RBE-LET dependence for multiple particle types. *Acta Oncologica*, 50, 757-762.
- SOLOWAY, M. S. (2013) Bladder cancer: Lack of progress in bladder cancer—what are the obstacles? *Nature Reviews Urology*, 10(1), pp. 5-6.
- SOURISSEAU, T., MANIOTIS, D., MCCARTHY, A., TANG, C., LORD, C. J., ASHWORTH, A. & LINARDOPOULOS, S. 2010. Aurora- A expressing tumour cells are deficient for homology- directed DNA double strand- break repair and sensitive to PARP inhibition. *EMBO molecular medicine*, 2, 130-142.
- SPEIT, G. & HARTMANN, A. 2006. The comet assay. *DNA Repair Protocols*. Springer.
- SRIVASTAVA, N., GOCHHAIT, S., DE BOER, P. & BAMEZAI, R. N. 2009. Role of H2AX in DNA damage response and human cancers. *Mutation Research/Reviews in Mutation Research*, 681, 180-188.

- STENZL, A., COWAN, N. C., DE SANTIS, M., KUCZYK, M. A., MERSEBURGER, A. S., RIBAL, M. J., SHERIF, A. and WITJES, J. A. (2011) Treatment of muscle-invasive and metastatic bladder cancer: update of the EAU guidelines. *European urology*, 59(6), pp. 1009-1018.
- STIFF, T., O'DRISCOLL, M., RIEF, N., IWABUCHI, K., LÖBRICH, M. & JEGGO, P. A. 2004. ATM and DNA-PK function redundantly to phosphorylate H2AX after exposure to ionizing radiation. *Cancer research*, 64, 2390-2396.
- STROBER, W. 2001. Trypan blue exclusion test of cell viability. *Curr Protoc Immunol*, Appendix 3, Appendix 3B.
- STROBER, W. 2015. Trypan Blue Exclusion Test of Cell Viability. *Curr Protoc Immunol*, 111, A3 B 1-3.
- STRUELENS, M. J., DE RYCK, R. & DEPLANO, A. 2001. Analysis of microbial genomic macrorestriction patterns by pulsed-field gel electrophoresis (PFGE) typing. *New approaches for the generation and analysis of microbial typing data*. Elsevier.
- SUTHERLAND, B. M., BENNETT, P. V., SIDORKINA, O. & LAVAL, J. 2000. Clustered DNA damages induced in isolated DNA and in human cells by low doses of ionizing radiation. *Proceedings of the National Academy of Sciences*, 97, 103-108.
- SUTHERLAND, B. M., BENNETT, P. V., SUTHERLAND, J. C. & LAVAL, J. 2002. Clustered DNA damages induced by x rays in human cells. *Radiation research*, 157, 611-616.
- SUZUKI, K., OJIMA, M., KODAMA, S. & WATANABE, M. 2003. Radiation-induced DNA damage and delayed induced genomic instability. *Oncogene*, 22, 6988.
- SVETLOVA, M., SOLOVJEVA, L. & TOMILIN, N. 2010. Mechanism of elimination of phosphorylated histone H2AX from chromatin after repair of DNA double-strand breaks. *Mutation Research/Fundamental and Molecular Mechanisms of Mutagenesis*, 685, 54-60.
- SWENBERG, J. A., FRYAR-TITA, E., JEONG, Y. C., BOYSEN, G., STARR, T., WALKER, V. E. & ALBERTINI, R. J. 2008. Biomarkers in toxicology and risk assessment: informing critical dose-response relationships. *Chem Res Toxicol*, 21, 253-65.



- TAKAHA, N., HAWKINS, A. L., GRIFFIN, C. A., ISAACS, W. B. & COFFEY, D. S. 2002. High mobility group protein I (Y): a candidate architectural protein for chromosomal rearrangements in prostate cancer cells. *Cancer research*, 62, 647-651.
- TAN, X., GROLLMAN, A. P. & SHIBUTANI, S. 1999. Comparison of the mutagenic properties of 8-oxo-7,8-dihydro-2'-deoxyadenosine and 8-oxo-7,8-dihydro-2'-deoxyguanosine DNA lesions in mammalian cells. *Carcinogenesis*, 20, 2287-92.
- THARIAT, J., HANNOUN-LEVI, J.-M., MYINT, A. S., VUONG, T. & GÉRARD, J.-P. 2013. Past, present, and future of radiotherapy for the benefit of patients. *Nature reviews Clinical oncology*, 10, 52.
- THIER, R. & BOLT, H. M. 2001. European aspects of standard setting in occupational hygiene and medicine. *Rev Environ Health*, 16, 81-6.
- TICE, R. R., AGURELL, E., ANDERSON, D., BURLINSON, B., HARTMANN, A., KOBAYASHI, H., MIYAMAE, Y., ROJAS, E., RYU, J. C. & SASAKI, Y. 2000. Single cell gel/comet assay: guidelines for in vitro and in vivo genetic toxicology testing. *Environmental and molecular mutagenesis*, 35, 206-221.
- TORNALETTI, S. 2009. DNA repair in mammalian cells. *Cellular and Molecular Life Sciences*, 66, 1010-1020.
- TORUDD, J., PROTOPOPOVA, M., SARIMOV, R., NYGREN, J., ERIKSSON, S., MARKOVA, E., CHOVANEC, M., SELIVANOVA, G. & BELYAEV, I. 2005. Dose-response for radiation-induced apoptosis, residual 53BP1 foci and DNA-loop relaxation in human lymphocytes. *International journal of radiation biology*, 81, 125-138.
- TOWNSEND, K. M. & DAWKINS, H. J. 1993. Field alternation gel electrophoresis--status quo. *J Chromatogr*, 618, 223-49.
- TRACHOOTHAM, D., ALEXANDRE, J. & HUANG, P. 2009. Targeting cancer cells by ROS-mediated mechanisms: a radical therapeutic approach? *Nature reviews Drug discovery*, 8, 579.
- TRETYAKOVA, N., GOGGIN, M., SANGARAJU, D. & JANIS, G. 2012. Quantitation of DNA adducts by stable isotope dilution mass spectrometry. *Chem Res Toxicol*, 25, 2007-35.
- TRETYAKOVA, N., VILLALTA, P. W. & KOTAPATI, S. 2013. Mass spectromet

- ry of structurally modified DNA. *Chem Rev*, 113, 2395-436.
- TURNER, H. C., BRENNER, D. J., CHEN, Y., BERTUCCI, A., ZHANG, J., WANG, H., LYULKO, O. V., XU, Y., SHURYAK, I. & SCHAEFER, J. 2010. Adapting the  $\gamma$ -H2AX assay for automated processing in human lymphocytes. 1. Technological aspects. *Radiation research*, 175, 282-290.
- URYGA, A., GRAY, K. & BENNETT, M. 2016. DNA damage and repair in vascular disease. *Annual review of physiology*, 78, 45-66.
- USHIO-FUKAI, M. & NAKAMURA, Y. 2008. Reactive oxygen species and angiogenesis: NADPH oxidase as target for cancer therapy. *Cancer Lett*, 266, 37-52.
- VADHAVKAR, N., PHAM, C., GEORGESCU, W., DESCHAMPS, T., HEUSKIN, A.-C., TANG, J. & COSTES, S. V. 2014. Combinatorial DNA damage pairing model based on X-ray-induced foci predicts the dose and LET dependence of cell death in human breast cells. *Radiation research*, 182, 273-281.
- VALDIGLESIAS, V., GIUNTA, S., FENECH, M., NERI, M. & BONASSI, S. 2013.  $\gamma$ H2AX as a marker of DNA double strand breaks and genomic instability in human population studies. *Mutation Research/Reviews in Mutation Research*, 753, 24-40.
- VALENTE, M. 2011. *Signalling detection of DNA damage induced by low doses of ionizing radiation in human lymphocytes*. Versailles-St Quentin en Yvelines.
- VALENTIN, J. 2006. *Low-dose extrapolation of radiation-related cancer risk*, Elsevier London.
- VILHAR, B. 2004. Help! There is a comet in my computer!  
[http://botanika.biologija.org/exp/comet/comet\\_guide01.pdf](http://botanika.biologija.org/exp/comet/comet_guide01.pdf)
- VALKO, M., RHODES, C. J., MONCOL, J., IZAKOVIC, M. & MAZUR, M. 2006. Free radicals, metals and antioxidants in oxidative stress-induced cancer. *Chem Biol Interact*, 160, 1-40.
- VALKO, M., MORRIS, H. & CRONIN, M. 2005. Metals, toxicity and oxidative stress. *Current medicinal chemistry*, 12, 1161-1208.
- VERELLEN, D., DE RIDDER, M., LINTHOUT, N., TOURNEL, K., SOETE, G. & STORME, G. 2007. Innovations in image-guided radiotherapy. *Nature Reviews Cancer*, 7, 949.

- VIGNARD, J., MIREY, G. & SALLES, B. 2013a. Ionizing-radiation induced DNA double-strand breaks: a direct and indirect lighting up. *Radiotherapy and Oncology*, 108, 362-369.
- VIGNARD, J., MIREY, G. & SALLES, B. 2013b. Ionizing-radiation induced DNA double-strand breaks: a direct and indirect lighting up. *Radiother Oncol*, 108, 362-9.
- VILENCHIK, M. M. & KNUDSON, A. G. 2003. Endogenous DNA double-strand breaks: production, fidelity of repair, and induction of cancer. *Proceedings of the National Academy of Sciences*, 100, 12871-12876.
- VILLALTA, P. W. & BALBO, S. 2017. The Future of DNA Adductomic Analysis. *International Journal of Molecular Sciences*, 18, 1870.
- VISCONTI, R. & GRIECO, D. 2009. New insights on oxidative stress in cancer. *Curr Opin Drug Discov Devel*, 12, 240-5.
- VOGELSTEIN, B., PARDOLL, D. M. & COFFEY, D. S. 1980. Supercoiled loops and eucaryotic DNA replication. *Cell*, 22, 79-85.
- VOGELSTEIN, B., PAPADOPOULOS, N., VELCULESCU, V. E., ZHOU, S., DIAZ, L. A. & KINZLER, K. W. 2013. Cancer genome landscapes. *science*, 339, 1546-1558.
- WANG, D., KREUTZER, D. A. & ESSIGMANN, J. M. 1998. Mutagenicity and repair of oxidative DNA damage: insights from studies using defined lesions. *Mutation Research/Fundamental and Molecular Mechanisms of Mutagenesis*, 400, 99-115.
- WARD, I. & CHEN, J. 2004. Early events in the DNA damage response.
- WARD, J. 1994. The complexity of DNA damage: relevance to biological consequences. *International journal of radiation biology*, 66, 427-432.
- WARD, J. F. 1981. Some biochemical consequences of the spatial distribution of ionizing radiation-produced free radicals. *Radiation research*, 86, 185-195.
- WARD, J. F. 1988. DNA damage produced by ionizing radiation in mammalian cells: identities, mechanisms of formation, and reparability. *Progress in nucleic acid research and molecular biology*. Elsevier.
- WARDMAN, P. 2009. The importance of radiation chemistry to radiation and free radical biology (The 2008 Silvanus Thompson Memorial Lecture). *The British journal of radiology*, 82, 89-104.

- WATSON, D. G., ATSRIKU, C. & OLIVEIRA, E. J. 2003. Review role of liquid chromatography–mass spectrometry in the analysis of oxidation products and antioxidants in biological systems. *Analytica Chimica Acta*, 492, 17-47.
- WATSON, J. D. & CRICK, F. H. 1953. Molecular structure of nucleic acids. *Nature*, 171, 737-738.
- WEINBERG, R. A. 2011. Hunting the elusive oncogene: a stroke of good luck. *Nat Cell Biol*, 13, 876.
- WIENCKE, J. K. 2002. DNA adduct burden and tobacco carcinogenesis. *Oncogene*, 21, 7376-91.
- WILLITZKI, A., LORENZ, S., HIEMANN, R., GUTTEK, K., GOIHL, A., HARTIG, R., CONRAD, K., FEIST, E., SACK, U. & SCHIERACK, P. 2013. Fully automated analysis of chemically induced  $\gamma$ H2AX foci in human peripheral blood mononuclear cells by indirect immunofluorescence. *Cytometry Part A*, 83, 1017-1026.
- WOGAN, G. N., HECHT, S. S., FELTON, J. S., CONNEY, A. H. & LOEB, L. A. 2004. Environmental and chemical carcinogenesis. *Semin Cancer Biol*, 14, 473-86.
- WOOD, R. D., MITCHELL, M., SGOUROS, J. & LINDAHL, T. 2001. Human DNA repair genes. *Science*, 291, 1284-1289.
- YANG, M. (2011) A current global view of environmental and occupational cancers. *Journal of Environmental Science and Health, Part C*, 29(3), pp. 223-249.
- YOUNG, I. & WOODSIDE, J. 2001. Antioxidants in health and disease. *Journal of clinical pathology*, 54, 176-186.
- ZOU, W., CHEN, H.-C., HISE, K. B., TANG, H., FOLEY, S. L., MEEHAN, J., LIN, W.-J., NAYAK, R., XU, J., FANG, H. & CHEN, J. J. 2013. Meta-Analysis of Pulsed-Field Gel Electrophoresis Fingerprints Based on a Constructed Salmonella Database. *PLoS ONE*, 8, e59224.

## **Appendix**

## **Methods for the genomic DNA extraction**

### **Isolation of DNA from bladder cancer cell lines using the QIAGEN Genomic-tip 100/G DNA extractor kit.**

#### **Cell preparation for X-ray radiation**

Cells were washed with PBS and trypsinised with 1-3ml using 1X trypsin EDTA (depending on the cell lines). After trypsinisation, the cell samples were then washed with cold medium and centrifuged at  $0.4 \times g$  for 4 minutes. The supernatant was discarded, and the cell pellets were washed twice with ice-cold PBS. The pellets were re-suspended at a final concentration of  $7 \times 10^6 - 10 \times 10^6$  cells in 1.5ml pre-labelled Eppendorf tubes in 100  $\mu$ l of ice-cold PBS.

The prepared cells were irradiated in the Eppendorf tubes as described in Section 2.11.1.2.

#### **DNA extraction by Qiagen Blood & Cell culture DNA Kit**

The Qiagen Blood & Cell culture DNA Kit (Qiagen Genomic-tips system) was used to extract DNA from bladder cancer cells line. All enzymes and buffers were contained in the kit. DNA was isolated according to manufacturer's instructions for direct isolation of chromosomal DNA 20-150Kb in size.

The irradiated samples were centrifuged at  $1500 \times g$  for 10 mins and the supernatant was removed. 0.5ml of ice-cold C1 buffer (438.14g sucrose, 4.06g  $MgCl_2 \cdot 6H_2O$  and 4.84g Tris base dissolved in 1L ddH<sub>2</sub>O, 42g Triton X-100 (100%) pH 7.5) and 1.5ml of ice-cold HPLC water were added to the cell pellet and briefly vortexed. The sample tubes were then incubated for 10mins on ice. The lysed cells were pelleted for 15 mins at  $1300 \times g$  at 4°C. The supernatant was then removed, and the pellets were re-suspended in 0.25ml C1 buffer + 0.75ml of HPLC water. The nuclear pellet samples were then vortexed for 10 seconds, centrifuged at 4°C for 15 mins at  $1300 \times g$  and re-suspended in 1ml of buffer G2 (76.42g guanidine HCL, 11.17g  $Na_2EDTA \cdot 2H_2O$ , 3.63g Tris base, 250ml of Tween-20 solution and 50ml 10% Triton X-100 adjusted to 1L with distilled water, pH 8). The nuclear pellet samples were then briefly vortexed for 10 seconds at maximum speed. Buffer G2 lysed the nuclei and

denatured the proteins such as nucleases, histones, and viral particles. Afterwards, 25µl of Qiagen protease was added to the samples to digest the denatured proteins into smaller fragments and the samples were incubated at 50°C for 30-60 mins. During this incubation period, the QIAGEN 100/G Genomic-tips were set up equilibrated before adding the samples by using 2ml of buffer QBT (43.83g NaCl, 10.46g MOPS, 150ml pure isopropanol and 15ml 10% Triton X-100 solution, adjusted to 1L with distilled water). After incubation, the sample was vortexed for 10 seconds at maximum speed, and the samples were applied to equilibrated columns. The samples were left to gravity flow. Next, the columns were washed twice with 2mL QC buffer (58.44g NaCl, 10.46g MOPS and 150ml pure isopropanol, adjusted to 1L, pH 7), and left to gravity flow. The columns were moved to new 15mL falcon tubes and the genomic DNA was finally eluted with 5ml of elution buffer QF (73.05g NaCl, 6.06 Tris-base, 15 % isopropanol and the volume was complete to 1L with ddH<sub>2</sub>O, pH 8.5) which was warmed to 50°C to increase the DNA yield. This elution step was undertaken twice, and left to gravity flow. 1.4ml of isopropanol was added to precipitate the DNA, then the precipitated DNA was mixed and centrifuged at 5000x g for 15mins at 4°C. The supernatant was then removed and the pellet was washed with 1ml of ice-cold 70% ethanol. After overtaxing and centrifugation at 5000 x g for 10 minutes at 4°C, the supernatant was carefully discarded. The resulting DNA (pellets) were dried at room temperature for ~5 mins and rehydrated in 100µl of HPLC water and incubated in at 4°C overnight. 10µl of the aliquot samples were collected and placed into pre-labelled Eppendorf tubes to measure DNA concentration. The concentration and purity of the extracted DNA were measured by a NanoDrop™ 1000 spectrophotometer.

## **The isolation of DNA from cultured cancer cells using the Wako DNA Extractor WB kit (NaI) method.**

### **Cells preparation for X-ray radiation**

The cell lines were washed with PBS and trypsinised using 1X trypsin EDTA when the confluent monolayers reached ~90% or ~ 10×10<sup>6</sup> - 12×10<sup>6</sup> cells/flask (to optimise maximum amount of DNA). Cells were then washed twice with cold medium and centrifuged, and the

supernatant discarded. Cell pellets were re-suspend with 500µl of ice-cold PBS and transferred to pre-labelled Eppendorf tubes (each tube contained  $\sim 10 \times 10^6$ - $12 \times 10^6$  cells).

The prepared cells were irradiated in the Eppendorf tubes as described in Section 2.11.1.2

### **DNA extraction by the Wako DNA Extractor kit**

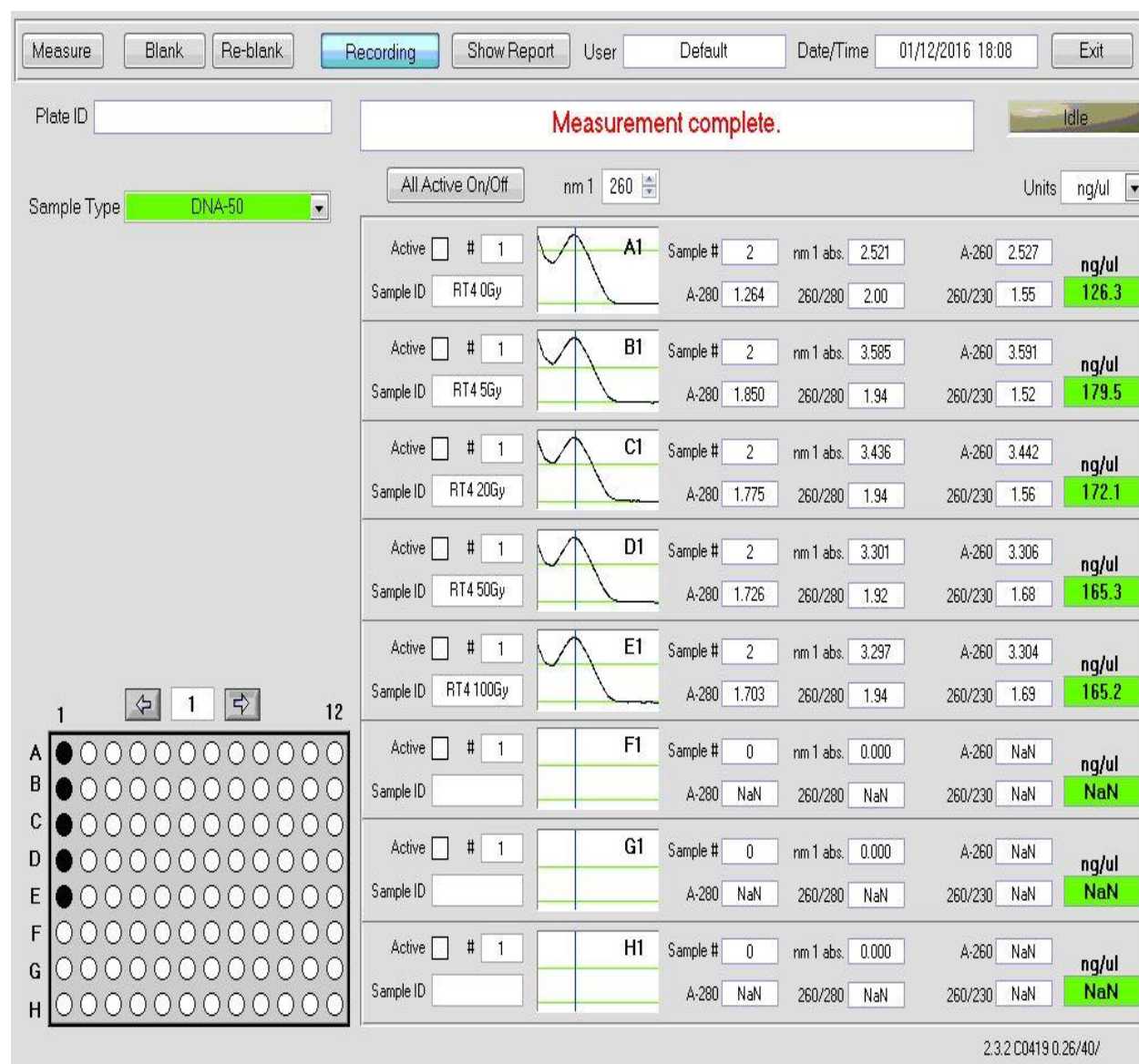
The Wako DNA Extractor WB kit (NaI) method was used to extract DNA from cells in culture. All enzymes and buffers were supplied with the kit, unless otherwise stated. Prior to cell lysis, treated cell pellets were defrosted, and centrifuged for 5 mins at 10000 x g at 4°C. The supernatant was then removed for each sample and the cell pellets were re-suspended with 2ml of lysis solution which contained 5mM desferrioxamine. The cell pellets were then vortexed for 30seconds at moderate speed. The supernatant was then carefully removed after a brief centrifugation of the suspension mixture at 10000 x g for 20 seconds at 4°C. The cells pellets were then re-suspended in 1ml of lysis solution (containing 5mM desferrioxamine) and were briefly vortexed for 30 seconds at moderate speed. Next, the supernatant was removed following brief centrifugation of the suspension mixture at 10000 x g for 20 seconds at 4°C. The resultant pellets were re-suspended in 200µl of enzyme reaction solution plus 7.24µl of RNase and 9.09µl of T1 and then incubated at 37°C for 30 mins. 10µl of proteinase K (10mg/ml of ddH<sub>2</sub>O) was added to each sample, mixed well by vortex and incubated at 37°C for 1-2 hrs. After incubation, the samples were centrifuged at 10000 x g for 5 mins at room temperature and supernatants were removed. 300µl of NaI solution was applied to each supernatant and mixed well by inversion for 5-10 mins followed by the addition of 500µl of ice-cold isopropanol and mixed well by inversion for at least 15 mins until the DNA, apparent as a whitish material, appeared. After the DNA precipitation, the DNA samples were centrifuged at 10000 x g for 10 mins at room temperature followed by supernatant removal and the DNA pellets were rinsed by adding 1ml of washing buffer A and were mixed thoroughly to remove the pellets from tube's wall. DNA pellets were centrifuged at 10000 x g for 10 mins. After centrifugation, the supernatant was discarded and pellets were rinsed by adding 1ml of washing buffer B. The DNA samples were left to dry at room temperature for 5 mins and were re-dissolved in 200µl of HPLC grade water, and the samples were left



overnight on a rotating table. 10µl of the aliquot samples were collected and placed into pre-labelled Eppendorf tubes to measure DNA concentration. The concentration and purity of the extracted DNA were measured by a NanoDrop™ 1000 spectrophotometer. (More information are given in the section 2.11 Liquid Chromatography-mass spectrometry/mass spectrometry (LC-MS/MS) method for the determination of 8-oxodG in DNA bladder cancer cell samples in Materials and Methods Chapter of this thesis).

The examples of the concentration and purity measures of the extracted DNA as determined using a NanoDrop™ 1000 spectrophotometer. (Information about Automated DNA Purification on the Maxwell® 16 MDx Instrument are given in section 2.11.1.5, in Materials and Methods Chapter of this thesis).

A:



**B:**

Measure Blank Re-blank **Recording** Show Report User Default Date/Time 07/12/2016 12:57 Exit

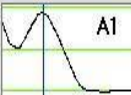
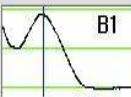
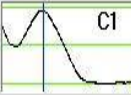
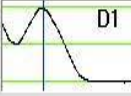
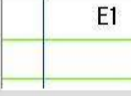
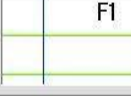

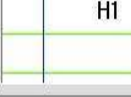
Plate ID


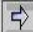
Sample Type **DNA-50**










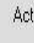
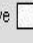

All Active On/Off nm 1 260 Units ng/ul










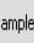

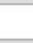
**Measurement complete.**










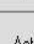

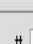
Idle










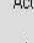


Active <input type="checkbox"/> # 1		Sample # 1	nm 1 abs. 1.843	A-260 1.847	ng/ul
Sample ID J82 Gy B		A-280 0.948	260/280 1.95	260/230 1.72	<b>92.37</b>
Active <input type="checkbox"/> # 1		Sample # 1	nm 1 abs. 1.867	A-260 1.870	ng/ul
Sample ID J82 20Gy B		A-280 0.960	260/280 1.95	260/230 1.78	<b>93.51</b>
Active <input type="checkbox"/> # 1		Sample # 1	nm 1 abs. 1.895	A-260 1.897	ng/ul
Sample ID J82 50Gy B		A-280 0.995	260/280 1.91	260/230 1.92	<b>94.87</b>
Active <input type="checkbox"/> # 1		Sample # 1	nm 1 abs. 1.943	A-260 1.947	ng/ul
Sample ID J82 100Gy B		A-280 1.037	260/280 1.88	260/230 1.86	<b>97.36</b>
Active <input type="checkbox"/> # 1		Sample # 0	nm 1 abs. 0.000	A-260 NaN	ng/ul
Sample ID		A-280 NaN	260/280 NaN	260/230 NaN	<b>NaN</b>
Active <input type="checkbox"/> # 1		Sample # 0	nm 1 abs. 0.000	A-260 NaN	ng/ul
Sample ID		A-280 NaN	260/280 NaN	260/230 NaN	<b>NaN</b>
Active <input type="checkbox"/> # 1		Sample # 0	nm 1 abs. 0.000	A-260 NaN	ng/ul
Sample ID		A-280 NaN	260/280 NaN	260/230 NaN	<b>NaN</b>
Active <input type="checkbox"/> # 1		Sample # 0	nm 1 abs. 0.000	A-260 NaN	ng/ul
Sample ID		A-280 NaN	260/280 NaN	260/230 NaN	<b>NaN</b>





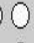





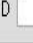

1  1  12


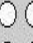








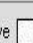

A            





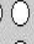







B            












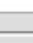
C            

D            

E            

F            

G            

H            

2.3.2 C0419 0.26/36/

Measure
Blank
Re-blank
Recording
Show Report
User
Default
Date/Time
02/02/2017 11:23
Exit


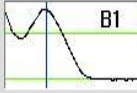
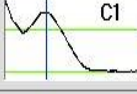

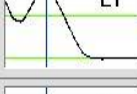

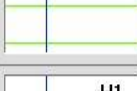
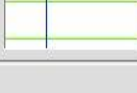
Plate ID

Sample Type DNA-50

Measurement complete.

Idle

All Active On/Off
nm 1 
Units ng/ul

A	1	←	1	→	12	Active <input type="checkbox"/>	# 1	 A1	Sample # <input style="width: 40px;" type="text" value="2"/>	nm 1 abs. <input style="width: 60px;" type="text" value="2.352"/>	A-260 <input style="width: 60px;" type="text" value="2.354"/>	ng/ul
						Sample ID <input style="width: 100%;" type="text" value="RT112 0Gy"/>	A-280 <input style="width: 60px;" type="text" value="1.191"/>	260/280 <input style="width: 60px;" type="text" value="1.98"/>	260/230 <input style="width: 60px;" type="text" value="1.09"/>	117.7		
B	1	←	1	→	12	Active <input type="checkbox"/>	# 1	 B1	Sample # <input style="width: 40px;" type="text" value="2"/>	nm 1 abs. <input style="width: 60px;" type="text" value="2.946"/>	A-260 <input style="width: 60px;" type="text" value="2.950"/>	ng/ul
						Sample ID <input style="width: 100%;" type="text" value="RT112 5Gy"/>	A-280 <input style="width: 60px;" type="text" value="1.532"/>	260/280 <input style="width: 60px;" type="text" value="1.93"/>	260/230 <input style="width: 60px;" type="text" value="1.58"/>	147.5		
C	1	←	1	→	12	Active <input type="checkbox"/>	# 1	 C1	Sample # <input style="width: 40px;" type="text" value="2"/>	nm 1 abs. <input style="width: 60px;" type="text" value="2.872"/>	A-260 <input style="width: 60px;" type="text" value="2.876"/>	ng/ul
						Sample ID <input style="width: 100%;" type="text" value="RT112 20Gy"/>	A-280 <input style="width: 60px;" type="text" value="1.489"/>	260/280 <input style="width: 60px;" type="text" value="1.93"/>	260/230 <input style="width: 60px;" type="text" value="1.26"/>	143.8		
D	1	←	1	→	12	Active <input type="checkbox"/>	# 1	 D1	Sample # <input style="width: 40px;" type="text" value="2"/>	nm 1 abs. <input style="width: 60px;" type="text" value="3.106"/>	A-260 <input style="width: 60px;" type="text" value="3.108"/>	ng/ul
						Sample ID <input style="width: 100%;" type="text" value="RT112 50Gy"/>	A-280 <input style="width: 60px;" type="text" value="1.591"/>	260/280 <input style="width: 60px;" type="text" value="1.95"/>	260/230 <input style="width: 60px;" type="text" value="1.85"/>	155.4		
E	1	←	1	→	12	Active <input type="checkbox"/>	# 1	 E1	Sample # <input style="width: 40px;" type="text" value="2"/>	nm 1 abs. <input style="width: 60px;" type="text" value="3.218"/>	A-260 <input style="width: 60px;" type="text" value="3.222"/>	ng/ul
						Sample ID <input style="width: 100%;" type="text" value="RT112 100Gy"/>	A-280 <input style="width: 60px;" type="text" value="1.671"/>	260/280 <input style="width: 60px;" type="text" value="1.93"/>	260/230 <input style="width: 60px;" type="text" value="1.79"/>	161.1		
F	1	←	1	→	12	Active <input type="checkbox"/>	# 1	 F1	Sample # <input style="width: 40px;" type="text" value="0"/>	nm 1 abs. <input style="width: 60px;" type="text" value="0.000"/>	A-260 <input style="width: 60px;" type="text" value="NaN"/>	ng/ul
						Sample ID <input style="width: 100%;" type="text"/>	A-280 <input style="width: 60px;" type="text" value="NaN"/>	260/280 <input style="width: 60px;" type="text" value="NaN"/>	260/230 <input style="width: 60px;" type="text" value="NaN"/>	NaN		
G	1	←	1	→	12	Active <input type="checkbox"/>	# 1	 G1	Sample # <input style="width: 40px;" type="text" value="0"/>	nm 1 abs. <input style="width: 60px;" type="text" value="0.000"/>	A-260 <input style="width: 60px;" type="text" value="NaN"/>	ng/ul
						Sample ID <input style="width: 100%;" type="text"/>	A-280 <input style="width: 60px;" type="text" value="NaN"/>	260/280 <input style="width: 60px;" type="text" value="NaN"/>	260/230 <input style="width: 60px;" type="text" value="NaN"/>	NaN		
H	1	←	1	→	12	Active <input type="checkbox"/>	# 1	 H1	Sample # <input style="width: 40px;" type="text" value="0"/>	nm 1 abs. <input style="width: 60px;" type="text" value="0.000"/>	A-260 <input style="width: 60px;" type="text" value="NaN"/>	ng/ul
						Sample ID <input style="width: 100%;" type="text"/>	A-280 <input style="width: 60px;" type="text" value="NaN"/>	260/280 <input style="width: 60px;" type="text" value="NaN"/>	260/230			

**D:**

Measure

Blank

Re-blank

Recording

Show Report

User

Default

Date/Time

01/12/2016 18:44

Exit

Plate ID

Measurement complete.

Idle

Sample Type

DNA-50

All Active On/Off

nm 1

260

Units

ng/ul

Active <input type="checkbox"/>	#	1		Sample #	1	nm 1 abs.	3.253	A-260	3.259	ng/ul	162.9
	Sample ID	UMUC3 0Gy				A-280	1.688	260/280	1.93	260/230	1.24
Active <input type="checkbox"/>	#	1		Sample #	1	nm 1 abs.	2.577	A-260	2.582	ng/ul	129.1
	Sample ID	UMUC3 5Gy				A-280	1.345	260/280	1.92	260/230	1.48
Active <input type="checkbox"/>	#	1		Sample #	1	nm 1 abs.	2.841	A-260	2.846	ng/ul	142.3
	Sample ID	UMUC3 20Gy				A-280	1.481	260/280	1.92	260/230	1.38
Active <input type="checkbox"/>	#	1		Sample #	1	nm 1 abs.	2.974	A-260	2.978	ng/ul	148.9
	Sample ID	UMUC3 50Gy				A-280	1.543	260/280	1.93	260/230	1.65
Active <input type="checkbox"/>	#	1		Sample #	1	nm 1 abs.	2.803	A-260	2.806	ng/ul	140.3
	Sample ID	UMUC3 100Gy				A-280	1.440	260/280	1.95	260/230	1.70
Active <input type="checkbox"/>	#	1		Sample #	0	nm 1 abs.	0.000	A-260	NaN	ng/ul	NaN
	Sample ID					A-280	NaN	260/280	NaN	260/230	NaN
Active <input type="checkbox"/>	#	1		Sample #	0	nm 1 abs.	0.000	A-260	NaN	ng/ul	NaN
	Sample ID					A-280	NaN	260/280	NaN	260/230	NaN
Active <input type="checkbox"/>	#	1		Sample #	0	nm 1 abs.	0.000	A-260	NaN	ng/ul	NaN
	Sample ID					A-280	NaN	260/280	NaN	260/230	NaN

1

↔

1

↔

12

A

B

C

D

E

F

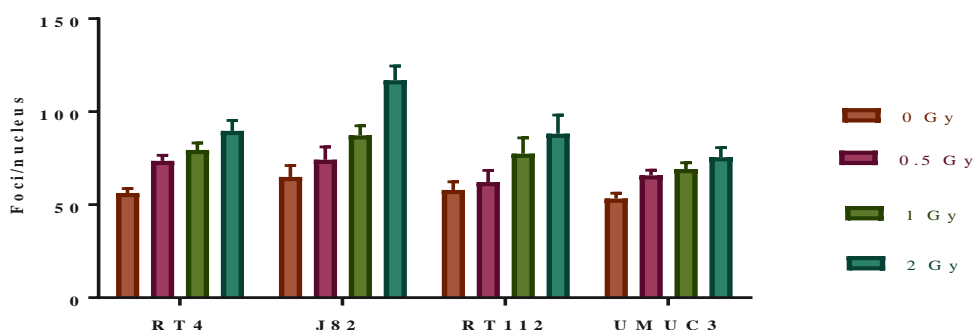
G

H

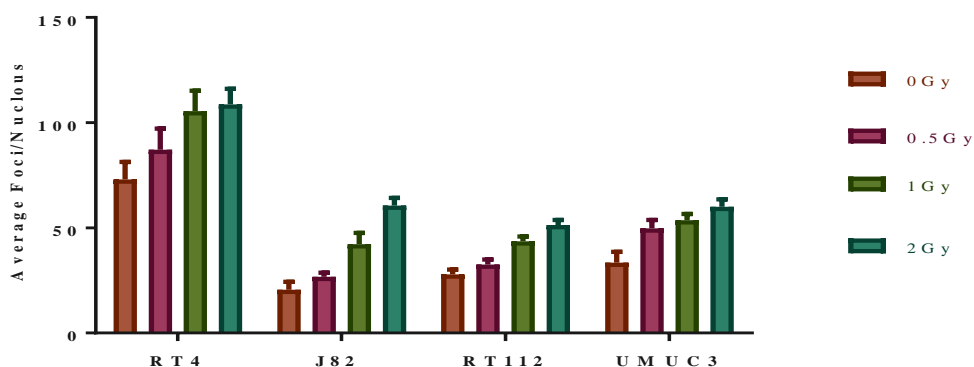
2.3.2 C0419 0.26/36/



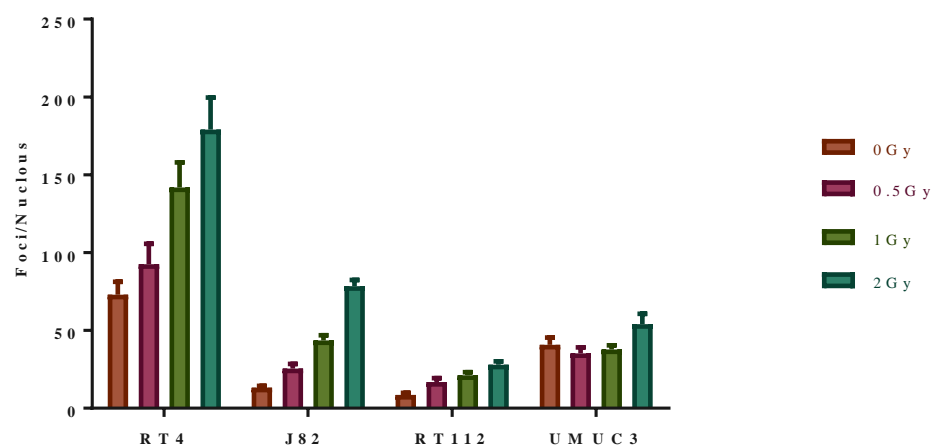
An example for some results obtained via Velocity program. (Information about  $\gamma$ -H2AX results obtained by Velocity program are given in section 6.4.1 Optimisation the  $\gamma$ -H2AX assay, in Materials and Methods Chapter of this thesis).



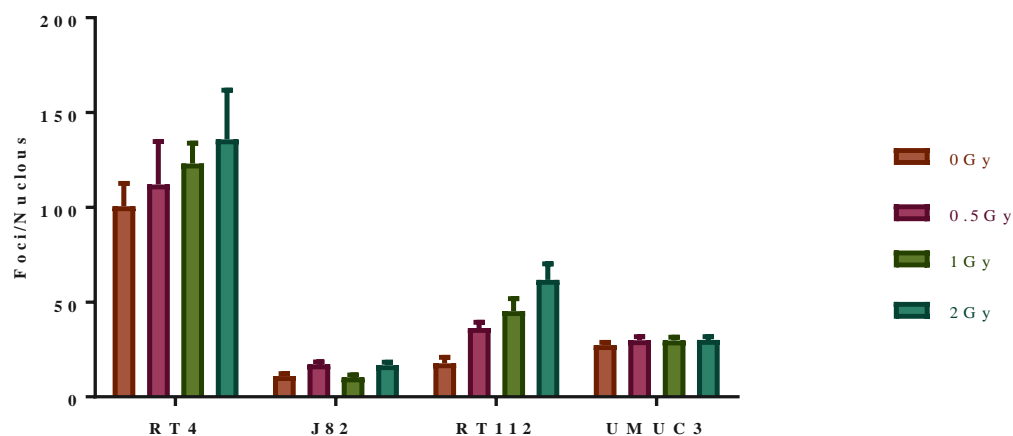
The DNA damage as assessed by average of Foci/ nucleus for four bladder cancer cell lines using  $\gamma$ -H2AX after treatment with 0, 0.5, 1, and 2 Gy of IR after 30 minutes incubation time. The data columns represent the Mean  $\pm$  SEM of two independent experiments (Velocity program).



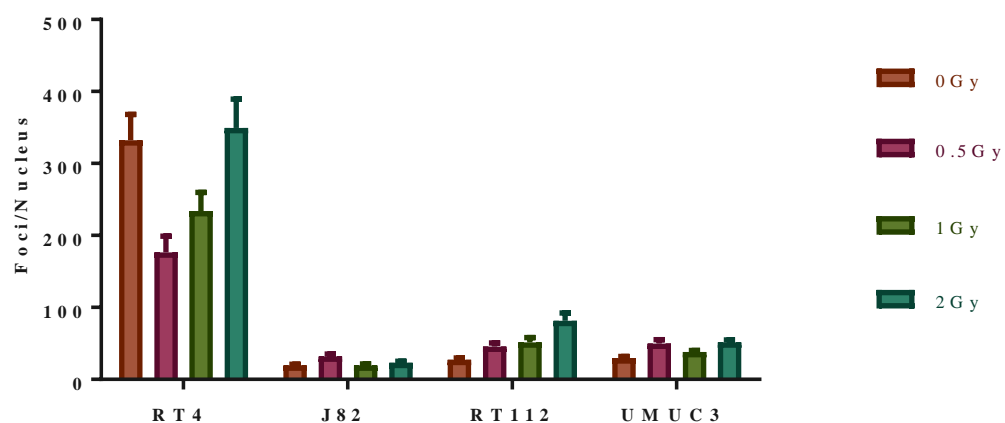
The DNA damage as assessed by average of Foci/ nucleus for four bladder cancer cell lines using  $\gamma$ -H2AX after treatment with 0, 0.5, 1, and 2Gy of IR after 2 hour incubation time. The data columns represent the Mean  $\pm$  SEM of two independent experiments (Velocity program).



The DNA damage as assessed by average of Foci/ nucleus for four bladder cancer cell lines using  $\gamma$ -H2AX after treatment with 0, 0.5, 1, and 2Gy of IR after 6 hour incubation time. The data columns represent the Mean  $\pm$  SEM of two independent experiments (Velocity program).



The DNA damage as assessed by average of Foci/ nucleus for four bladder cancer cell lines using  $\gamma$ -H2AX after treatment with 0, 0.5, 1, and 2Gy of IR within 16 hour incubation time. The data columns represent the Mean  $\pm$  SEM of two independent experiment (Velocity program).



The DNA damage as assessed by average of Foci/ nucleus for four bladder cancer cell lines using  $\gamma$ -H2AX after treatment with 0, 0.5, 1, and 2 Gy of IR after 24 hour incubation time. The data columns represent the Mean  $\pm$  SEM of two independent experiment (Velocity program).